Polluted soil remediation using surfactant foam injection : experiments and upscaling

Sagyn Omirbekov

HESAM UNIVERSITÉ

Arts et Métiers Sciences et Technologies

ÉCOLE DOCTORALE SCIENCES DES MÉTIERS DE L'INGÉNIEUR
I2M – TREFLE ENSAM UMR 8508 – Campus de Bordeaux

THÈSE

présentée par : **Sagyn OMIRBEKOV**

soutenue le : **15 juillet 2020**

pour obtenir le grade de : **Docteur d'HESAM Université**

préparée à : **École Nationale Supérieure d'Arts et Métiers**

Spécialité : **Mécanique-matériaux**

Polluted soil remediation using surfactant foam injection: experiments and upscaling

THÈSE dirigée par :

Mme. AHMADI-SÉNICHAULT Azita

M. DAVARZANI Hossein

Jury

M. Michel QUINTARD, Directeur de Recherche CNRS, IMFT	Président
M. William R. ROSSEN, Professeur, Delft University of Technology	Rapporteur
M. Fabrice GOLFIER, Maître de conférences, ENSG, Université de Lorraine	Rapporteur
M. Henri BERTIN, Directeur de Recherche CNRS, Université de Bordeaux	Examinateur
Mme. Azita AHMADI-SÉNICHAULT, Professeure, Arts et Métiers ParisTech	Examinatrice
M. Hossein DAVARZANI, Ingénieur de recherche, BRGM	Examinateur
M. Stéfan COLOMBANO, Ingénieur de recherche, BRGM	Invité

THÈSE

Acknowledgment

First of all, I would like to express my gratitude to the people who surrounded me during these three years of PhD project.

I would like to thank my thesis supervisors Azita Ahmadi-Sénichault and Hossein Davarzani, for their guidance through each research stage and their advice to conduct this project. Thanks to them, I learned many things and gained many skills during these past three years.

I would like to acknowledge Stéfan Colombano for inspiring my interest in the experiments and his motivation and support. I do not forget his sense of humor and his menu translations at the BRGM restaurant. I would also like to thank Michaelle Didier and Fabien Lion for the administrative procedures and help during the moving to Orleans and all the colleagues from the 3SP/DEPA division of the BRGM.

I am also grateful to Henri Bertin for his help and advice on experiments, Bauyrzhan Satken for his advice on the experimental setup, Muriel Ezan-Bore, and Valérie Pernot for the administrative procedures, Audrey Duphil for the help in the laboratory, and all other members of I2M laboratory.

I would like to thank Korlan Rysbayeva and Bexultan Sabyrbay for their assistance in conducting the experiments, and doctoral students Nicolas Philippe, Maxime Cochennec, Romain Aranda, Mohammad Ali Iravani, Sofia Visitacion, Safae El Farricha, Terence Mackaya, Vincent Le Maout, and Mohamed Bensalem for the kindness and friendliness.

Very special gratitude goes to Bolashaq international scholarship of the president of the Republic of Kazakhstan for providing the PhD grant. Also, I would like to thank the Centre of International Programs for their supports.

Last but not least, I would like to thank my whole family and friends for supporting me spiritually throughout this thesis and my life in general.

Contents

Nomenclature

Greek Letters

$A_{\beta\sigma}$	Area of solid-fluid interface (m^2)
α	Empirical shift parameter associated with the bulk rheology of the fluid and the tortuosity of porous media (-)
β	Liquid-phase
γ	Gas-liquid interfacial tension (N/m)
$\dot{\gamma}$	Shear rate (1/s)
$\dot{\gamma}_{eq}$	Equivalent/In-situ shear rate (1/s)
ΔP	Pressure drop (Pa)
$\Delta\rho$	Gas-liquid density difference (kg/m^3)
ε	The foam expansion ratio (-)
ζ	Scale-separation parameter (-)
μ	Fluid viscosity (Pa.s)
μ_{app}	Foam apparent viscosity (Pa.s)
∇P	Pressure gradient (Pa/m)
∇P^*	Critical pressure gradient (Pa/m)
ρ	Fluid density (kg/m^3)
ρ_f	Foam density (kg/m^3)
σ	Solid-phase
τ	Shear stress (Pa)
τ_0	Yield stress (Pa)
τ_w	Shear stress at the tube wall (Pa)
$\emptyset$	Porosity (%)
χ	Dimensionless fitting coefficient (-)
Ω	Total volume of representative elementary volume (REV)
Ω_β	Liquid-phase domain
Ω_σ	Rigid solid-phase domain
ω	Dimensionless fitting coefficients (-)

Roman Letters

a	Consistency index of power-law model ($Pa.s^n$)
D	Porous column diameter (m)
d	Grain size diameter (mm)
f_g	Fraction of gas/foam quality (%)

f_g^*	Transition foam quality (%)
f_{gc}	Critical gas fraction (%)
G'	Storage modulus (Pa)
G''	Loss modulus (Pa)
g	Acceleration of gravity (m/s^2)
i	Natural number (1, 2, 3 …)
K	Intrinsic permeability (m^2; D)
k_i	Relative permeability of phase i (-)
k_{rw}	Relative permeability of water (-)
L	Characteristic macroscopic length (m)
l	Characteristic length of REV (m)
L_{eff}	Effective length, length of the tortuous capillaries (m)
m	Exponent index of Herschel-Bulkley-Papanastasiou (s)
m_g	Mass of liquid phase (kg)
m_l	Mass of gas phase (kg)
n	Power-law flow index (-)
n_f	Number of lamella/Foam texture (-)
n_t	Number of trapped gas (-)
N_{Bo}	Bond number (-)
N_{ca}	Capillary number in porous media (-)
N_{cL}	Capillary number for foam generation in porous media (-)
P	Fluid pressure (Pa)
P_i	Fluid pressure of phase i (Pa)
Q	Volumetric (total) flow rate (m^3/s; mL/min)
Q_b	Source-sink term for foam bubbles (-)
Q_f	Volumetric flow rate due to the fluidity (m^3/s; mL/min)
Q_G	Volumetric gas flow rate (m^3/s; mL/min)
Q_L	Volumetric liquid flow rate (m^3/s; mL/min)
Q_s	Volumetric flow rate due to the slip velocity (m^3/s; mL/min)
Q_t	Volumetric total flow rate (m^3/s; mL/min)
R	Radius of circular capillary (m)
R_c	Foam coalescence rate (-)
R_g	Grain radius (m)
R_{gr}	Foam generation rate (-)
R_{eq}	Equivalent radius (m)
RF	Resistance factor (-)

S	Cross-sectional area (m^2)
S_g	Saturation of gas (-)
S_{gf}	Flowing-gas saturation (-)
S_{gt}	Saturation of trapped-gas (-)
S_i	Saturation of phase i (-)
S_w	Saturation of liquid (-)
S_{wi}	Initial liquid saturation (-)
u	Darcy velocity (m/s)
u_i	Darcy velocity of phase i (m/s)
v	Fluid velocity field (m/s)
V_g	Volume of gas (m^3)
V_l	Volume of liquid (m^3)
V_p	Volume of pore (PV) within the porous medium (m^3; mL)
X_f	Fraction of flowing gas (-)
X_t	Fraction of trapped gas (-)
z	Vertical axis

Abbreviations

AOS	Alpha olefin sulfonate
CGA	Colloidal Gas Aphrons
CMC	Critical Micelle Concentration
DNAPL	Dense Non-Aqueous Phase Liquid
EOR	Enhanced Oil Recovery
FEP	Fluorinated Ethylene Propylene
FG	Foam Generator
GB	Glass Beads
GT	Glass Tube
H-B	Herschel-Bulkley model
H-B-P	Herschel-Bulkley-Papanastasiou model
HCB	Hexachlorobenzene
LNAPL	Light Non-Aqueous Phase Liquids
M	Main column
NAPL	Non-Aqueous Phase Liquids
PAH	Polyaromatic Hydrocarbons
PCE	Tetrachloroethene
PCP	Pentachlorophenol

PTFE	Polytetrafluoroethylene
PV	Pore Volume
PVC	Polyvinyl Chloride
REV	Representative Elementary Volume
TCA	Trichloroethane
TCE	Trichloroethylene
YSF	Yield Stress Fluid

Part 1 – Substantial summary in French

1. Introduction générale

La mousse aqueuse est un système à deux phases, dans lequel des bulles de gaz (déconnectées) sont dispersées au sein d'une phase liquide continue (Bikerman, 1973). Cette phase liquide continue séparant les bulles de gaz forme des films liquides minces dénommés lamelles. Dans la plupart des mousses, la fraction de gaz est élevée. Le tensioactif ajouté dans la phase aqueuse stabilise les lamelles en réduisant la mobilité des bulles de gaz et en maintenant la phase gazeuse discontinue. Ainsi, réduire la mobilité des gaz diminue la mobilité de la mousse. Cette propriété de la mousse est la plus cruciale en termes d'application.

Le comportement mécanique particulier de la mousse, combiné à sa surface spécifique importante par rapport à sa densité, font en sorte qu'elle est utilisée dans de nombreux types d'applications : industrie alimentaire, entreprises de cosmétiques et de blanchisserie, produits chimiques ménagers, fluides anti-incendie et matériaux de construction (Prud'homme & Khan, 1996). L'utilisation de mousse aqueuse dans les milieux poreux est également très répandue, notamment dans l'industrie pétrolière (Lake, 1989); ainsi, les procédés de récupération assistée du pétrole, RAP, (EOR en anglais) à l'aide de mousse ont commencé depuis le début des années 1960 (Patzek, 1996). Dans l'industrie pétrolière, la mousse peut être utilisée comme fluide de forage, comme agent de contrôle de la mobilité dans les processus RAP (Chen, et al., 2014), dans les traitements d'acidification de la matrice (Rossen & Wang, 1999) et dans la prévention des fuites de gaz (Bernard & Holm, 1970). À la fin du siècle dernier, la technologie d'injection de mousse dans des milieux poreux a commencé à être utilisée pour les processus de dépollution des aquifères contaminés (Hirasaki, et al., 1997).

La principale utilisation de la mousse dans la dépollution des sols consiste à contrôler la perméabilité des milieux poreux, afin de diriger les réactifs utilisés pour la dépollution des zones plus perméables vers les zones moins perméables de l'aquifère. Cependant, les différences entre les applications dans les réservoirs de pétrole et les aquifères sont notables. Par exemple, les milieux poreux dans les réservoirs de pétrole sont principalement consolidés avec une faible perméabilité, tandis que les aquifères pollués sont souvent non consolidés et relativement perméables. Par conséquent, l'application d'un écoulement de mousse dans des milieux poreux hautement perméables fait toujours face à des défis spécifiques.

- Mousse hors milieu poreux

Le comportement mécanique de la mousse est complexe en raison de ses propriétés élastiques, plastiques et visqueuses. La mousse est par conséquent souvent analysée rhéologiquement hors milieu poreux (« bulk foam » en anglais) (Coussot, 2005; Larson, 1999; Macosko, 1994). De nombreux auteurs ont étudié expérimentalement la rhéologie de la mousse hors milieu poreux au cours des soixante dernières années (Cohen-Addad, et al., 2013; Denkov, et al., 2009; Hohler & Cohen-Addad, 2005; Katgert, et al., 2013; Kraynik, 1988; Dollet & Raufaste, 2014; Khan, et al., 1988; Herzhaft, 1999; Denkov, et al., 2005).

Dans la plupart des études, la mousse hors milieu poreux a été mise en évidence comme un fluide à seuil ; la majorité des résultats expérimentaux relatifs au comportement des mousses peut être bien décrites par la loi de Herschel-Bulkley. Par exemple, Khan et al. (1988) ont étudié la mousse à l'aide d'un rhéomètre en utilisant une géométrie à plaques parallèles. La géométrie a été recouverte de papier de verre pour éliminer la vitesse de glissement à la paroi. Le diamètre moyen des bulles de mousse était de 65 µm (mesures réalisées par une méthode optique). Ils ont démontré l'existence d'un seuil de contrainte (ou limite d'élasticité) pour les mousses avec 92%, 95% et 97% de fractions gazeuses (f_g, qualité de la mousse) ; celui-ci augmentant avec f_g.

- Mousse en milieu poreux

Dans les milieux poreux, une compréhension complète de l'écoulement de la mousse est également entravée par le comportement complexe de la mousse associé à la microstructure complexe des milieux poreux. De plus, il existe des contradictions apparentes dans les conclusions des études sur l'écoulement de mousse présentées dans la littérature. Par exemple, certains auteurs ont montré un comportement de type newtonien d'écoulement de mousse dans des milieux poreux (Persoff, et al., 1991), ou rhéofluidifiant (Hirasaki & Lawson, 1985; Falls, et al., 1989), ou newtonien et rhéofluidifiant (Vassenden & Holt, 2000) ou un comportement dépendant de la qualité de la mousse (Alvarez, et al., 2001). Hirasaki et Lawson (1985) ont rapporté un comportement non linéaire de la mousse lors de son écoulement à travers d'un tube capillaire lisse et ont souligné l'impact de la texture de la mousse (i.e. taille des bulles) sur la viscosité apparente de la mousse. Le comportement rhéofluidifiant de l'écoulement de la mousse dans un milieu poreux constitué de billes homogènes a été mis en lumière par Falls et al. (1989). Rossen et Wang (1999) ont modélisé la mousse comme un fluide de Bingham s'écoulant dans des grès. Ils ont supposé que la taille des bulles était fixe et à peu près égale à la taille des pores pour des mousses de faible qualité. Certains auteurs ont également considéré la présence d'un seuil de contrainte basé sur un gradient de pression seuil, qui était lié aux types de gaz et de surfactant, à la concentration en surfactant et aux propriétés pétrophysiques des milieux poreux (Rossen & Gauglitz, 1990; Dicksen, et al., 2002; Ransohoff & Radke, 1988; Gauglitz, et al., 2002; Omirbekov, et al., 2020). Cependant, dans la plupart des études de modélisation de mousse dans des milieux poreux, la mousse a été caractérisée comme un fluide à rhéologie en loi de puissance sans supposer un seuil de contrainte (Friedmann, et al., 1991; Kovscek, et al., 1997; Bertin, et al., 1998; Myers & Radke, 2000; Kam, 2008; Kovscek, et al., 2010; Ashoori, et al., 2012). De plus, la génération de mousse in situ dans des milieux poreux hautement perméables, principalement lorsque les tailles de pores sont beaucoup plus grandes que celles des bulles, est mal connue ; dans ce cas, le comportement et la stabilité de la mousse dépendent fortement des processus de génération.

- Mousse en tube capillaire

La rhéologie de la mousse en tubes capillaires (avec des géométries simples) est souvent décrite comme un fluide rhéofluidifiant avec ou sans seuil de contrainte ; plusieurs types de modèle ont été utilisés pour représenter l'écoulement de la mousse comme le modèle de Bingham (Khan, et al., 1988), le modèle de loi de puissance (Enzendorfer, et al., 1995; Gardiner, et al., 1999) et le modèle Herschel-Bulkley (Harris, 1989; Burley & Shakarin, 1992; Herzhaft, et al., 2005). Par exemple, David et Marsden (1969) ont étudié l'écoulement de la mousse dans des tubes de verre avec des diamètres de 0,4 ; 0,6 ; 0,7 et 0,8 mm. Ils ont mis en lumière le comportement rhéofluidifiant de la mousse avec une contrainte seuil très faible, et ont également corrigé la viscosité apparente de la mousse en tenant compte de la vitesse de glissement le long de la paroi. Hirasaki et Lawson (1987) ont décrit la viscosité apparente de l'écoulement de la mousse dans des tubes capillaires lisses sur la base de la loi de Hagen-Poiseuille. Les mousses générées avec une fraction de gaz (f_g, qualité de mousse) d'au moins 70% s'écoulaient à travers des capillaires en verre avec des rayons de 0,1 ; 0,2 ; 0,25 ; 1 et 2,5 mm. La plus petite bulle était équivalente à la taille du plus petit tube capillaire. Ils ont observé le comportement rhéofluidifiant de la mousse s'écoulant dans les tubes et ont décrit que la viscosité apparente de la mousse était affectée par trois principaux facteurs : 1) des zones de liquide entre les bulles de gaz ; 2) déformation des formes des bulles due aux forces visqueuses et capillaires ; 3) le gradient de tension superficielle, qui s'explique par l'accumulation de matière active de surface à l'arrière des bulles. Ils ont également noté la dépendance de la viscosité apparente de la mousse de la taille des bulles (texture), du rayon du capillaire et à la fraction de gaz dans la mousse. Cependant, le changement de longueur des tubes capillaires n'a pas affecté le comportement de la mousse dans les tubes capillaires. Herzhaft et al. (2005) ont étudié une mousse pré-générée dans un rhéomètre à tube à recirculation constitué de deux tubes parallèles en acier inoxydable d'un diamètre interne de 7,7 et 10,9 mm respectivement. L'écoulement de la mousse a été examiné par rapport à la qualité de la mousse variant de 20% à 85% pour différentes concentrations de tensioactif et à différentes pressions statiques. Ils ont trouvé un comportement newtonien et de type fluide à seuil respectivement pour les mousses de faible qualité ($f_g \leq$ 50%) et de haute qualité ($f_g \geq$ 60%). Bogdanovic et al. (2009) ont étudié le comportement rhéologique des mousses avec une qualité de mousse allant de 86,2% à 99,6% dans des conduites horizontales en acier inoxydable de diamètres respectives 0,5 et 1 pouce (correspondant respectivement à 12,7 et 25,4 mm). La mousse a été générée par co-injection d'azote et d'une solution de tensioactif en utilisant un filtre (taille d'ouverture de 50 µm ou 90 µm). Ils ont étudié cinq différents tensioactifs à trois concentrations différentes. Ils ont trouvé un impact du type de surfactant sur la valeur de transition de la qualité de la mousse (f_g^*), pour lesquels des valeurs plus élevées ont été trouvées pour des mousses plus stables. Il faut noter que f_g^* correspond à la valeur de transition entre les régimes de faible et forte qualité de mousse. Cependant, le changement de diamètre du tuyau n'a pas modifié de manière significative la valeur de f_g^*. Ils ont également observé un comportement rhéoépaississant de la mousse dans des régimes de haute qualité ($f_g > f_g^*$). Dans les régimes de faible qualité ($f_g < f_g^*$), les mousses se comportaient

principalement comme un fluide rhéoépaississant dans la conduite de 0,5 pouce de diamètre, mais dans la conduite de 1 pouce, les mousses présentaient un comportement presque newtonien (légèrement rhéofluidifiant). Gajbhiye et Kam (2011) ont mené des expériences d'écoulement de mousse dans des conduites en acier inoxydable et en nylon. L'écoulement de la mousse a été étudié par la mesure de la chute de pression et également visuellement en filmant les bulles de mousse puisque les tubes en nylon étaient transparents. Ils ont souligné le comportement rhéoépaississant de l'écoulement de la mousse dans le régime de faible qualité et ont indiqué l'effet du surfactant sur la valeur de f_g^*. Ils ont montré l'existence de deux régimes d'écoulement observés sur la base de la texture de la mousse pendant les expériences. Le régime de haute qualité a été décrit par des mousses à texture fine et un écoulement en gouttelettes. En revanche, l'écoulement de la mousse dans le régime de faible qualité était caractérisé par un écoulement stable de mousse uniforme et illustré par un écoulement en piston.

Une autre caractéristique essentielle de l'écoulement de la mousse dans les tubes est la vitesse de glissement à la paroi, qui dépend du type de matériau du tube, de sa rugosité de surface et de son diamètre (Stevenson, 2012). Cette vitesse de glissement est simplement utile pour une description macroscopique de la condition aux limites aux parois. Le mécanisme de glissement à l'échelle des pores dépend de la présence d'une fine couche de liquide qui ne glisse pas elle-même, mais mouille la paroi et lubrifie l'écoulement de la mousse. Ainsi, lorsque la mousse est cisaillée, un gradient de vitesse important apparaît dans cette couche liquide. Ce liquide de faible viscosité conduit à un glissement de la mousse ; son existence a été trouvée dans la plupart des études relatives aux mousses dans des conduites. Par exemple, Jastrzebski (1967) a supposé que la vitesse de glissement de la paroi était inversement proportionnelle au diamètre de la conduite. Il a également, pour la première fois, proposé de corriger la vitesse de glissement à la paroi. Harris et Reidenbach (1987) n'ont observé aucune vitesse de glissement à la paroi dans leur tuyau d'acier de 3 m de long et d'un diamètre de 7,75 mm. Thondavadi et Lemlich (1985) ont mis en lumière un glissement à la paroi pour des conduites en acrylique (Perspex), mais n'ont pas observé de glissement de paroi dans des conduites en acier galvanisé (d'une rugosité de 100 à 500 µm). Ils ont noté que la surface acrylique n'est pas mouillée par la mousse, mais que l'acier galvanisé est bien mouillé. Cependant, Denkov et al. (2012) ont constaté que l'angle de contact statique de l'eau déionisée était de 77,0 ° et 77,8 °, respectivement, pour le Perspex et l'acier galvanisé (Stevenson, 2012). De plus, il a été démontré que la vitesse de glissement à la paroi est dépendante de l'épaisseur du film liquide (Enzendorfer, et al., 1995), ceci est d'autant plus vrai pour les faibles qualités de mousse (Calvert & Nezhati, 1986).

A notre connaissance, la rhéologie de l'écoulement de la mousse dans les tubes capillaires est toujours en débat. En effet, comme mentionné ci-dessus, divers comportements rhéologiques sont observés pour différentes conditions expérimentales : newtonien, rhéofluidifiant, rhéoépaississant, avec ou sans seuil de contrainte. De plus, l'impact du matériau dont est fait le tube, qui est en relation avec la mouillabilité et la vitesse de glissement de la paroi, n'a pas été étudié en détail dans les études précédentes.

- Modélisation de l’écoulement des mousses en milieu poreux

Depuis les années 1980, plusieurs techniques de modélisation de la mousse ont été développées pour comprendre et prédire le comportement complexe de l'écoulement de la mousse en milieux poreux (Ma, et al., 2015). Ma et al. (2015) ont fourni un aperçu complet des méthodes existantes de modélisation de la mousse en milieu poreux. Ils ont classé les techniques de modélisation en trois groupes en fonction des textures de mousse implicites ou dynamiques : modèles d'équilibre local, modèles d'équilibre de population (« Population balance Models »), etc. Ils ont également indiqué la possibilité d'utiliser tous les modèles pour une incorporation directe dans des simulateurs de réservoir basés sur le bilan matière et la loi de Darcy. Ils ont répertorié certaines études sur le changement d'échelle de la mousse (de l'échelle du laboratoire à l'échelle du terrain) ; certains problèmes ont été signalés notamment les effets d'entrée et de bout dans les expériences de base en laboratoire.

En revanche, un lien entre la physique à l'échelle des pores ou des bulles (discontinue) et les modèles à l'échelle de Darcy (continuum) est encore manquant. Ce lien est souvent établi au moyen de diverses approches de mise à l'échelle (« upscaling » en anglais) (Berryman, 2005). Par exemple, la loi de Darcy est obtenue à partir de l'écoulement incompressible rampant d'un fluide newtonien via la méthode de prise de moyenne volumique avec une condition aux limites de non-glissement aux interfaces liquide-solide (Quintard & Whitaker, 1993; Quintard & Whitaker, 1994). Dans cette méthode, la perméabilité intrinsèque est calculée en fonction des variables de fermeture pour une géométrie donnée (une cellule unitaire périodique représentative du milieu poreux) (Whitaker, 1999). Cependant, le changement d'échelle est toujours un défi pour les fluides non newtoniens, qui sont décrits par des équations aux dérivées partielles non linéaires. Il existe très peu d'études expérimentales, numériques ou analytiques sur le changement d’échelle de l'écoulement des fluides non newtoniens dans les milieux poreux. Plusieurs auteurs ont étudié théoriquement ou numériquement le changement d’échelle des écoulements de fluides suivant les lois de puissance (Idris, et al., 2004; Wang, et al., 2014; Woods, et al., 2003; Orgéas, et al., 2006), les fluides viscoélastiques, les fluides à seuil, ou ont considéré le cas des fluides non newtoniens généralisés (Orgéas, et al., 2007). Par conséquent, le changement d’échelle de la mousse dans les milieux poreux est encore sujet à débat (Ma, et al., 2015), en particulier dans la dépollution des sols, où la perméabilité des milieux poreux est considérablement élevée. Certains auteurs ont également proposé empiriquement une équation à l'échelle de Darcy pour les fluides non newtoniens (Larry, et al., 1986; Chauveteau, 1982; Chevalier, et al., 2013; Castro, 2019). En termes simples, l'extension de l'équation à l'échelle de Darcy pour un fluide à seuil dans les milieux poreux anisotropes est très complexe et reste ouverte.

L'objectif final de cette thèse est d'améliorer nos connaissances sur les possibilités d'utilisation de la mousse dans des milieux poreux très perméables pour la dépollution de sols contaminés. Par conséquent, la rhéologie de la mousse pré-générée et le comportement de la mousse dans des milieux poreux de grande

perméabilité et dans différents tubes capillaires ont été principalement étudiés. De plus, le changement d'échelle de l'écoulement de la mousse de l'échelle des pores à l'échelle locale (échelle de Darcy) a été étudié en utilisant, comme paramètres d'entrée, les mesures expérimentales de la rhéologie de la mousse hors milieux poreux.

2. Considerations théoriques

Trois mécanismes majeurs de génération de mousse sont identifiés à l'échelle du pore dans les milieux poreux : rupture (« snap-off » en anglais) , abandon (« leave-behind » en anglais) et division lamellaire (« lamella division » en anglais) (Kovscek & Radke, 1994). Selon les processus de génération, le débit, la perméabilité, la compressibilité et la longueur du système, la mousse peut être classée comme "faible" ou "forte" (Ransohoff & Radke, 1988; Rossen, 1990), ce qui peut être décrit comme la transition d'une mousse faible de gaz continue à une mousse forte de gaz discontinue (voir Fig. 1). Une mousse faible est produite généralement avec des processus d'abandon, tandis que des mousses fortes sont générées par les trois mécanismes. Comme l'ont indiqué des études antérieures (Rossen & Gauglitz, 1990; Dicksen, et al., 2002; Ransohoff & Radke, 1988; Gauglitz, et al., 2002; Rossen, 1990), de la mousse est générée lorsque le gradient de pression dépasse le gradient de pression critique noté ∇P^* (Fig. 1). Ce gradient de pression dépend d'un nombre capillaire minimum pour entrer dans les pores par le mécanisme de rupture.

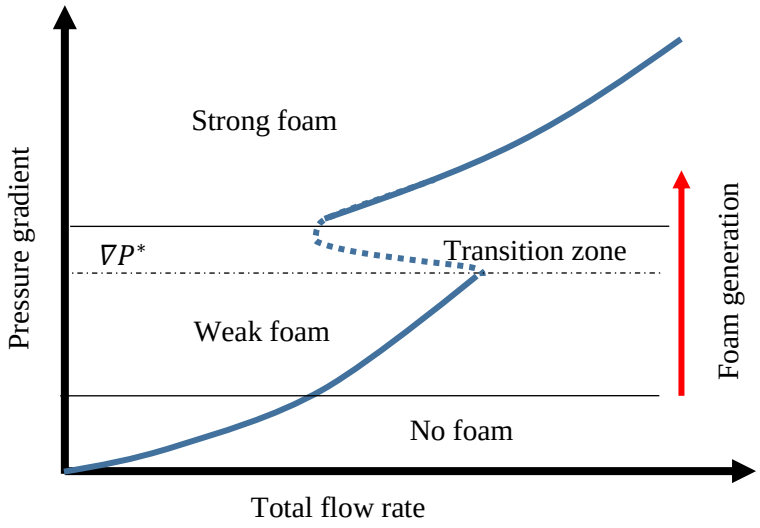

Fig. 1 Mécanisme de formation de mousse dans un milieu poreux, inspiré de (Gauglitz, et al., 2002)

Plusieurs auteurs ont calculé le nombre capillaire minimum pour générer de la mousse dans un milieu poreux (Rossen & Gauglitz, 1990; Dicksen, et al., 2002; Ransohoff & Radke, 1988; Tanzil, et al., 2000). En examinant différents milieux poreux, Tanzil et al. (2000; 2002) ont calculé le nombre capillaire minimum N_{cL}=2, avec le nombre capillaire N_{cL} défini comme :

$$N_{cL} = \frac{\Delta P}{\gamma}\sqrt{\frac{K}{\emptyset}} \qquad (1)$$

où γ (N/m) est la tension interfaciale gaz-liquide, K (m^2) est la perméabilité du milieu poreux dans la colonne, $\emptyset$ (-) est la porosité, et ΔP (Pa) est la baisse de pression mesurée le long de la colonne. ΔP

dépend de la qualité de la mousse, qui est le rapport entre le volume de gaz injecté et le volume total de liquide et de gaz, il peut être exprimé comme :

$$f_g = \frac{Q_G}{Q_G + Q_L} \tag{2}$$

où Q_G (mL/min) et Q_L (mL/min) sont respectivement les débits de gaz et de liquides. La somme de Q_G et Q_L donne la valeur du débit total Q_t. Selon la valeur de la fraction gazeuse, la mousse peut être sèche (f_g>99%), humide (64%<f_g<99%), ou considéré comme un liquide avec des bulles en suspension (f_g<64%) (Langevin, 2017). De plus, la forme de la bulle de mousse peut être transformée de sphérique en polyédrique en augmentant la fraction gazeuse (Kovscek & Radke, 1994). Dans les milieux poreux, Osterloh et Jante (1992) ont distingué deux régimes d'écoulement de mousse particuliers en régime stationnaire en fonction de la qualité de la mousse (dans des expériences avec du sable). Ils ont trouvé un régime de faible qualité (humide), dans lequel le gradient de pression était constant quel que soit le débit du liquide, et un régime de haute qualité (sec), dans lequel le gradient de pression était indépendant du débit de gaz. Une valeur particulière de qualité de mousse, f_g^*, divise ces deux régimes. Cette valeur de transition dépend des caractéristiques des milieux poreux, des types de tensioactifs et du gaz (Alvarez, et al., 2001).

L'écoulement de la mousse dans les milieux poreux est également affecté par la gravité. La compétition entre la gravité et les forces capillaires peut conduire à des configurations d'écoulement différentes. Cette compétition est quantifiée par le nombre de Bond, qui est calculé à l'aide de l'équation suivante (Ransohoff & Radke, 1988):

$$N_{Bo} = \frac{\Delta\rho g R_g D}{\gamma} \tag{3}$$

où $\Delta\rho$ (kg/m^3) est la différence de masse volumique gaz-liquide, g (m/s^2) est l'accélération gravitationnelle, R_g (m) est le rayon du grain, D (m) est le diamètre de la colonne poreuse.

L'écoulement de fluide newtonien dans des milieux poreux peut être considéré idéalisé comme un écoulement à travers un faisceau de tubes capillaires tortueux qui ont des rayons uniformes, R. La théorie de Kozeny-Carman (Kozeny, 1927; Carman, 1997) définit la tortuosité dans les capillaires comme le rapport entre la longueur effective (L_{eff}), c'est-à-dire la longueur des capillaires tortueux et les longueurs de tubes capillaires droits équivalents (L). Par conséquent, il a été supposé que le fluide entrant dans les capillaires tortueux s'écoule plus rapidement que le fluide s'écoulant à travers les capillaires droits équivalents afin d'atteindre l'extrémité du tube en même temps. En utilisant ce concept, l'écoulement dans des milieux poreux peut être présenté comme suit :

$$u = \frac{\emptyset R^2 \Delta P}{8\mu L}\left(\frac{L}{L_{eff}}\right)^2 \tag{4}$$

Où u (m/s) et ΔP (Pa) sont la vitesse de Darcy et la chute de pression dans la direction parallèle à la longueur L (m), μ (Pa.s) est la viscosité dynamique du fluide, $\emptyset$ est la porosité du milieu poreux. La vitesse de Darcy pour l'écoulement des fluides newtoniens en milieu poreux est alors définie comme suit (Eq. (4)) (Darcy, 1856).

$$u = \frac{Q}{A} = \frac{K\,\Delta P}{\mu\,L} \tag{5}$$

où Q (m^3/s) and A (m^2) sont le débit et la surface de la section transversale du milieu poreux. Le rayon moyen des pores pourrait être calculé comme le rayon des capillaires droits composant un faisceau donnant le même flux :

$$R_{eq}^2 = (R\frac{L}{L_{eff}})^2 = \frac{8K}{\emptyset} \tag{6}$$

Dans l'équation précédente, R_{eq} (m) est le rayon moyen des pores, K (m^2) est la perméabilité intrinsèque du milieu poreux. Le terme $(\frac{L}{L_{eff}})^2$ représente la tortuosité dans le milieu poreux. Par conséquent, un taux de cisaillement équivalent ($\dot{\gamma}_{eq}$) pour l'écoulement dans les milieux poreux peut être exprimé comme suit (Darby, et al., 2001),

$$\dot{\gamma}_{eq} = \frac{4\alpha u/\emptyset}{R_{eq}} \tag{7}$$

où α est un paramètre de décalage empirique associé à la rhéologie du fluide hors milieu poreux et à la tortuosité des milieux poreux (Chauveteau & Zaitoun, 1981). On a supposé que la tortuosité des sphères compactées était de 25/12 à partir de la dérivation de l'équation de Blake-Kozeny en utilisant le modèle capillaire (Christopher & Middleman, 1965; Hirasaki & Pope, 1974). En conséquence, Hirasaki et Pope (1974) ont proposé d'utiliser α ≈0,69 avec $\alpha = 1/\sqrt{L/L_{eff}}$ pour les fluides newtoniens. Récemment, Rodriguez de Castro (2019) a trouvé expérimentalement α égal à 0,68 dans des milieux poreux constitués de billes de verre.

Si l'on considère la loi de Darcy comme applicable pour l'écoulement d'un fluide non newtonien en milieu poreux, l'effet de la rhéologie non linéaire du fluide peut être incorporé dans la définition d'une viscosité apparente donnée par :

$$\mu_{app} = \frac{K\,\Delta P}{u\,L} \tag{8}$$

Cette viscosité apparente μ_{app} n'est pas une propriété intrinsèque du fluide et varie avec le débit. C'est une fonction non linéaire du taux de cisaillement équivalent donné dans l'Eq. (7), qui peut être modifiée en fonction du débit. De plus, le taux de cisaillement varie considérablement en fonction de la structure et de l'hétérogénéité des milieux poreux qui modifient la vitesse interstitielle.

Le comportement rhéologique du fluide à seuil pour un cisaillement simple peut être décrit par le modèle de Herschel-Bulkley (Herschel & Bulkley, 1926) :

$$\tau < \tau_0 \Rightarrow \dot{\gamma} = 0 \text{ (solid regime)}; \tau > \tau_0 \Rightarrow \tau = \tau_0 + a\dot{\gamma}^n \text{ (liquid regime)} \quad (9)$$

où τ (Pa) est la contrainte de cisaillement, $\dot{\gamma}$ (1/s) est le taux de cisaillement, τ_0 (Pa) est la limite d'élasticité ou le seuil de contrainte, a (Pa.s^n) et n (-) sont respectivement les indices de consistance et de fluidité. Le modèle continu et visqueux proposé par Papanastasiou (Papanastasiou, 1987) est utilisé pour éviter la principale difficulté causée par le modèle de Herschel-Bulkley dans les études numériques en raison d'un comportement discontinu à des taux de cisaillement faibles qui tendent la viscosité apparente vers l'infini. Le modèle Herschel-Bulkley-Papanastasiou (H-B-P) peut s'écrire comme suit :

$$\mu(\dot{\gamma}) = a(\dot{\gamma})^{n-1} + \frac{\tau_0}{\dot{\gamma}}\,[1 - exp(-m\dot{\gamma})] \quad (10)$$

où m (s) est un paramètre de régularisation qui doit avoir une très grande valeur.

Par conséquent, le débit volumétrique dans un tube circulaire pour les fluides Herschel-Bulkley peut être défini par la relation suivante (Skelland, 1967) :

$$Q = \frac{8\pi}{a^{\frac{1}{n}}}\left(\frac{L}{\Delta P}\right)^3 (\tau_w - \tau_0)^{1+\frac{1}{n}}\left[\frac{(\tau_w - \tau_0)^2}{3 + 1/n} + \frac{2\tau_0(\tau_w - \tau_0)}{2 + 1/n} + \frac{{\tau_0}^2}{1 + 1/n}\right](\tau_w > \tau_0) \quad (11)$$

qui a été dérivée par l'équation bien connue de Weissenberg-Rabinowitsch (Rabinowitsch, 1929; Mooney, 1931). Dans l'équation précédente, la contrainte de cisaillement à la paroi τ_w (Pa) est donnée par :

$$\tau_w = \frac{\Delta PR}{2L} \quad (12)$$

3. Etude expérimentale

Dans cette section, nous présentons les fluides et matériaux utilisés, la configuration expérimentale et les procédures pour les études d'écoulement de mousse en milieu poreux et dans des tubes capillaires.

3.1. Fluides et matériels

Solution de surfactant

Le tensioactif à base d'alpha-oléfine sulfonate (AOS) C14-16 Rhodacal® LSS-40 / AX (Solvay Novecare) et de l'eau déminéralisée / dégazée ont été utilisés pour préparer une solution de tensioactif. Le tensioactif contenait 40% en poids de matières actives dans la solution aqueuse. Le surfactant chimique a été choisi sur la base de plusieurs facteurs tels que la biodégradabilité du sol (Tuvell, et al., 1978; Talmage, 1994), l'accessibilité du marché (Cserháti, et al., 2002), et les tests sur le terrain à des fins d'assainissement des sols (Svab, et al., 2009). La concentration micellaire critique (CMC) du surfactant est de 1,8±0.1 g/L, qui est mesurée par la méthode de la goutte pendante (Stauffer, 1965) à l'aide d'un analyseur de forme de

goutte (DSA-100S, KRUSS). La solution de tensioactif a été préparée à une concentration de quatre fois la CMC pour éviter l'adsorption (Paria, 2008; Omirbekov, et al., 2020; Aranda, et al., 2020) à de faibles concentrations et respecter la biodégradabilité à fortes concentrations.

Gaz

Le gaz utilisé pour générer de la mousse dans toutes les expériences était de l'azote, fourni par Air Liquide, avec une pureté de 99,98%. Le N_2 a été sélectionné après avoir examiné plusieurs études présentées dans la littérature portant, notamment la stabilité de la mousse (Farajzadeh, et al., 2009; Zeng, et al., 2016) et la solubilité (Sander, 1999) des gaz. De plus, le dioxyde de carbone (pureté> 99,7%), fourni par Air Liquide, est utilisé pour les procédures de pré-saturation afin d'éviter le piégeage de bulles de gaz.

Milieu poreux

Des milieux poreux non consolidés fabriqués à partir de sable de silice calibré (BR-37) et de billes de verre de tailles différentes sont utilisés ; ils sont respectivement fournis par les sociétés Sibelco ™ et Sigma-Aldrich. Les caractéristiques de granulométrie du sable étaient les suivantes : le coefficient d'uniformité (C_u) est de 0,72, le coefficient de courbure (C_c) est de 0,98; la taille effective (d_{10}) et la taille moyenne des grains (d_{50}) sont respectivement de 0,180 et 0,135 mm. Un empilement de sable fin a été utilisé pour générer de la mousse, tandis que l'écoulement de la mousse a été examiné dans des empilements de billes de verre (GB) de 1, 2, 4 et 8 mm. Contrairement au sol naturel, les milieux poreux fabriqués des billes de verre empêchent l'adsorption et garantissent une distribution homogène des pores. Les caractéristiques des milieux poreux sont présentées dans le Table 1.

Table 1 Propriétés des milieux poreux

Milieu poreux	**Diamètre granulométrique moyen, d (mm)**	**Porosité,Ø (%)**	**Perméabilité, K (darcy)**	**Volume poral, PV (mL)**	**Rayon moyen des pores, R_{eq} (µm)**
Sable BR37	0,135	38±1	7±1	51±2	11,5
GB 1	1	36±1	830±10	181±2	133,5
GB 2	2	35±1	3017±10	181±2	257,9
GB 4	4	40±1	11032±10	185±2	467,2
GB 8	8	41±1	41125±10	191±2	886,4

La porosité du milieu a été déterminée en mesurant la masse de la colonne principale avant et après les processus de saturation en eau. La perméabilité a été calculée en reliant les valeurs mesurées de la différence de pression pour différents débits d'eau aux débits imposés correspondants par la loi de Darcy.

Tubes capillaires

La rhéologie de la mousse pré-générée est également examinée dans des tubes capillaires, dont les diamètres ont été choisis en considérant les milieux poreux de notre expérience précédente comme un

faisceau de tubes capillaires (Omirbekov, et al., 2019). Les diamètres des tubes ont été calculés par l'Eq. (6), qui est égal à deux fois la valeur de R_{eq}. De plus, selon Prud'homme et Khan (1996), le diamètre du tube doit être au moins dix fois plus grand que celui des bulles de gaz pour mesurer de manière appropriée la rhéologie de la mousse en milieu continu dans des tubes capillaires.

Deux types de systèmes de tubes capillaires sont considérés pour étudier l'influence du matériau du tube sur les propriétés de la mousse : les systèmes hydrophobes (PTFE – polytetrafluoroéthylène et FEP - Éthylène propylène fluoré) et hydrophiles (GT - tubes en verre lisse). Les tubes PTFE et FEP ont été fournis respectivement par les sociétés Darwin Microfluidics (France) et Adtech (Royaume-Uni). Les tubes en verre ont été obtenus auprès de DWK Life Sciences GmbH (Allemagne). Puisque la longueur des capillaires n'affecte pas le comportement d'écoulement de la mousse (Hirasaki & Lawson, 1985), la longueur des tubes hydrophobe et hydrophile a été choisie pour être respectivement de 30 cm et 40 cm. Ces longueurs ont été choisies en fonction des longueurs de colonnes considérées dans nos expériences précédentes (Omirbekov, et al., 2020). Les tubes capillaires utilisés avec leurs diamètres internes (id) sont présentés sur la Table 2.

Table 2 Type de matériau et diamètres internes des tubes capillaires utilisés dans cette étude

Type de matériau du tube capillaire		Diamètre interne du tube (mm)			
Matériaux hydrophobes	FEP	0,25 (±0,01)	0,3 (±0,01)	0,4 (±0,01)	0,8 (±0,01)
	PTFE	-	0,3 (±0,01)	0,5 (±0,01)	0,8 (±0,01)
Matériau hydrophile	Tube de verre (GT)	0,2 (±0,01)*	0,4 (±0,01)*	0,5 (±0,01)*	0,8 (±0,01)

*ces tubes capillaires en verre n'ont pas été étudiés en raison du retard de livraison

3.2. Dispositifs expérimentales

Les dispositifs utilisés pour conduire les expériences sont présentées en Fig. 2. Pour générer de la mousse, du N_2 et la solution de tensioactif ont été co-injectés dans la colonne de générateur de mousse. Ensuite, la rhéologie de la mousse pré-générée a été étudiée avec différentes méthodes : A) à l'aide d'un rhéomètre (mousse hors milieu poreux) ; B) dans les tubes capillaires ; C) dans la colonne principale de milieu poreux (p.m.).

Le contrôleur de débit massique El-Flow Select F-201CV (Bronkhorst), offrant une plage de 0,16 à 10 mL_n/min (lecture de ± 0,5%, plus ± 0,1% de la pleine échelle), a été utilisé pour contrôler le débit de gaz et garantir la stabilité d'écoulement de gaz depuis la bouteille de gaz. Une pompe à piston modèle 1HM (Eldex), avec une précision de ± 0,3%, a été utilisée pour injecter la solution de tensioactif à un débit constant. La colonne génératrice de mousse avait une longueur de 10 cm, un diamètre intérieur de 4 cm et était constituée de chlorure de polyvinyle transparent (PVC). Le garnissage à base de sable a été contenu

au sein de la colonne en utilisant une grille métallique de taille 42 µm. Les configurations suivantes ont été utilisées pour étudier les propriétés de la mousse pré-générée.

A) Un rhéomètre rotatif Haake Mars 60, Thermofisher (rotation de couple min. 0,02 µNm, résolution de couple 0,1 nNm) à géométrie de plaques parallèles dentelées (P60 / Ti / SE et TMP60 / SE) a été utilisé pour examiner la rhéologie de la mousse pré-générée.

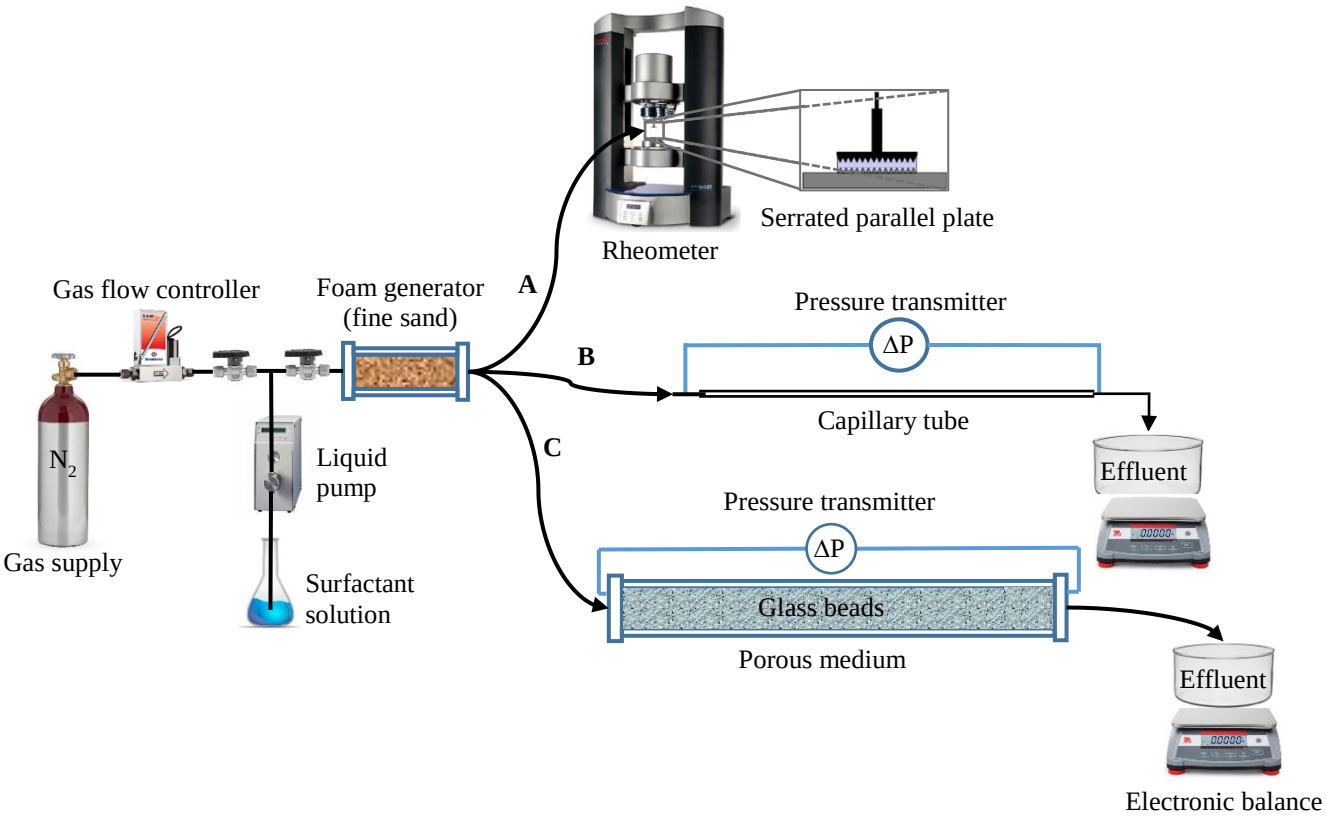

Fig. 2 Schéma des montages expérimentaux utilisés pour caractériser la rhéologie de A) mousse en milieu libre, B) mousse dans les tubes capillaires, C) mousse dans les milieux poreux

B) Pour étudier la mousse pré-générée, nous avons utilisé des tubes capillaires de 40 cm de long avec différents diamètres intérieurs. Le transmetteur de pression différentielle Rosemount 3051S (Emerson) dans la plage de 0 à 620 mbar (± 0,5 mbar à la valeur maximale) a été utilisé pour mesurer la différence de pression le long des tubes capillaires pour une baisse chute de pression inférieure à 620 mbar. Lorsque l'amplitude de la pression était supérieure à 620 mbar, nous avons utilisé deux capteurs de pression PR-33X (Keller) jusqu'à un maximum de 3000 mbar (avec une précision de 0,01%), installés aux deux extrémités des tubes capillaires. En outre, le capteur de pression Rosemount 3051S (Emerson) dans la plage de 0 à 2500 mbar (± 5 mbar à la valeur maximale) a également été utilisé pour les tubes avec un diamètre intérieur de 0,4, 0,5 et 0,8 mm.

C) La colonne principale (en PVC) d'une longueur de 40 cm et d'un diamètre intérieur de 4 cm remplie de billes de verre de 1 mm a été utilisée pour étudier la mousse pré-générée. Des grilles métalliques d'une taille 150 µm ont été utilisées de chaque côté de la colonne pour contenir les billes de verre dans la colonne. La chute de pression le long de la colonne principale a été mesurée par un transmetteur de pression différentielle Rosemount 2051 (Emerson) avec une plage de 0 à 2500 mbar (± 7 mbar à la valeur maximale). Une balance électronique modèle STX 6201 (OHAUS) avec une précision de 0,1 g a été utilisée pour mesurer la masse de l'effluent. La limite de pression maximale de ce dispositif expérimental était jusqu'à 6 bars contrôlée par le capteur de pression de la pompe.

3.3. Procédures expérimentales

Tout d'abord, les colonnes poreuses ont été soigneusement remplies et contrôlées pour les fuites. Les colonnes ont subies une injection de CO2 gazeux pour éliminer tout air. Ensuite, de l'eau dégazée / déminéralisée a été injectée dans les colonnes, en position verticale, avec 0,5 mL/min (au moins cinq volumes de pores (PV) pour dissoudre tout CO_2 et ainsi saturer complètement la colonne). Le CO_2 étant hautement soluble dans l'eau, cette étape a été utilisée pour garantir 100% de saturation des milieux poreux par l'eau. Pour mesurer le volume des pores et la porosité, les colonnes ont été pesées avant et après la saturation en eau. Les étapes expérimentales ultérieures ont été réalisées avec la colonne en position horizontale. La perméabilité du milieu poreux a été mesurée avec l'injection d'eau dégazée à différents débits tout en mesurant la différence de pression et calculée via la loi de Darcy (Eq. (5)). Les propriétés mesurées des milieux poreux ont été présentées dans le Table 1. Ensuite, la colonne a été traversée par 3 PV de solution de tensioactif pour achever l'adsorption. Enfin, pour générer de la mousse, la solution de tensioactif et l'azote gazeux ont été simultanément injectés dans le générateur de mousse. 5 PV de fluides ont été co-injectés pour obtenir une mousse pré-générée stable. La mousse pré-générée a été étudiée plus en détail dans des différentes configurations A) en utilisant le rhéomètre, B) dans des tubes capillaires C) dans un empilement de billes de verre.

Dispositif A) Des mousses pré-générées avec des qualités de mousse de 60%, 85% et 95%, générées au même débit total (Q =2 mL/min, u =2.65×10^{-05} m/s), ont été étudiées en utilisant le rhéomètre. Les propriétés rhéologiques de la mousse ont été étudiées à l'aide du rhéomètre, compte tenu des études précédentes (Larson, 1999; Macosko, 1994). La géométrie à plaques parallèles avec des surfaces dentelées a été utilisée pour éviter la vitesse de glissement sur la paroi (Herzhaft, 1999; Marze, et al., 2008; Princen & Kiss, 1989). L'espace de cisaillement de la géométrie était de 1 mm, ce qui a été choisi en tenant compte des études précédentes (Herzhaft, 1999). De plus, avant de commencer les expériences, la stabilité dynamique de la mousse à chaque qualité a été vérifiée, sur la base de l'étude de (Khan, et al., 1988), en examinant des échantillons à un taux de cisaillement constant. L'idée était d'observer combien de temps la mousse pouvait résister à un torque constant. La diminution des valeurs de torque indique le

changement de la structure de la mousse. Le volume de 3,1 ml de l'échantillon de mousse a été examiné, et les expériences ont été exécutées en triplicat pour chaque qualité de mousse.

Dispositif B) La mousse pré-générée a été injectée horizontalement dans des tubes capillaires. Le débit de mousse dans chaque tube capillaire a été étudié lors de l'injection d'un volume équivalent à 1 PV du générateur de mousse en mesurant la perte de charge à l'aide des transmetteurs de pression. Afin d'examiner l'impact de la qualité de la mousse sur le comportement d'écoulement de la mousse dans les tubes capillaires, des tubes FEP, PTFE et GT avec un diamètre intérieur de 0,8 mm et un tube en PTFE avec un diamètre intérieur de 0,5 mm ont été étudiés à un débit total fixe de 1 mL/min tandis que la qualité de la mousse variait de f_g= 50% à f_g = 99%. Pour étudier la rhéologie de la mousse dans les tubes capillaires de qualité f_g = 85%, nous avons mesuré la perte de charge le long des tubes capillaires en changeant le débit. Le débit total variait de 0,2 mL/min à 1 mL/min . De plus, nous prenions des photos des bulles de mousse pour chaque débit et qualité de mousse pour étudier l'évolution de la texture de la mousse dans le cas du tube en verre de 0,8 mm.

Dispositif C) La mousse pré-générée a été connectée à la colonne principale pour étudier l'impact de f_g et pour déterminer sa valeur de transition f_g^*. La mousse à débit total fixe (2 mL/min) a été étudiée pour différentes qualités de mousse (40% -99%). Les fractions de gaz et de liquide injectées étaient contrôlées par le contrôleur de débit massique et la pompe. Les expériences d'écoulement de mousse ont été examinées à travers les mesures de débit et de pression le long de la colonne. Par conséquent, la viscosité apparente de la mousse a été dérivée de la loi de Darcy (Eq. (5)). Après avoir déterminé f_g^*, l'écoulement de mousse dans un empilement de billes de verre de 1 mm (1mm GB) a été étudié à des régimes de faible qualité. Le débit de mousse avec f_g = 60%, 85% et 95% a été étudié pour différents débits totaux augmentés progressivement à partir du débit minimum (Q=0.2 mL/min, u=2.65×10^{-06} m/s) jusqu'au débit maximum (Q =2.2 mL/min, u =2.92×10^{-05} m/s). Ainsi, 905 et 82 minutes ont été respectivement nécessaires pour injecter 1 PV de mousse pré-générée à travers la colonne principale aux débits minimum et maximum. Les expériences ont été dupliquées par au moins une expérience de débit décroissant. Dans le même temps, la balance électronique a permis de mesurer la masse de l'effluent liquide pour déterminer le changement de saturation de la solution de surfactant (S_w) à l'intérieur de la colonne principale.

Toutes les expériences ont été réalisées à température ambiante (20 ° C) et à pression atmosphérique.

4. Etude théorique : technique de changement d'échelle

Étant donné que le changement d'échelle directe de l'écoulement de mousse de l'échelle du pore à l'échelle du laboratoire est complexe, nous avons utilisé la technique de changement d'échelle avec comme entrée les données rhéologiques de la mousse mesurées hors milieu poreux. L'objectif était

d'examiner si le comportement d'écoulement de la mousse dans les milieux poreux peut être prédit à partir des données rhéologiques obtenues en milieu libre (hors milieu poreux). Pour une application sur le terrain dans les aquifères, un deuxième changement d'échelle doit être envisagée. Cela sort du cadre de cette étude.

Afin d'étudier numériquement le comportement macroscopique de l'écoulement de la mousse, il a d'abord été nécessaire d'établir la géométrie du volume élémentaire représentatif (REV) pour correspondre à la perméabilité des milieux poreux obtenue à partir des expériences de laboratoire. Pour ce faire, nous avons résolu le problème de fermeture pour l'écoulement rampant des fluides newtoniens à l'état stationnaire développé par la méthode de la prise de moyenne volumique (Quintard & Whitaker, 1994; Whitaker, 1999) pour définir la perméabilité des cellules unitaires en 2D et en 3D (voir Fig. 4). La porosité de chaque type de cellule unitaire a été ajustée pour obtenir la même perméabilité que dans l'expérience sur la colonne 1D. Ensuite, le problème aux limites développé a été résolu en utilisant la méthode d'homogénéisation (Auriault, 1991) et ce, dans le but d'étudier davantage le comportement macroscopique de l'écoulement de la mousse. Les objectifs du changement d'échelle étaient d'étudier l'impact de f_g et l'effet de différentes géométries de cellules unitaires sur l'écoulement de la mousse. Ensuite, le résultat des expériences sur colonne poreuse 1D a été utilisé pour corréler et valider les résultats de changement d'l'échelle.

4.1. Description de l'écoulement de la mousse à l'échelle du pore

Le concept de milieu poreux est présenté sur la Fig. 3, dans laquelle nous considérons le flux de mousse à travers un REV périodique avec Ω étant le volume total de REV.

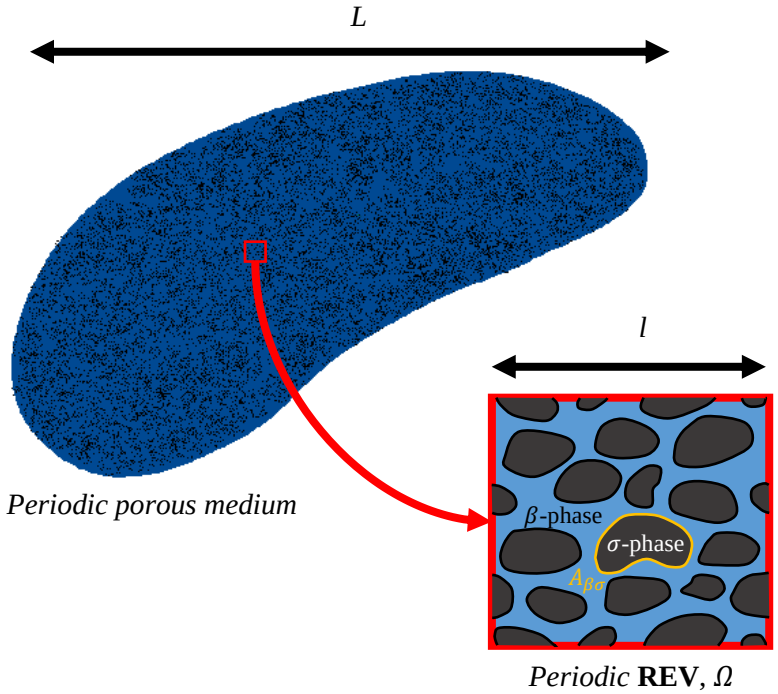

Fig. 3 Illustration schématique d'un milieu poreux périodique avec le REV associé

Le volume considéré, Ω, est constitué de la phase solide rigide Ω_σ et de la phase fluide (mousse) β de volume Ω_β. La porosité du milieu poreux peut être définie par $\emptyset = \Omega_\beta/\Omega$. Une condition aux limites sans glissement est considérée à l'interface solide-fluide notée ($A_{\beta\sigma}$). En outre, le fluide est considéré comme incompressible, purement visqueux et isotrope. Puisque l'écoulement est en régime rampant (les effets d'inertie sont négligés) et en régime stationnaire, les équations de conservation de masse et de quantité de mouvement pour un fluide à seuil sont écrites comme

$$0 = \boldsymbol{\nabla} \cdot \left(-P\mathbf{I} + \mu(\dot{\gamma})\left(\boldsymbol{\nabla}\mathbf{v} + (\boldsymbol{\nabla}\mathbf{v})^{\mathrm{T}}\right)\right) \qquad \text{in } \Omega_\beta \tag{13}$$

$$\boldsymbol{\nabla} \cdot \mathbf{v} = 0 \qquad \text{in } \Omega_\beta \tag{14}$$

$$\mathbf{v} = 0 \qquad \text{on } A_{\beta\sigma} \tag{15}$$

où $\mathbf{v}$ est la vitesse du fluide et P est la pression. μ est la viscosité dynamique du fluide, qui peut être définie par le modèle H-B-P (Eq. (10)) dans notre cas. Par conséquent, l'ensemble d'équations constitue la description à l'échelle du pore de l'écoulement de la mousse dans des milieux poreux hautement perméables.

4.2. Caractéristiques des cellules unitaires

L'écoulement de la mousse dans un milieu poreux modèle a été étudié avec une perméabilité fixe. L'étude a été menée dans quatre différentes cellules unitaires 2D périodiques et deux différentes cellules unitaires

3D. La fraction poreuse (porosité) a été ajustée pour obtenir la même perméabilité que la perméabilité de notre colonne principale. Les types de cellules unitaires avec leurs valeurs de porosité sont présentés dans la Fig. 4, avec a) arrangement carré de cylindres de section circulaire (SPC), b) arrangement carré avec de cylindres de section carrée (SPS), c) arrangement carré face centrée de cylindres de section circulaire (CPC), d) arrangement carré face centré de cylindres de section carrée (CPS), e) empilement cubique simple de cubes (SCP), f) empilement cubique centré de sphères (BCP).

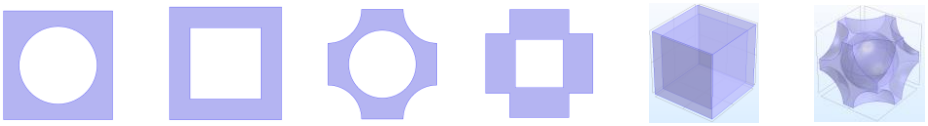

	a) SPC	b) SPS	c) CPC	d) CPS	e) SCP	f) BCP
∅ (-)	0.43	0.37	0.49	0.63	0.41	0.42

Fig. 4 Cellules unitaires périodiques 2D et 3D pour un réseau de cylindres parallèles de sections transversales circulaires (a, c), carrées (b, d), (e, f) empilements cubique simple de cubes et cubique centré de sphères

La longueur des cellules unitaires a été choisie pour être de 1 mm pour tous les cas afin d'être proche de la taille des billes de verre de 1 mm, et la perméabilité a été fixée à $8{,}3 \times 10^{-10}$ m^2. La perméabilité de chaque milieu poreux a été calculée en résolvant le problème de fermeture de l'écoulement de fluide newtonien par la méthode de prise de moyenne volumique (Quintard & Whitaker, 1994; Whitaker, 1999). Il est à noter qu'idéalement, les cellules unitaires choisies doivent avoir la même porosité et perméabilité que l'échantillon expérimental. De plus, ils devraient présenter des microstructures similaires en termes de désordre. Bien que toutes les cellules unitaires considérées ici soient des géométries ordonnées, les valeurs de porosité des cellules SPC, SPS, SCP et BCP sont relativement proches les unes des autres et également proches de la valeur trouvée pour l'empilement de billes de verre. La porosité pour CPC et CPS est significativement plus élevée pour la même valeur de perméabilité.

4.3. Changement d'échelle

Séparation des échelles

Afin de répondre aux exigences de la méthode d'homogénéisation (Idris, et al., 2004; Orgéas, et al., 2007; Auriault, 1991; Papanicolau, et al., 1978; Sanchez-Palencia, 1980), la condition de séparation des échelles doit être satisfaite pour les milieux poreux considérés. Comme le décrit Fig. 3, la longueur caractéristique l du REV est supposée être petite par rapport à la longueur macroscopique caractéristique L. Ceci peut être exprimé comme suit :

$$\zeta = \frac{l}{L} \ll 1 \tag{16}$$

où ζ représente le paramètre de séparation d'échelle.

Problème aux limites

Dans ce travail, la procédure d'homogénéisation proposée par Orgeas (2007) a été utilisée. Ainsi, l'écoulement d'un fluide newtonien généralisé à travers des cellules unitaires 2D et 3D est étudié à l'aide de simulations numériques. Un problème aux limites concernant la vitesse au premier ordre $\mathbf{v}^{(0)}$ et également la pression au second ordre $\nabla \mathrm{P}^{(1)}$ ont dû être abordés comme suit afin d'étudier l'écoulement de la mousse en milieu poreux :

$$\boldsymbol{\nabla} \cdot \left(-\zeta P^{(1)} + \left(\frac{\tau_0}{|\dot{\gamma}|} \left[1 - \exp(-m|\dot{\gamma}|) \right] + a|\dot{\gamma}|^{n-1} \right) \left(\boldsymbol{\nabla}\mathbf{v}^{(0)} + \left(\boldsymbol{\nabla}\mathbf{v}^{(0)} \right)^{\mathrm{T}} \right) \right) = \boldsymbol{\nabla} P_{\mathrm{x}}^{(0)} \quad \text{in } \Omega_\beta \qquad (17)$$

$$\boldsymbol{\nabla} \cdot \mathbf{v}^{(0)} = 0 \quad \text{in } \Omega_\beta \qquad (18)$$

$$\mathbf{v}^{(0)} = 0 \quad \text{on } A_{\beta\sigma} \qquad (19)$$

Ici, les inconnues $\zeta P^{(1)}$ et $\mathbf{v}^{(0)}$ sont périodiques, et le gradient de pression macroscopique $\boldsymbol{\nabla} P_{\mathrm{x}}^{(0)}$ est donné sur l'ensemble du REV comme terme source. La mousse a été considérée comme un fluide à seuil suivant le modèle rhéologique H-B-P (Eq. (10)), où la viscosité du fluide est supposée être fonction du taux de cisaillement $|\dot{\gamma}|$ donné par :

$$|\dot{\gamma}| = \sqrt{2\mathbf{S}:\mathbf{S}} \qquad (20)$$

où la vitesse de déformation **S** est définie en fonction du champ de vitesse **v** à l'échelle du pore,

$$\mathbf{S} = \frac{1}{2}\left(\boldsymbol{\nabla}\mathbf{v}^{(0)} + \left(\boldsymbol{\nabla}\mathbf{v}^{(0)} \right)^{\mathrm{T}} \right) \qquad (21)$$

Le problème aux limites ci-dessus a été résolu dans la cellule unitaire périodique 2D de section circulaire (Fig. 4, a) pour f_g= 60%, 85% et 95%, où les paramètres rhéologiques du modèle continu et visqueux étaient obtenus à partir de l'étude expérimentale. La mousse avec f_g= 85% a été étudiée pour toutes les géométries présentées sur la Fig. 4. Pour toutes les simulations dans les milieux poreux isotropes ordonnés, le gradient de pression macroscopique imposé $\boldsymbol{\nabla} P_{\mathrm{x}}^{(0)}$ était dans la direction de l'axe x. Le problème aux limites non linéaire (Eqs. (17)-(19)) a été résolu en utilisant Comsol Multiphysics® avec une formulation mixte pression-vitesse (P1-P2). Les problèmes d'écoulement ont été résolus grâce au module d'écoulement rampant, qui est conçu pour résoudre les écoulements de Stokes. La viscosité dynamique du module était défini par l'utilisateur via la section « Equation view ». La résolution de ce problème était similaire à la résolution du problème d'écoulement direct dans des cellules unitaires simples. Les éléments finis-triangulaires ont été utilisés pour mailler les géométries 2D. Un exemple de maillage et de conditions aux limites utilisées est illustré sur la Fig. 5.

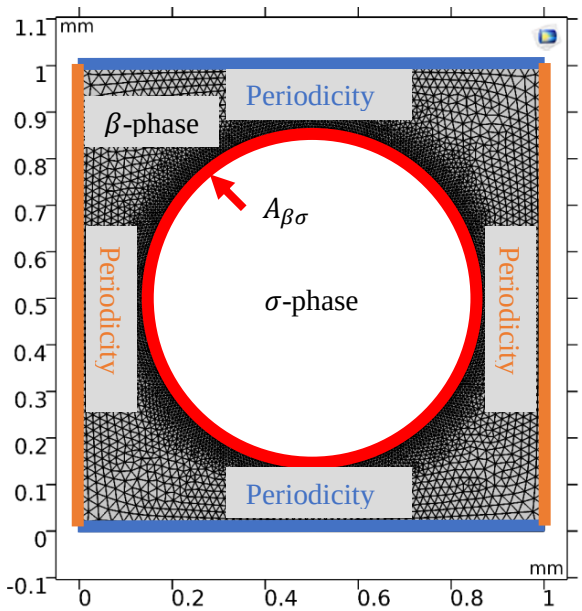

Fig. 5 Maillage et conditions aux limites utilisés pour réaliser les simulations

Les résultats présentés dans la littérature pour les mêmes géométries (Idris, et al., 2004; Orgéas, et al., 2007) ont permis de valider le modèle numérique adopté ici dans le cas des fluides à rhéologie en loi de puissance et des fluides newtoniens généralisés.

5. Résultats et discussion

5.1. Etude expérimentale

5.1.1. Génération de mousse en milieu poreux

La génération de mousse *in situ* (co-injection de gaz et de tensioactif) dans la colonne du générateur de mousse après l'injection de 0,6 PV est représentée sur la Fig. 6, pour différents types de sol et différents débits. La Fig. 6a montre le processus pendant la première expérience de drainage dans la colonne de générateur de mousse remplie de sable fin, où le débit total était égal à 2 mL/min. Le déplacement de mousse en forme de piston dans le pré-générateur poreux a été observé avec une zone de transition verticale.

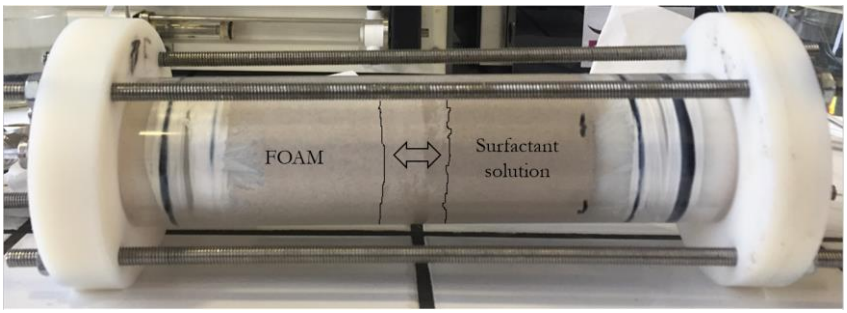

a)

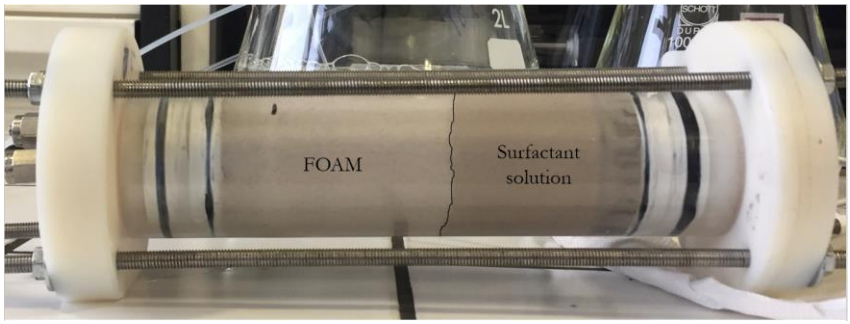

b)

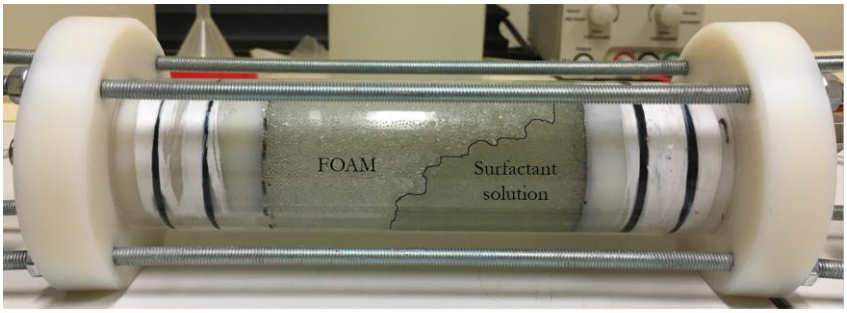

c)

Fig. 6 Génération de mousse in situ dans la colonne du générateur de mousse (après injection de 0,6 PV) : a) sable BR37, à Q_t=2 mL/min, b) sable BR37, à Q_t=8 mL/min, and c) billes de verre de 1 mm , à Q_t = 2 mL/min

Cette zone de transition se produit en raison de la transition de la «mousse faible» à la «mousse forte», ce qui s'explique par le processus de génération de mousse dans les milieux poreux (voir Fig. 1). A ce débit total, le mécanisme de génération de mousse est appelé «snap-off» (rupture) et dépend de la pression capillaire dynamique locale. Cependant, lorsque le débit total augmente encore, la baisse de pression augmente brusquement à des valeurs beaucoup plus élevées en raison des mécanismes de génération de mousse dans les milieux poreux. Ainsi, la génération de mousse résistante nécessite un gradient de pression élevé ou dépend des débits d'injection où le mécanisme de «division lamellaire» peut jouer un rôle crucial. Le mécanisme de division des lamelles concerne les lamelles de mousse déjà existantes et augmente le nombre de bulles. Pour cela, il est nécessaire que les lamelles statiques dans les gorges interstitielles soient déplacées avec un gradient de pression suffisant. Pour vérifier ce fait, nous avons mené une autre expérience de drainage en augmentant le Q_t. Dans cette expérience (voir Fig. 6b), le débit

total était quatre fois plus élevé (8 mL/min) que le précédent, et aucune zone de transition n'a été observée (déplacement de type piston). Néanmoins, au cours de l'expérience, le gradient de pression a fortement augmenté et nous avons été contraints d'arrêter l'expérience en raison de la limitation de pression du dispositif expérimental. Après cela, nous avons effectué le processus de co-injection à Q_t=2 mL/min dans la colonne du générateur de mousse remplie de billes de verre de 1 mm. Le drainage de la solution de tensioactif à 0,6 PV est présenté sur la Fig. 6c. On montre clairement que la frontière entre la mousse et la zone saturée a une pente donnée en raison de la qualité de mousse faible et des effets de gravité. En effet, le nombre de Bond (Eq. (3)) était d'environ dix fois plus grand pour le pré-générateur poreux réalisé avec les billes de verre de 1 mm que celui réalisé avec du sable.

5.1.2. Rhéologie de la mousse

Fig. 7 présente la rhéologie de la mousse pré-générée pour différentes qualités de mousse. La contrainte de cisaillement τ est affichée en fonction du taux de cisaillement $\dot{\gamma}$. Les points représentent la valeur moyenne des résultats expérimentaux et les lignes décrivent les résultats du modèle H-B-P. Le Table 3 montre les paramètres d'ajustement avec les coefficients du modèle H-B-P. Le paramètre de régularisation m a été choisi égal à 10000 afin de mieux représenter le comportement du seuil de contrainte dans les études numériques. À partir de ces résultats, on observe un comportement de fluide non newtonien à seuil de contrainte (« yield stress » en anglais) en cohérence avec le modèle Herschel-Bulkley-Papanastasiou. De plus, nous avons vu que le seuil de contrainte augmente avec l'augmentation de la qualité de la mousse, ce qui augmente la viscosité de la mousse ; notons que la valeur du seuil croit avec la qualité de la mousse. Ces résultats sont cohérents avec ceux de la littérature (Khan, et al., 1988), où le module de stockage (G') et τ_0 ont été mesurés en fonction de la qualité de la mousse (Marze, et al., 2009; Saint-Jalmes & Durian, 1999). La valeur du seuil de contrainte augmente d'un facteur deux entre f_g= 85% et f_g= 95%, ce qui peut s'expliquer par l'évolution de la forme des bulles de forme sphérique à polyédrique, augmentant ainsi le frottement entre les bulles (Denkov, et al., 2009).

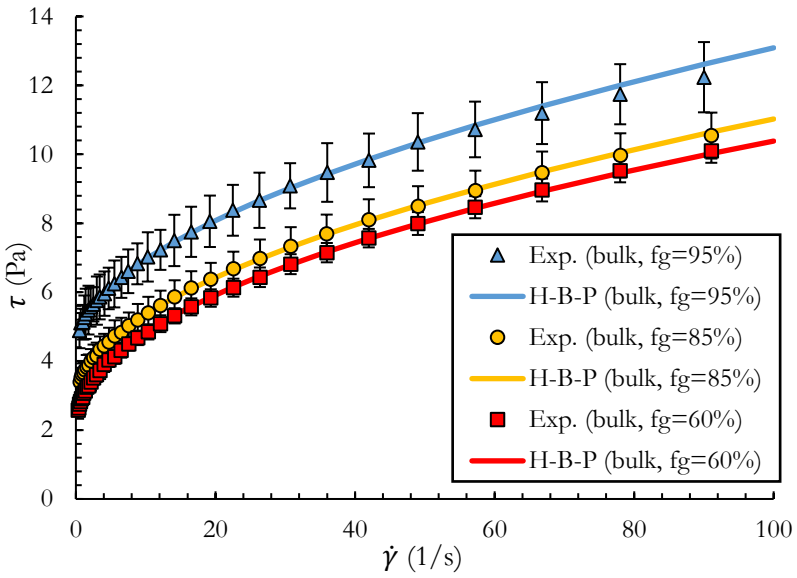

Fig. 7 Rhéologie de la mousse avec différentes qualités de mousse

Table 3 Paramètres de calage du modèle H-B-P

f_g (%)	**60%**	**85%**	**95%**
n (-)	0,48	0,52	0,54
τ_0 **(Pa)**	2,03	2,87	4,49
a **(Pa.s^n)**	0,94	0,76	0,7
m **(s)**	10000	10000	10000
R^2	0,99	0,99	0,99

On peut donc en conclure que dans nos expériences, la mousse peut être clairement considérée comme un fluide à seuil. Ceci est en accord avec des études antérieures dans lesquelles la valeur de l'indice de fluidité, n, obtenue expérimentalement était proche de 0,5 (Denkov, et al., 2009; Marze, et al., 2008; Princen & Kiss, 1989; Ovarlez, et al., 2008; Ovarlez, et al., 2010; Tcholakova, et al., 2008).

Il convient de noter que la mesure de la rhéologie de la mousse de qualité f_g=60% s'est avérée compliquée en raison du drainage de la phase liquide de la mousse au sein du rhéomètre. Par conséquent, pour éviter que le liquide ne sorte des plaques, nous avons introduit la quantité nécessaire exacte de l'échantillon de mousse (3,1 mL) en réglant l'espace à 3 mm (l'échantillon de mousse a été placé entre deux plaques). Ensuite, l'écart a été réduit lentement jusqu'à 1 mm pour effectuer des tests à différents taux de cisaillement. La mousse de qualité f_g= 60% a été étudiée avec grand soin à chaque taux de cisaillement en réalisant des expériences supplémentaires pour garantir des résultats précis.

Ces résultats sont analysés avec ceux de l'étude expérimentale sur les milieux poreux. Ils sont ensuite utilisés comme données d'entrée pour le changement d'échelle de l'écoulement de la mousse dans des milieux poreux hautement perméables en considérant la mousse comme un fluide à seuil.

5.1.3. Écoulement de mousse en milieu poreux (échelle de Darcy)

La Fig. 8 présente le front de propagation de mousse dans les colonnes principales remplies de billes de verre de 1 mm. On y voit la mousse qui a été respectivement pré-générée dans le sable fin (a) et dans l'empilement de billes de verre de 1 mm (b).

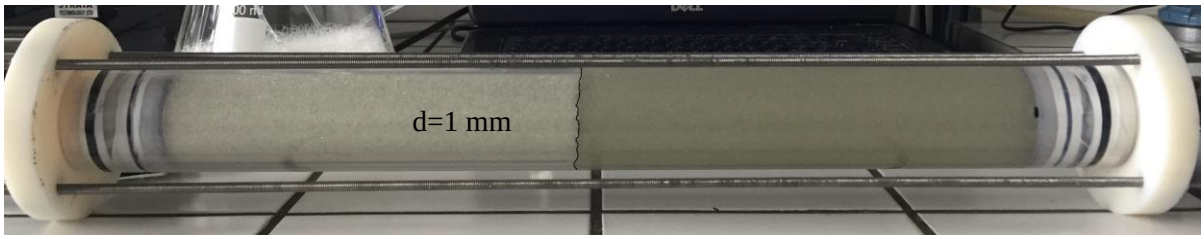

a)

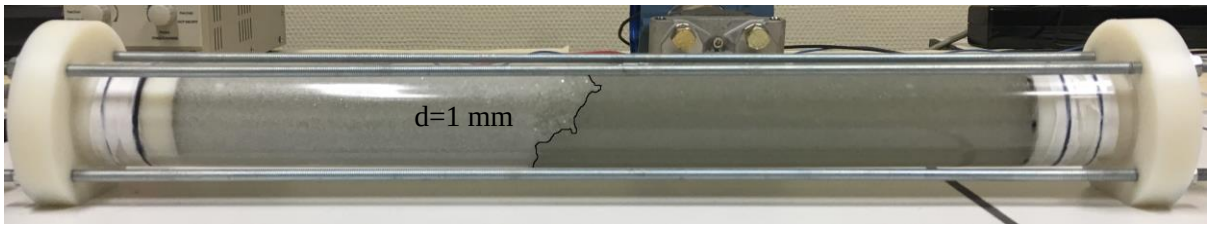

b)

Fig. 8 Injection de la mousse pré-générée dans les colonnes principales à Q_t=2 mL/min : mousse générée a) dans le sable fin b) dans les billes de verre de 1 mm (t = 0,5 PV)

Nous pouvons comparer visuellement les deux colonnes. La mousse générée dans le sable fin présente un comportement de mousse forte (front de déplacement net). Cependant, la mousse générée à l'aide d'un pré-générateur de billes de verre de 1 mm présente une zone de transition avec une pente particulière, ce qui pourrait s'expliquer par la présence de mousse faible à l'interface. Ces circonstances se sont produites lorsque la perte de charge était inférieure à ∇P^* dans l'interface ; par conséquent, la mousse faible s'est formée. Toutes les conditions expérimentales étant identiques à l'exception des colonnes pré-génératrices, les valeurs des nombres capillaires et Bond et la taille des bulles peuvent expliquer ce phénomène.

La Fig. 9 montre les valeurs des nombres capillaires et de Bond pour différents systèmes de générateur de mousse et de colonne principale (les calculs ont été réalisés à l'état stationnaire). Puisque la valeur du nombre de Bond est la même et dépasse un (N_{Bo}=10,9), les forces capillaires sont faibles par rapport aux forces de gravité. Cependant, les valeurs du nombre capillaire dans la colonne principale, pour Q_t=2 mL/min, étaient respectivement de 94 et 79,9 pour la mousse générée dans le sable et les billes de verre de 1 mm. Il faut noter que la taille moyenne des bulles dans le générateur de mousse rempli de sable était 11 fois plus petite que celles fabriquées dans des billes de verre de 1 mm (si nous supposons que les

bulles avaient à peu près la même taille que les pores) (voir Table 1). Par conséquent, la mousse produite à l'aide d'un prégénérateur en sable était plus visqueuse, et nous pouvons confirmer que la variation de viscosité de la mousse dépend de la taille des bulles. De plus, plusieurs auteurs ont montré expérimentalement que la viscosité apparente de la mousse dépend fortement de la texture ou de la taille des bulles à l'échelle des pores (Hirasaki & Lawson, 1985; Falls, et al., 1988; Roof, 1970; Ma, et al., 2012; Ramadan, et al., 2003). Étant donné que la plupart des recherches effectuées concernaient des applications dans l'industrie pétrolière, où les tailles de pores sont beaucoup plus petites que dans les aquifères, la taille des bulles a été considérée comme étant à peu près égale à la taille des pores (en raison du grossissement des petites bulles liées à la diffusion de gaz). Cependant, il faut noter que le grossissement des bulles dans les aquifères nécessite beaucoup plus de temps en raison de la grande taille des pores.

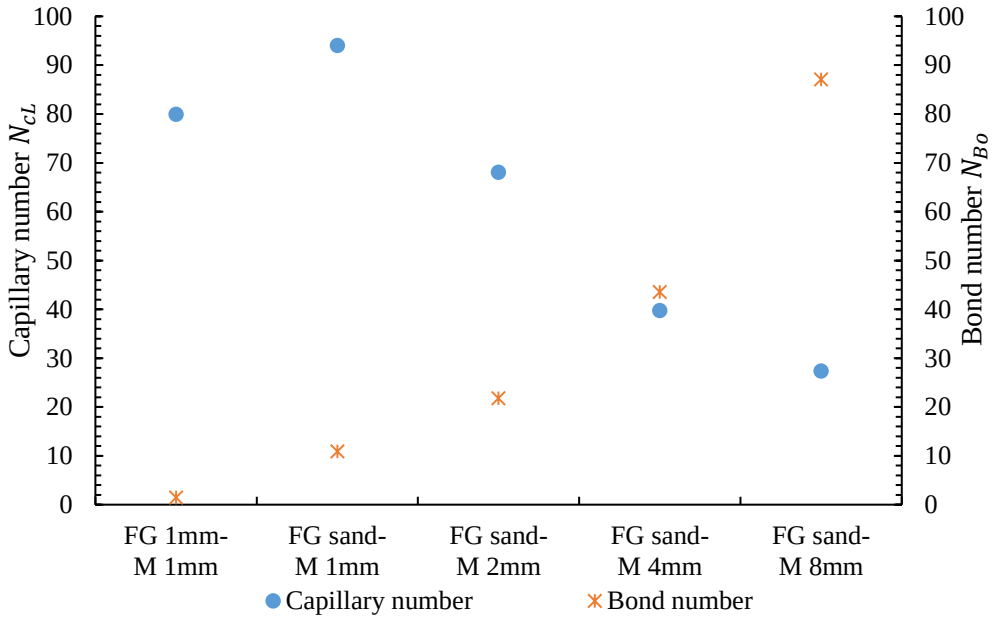

Fig. 9 Nombres capillaire et de Bond pour différents générateurs de mousse et différentes colonnes principales (f_g=85%, Q_t=2 mL/min)

De plus, après la première expérience de drainage, nous avons déterminé la saturation initiale (S_{wi}) de la solution de tensioactif pour chaque colonne poreuse (Table 4). S_w a augmenté avec la taille des grains. Étant donné que les forces de gravité étaient plus importantes avec les billes de verre de 4 et 8 mm (voir Fig. 9), l'effet du drainage par gravité augmentait la saturation en liquide des milieux poreux lorsque la taille des pores devenait plus grande. Nous avons également observé la dépendance de S_{wi} sur le générateur de mousse (taille des bulles) : S_{wi} augmentait avec la taille des bulles.

Table 4 Saturation initiale de la solution de surfactant après le premier drainage (f_g=85%, Q_t=2 mL/min)

Générateur de mousse	Colonne principale	S_{wi} (%)
Sable BR37	GB 1	2,82
	GB 2	2,99
	GB 4	4,10
	GB 8	5,58
Billes de verre : GB 1	GB 1	4,10

5.1.3.1. Influence de la qualité de la mousse sur le comportement d'écoulement de la mousse

Nous avons déterminé la valeur de la qualité de la mousse correspondant à la transition entre les régimes de faible qualité et de haute qualité, f_g^*, afin de sélectionner une qualité de mousse unique pour une étude plus approfondie de la rhéologie de ladite mousse.

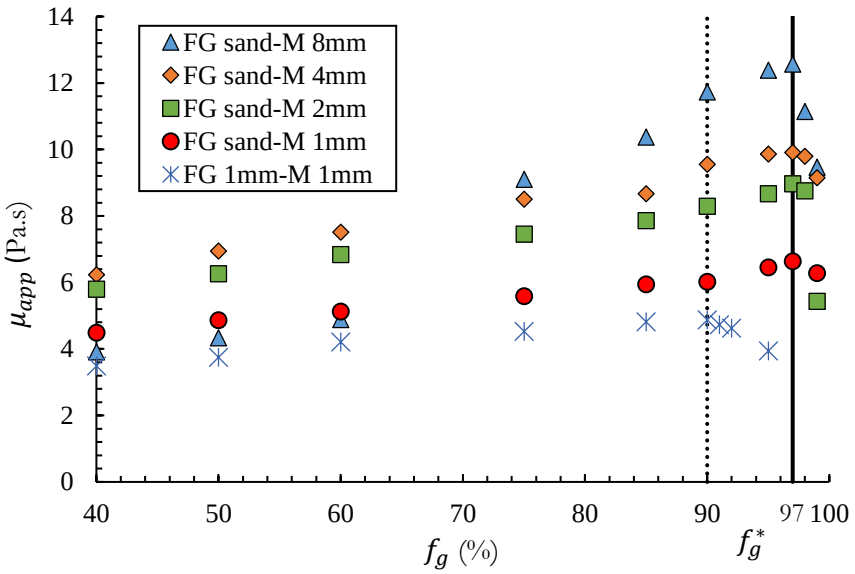

Fig. 10 Viscosité apparente de la mousse en fonction de la qualité de la mousse à débit total fixe (Q_t=2 mL/min)

La Fig. 10 montre l'évolution de la viscosité apparente de la mousse calculée en utilisant la loi de Darcy en fonction de la qualité de la mousse. Sur cette figure, les points colorés représentent les résultats de la mousse générée par le générateur de mousse rempli de sable, et les points en étoile sont le résultat de la mousse fabriquée à travers le générateur de billes de verre de 1 mm. Par comparaison des résultats pour la mousse générée par la colonne de sable, on voit que la viscosité apparente de la mousse augmente avec la taille du diamètre des éléments constitutifs de l'empilement. Les lignes verticales repèrent la qualité de la mousse correspondant à la transition, f_g^*, qui est la limite entre les régimes de basse qualité et de haute

qualité. La qualité de la mousse de transition (f_g^*) est de 97% pour toutes les billes de verre et est indépendante de la granulométrie (et de la perméabilité du milieu poreux). La figure met en lumière que la viscosité apparente des mousses augmente avec la qualité de la mousse jusqu'à f_g^*. Osei-Bonsu et al. (2016) ont également constaté une augmentation de la viscosité apparente de la mousse avec la qualité de la mousse à travers une cellule Hele-Shaw. Cependant, ils n'ont pas remarqué une transition f_g^* même lorsque f_g=99%. Alvarez et al. (2001) ont montré une valeur f_g^* élevée (97%) pour une mousse produite à partir de laine de bronze dans un milieu de grande perméabilité (colonne de sable, perméabilité de 3,1 Darcy). Ils ont démontré que le f_g^* augmente avec la perméabilité en supposant que la taille de la bulle est fixée au régime de basse qualité (Rossen & Wang, 1999). Des pressions capillaires plus faibles dans des pores plus grands accompagnaient l'idée de valeurs élevées de f_g^* (ce qui explique un f_g^* beaucoup plus élevé avec le prégénérateur rempli de sable).

Si l'on considère que la taille des bulles peut être fixée dans un régime de faible qualité, les résultats sont cohérents avec le modèle de Rossen et Wang (1999), où la viscosité apparente ne dépend que de la structure du milieu poreux et de la tension de surface. Cependant, nous admettons que la taille des bulles peut être modifiée du fait de l'effet de diffusion à de faibles débits. De plus, la diminution de la viscosité apparente pour une qualité de mousse inférieure à 75% pour 8 mm GB peut être expliquée par le passage de la mousse à l'état de liquide pétillant (Ramadan, et al., 2003).

Au contraire, la mousse générée à partir des billes de 1 mm, et injectée dans le même milieu poreux, a une valeur de qualité de mousse correspondant à la transition faible/forte inférieure (90%), ce qui pourrait s'expliquer par la différence de taille de bulles des mousses pré-générées. Comme mentionné précédemment, la taille moyenne des bulles générées dans le sable est inférieure à la taille des pores des billes de verre. Par conséquent, si la taille de pore équivalente est plus grande que la taille de bulle équivalente, la mousse peut se comporter comme une mousse en milieu libre (hors milieu poreux). Ces circonstances sont proches de l'écoulement de la mousse dans les fractures, où le f_g^* pour la pression capillaire limite était estimée à une valeur aussi élevée que 99,95% (Pancharoen, et al., 2012). Par conséquent, nous pouvons conclure que f_g^* dépend étroitement de la taille des bulles (et donc de la structure du générateur de mousse).

5.1.3.2. Rhéologie de la mousse en milieu poreux (échelle de Darcy)

La Fig. 11 montre les résultats expérimentaux en termes de gradient de pression le long de la colonne poreuse remplie de billes de verre de 1 mm en fonction de la vitesse d'écoulement de la mousse, pour f_g= 0%, 85% et 95%. Un comportement non linéaire a été observé avec une augmentation dugradient de pression avec la qualité de la mousse. Nous n'avons pas pu obtenir des valeurs de ∇P supérieures correspondant aux débits d'injection de mousse de 3-4 mL/m en raison de la limite de pression maximale de notre dispositif expérimental pour des mousses de qualité f_g=60% et 85%.

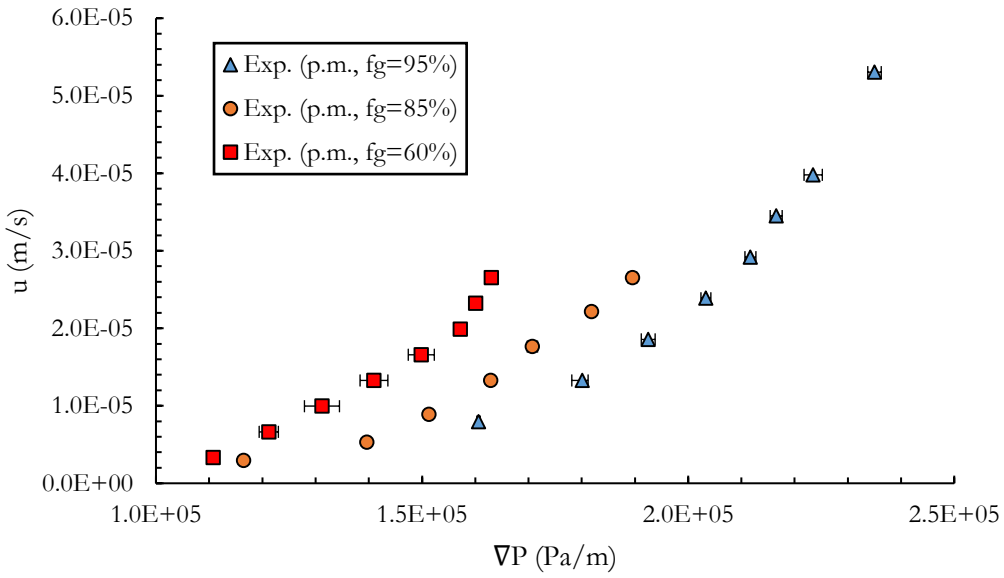

Fig. 11 Gradient de pression le long de la colonne remplie de bille de 1mm en fonction de la vitesse superficielle, pour f_g=60%, 85%, 95%

Les variations de viscosité apparentes en fonction du taux de cisaillement équivalent (Eq. (7)) ont été analysées afin d'étudier la rhéologie de la mousse. La viscosité apparente de la mousse en fonction du taux de cisaillement équivalent (Eq. (8)) est présenté en Fig. 12 ; les points représentent des données expérimentales et les lignes correspondent aux courbes d'ajustement par le modèle H-B-P. Les résultats montrent que les mousses dans les milieux poreux se comportent comme des fluides à seuil non newtoniens, et la viscosité apparente de la mousse augmente avec la qualité de la mousse. Par conséquent, nous avons constaté que l'écoulement de mousse dans les milieux poreux se comportait comme une mousse hors milieu poreux si les bulles étaient plus petites que la taille des pores et pour un régime d'écoulement de mousse de faible qualité. De plus, nous avons observé que les valeurs de seuil de contrainte pour les mousses dans des milieux poreux étaient environ deux fois plus élevées que celles trouvées pour les mousses en milieu libre (voir Table 3). De plus, l'indice de fluidité n augmentait lorsque les fractions de gaz diminuaient et avait une valeur de 0,65 pour f_g=60%. Dans la littérature, la valeur de n>0.5 a été trouvée pour les mousses hors milieu poreux de faible qualité (f_g<75%) (Otsubo & Prud'homme, 1994; Otsubo & Prud'homme, 1994; Larmignat, et al., 2008). Nos résultats sont donc cohérents avec ces études. Cependant, il faut noter que l'indice de loi de puissance n était d'environ 0,5 pour toutes les mousses en milieu libre. Ceci peut être une conséquence de la rugosité de surface puisque notre milieu poreux était constitué d'un empilement de billes de verre, et les parois des pores sont lisses par rapport à la géométrie à surface dentelée du rhéomètre. De plus, cela peut être le résultat du temps de préparation de l'échantillon pour la mousse de qualité f_g=60% mentionnée à la section 5.1.2. Par conséquent, les mousses peuvent être classées en deux groupes en fonction de la qualité de la mousse et

des valeurs de l'indice de puissance : nous avons observé n≈0.5 pour f_g=85% et 95% et n>0.5 pour f_g=60%.

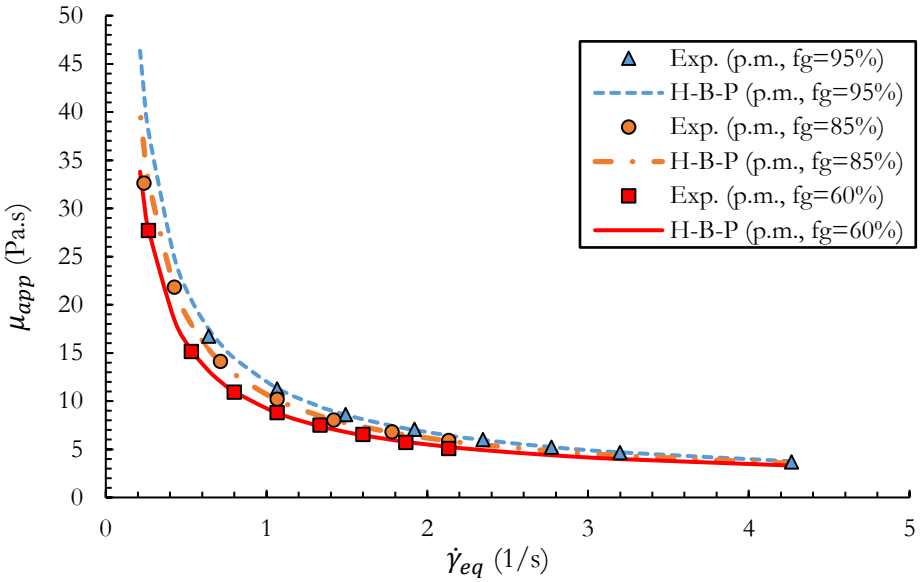

Fig. 12 Viscosité apparente en fonction du taux de cisaillement équivalent : f_g=60%, 85% et 95%

Table 5 Paramètres de calibration du modèle H-B-P

f_g (%)	60%	85%	95%
n (-)	0,65	0,53	0,49
τ_0 (Pa)	6,05	6,86	8,06
a (Pa.s^n)	3,15	3,88	3,90
m (s)	10000	10000	10000
R^2	0,99	0,99	0,99

5.1.4. Rhéologie de la mousse dans les tubes capillaires : effet du diamètre du tube, du matériau et de la texture de la mousse

Afin d'étudier la rhéologie de la mousse dans les tubes capillaires, nous avons tracé la viscosité apparente en fonction du taux de cisaillement équivalent, à f_g= 85% (fixe). La variation de la viscosité apparente de la mousse dans des tubes capillaires FEP avec différents diamètres intérieurs en fonction du taux de cisaillement est présentée sur la Fig. 13. Les résultats expérimentaux montrent le comportement non newtonien de la mousse lors de son écoulement à travers un tube capillaire ; les résultats ont été comparés (après calage) avec le modèle Herschel-Bulkley (Eq. (10)). Sur les figures Fig. 13, Fig. 14, Fig. 15, Fig. 17, les points colorés et les lignes correspondent respectivement aux données expérimentales et aux

courbes ajustées en utilisant le modèle de Herschel-Bulkley. Les paramètres d'ajustement pour chaque tube avec le coefficient de détermination sont présentés dans le Table 6.

Les mêmes expériences dans des conditions identiques ont également été réalisées dans tous les tubes capillaires en PTFE. Les résultats avec les courbes d'ajustement sont montrés sur la Fig. 14 ; les paramètres d'ajustement sont présentés dans le Table 6. Les deux figures montrent la dispersion des résultats par rapport aux lignes d'ajustement H-B, cette dispersion augmente avec la réduction du diamètre du tube. Lorsque nous examinons le tube de plus petit diamètre, la taille des bulles devient plus significative par rapport au diamètre du tube puisque le nombre de bulles diminue par section des tubes. Il en résulte une instabilité de la mesure de la perte de charge due aux différences de pression entre les phases gazeuse et liquide.

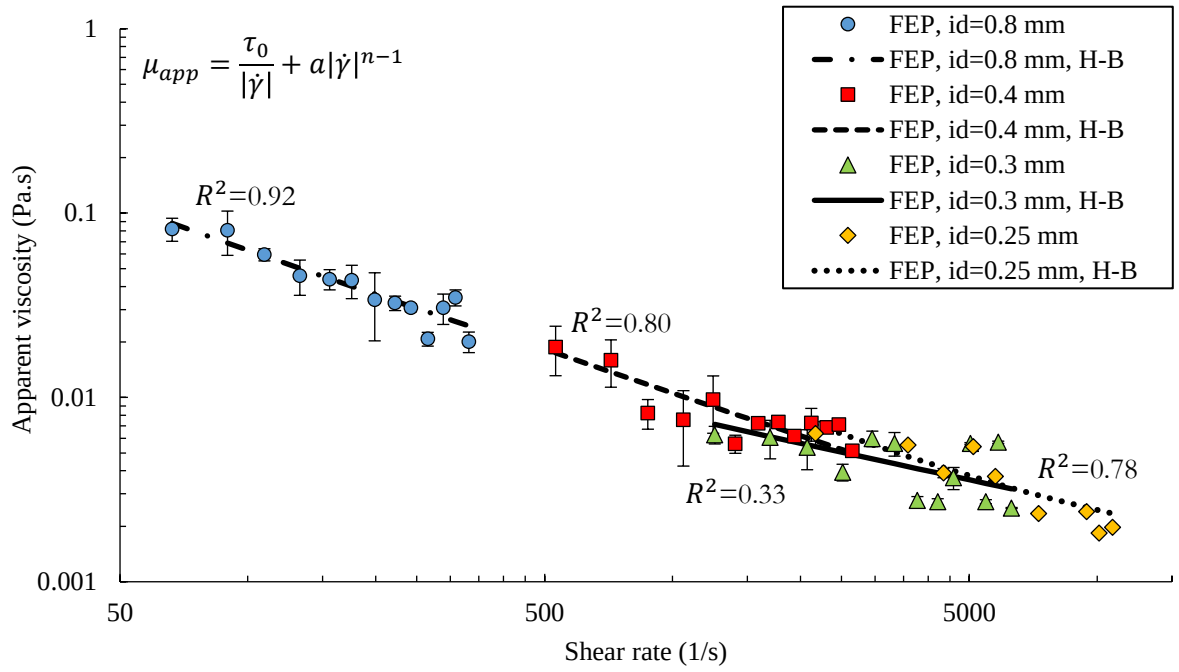

Fig. 13 Viscosité apparente de la mousse en fonction du taux de cisaillement dans les tubes FEP avec un id=0,25 ; 0,3 ; 0,4 ; et 0,8 mm (f_g=85%)

Comme le montre le Table 6, nous avons observé l'impact du diamètre du tube sur la rhéologie de la mousse. Le comportement rhéofluidifiant de la mousse a été trouvé pour tous les tubes. Dans les tubes en PTFE, nous avons remarqué une augmentation des indices de fluidité n avec la taille du diamètre du tube. Cependant, pour les tubes FEP, nous avons trouvé un effet inverse, où les valeurs de n augmentaient avec une réduction du diamètre du tube. La mousse se comportait quasiment comme un fluide de Bingham pour les tubes FEP avec un diamètre intérieur de 0,25 et 0,3 mm, dont les indices de fluidité étaient respectivement de 0,95 et 0,99. De plus, les valeurs de la contrainte seuil augmentaient avec la diminution

du diamètre des tubes FEP. Néanmoins, les valeurs de contrainte seuil obtenues par calage étaient presque nulles dans tous les tubes en PTFE, montrant ainsi l'absence de seuil de contrainte dans ces tubes.

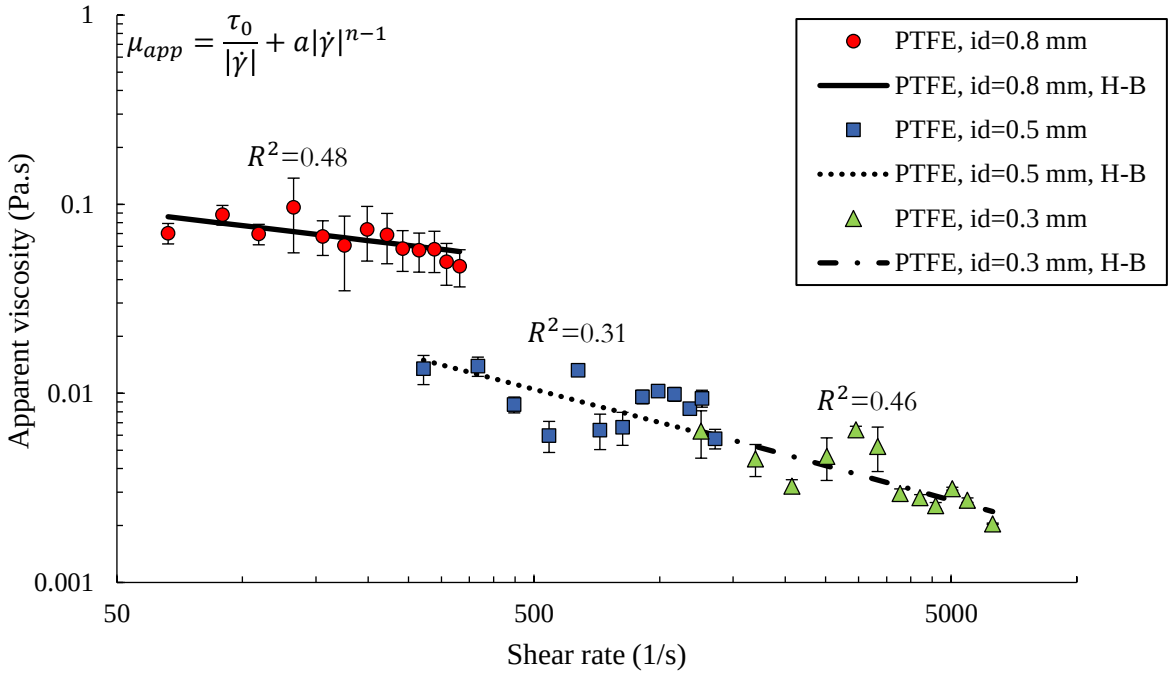

Fig. 14 Viscosité apparente de la mousse en fonction du taux de cisaillement dans les tubes PTFE avec un id=0,3 ; 0,5 ; et 0,8 mm (f_g=85%)

Sur la Fig. 15, nous avons tracé la viscosité apparente de la mousse en fonction du taux de cisaillement pour un tube de diamètre intérieur de 0,8 mm ; les paramètres d'ajustement avec le coefficient de détermination sont présentés dans le Table 6. Nous pouvons voir que la mousse dans le tube de verre se comporte également comme un fluide rhéofluidifiant. Cependant, les résultats ne suivent pas le modèle de Herschel-Bulkley entre des valeurs de taux de cisaillement de 66,3 1/s et 155,8 1/s.

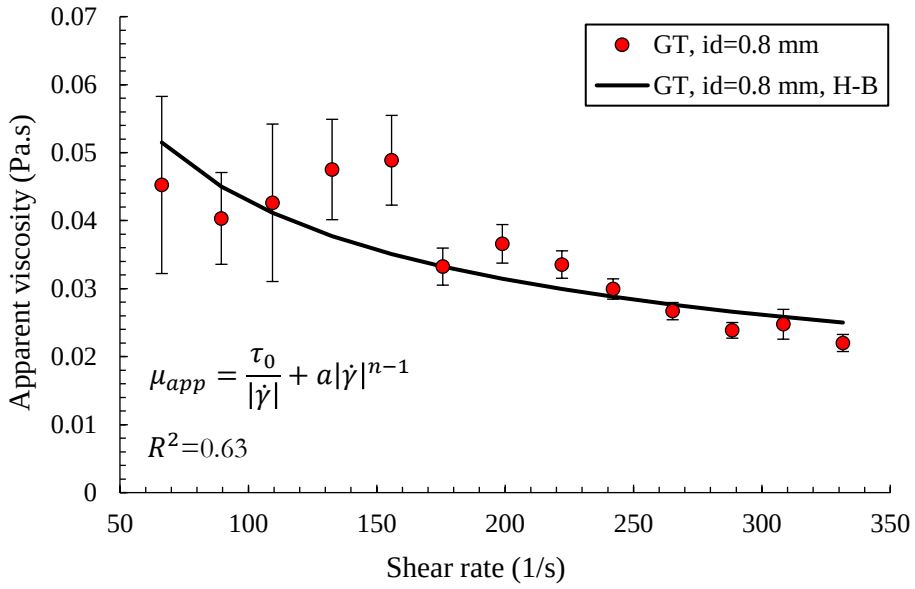

Fig. 15 Viscosité apparente de la mousse v. taux de cisaillement dans le tube de verre avec un id=0.8 mm (f_g=85%)

Pour de faibles taux de cisaillement (c'est-à-dire faibles débits) jusqu'à 155 1/s, les barres d'erreur des valeurs de viscosité apparente sont relativement élevées par rapport aux celles obtenues à des taux de cisaillement plus élevés. Ce phénomène peut s'expliquer par le passage de la formation de mousse d'un état faible à un état fort dans la colonne génératrice, ceci se produit lorsque le débit total augmente. Au cours de ce processus, la texture de la mousse passe de grossière à fine, réduisant ainsi considérablement la mobilité du gaz. Ainsi, l'écoulement de mousse à de faibles taux de cisaillement présente un état de faiblesse, ceci génère des oscillations plus élevées des mesures de chute de pression (i.e. viscosité apparente de la mousse).

La Fig. 16 permet de mieux appréhender ce phénomène ; elle regroupe les photographies d'écoulement de mousse à l'état stationnaire dans un tube en verre de 0,8 mm pour des débits de l'ordre de 0,20 à 1 mL/min et une qualité de mousse de 85%. D'après les images, on voit que les barres d'erreur élevées de la viscosité apparente dépendent du changement de texture de la mousse en fonction des débits. Notamment, à de faibles débits de 0,20 mL/min à 0,47 mL/min, nous avons observé des gouttelettes de gaz libre qui sont responsables de l'importante fluctuation des mesures de baisse de pression. Comme mentionné ci-dessus, ce phénomène est lié à la présence de mousse faible, qui se produit en raison de l'excès du taux de coalescence des bulles par rapport à la création de lamelles (c'est-à-dire de bulles) dans le générateur de mousse (Sheng, 2013).

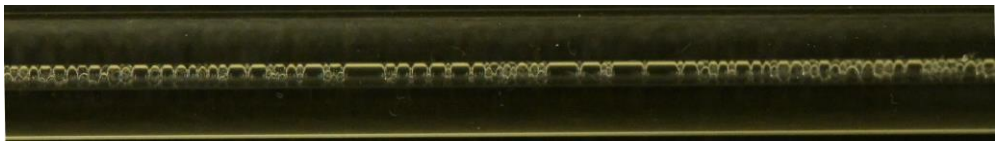

0.20 mL/min (66.3 1/s)

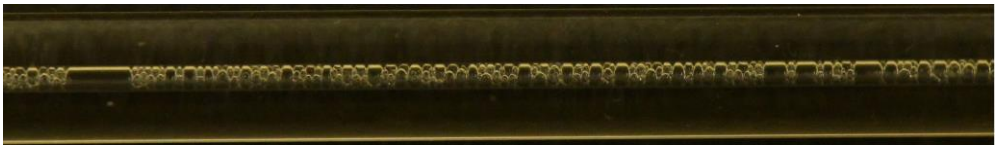

0.27 mL/min (89.5 1/s)

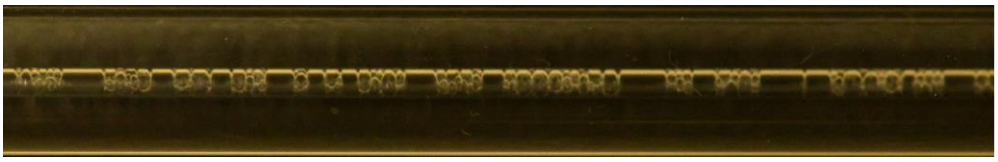

0.33 mL/min (109.4 1/s)

0.40 mL/min (132.6 1/s)

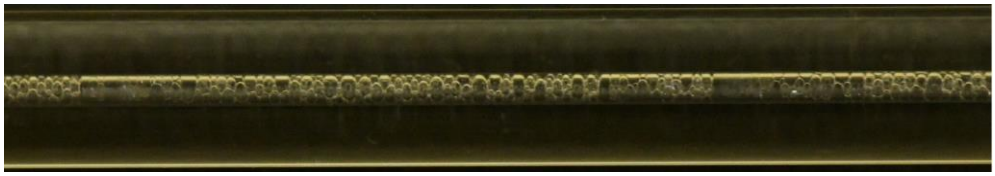

0.47 mL/min (155.8 1/s)

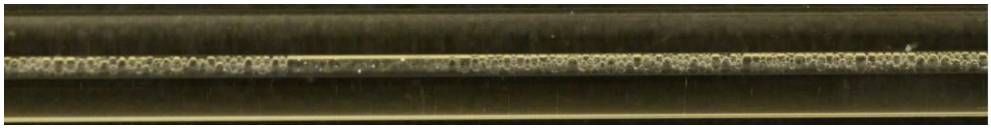

0.53 mL/min (175.7 1/s)

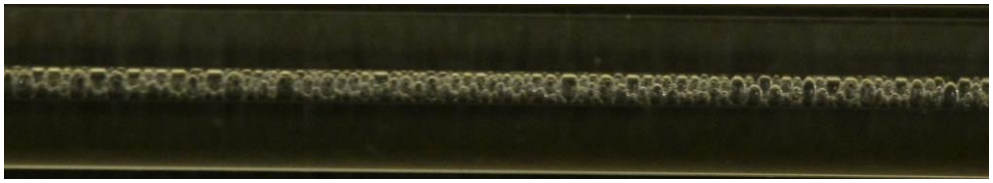

0.60 mL/min (198.9 1/s)

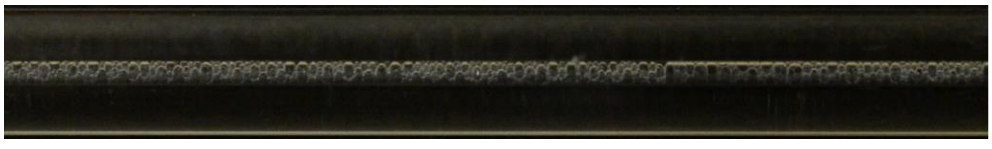

0.67 mL/min (222.1 1/s)

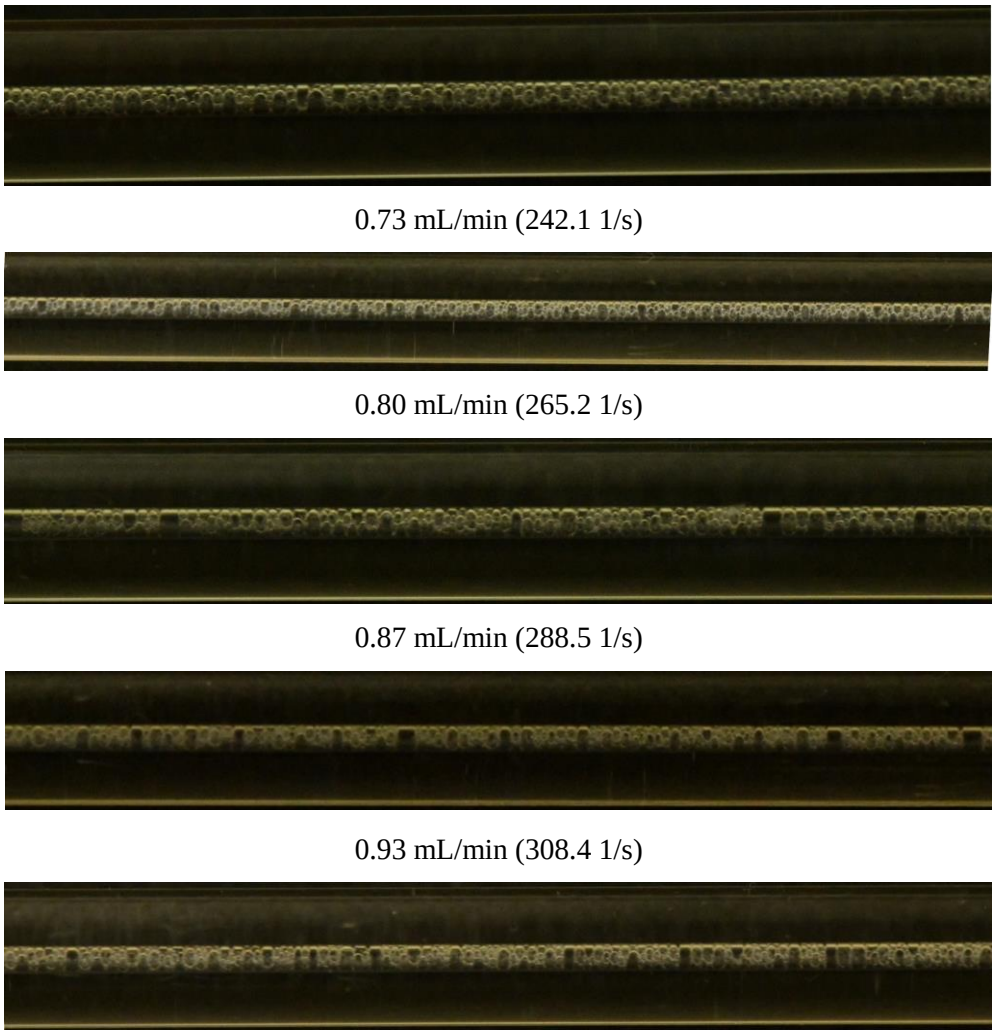

Fig. 16 Images de mousse dans des tubes en verre de 0,8 mm à différents débits (f_g=85%)

Pour comparer les résultats de la viscosité apparente de la mousse dans des tubes constitués de différents matériaux, nous avons tracé les résultats de la viscosité apparente de la mousse obtenue à partir de tubes FEP, PTFE et GT de même diamètre sur la Fig. 17. A première vue, nous avons observé que la viscosité apparente de la mousse dans les systèmes hydrophobes (c'est-à-dire dans les tubes en PTFE et FEP) est plus élevée que dans le tube en verre, qui est un matériau hydrophile.

Selon les paramètres d'ajustement présentés dans le Table 6, la mousse dans les tubes PTFE et GT (tube de verre) se comportait comme un fluide à une loi de puissance tandis que dans le tube FEP, la mousse s'écoulait comme un fluide à seuil. La mousse générée étant identique, l'écart ne peut être attribué qu'au matériau utilisé pour chaque tube. Cependant, selon les images présentées sur la Fig. 16, nous avons observé que la texture de la mousse est grossière aux faibles débits de 0,20 mL/min (66,3 1/s) à 0,47 mL/min (155,8 1/s). Si l'on ne prend pas en compte les données de ces débits, les résultats du FEP et des tubes en verre se chevauchent presque. Néanmoins, même à des taux de cisaillement élevés, supérieurs à

155,8 1/s, on observe des différences de viscosité apparente de la même mousse dans les tubes PTFE et FEP (que les deux tubes soient en matériaux hydrophobes ou non).

Enfin, nous avons constaté que le comportement de la mousse dépend du type de matériau (ceci peut être lié à la rugosité de la surface ou sa mouillabilité).

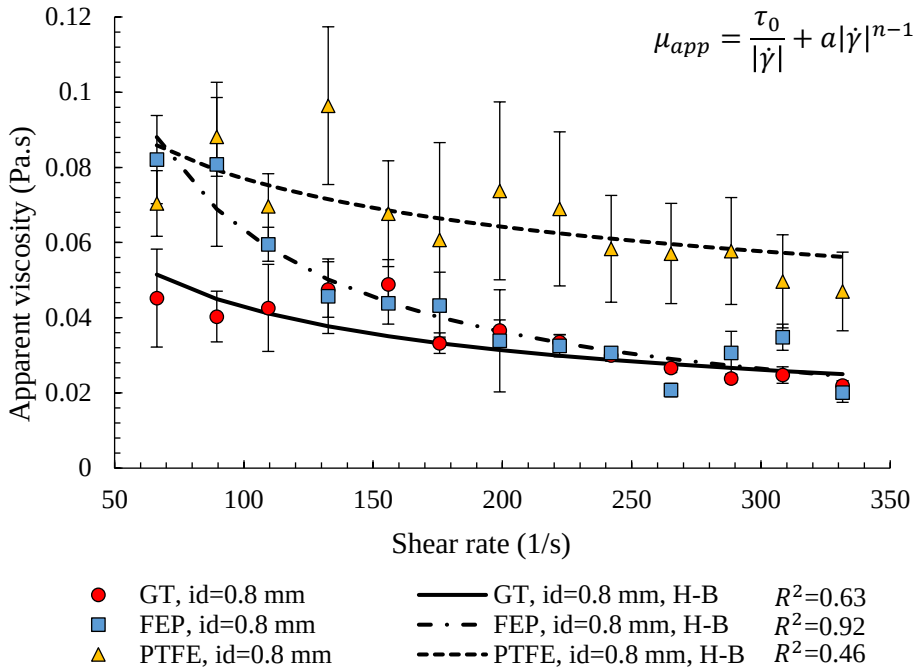

Fig. 17 Comparaison des viscosités apparentes de la mousse pour les tubes FEP, PTFE et GT avec un id = 0,8 mm dans la même plage de taux de cisaillement (f_g=85%)

Table 6 Paramètres de calibration du modèle H-B-P pour des tubes en FEP, PTFE et GT

Tube types	**FEP**				**PTFE**			**GT**
id (mm)	0,25	0,3	0,4	0,8	0,3	0,5	0,8	0,8
$\boldsymbol{n}$ (-)	0,95	0,99	0,36	0,36	0,39	0,42	0,74	0,55
$\boldsymbol{\tau_0}$ (Pa)	12,69	4,49	4,12	2,95	0,01	0	0	0
$\boldsymbol{a}$ (Pa.s^n)	0,01	0,01	0,54	0,64	0,48	0,39	0,26	0,34
R^2	0,78	0,33	0,80	0,92	0,48	0,31	0,46	0,63

5.1.4.1. Cohérence du comportement de la mousse dans les tubes capillaires avec la rhéologie de la mousse en milieu libre (« bulk foam » en angalais)

Dans cette section, nous avons utilisé l'expression analytique du modèle de Herschel-Bulkley (Eq. (11)) pour l'écoulement à travers les tubes de section circulaire. Les caractéristiques rhéologiques mesurées de la mousse en milieu libre de notre expérience précédente (Omirbekov, et al., 2019) sont utilisées comme données d'entrée de ce modèle pour étudier la cohérence avec le comportement de la mousse dans les

tubes capillaires. Les paramètres d'ajustement H-B suivants de la mousse en milieu libre (avec une qualité de mousse de f_g=85%) sont utilisés dans l'expression analytique : n=0,52, τ_0=2,87 et a=0,76 (Table 3).

Sur la Fig. 18, nous avons tracé le débit total en fonction de la perte de charge par unité de longueur d'écoulement de mousse à travers les tubes GT, FEP, PTFE de 0,8 mm et la solution analytique du modèle H-B (en utilisant la rhéologie de la mousse en milieu libre). Sur cette figure, les données expérimentales et les résultats de la solution analytique correspondent respectivement aux points colorés et à la ligne en pointillés. Ici, on observe que la mobilité de la mousse dans les tubes capillaires est supérieure à celle simulée en utilisant la rhéologie de la mousse en milieu libre. Cela peut être une conséquence de la vitesse de glissement sur la paroi dans les tubes capillaires puisque la rhéologie de la mousse en milieu libre a été mesurée à travers la géométrie à plaques parallèles dentelées pour éliminer la vitesse de glissement sur la paroi.

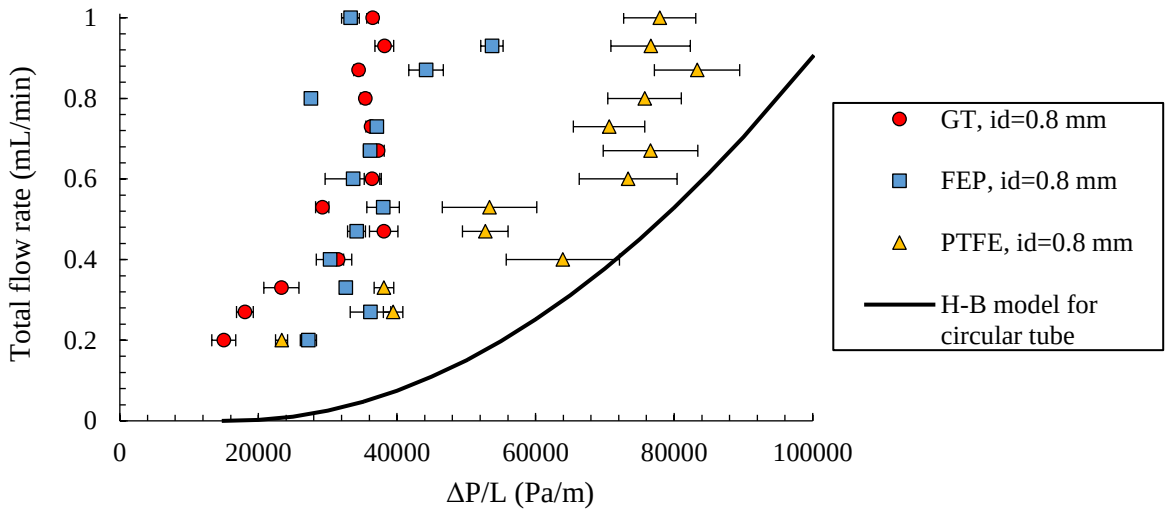

Fig. 18 Débit total en fonction de la perte de charge par unité de longueur pour les tubes en GT, FEP, PTFE avec un id de 0,8 mm et comparaison avec la solution analytique pour le fluide à seuil de contrainte (f_g=85%)

Puisque les diamètres des tubes sont les mêmes, seules la rugosité de surface et la mouillabilité de la mousse peuvent affecter la condition aux limites de la surface (c'est-à-dire le glissement sur la paroi).

Le verre est un matériau hydrophile dont l'angle de contact statique est de 47-58 ° (Mitra, et al., 2016), ce qui est donc inférieur à 90°. Selon Lee et al. (2008), les angles de contact avant et arrière de la goutte d'eau sur les surfaces en PTFE sont respectivement de 122° et 94°. Sur les surfaces en FEP, les valeurs des angles de contact d'avancée et de recul sont quasiment identiques et correspondent respectivement à 119° et 98°. Étant donné que la solution de surfactant est capable de changer l'angle de contact (Singh & Mohanty, 2016), l'angle de contact entre la solution de surfactant et le PTFE (ou FEP) peut être modifié

(Chaudhuri & Paria, 2009; Henrich, et al., 2016). Cependant, sur la Fig. 18, nous pouvons voir que les résultats des tubes en FEP et en PTFE sont différents et que les résultats du tube FEP sont proches des résultats du tube en verre lisse. La seule raison de cette différence peut être l'effet de la rugosité de surface. Selon Lee et al. (2008), la rugosité superficielle moyenne quadratique (R_{rms}) des matériaux PTFE et FEP correspond respectivement à 58,6 et 10,5 (la R_{rms} a été mesurée par un microscope à force atomique sur des zones balayées de 10×10 μm^2). On voit que la rugosité des surfaces en PTFE est environ 6 fois supérieure à celle en FEP. Aussi, nous pouvons supposer que la rugosité de paroi du tube PTFE supprime la vitesse de glissement sur la paroi, mais ne l'élimine pas complètement par rapport aux résultats de la rhéologie de la mousse en milieu libre. En conséquence, le débit total doit être présenté comme suit :

$$Q_t = Q_f + Q_s \tag{22}$$

dans laquelle Q_f (mL/min) et Q_s (mL/min) sont le débit volumétrique dû respectivement à la fluidité et au glissement. A partir de l'équation précédente, Q_s a été approximativement estimé à 0,19 mL/min pour le tube en PTFE de 0,8 mm de diamètre. Cependant, la vitesse de glissement sur la paroi doit être évaluée avec beaucoup de soin, en fonction du diamètre du tube (Jastrzebski, 1967). Par conséquent, la vitesse de glissement sur la paroi sera calculée pour tous les tubes (une fois que les expériences sur des tubes en verre de plus petit diamètre seront terminées).

Afin de comparer et de combiner nos résultats, nous avons rassemblé les résultats de la rhéologie de la mousse en milieu libre (acquis à l'aide d'un rhéomètre), ainsi que les résultats de l'écoulement de la mousse à travers des milieux poreux hautement perméables (Omirbekov, et al., 2019). La Fig. 19 présente la viscosité apparente de la mousse mesurée en fonction du taux de cisaillement dans les tubes capillaires en GT, FEP et PTFE, en comparaison avec les résultats de l'écoulement de mousse dans la colonne poreuse et le comportement de la mousse en milieu libre avec le rhéomètre. Toutes les mousses étudiées ont été pré-générées à travers le même type de sable et avec une qualité de mousse f_g= 85%. Les résultats expérimentaux de la colonne de billes de verre et de la mousse en milieu libre (mesurés à l'aide du rhéomètre) ont été tirés de section 5.1.2. Tous les résultats ont été ajustés en utilisant le modèle Herschel-Bulkley ; les paramètres d'ajustement (avec le coefficient de détermination) sont présentés à la Fig. 19.

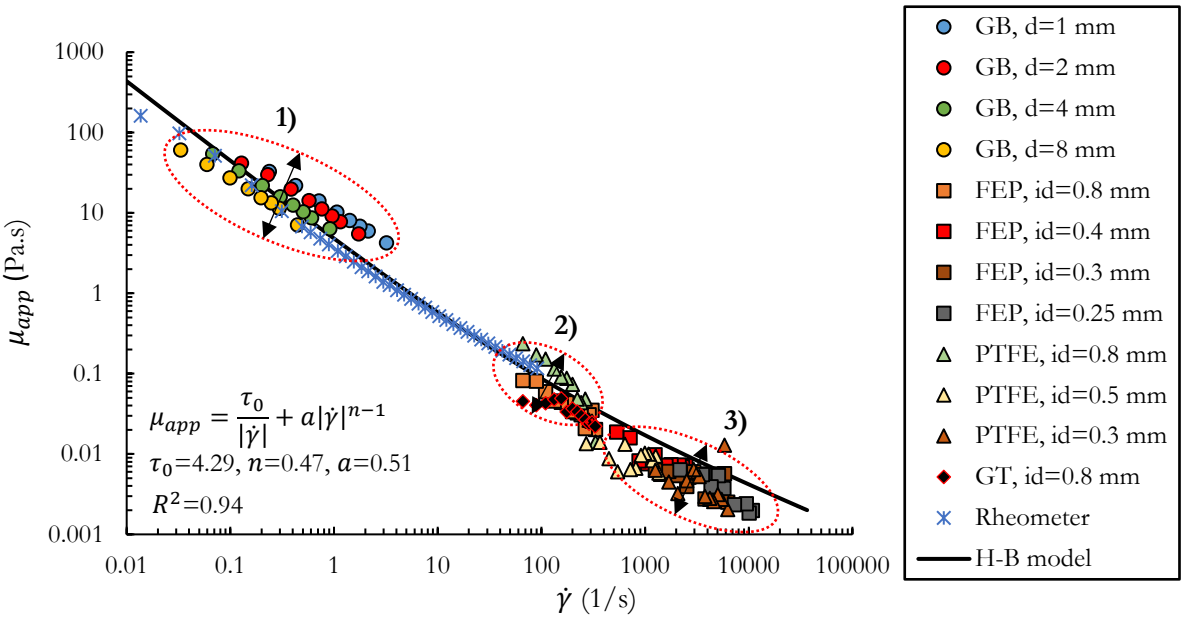

Fig. 19 Viscosité apparente de la mousse de f_g=85% en fonction du taux de cisaillement par différentes méthodes : dans des empilements de billes de verre (GB id = 1, 2, 4 et 8 mm), à l'aide d'un rhéomètre (géométrie à plaques parallèles dentelées), et dans des tubes capillaires (FEP, id = 0,25, 0,3, 0,4 et 0,8 mm; PTFE, id = 0,3, 0,5 et 0,8 mm)

Ces résultats montrent globalement que la mousse pré-générée dans la présente étude peut être considérée comme une mousse en milieu libre si les bulles sont beaucoup plus petites que les pores dans le cas des colonnes poreuses ou bien plus petites que le diamètre du tube pour les écoulements dans les tubes capillaires. Cependant, les inférences suivantes peuvent être tirées de chaque zone de la Fig. 19 (ces interférences sont numérotées sur ladite figure).

1) La mousse en écoulement dans un milieu poreux, c'est-à-dire dans un milieu confiné, se comporte différemment de la mousse en milieu libre dans les conditions ambiantes. La viscosité apparente de la mousse augmente avec la diminution de la taille des grains. Ceci peut être un effet de compressibilité qui est plus important dans les milieux poreux moins perméables. Par conséquent, les résultats obtenus pour des écoulements dans des empilements de billes de 4 mm et de 8 mm semblent cohérents avec les résultats du rhéomètre.

2) L'effet du matériau du tube sur la viscosité apparente de la mousse est mis en exergue. Cela peut être lié à l'impact de la vitesse de glissement sur la paroi, qui est donc liée à la rugosité de surface et à la mouillabilité. Par conséquent, la vitesse de glissement sur la paroi peut entraîner une modification de la mobilité de l'écoulement de la mousse dans les tubes. Cependant, comme cela a été mentionné dans la section précédente, il doit être à nouveau étudié avec beaucoup de soin.

3) Nous avons remarqué une dispersion des résultats de l'écoulement de la mousse dans des tubes de plus petit diamètre, en particulier pour des taux de cisaillement très élevés. Cela peut également être

dû à la diminution du rayon du tube, donc à une diminution du rapport taille de pore sur la taille des bulles. L'écoulement de mousse à des débits élevés et dans des tubes de plus petit diamètre doit être considéré avec une attention particulière.

5.2. Etude théorique : changement d'échelle de l'écoulement de mousse en milieu poreux

5.2.1. Influence de la qualité de la mousse

Le résultat de l'étude numérique sur l'écoulement de la mousse dans la cellule unitaire périodique 2D SPC est comparé aux résultats expérimentaux en termes de relation vitesse vs gradient de pression sur la Fig. 20, pour différentes qualités de mousse. La Fig. 20 a été tracée sur une échelle semi-logarithmique afin de comparer les résultats du modèle et les données expérimentales. Les lignes en pointillés représentent les résultats numériques, dans lesquels la taille du cylindre solide (la porosité de la cellule unitaire) a été définie afin d'ajuster les données expérimentales en termes de perméabilité (K=8.3×10^{-10} m^2). Les points colorés correspondent aux résultats expérimentaux dans un empilement de billes de verre de 1 mm. Ainsi, l'écoulement de mousse avec des valeurs de qualité de 60, 85 et 95% a été examiné afin d'étudier l'influence de la qualité de la mousse sur le comportement d'écoulement de la mousse. Concernant les résultats expérimentaux, on observe que la viscosité d'écoulement de la mousse dans les milieux poreux augmente avec f_g. Cependant, les résultats de l'étude numérique montrent une mobilité de la mousse beaucoup plus élevée que pour les résultats expérimentaux (même à des gradients de pression plus faibles). Néanmoins, la tendance globale des courbes et le comportement en termes de f_g sont relativement similaires à ceux des résultats expérimentaux.

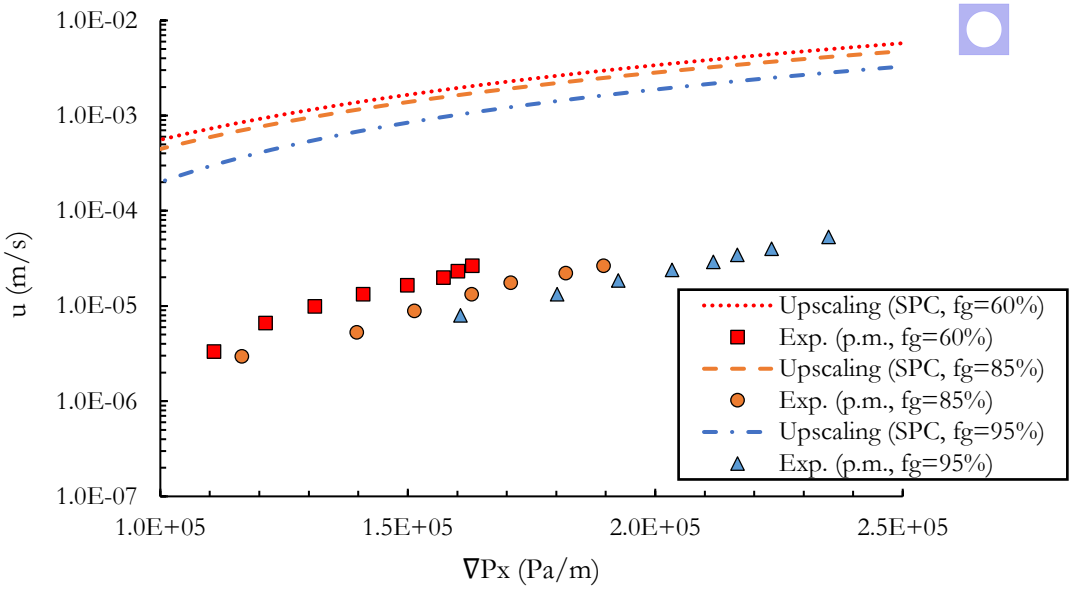

Fig. 20 Evaluation de la vitesse superficielle en fonction du gradient de pression macroscopique en géométrie SPC périodique 2D, pour différentes qualités de mousse (f_g = 60, 85 et 95%)

5.2.2. Effet de la géométrie des milieux poreux

La Fig. 21 présente la vitesse superficielle de la mousse en fonction du gradient de pression dans différentes géométries 2D et 3D pour f_g=85%. Les lignes en pointillés correspondent aux résultats numériques où la géométrie de la cellule unitaire a été ajustée pour correspondre à la valeur K=8.3×10^{-10} m^2 dans le cas newtonien, et les points colorés représentent les résultats expérimentaux correspondants au garnissage avec les billes de verre pour f_g=85%.

Comme le montre la Fig. 21, l'écoulement est non linéaire et dépend de la géométrie du milieu poreux, qui joue un rôle crucial dans l'écoulement des fluides à seuil. De plus, les flux dans les géométries 2D-SPC et 2D-SPS sont, d'une part, proches les uns des autres mais, d'autre part, diffèrents des résultats des autres cellules unitaires. De plus, les résultats pour les cellules unitaires 2D plus complexes CPC et CPS sont très proches de ceux des cellules unitaires 3D SCP et BCP. Étant donné que les résultats de changement d'échelle ont été tracés sur l'échelle semi-logarithmique, la petite différence entre les résultats n'a pas été explicitement visible. La porosité des cellules 2D-SPC et 2D-CPS est respectivement égale à 0,49 et 0,63, ce qui est supérieur à la porosité des autres cellules unitaires où les valeurs sont proches de 0,4. Par conséquent, nous concluons que le comportement de la mousse dépend de la structure du support poreux. Les résultats pour les géométries 2D et 3D complexes sont plus proches des données expérimentales que les géométries 2D simples. Les vitesses superficielles de mousse prédites sont cependant encore de quelques ordres de grandeur plus élevées que les données expérimentales.

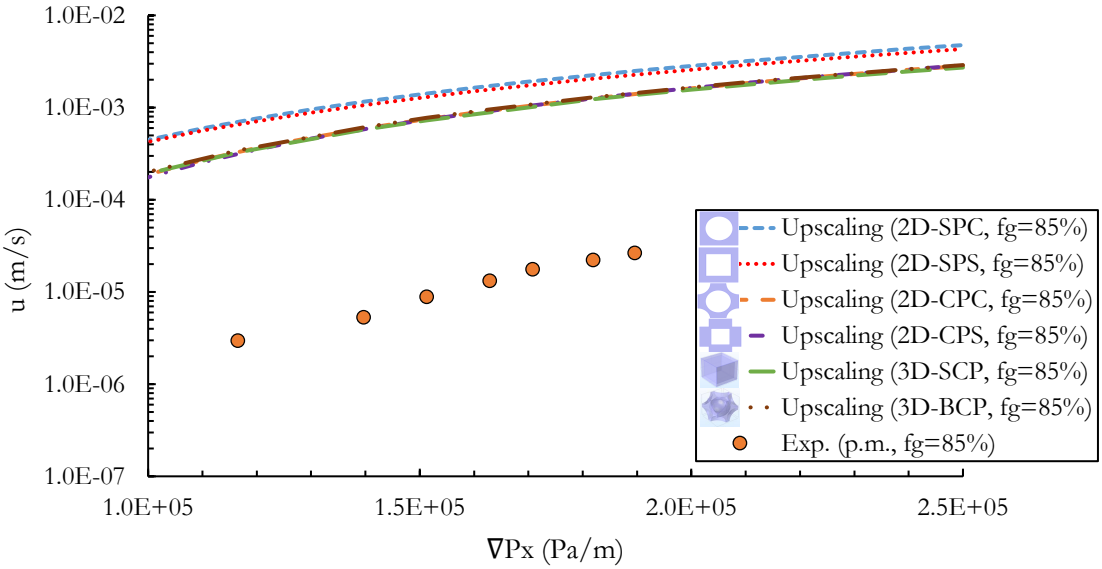

Fig. 21 Gradient de pression macroscopique par rapport à la vitesse superficielle de l'écoulement de la mousse dans les cellules unitaires 2D SPC, SPS, CPC, CPS et 3D SCP, BCP (f_g=85%)

Cet écart peut être attribué aux effets de compressibilité et de piégeage de gaz, qui doivent être pris en compte lors de l'étude de l'écoulement de la mousse en milieu poreux.

Nous avons calculé le nombre capillaire N_{ca} en utilisant l'équation suivante pour estimer l'effet de piégeage dans les expériences d'injection de mousse (Satter & Iqbal, 2015),

$$N_{ca} = \frac{K\nabla P}{\gamma} \tag{23}$$

où γ=0.036 (N/m) est la tension interfaciale gaz-liquide. Par conséquent, le nombre capillaire en fonction du gradient de pression peut s'écrire $N_{ca} = 2.31 \times 10^{-8}\nabla P$. La valeur minimale de N_{ca} est alors de $2{,}55\times10^{-3}$ ce qui correspond à notre gradient de pression minimum mesuré (110782 Pa/m) auquel la qualité de la mousse était de 60%. Ce nombre capillaire est même supérieur au nombre capillaire critique de 10^{-5}, au-dessus duquel les forces capillaires deviennent négligeables selon plusieurs études (Chatzis & Morrow, 1984; Ding & Kantzas, 2007). Par conséquent, le piégeage de gaz peut être négligeable dans nos expériences.

Pour mieux observer les effets du piégeage de gaz et de la compressibilité de la mousse avec f_g=85% dans le milieu poreux, nous avons fermé la sortie de la colonne de pré-générateur et mesuré la perte de charge le long de la colonne principale à la fin de l'expérience. La Fig. 22 montre que la pression dans la colonne a diminué progressivement même après l'arrêt de l'alimentation en mousse. Au cours des deux premières heures, le gradient de pression a fortement chuté de 140 000 Pa/m à 37 000 Pa/m, après avoir progressivement diminué ; l'expérience a duré quatre jours.

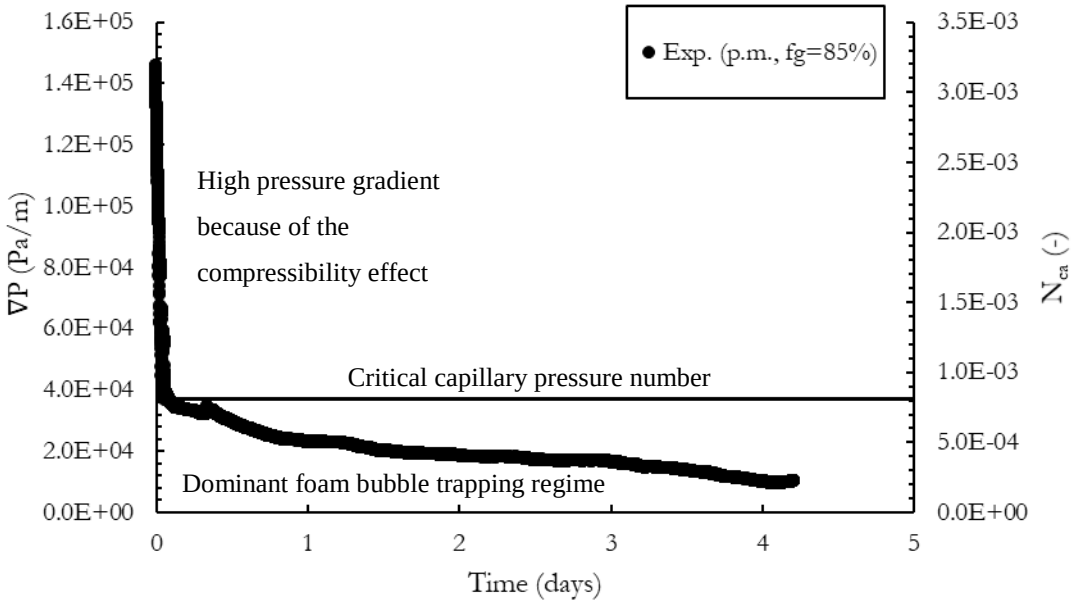

Fig. 22 Gradient de pression et nombre capillaire en fonction du temps après l'arrêt de l'écoulement de mousse (f_g=85%)

Après avoir fermé la sortie du générateur de mousse, la mousse continue de s'écouler à travers la colonne. Cela peut s'expliquer par l'effet de compressibilité de la mousse. Cependant, le gradient de pression

diminue d'abord très rapidement puis plus lentement à cause du piégeage de gaz. À partir des valeurs du nombre capillaire représentées sur la Fig. 22, nous pouvons dire que le piégeage de gaz se produit en dessous d'un nombre critique de pression capillaire, N_{ca}=7×10^{-4}. Cela montre que nos expériences d'écoulement de mousse dans un empilement de billes de verre de 1 mm (2,55×10^{-3}<N_{ca}<5,42×10^{-3}) ne sont pas affectées par le piégeage de gaz.

Nous avons également observé la compressibilité de la mousse et les effets de piégeage de gaz en mesurant le gradient de pression le long de la colonne et en pesant l'effluent. La colonne de mousse pré-générée a d'abord été connectée à la colonne de billes de verre qui était initialement saturée par la solution de tensioactif. La Fig. 23 représente la masse d'effluent et le gradient de pression en fonction des volumes de pores (PV) de la colonne principale. Le volume de pores (PV) du garnissage des billes de verre était de 180,9 ml, ce qui est illustré sur la Fig. 23 par la ligne noire continue. Le débit d'injection totale dans le générateur de mousse était de 2 ml/min (comprenant 1,20 ml/min de gaz N_2 et 0,80 ml/min de solution de surfactant). Cependant, la percée gazeuse s'est produite après la production de 2,94 PV de liquide, ce qui correspond à un changement de pente sur la figure (ligne noire en pointillé). Ainsi, 2,94 fois plus de liquide a été récupéré que ce qui était initialement indiqué dans la colonne.

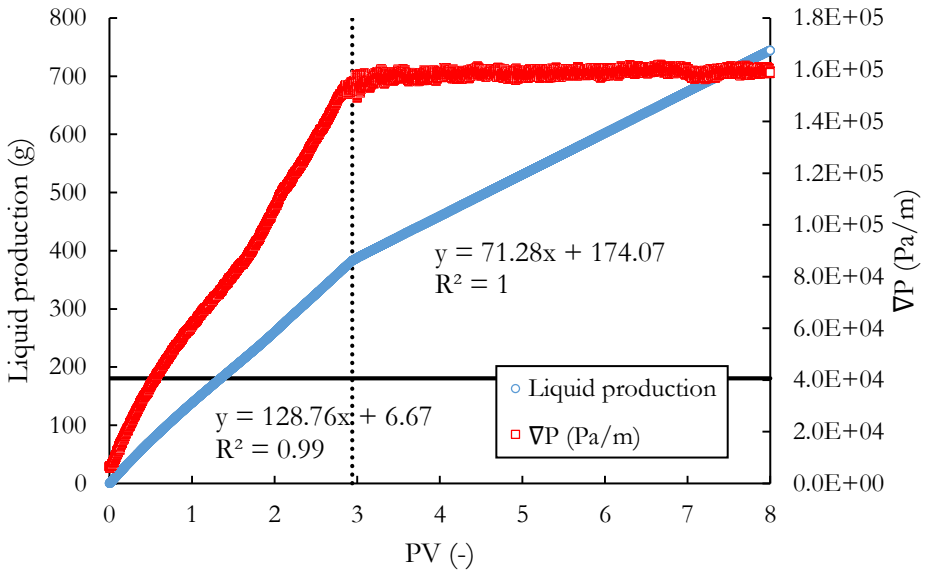

Fig. 23 Masse liquide d'effluent en fonction du PV pour le garnissage GB à Q_t = 2 mL / min pour f_g=60%

Le graphe met en lumière la compressibilité et le piégeage du gaz dans les milieux poreux (qui ont retardé le temps de pénétration du gaz). La Fig. 22 démontre que le gaz était piégé de manière considérable en dessous de 37 000 Pa/m. Ainsi, le liquide s'écoulait à l'intérieur des lamelles de mousse aux faibles gradients de pression. Ce phénomène a également été observé par Falls et al. (1989). Ils ont trouvé l'écoulement des lamelles de mousse à travers un chemin préférentiel unique avecles lamelles

stationnaires bloquant la majeure partie de la section transversale de la colonne de billes à des gradients de pression suffisamment faibles. Le gaz étant piégé dans le milieu poreux, tout le liquide a été transporté à travers les lamelles, retardant ainsi la percée du gaz. Ainsi, nous avons récupéré 385 mL de liquide lors de la percée gazeuse, soit 2,1 fois plus que le PV. De plus, sur la base de l'équation de tendance de la production de liquide pour la première moitié de la courbe, le taux de récupération de liquide était d'environ 128,8 ml par PV injecté, soit 24% de moins que le volume d'injection (180,9 ml). Si l'on considère que le liquide est un fluide incompressible, le volume de gaz est réduit à 40%. Par conséquent, nous pouvons conclure que l'écoulement de la mousse à des gradients de basse pression est influencé par l'effet de piégeage et à des gradients de pression élevés par la compressibilité (qui tend à diminuer le volume de gaz de la mousse). Après la percée, lorsque la mousse a atteint la sortie de la colonne, le changement de masse d'effluent correspond à la masse du fluide injecté. Fort de ces résultats, il faut noter que la compressibilité de la mousse doit être prise en compte lors de l'étude de la rhéologie de la mousse en milieu poreux.

La majeure partie du volume de mousse étant constituée de gaz, la compressibilité est l'un des paramètres essentiels à prendre en compte. La compressibilité est souvent décrite en termes de rapport d'expansion ε qui est défini comme le rapport entre la masse volumique de la phase liquide ρ_l et celle de la mousse ρ_f (ε=ρ_l/ρ_f) (Valko & Economides, 1992). La pression d'expansion doit être déterminée pour chaque perte de charge. En utilisant la méthode d'égalisation du volume proposée par (Valko & Economides, 1992), on devrait obtenir une seule courbe de référence en traçant la contrainte de cisaillement normalisée (τ/ε) en fonction du taux de cisaillement normalisé ($\dot{\gamma}/\varepsilon$) indépendamment de la pression et de la qualité de la mousse. Selon Valko et Economides (1992), cette méthode est pertinente pour les mousses à faible expansion (ε <4) à bulles sphériques. Gardiner et coll. (1999) ont mis en évidence une augmentation de la viscosité apparente de la mousse avec le taux d'expansion en analysant et en ajustant les données de viscosité de la mousse issues de recherches antérieures. Ils ont également découvert que la méthode d'égalisation du volume, proposée par Valko et Economides (1992), est applicable aux mousses polyédriques (ε> 5) et pétillantes à polyédriques (5≥ε≥4) (Gardiner, et al., 1998). La plupart de ces études ont été réalisées à l'aide de géométries simples telles que des conduites. Par conséquent, la détermination du taux de dilatation en milieu poreux est plus difficile, si seule la perte de charge le long de la colonne est mesurée.

Pour éviter l'effet de compressibilité, nous avons étudié le changement d'échelle de l'écoulement de la mousse dans un milieu poreux hautement perméable sur la base des résultats d'un epilement de billes de verre de 4 mm d'Omirbekov et al. (2020). Dans ce cas, la mousse a été pré-générée en utilisant la même solution de tensioactif et le même colonne de prégénération remplie de sable. Le gradient de pression maximal était de 23 210 Pa/m au débit de 3 ml/min à f_g=85%. Par conséquent, la perméabilité des cellules unitaires a été ajustée à la perméabilité d'un empilement de billes de verre de 4 mm, K=1,09×10^{-8} m^2.

Aucun piégeage de gaz n'était prévu car les nombres de capillaires étaient respectivement de $4{,}5\times10^{-3}$ et 7×10^{-3} aux débits de 0,22 et 3 mL/min. La Fig. 24 montre les résultats de changement d'échelle à travers les différentes géométries 2D et 3D avec les résultats expérimentaux d'Omirbekov et al. (2020). Dans ce cas, les résultats de la mise à l'échelle sont proches des données expérimentales.

Comme l'effet de compressibilité est insignifiant dans un empilement de billes de verre de 4 mm ($\varepsilon\cong1$), nous avons estimé le taux de dilatation pour un empilement de billes de verre de 1 mm en utilisant la méthode d'égalisation du volume de Valko et Economides (1992). Sur la Fig. 25, nous avons tracé la contrainte de cisaillement en fonction du taux de cisaillement de mousse (f_g=85%) dans des colonnes remplies de billes de verre de 1 mm sans et avec un facteur de dilatation moyen, sur la base des résultats de l'empilement avec des billes de verre de 4 mm GB. Nous avons trouvé un facteur d'expansion moyen de $\varepsilon = 2{,}1$ pour un empilement de billes de verre de 1 mm. Comme la forme des bulles de la mousse dans les milieux poreux est plus sphérique, la méthode de Valko et Economides (1992) pour les mousses à faible expansion est applicable.

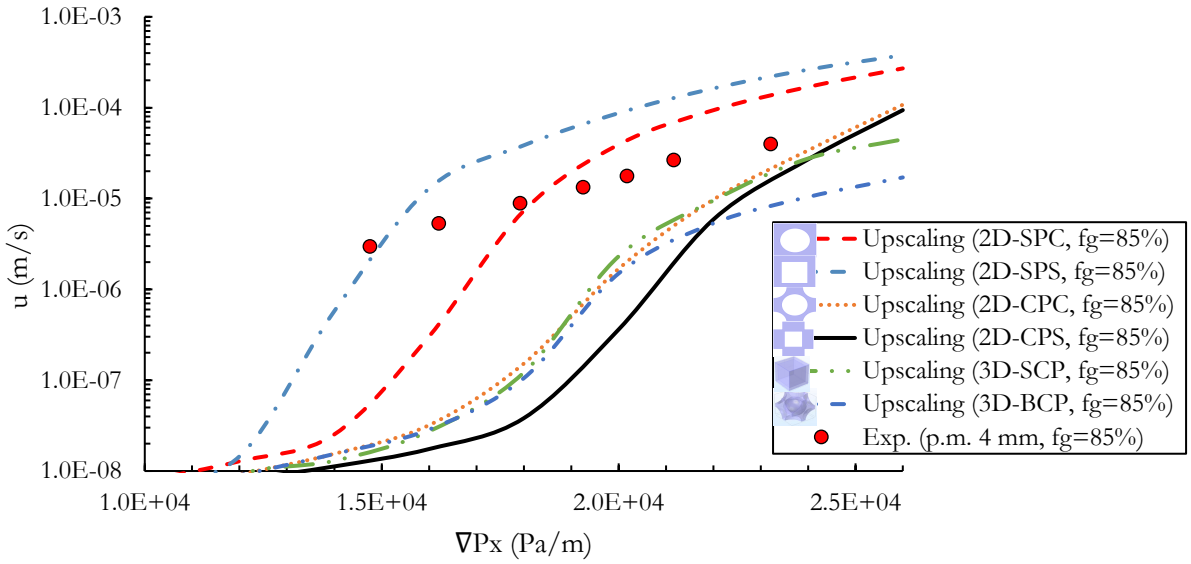

Fig. 24 Vitesse superficielle de l'écoulement de la mousse par rapport au gradient de pression macroscopique dans les cellules unitaires 2D et 3D et résultats expérimentaux dans un empilement de 4 mm GB de Omirbekov et al. 2020 (f_g=85%)

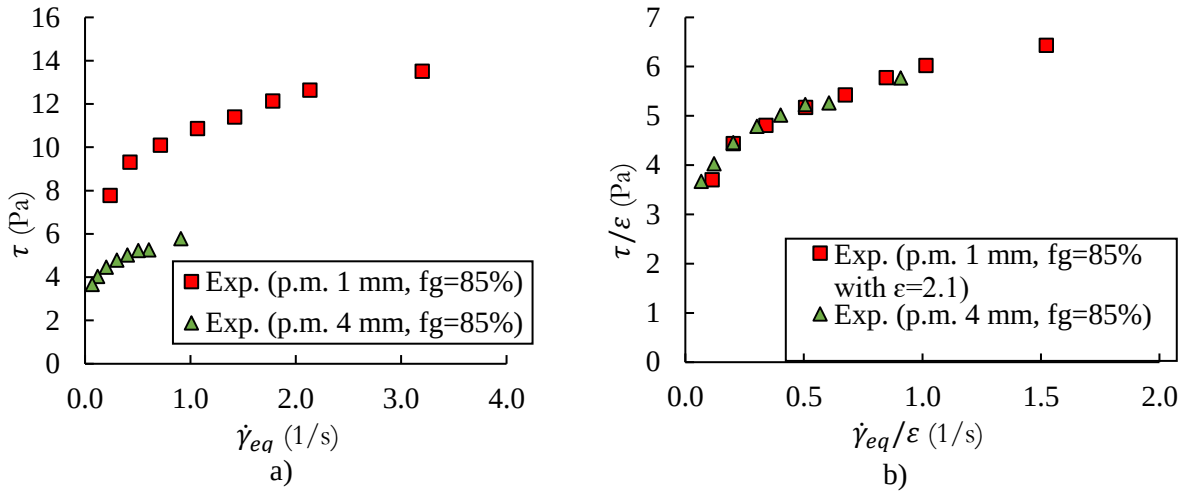

Fig. 25 Contrainte de cisaillement en fonction du taux de cisaillement pour la qualité de la mousse f_g=85% dans les empilements GB de 1 et 4 mm a) sans facteur de dilatation b) avec ε = facteur de dilatation de 2,1 pour un empilement GB 1 mm

On note également la simplicité des cellules unitaires considérées ici où la structure à l'échelle des pores est très ordonnée ce qui peut également influencer les résultats et expliquer en partie les écarts observés. Par conséquent, le changement d'échelle est un outil prometteur si les paramètres d'entrée sont réglés en tenant compte non seulement de la structure réelle du milieu poreux mais également de tous les phénomènes impliqués pour l'écoulement de la mousse en milieu confiné. Nous avons uniquement étudié le changement d'échelle du flux de mousse de l'échelle des pores à l'échelle du laboratoire. Par conséquent, le deuxième passage de l'échelle du laboratoire à l'échelle du terrain devrait être envisagé à l'avenir. Ensuite, la stabilité de la mousse, y compris la coalescence et la ségrégation par gravité, doit être étudiée. Nous savons que dans les applications sur le terrain, la texture de la mousse et la taille des bulles peuvent être différentes, car le temps de séjour de la mousse peut être beaucoup plus long.

6. Conclusion générale

Cette thèse visait à apporter de nouvelles contributions à l'étude du comportement de la mousse dans les milieux poreux très perméables que l'on trouve principalement dans les aquifères. Plus spécifiquement, le comportement de la mousse pré-générée dans des milieux poreux à grande perméabilité, où les bulles de mousse sont bien plus petites que les dimensions des pores, fait encore défaut. Par conséquent, nous avons étudié l'écoulement de la mousse pré-générée à travers des milieux poreux très perméables et des tubes capillaires, ainsi que le comportement rhéologique de la mousse en milieu libre à l'aide d'un rhéomètre. De plus, le changement d'échelle de la mousse de l'échelle du pore à l'échelle de Darcy a été réalisé en utilisant la technique d'homogénéisation en tenant compte des caractéristiques rhéologiques mesurées de la mousse comme donnée d'entrée. La caractérisation de la mousse en milieu libre, y compris

la concentration d'agent tensioactif, le type de gaz et la formation de mousse en fonction d'une concentration d'agent tensioactif alpha-oléfine sulfonate, a été examinée. Nous avons considéré la formation de mousse en utilisant un empilement de sable (d_{50}=0,135 mm) et un empilement de billes de verre de 1 mm, dans lequel la mousse était pré-générée par co-injection de solution de tensioactif et d'azote.

Nous tirons les conclusions suivantes de la caractérisation de la mousse en milieu libre (hors milieu poreux).

- La concentration micellaire critique (CMC) du surfactant utilisé a été déterminée expérimentalement à 1,8 g/L.
- La stabilité maximale (c.-à-d. durée de demi-vie) de la mousse a été observée à 2 × CMC, et la plus grande capacité de moussage a été obtenue à 3 × CMC. La concentration en tensioactif a été choisie pour être 4 × CMC avec une marge, pour assurer non seulement la stabilité et la moussabilité, mais également une concentration élevée en tensioactif en cas d'adsorption.
- La mousse générée via N_2 s'est avérée beaucoup plus stable et moussable qu'avec le CO_2. Plus précisément, la stabilité et la moussabilité ont été dépassées respectivement de 42 et 3 fois.

Après avoir sélectionné le tensioactif, la concentration du tensioactif et le type de gaz, le comportement de la mousse lors de son écoulement a été étudié dans des empilements de billes de verre (GB) de taille différentes. La génération de mousse dans un empilement de sable et un empilement de billes de verre de 1 mm a été analysée pour étudier l'effet de la taille des bulles sur la viscosité apparente de la mousse. L'impact de la qualité de la mousse (pré-générée) sur la viscosité apparente de la mousse à un débit fixe a été examiné pour distinguer les régimes de qualité faible et élevée. La rhéologie de la mousse pré-générée avec différentes qualités de mousse a été étudiée dans une colonne poreuse remplie de billes de verre de 1 mm. De plus, la rhéologie de la mousse avec une qualité de f_g= 85% a été examinée dans des colonnes remplies de billes de verre de 1 mm, 2 mm, 4 mm et 8 mm. Les conclusions suivantes ont été extraites des résultats.

- Le générateur de mousse joue un rôle crucial dans le comportement de la mousse dans les milieux poreux. La mousse générée dans la colonne de sable présentait un front vertical net par rapport à la colonne de billes de verre GB de 1 mm (interface inclinée) au même débit total, démontrant ainsi le fort de balayage de la mousse générée dans des milieux poreux plus fins.
- La pré-génération de mousse dans un milieu moins perméable que le milieu poreux de la colonne principale améliore la viscosité apparente de la mousse et la stabilité de la mousse. Ce phénomène peut être lié à la taille des bulles car la viscosité est plus élevée pour une mousse contenant des bulles de gaz plus petites. Par cela, nous confirmons la dépendance de la viscosité apparente de la mousse sur la texture de la mousse et la taille des bulles.

- Nous avons constaté que la saturation initiale en liquide (S_{wi}) (c'est-à-dire la teneur en liquide) dans la colonne remplie de billes de verre de 1 mm est inférieure à la fraction liquide de mousse injectée. De plus, nous avons observé que la S_{wi} dépend du débit par rapport aux milieux poreux à faible perméabilité. Cela peut être dû à la compressibilité de la mousse, dans laquelle des bulles de gaz compressées et déconnectées déplacent la phase liquide continue, réduisant ainsi la fraction liquide de la mousse dans un milieu poreux.
- La mousse pré-générée dans l'empilement de sable présentait une qualité de mousse correspondant à la transition faible/forte supérieure (f_g^*) dans une colonne remplie de billes de verre d'1 mm GB que la mousse générée directement à travers l'empilement de billes d'1 mm GB. Ainsi, la mousse pré-générée dans les milieux poreux moins perméables a démontré une meilleure stabilité. Ceci est lié à la pression capillaire limite plus élevée de la mousse plus fine, qui retarde le grossissement de la bulle (instabilité de la mousse).
- Des valeurs identiques de f_g^* qualité de la mousse correspondant à la transition ont été obtenues dans tous les empilements de billes de verre pour la mousse générée à travers la colonne remplie de sable. Par conséquent, nous en avons conclu que f_g^* était indépendante de la perméabilité du milieu poreux pour les milieux poreux hautement perméables lorsque les bulles sont beaucoup plus petites que les pores. La qualité de la mousse de transition, f_g^*, était égale à 97%.
- Si la taille de la bulle est la même que la taille des pores, la mousse se comporte comme un fluide newtonien à de faibles débits et présente un comportement de fluide rhéofluidifiant en augmentant les débits. Lorsque les bulles de mousse sont beaucoup plus petites que les pores, la mousse dans les milieux poreux s'est avérée se comporter comme un fluide rhéofluidifiant à seuil quelle que soit la taille moyenne des grains poreux. Le comportement rhéologique de cette mousse est bien adapté au modèle Herschel-Bulkley. Par conséquent, nous proposons de considérer la mousse comme un fluide à seuil dans des milieux poreux hautement perméables où les bulles de mousse sont beaucoup plus petites que les pores.
- Il a également été montré que la viscosité apparente de la mousse (μ_{app}) dans les milieux poreux augmentait avec la taille du diamètre des grains (c'est-à-dire la perméabilité) au même débit total. Cependant, pour un taux de cisaillement constant, le μ_{app} de la mousse diminue avec l'augmentation de la granulométrie, ce qui peut être un effet de la compressibilité de la mousse dans des milieux moins perméables.

La rhéologie de la mousse pré-générée à travers le sable fin a également été étudiée, sous forme de mousse en milieu libre (hors milieu poreux) dans un rhéomètre à géométrie à plaques parallèles dentelées, afin d'examiner la différence de comportement de ladite mousse hors et dans le milieu poreux. Les résultats obtenus avec le rhéomètre ont été ajustés à l'aide d'un modèle rhéologique (modèle Herschel-Bulkley-

Papanastasiou) et ont été analysés en fonction des résultats obtenus en milieu poreux. Les conclusions suivantes ont été tirées de ces résultats :

- Il a été constaté que la viscosité de la mousse en milieu libre peut être considérée comme celle d'un fluide à seuil et que le comportement rhéologique de la mousse correspond bien au modèle Herschel-Bulkley-Papanastasiou (H-B-P). Nous avons également observé que les valeurs du seuil de contrainte déterminées par le modèle H-B-P, augmentaient avec la qualité de la mousse.
- Nous avons constaté que la viscosité apparente de la mousse dans les milieux poreux hautement perméables est 3 à 4 fois plus élevée que la viscosité de la mousse hors milieu poreux au même taux de cisaillement, ce qui est dû à la complexité de l'écoulement de la mousse dans les milieux poreux.

Les données rhéologiques de la mousse hors milieu poreux ont été utilisées comme données d'entrée pour les changements d'échelle ultérieures, dans lesquelles le comportement macroscopique de l'écoulement de la mousse a été étudié numériquement dans différentes cellules unitaires périodiques 2D et 3D (par exemple, des arrangements carrés de cylindres avec une section circulaire (SPC), des arrangements carrés de cylindres à section carrée (SPS), des arrangements carrés faces centrées de cylindres de section circulaire (CPC), des arrangements carré faces centrées de cylindres de section carrée (CPS), des empilements cubiques simples de cubes (SCP), et des empilements cubiques centrés de sphères (BCP)). Pour ce faire, nous avons résolu le problème de fermeture non linéaire pour un fluide newtonien généralisé proposé par Orgeas (2007) à travers des cellules unitaires périodiques 2D et 3D ; nous avons, par la suite, comparé ces résultats avec les résultats expérimentaux obtenus à partir de d'expériences dans des colonnes de milieux poreux. Nous avons effectué également un changement d'échelle en utilisant la loi de Darcy proposée par Chevalier et al. (2013) pour dériver des coefficients sans dimension à partir de nos résultats expérimentaux. Les conclusions suivantes ont été tirées des résultats.

- La mousse étant un fluide non newtonien, la structure géométrique des milieux poreux joue un rôle crucial dans le comportement de la mousse. Cependant, nous n'avons pas observé de variations significatives des résultats entre les écoulements dans les géométries 2D-CPC et 3D-BCP de même porosité.
- Nous avons trouvé des différences considérables entre les résultats de changement d'échelle et les résultats expérimentaux. Néanmoins, la tendance globale de la courbe de la vitesse superficielle en fonction du gradient de pression (issue des résultats de changement d'échelle et du comportement en termes de f_g) a suivi la même tendance que celles des résultats expérimentaux.
- Les valeurs d'ajustement des coefficients sans dimension (χ et ω) de la loi de Darcy empirique étendue ont montré des valeurs élevées pour les mousses par rapport à d'autres fluides à seuil ; ces valeurs variaient en fonction de la qualité de la mousse.

Nous avons observé des différences considérables entre les résultats expérimentaux et les résultats numériques de changement d'échelle ; celles-ci pourraient être causées par la complexité de la mousse dans les milieux poreux. Le changement d'échelle de la mousse dans des milieux poreux à haute perméabilité peut être un outil prometteur si les paramètres d'entrée sont réglés avec précision en considérant les phénomènes particulières en jeu lors de l'écoulement de mousse dans des milieux confinés.

Afin d'éviter la microstructure très compliquée des milieux poreux et d'étudier la rhéologie de la mousse, nous avons étudié l'écoulement de mousse pré-généré dans des tubes capillaires de différents diamètres et constitués de différents matériaux (PTFE - polytétrafluoroéthylène, FEP - éthylène propylène fluoré et verre). Les objectifs étaient d'étudier l'effet de la qualité de la mousse, du type de matériau, du diamètre du tube et de la taille des bulles sur l'écoulement de la mousse. Ces résultats ont été comparés, à la fois avec la rhéologie des mousses pré-générées s'écoulant dans des milieux poreux, et avec le comportement de mousse en milieu libre déterminées à l'aide d'un rhéomètre. Les résultats suivants ont été tirés des résultats de cette étude.

- La viscosité apparente de la mousse en fonction de la qualité de la mousse suit généralement la tendance classique, qui se produit dans les milieux poreux, avec deux régimes correspondant aux régimes de basse qualité et de haute qualité séparés par une valeur de qualité de mousse correspondant à la transition (f_g^*). Cependant, la viscosité apparente de la mousse augmentait avec la qualité de la mousse jusqu'à l'instabilité qui se produisait au-dessus d'une qualité de la mousse de 90% en raison du changement des textures de la mousse. Par conséquent, pour les tubes d'un diamètre interne de 0,8 mm, f_g^*=98% dans les tubes FEP et PTFE, et f_g^*=97% dans le tube en verre. Cependant, pour les tubes FEP de 0,5 mm, la transition a été observée à f_g^*=96%, ce qui indique que l'instabilité de la pression capillaire limite est plus faible dans les tubes de plus petit diamètre. Ainsi, nous confirmons que f_g^* dépend du type de matériau et du diamètre du tube. De plus, les valeurs de f_g^* trouvées pour le tube de verre sont compatibles avec les résultats trouvés dans les empilements de billes de verre.
- Nous avons observé que la texture de la mousse passe du liquide pétillant (bulles en suspension) à de faibles qualités de mousse (f_g<70%) à une mousse homogène polydisperse à 70% ≤f_g<90% et à une mousse à piston au-dessus de f_g≥90%. La texture de la mousse a également changé en fonction du débit. A faibles débits, la texture de la mousse est grossière, ce qui est dû à la génération de mousse faible où le taux de coalescence des bulles augmente par rapport au taux de génération de bulles. Ainsi, la rhéologie de la mousse doit être étudiée avec un soin particulier pour la texture de la mousse.
- La mousse se comporte comme un fluide à seuil dans les tubes FEP, et son comportement peut être bien ajusté par le modèle de Herschel-Bulkley. Cependant, les valeurs de la contrainte seuil

se sont avérées nulles dans les tubes GT et PTFE. La viscosité apparente de la mousse dans les empilements de billes de verre et avec le rhéomètre laissent à penser qu'il s'agit d'un fluide à seuil. Cela peut être une conséquence de l'existence d'une vitesse de glissement sur la paroi dans les tubes capillaires.

- La viscosité de la mousse est plus importante dans le tube en PTFE que dans le tube en FEP et en verre, ce qui peut être une conséquence de la rugosité de la surface. Cependant, nous n'avons pas pu définir l'effet de paroi du tube ; par conséquent, des recherches supplémentaires pour éclaircir cet aspect sont en cours.
- La rhéologie de la mousse déduite de l'écoulement dans les tubes capillaires pourrait être compilée dans une courbe maitresse avec celle obtenue par l'étude de l'écoulement de la mousse dans les empilements de billes de verre et celle mesurée par un rhéomètre. Ces données pourraient être intégrées ensemble par un modèle HB permettant des comparaisons différentes et des discussions.
- La dispersion des résultats trouvés pour l'écoulement de la mousse dans de petits capillaires peut être attribuée au caractère polydisperse de la mousse générée à travers la colonne remplie de sable puisque le nombre de bulles diminue avec la section des tubes.

Ces informations peuvent guider l'étude de la mousse pré-générée dans des milieux poreux fortement perméables, en particulier pour l'application dans les processus de dépollution des sols. Nous espérons que notre étude sera un point d'ouverture pour d'autres recherches sur l'écoulement de mousse dans les aquifères de forte perméabilité.

Part 2 – Dissertation in English

Chapter 1

General Introduction

Aqueous foam is a two-phase system, where (disconnected) gas bubbles are dispersed in a continuous liquid phase (Bikerman, 1973). In most foams, the fraction of gas is high, and the thin liquid film separating regions of gas are called lamella. The surfactant in the aqueous phase stabilizes the lamellae by reducing the gas mobility and keeping the gas phase discontinuous. Thus, reducing the gas mobility decreases the mobility of the whole system, which is the most crucial property of foam in terms of application.

Due to the mechanical behavior of foam combined with its sizeable specific area relative to the density (Prud'homme & Khan, 1996), the use of liquid foam can be found in many very different types of applications, such as in the food industry, in cosmetic and laundry businesses, in household chemicals, as fire fighting fluids, and in construction materials. The use of aqueous foam in porous media is also extensive, and the application of foam in the oil industry, particularly in the enhanced oil recovery (EOR) processes (Lake, 1989), has started since the early 1960s (Patzek, 1996). In the petroleum industry, foam can be used as a drilling fluid, as a mobility-control agent in EOR processes (Chen, et al., 2014), in matrix-acidization treatments (Rossen & Wang, 1999), and gas-leakage prevention (Bernard & Holm, 1970). At the end of the last century, foam injection technology in porous media has begun to be used for contaminated-aquifer remediation processes (Hirasaki, et al., 1997).

The primary use of foam for contaminated-soil remediation processes is to control the permeability of porous media, thereby diverting remediation agents from high to low permeable zones of aquifers. However, the inconsistencies between applications in oil reservoirs and aquifers are notable. For instance, porous media in oil reservoirs are mainly consolidated with low permeability, while polluted aquifers are mostly unconsolidated and highly permeable. Therefore, the application of foam flow in highly permeable porous media still faces specific challenges. First, in-situ foam generation in very highly permeable porous media, mainly where pore sizes are much larger than bubbles, is doubtful. Second, the behavior and stability of foam are highly dependent on the generation processes. Moreover, there is lingering uncertainty about the behavior of foam in highly permeable porous media when bubbles are much smaller than aquifer pores. In addition, the upscaling of foam flow in porous media, starting from the bulk-form fluid properties and porous space geometry, still begs questions.

We indicated above some essential questions on the application of foam in highly permeable porous media that will be considered in this thesis. Consequently, the rheological behavior of pre-generated foam in bulk-form, as well as in porous media, will be experimentally studied. The influence of the foam generator on the rheology of the foam will also be examined. The flow of a pre-generated foam will be analyzed in different capillary tubes at higher shear rates. Moreover, an upscaling of foam flow through porous media from the pore-scale to the Darcy scale will be conducted using the measured rheological characteristics of bulk foam as input, and the results will be compared to experimental ones. The main objectives and scope of the thesis will be drawn at the end of this chapter. First, we start with a problem statement and a

discussion of bulk foam, foam in porous media, and the different applications of foam in contaminated-soil remediation.

1.1. Statement of the problem

This research is a part of the project entitled "Using the foams with blocking effect and the desorption/iron delivery foams for the treatment of heterogeneous high-velocity groundwater polluted by heavy chloride compounds," with an acronym of FAMOUS (in French: "Utilisation des mousses à effets bloquants et des mousses de désorption/vectorisation du Fer pour le traitement de nappes phréatiques hétérogènes à forte vélocité polluées par des composés chlorés lourds"). This project is conducted by SOLVAY, SERPOL, BRGM (French Geological Survey) companies, I2M laboratory in Bordeaux, the University of Franche – Comté (UTINAM laboratory) in the framework of GESIPOL call for projects of ADEME (Environment and Energy Management Agency). The aim of the FAMOUS project is the remediation of DNAPL contaminated soil using two different foam types: 1) to divert the high-speed groundwater flow from polluted zones, 2) to dissolve and treat the contaminants.

The contaminated site is located in southeastern France on the western foothills of the Alps mountain range system shown in Fig. 1.1. The water table of the site is 10 m deep with ±1 m amplitude, and the thickness of the aquifer is about 65 m. The aquifer is heterogeneous with the hydraulic conductivity from 10^{-4} to 10^{-2} m/s (corresponding permeability from 10^{-11} to 10^{-9} m^2), and the average groundwater velocity is 10 m/day. The direction of the aquifer flow is from the south-southeast (SSE) to the north-northwest (NNW).

Fig. 1.1 Hydro-physical map of the contaminated site area: the red zone refers to the contaminated area

We also know that the mean porosity of the site is equal to 40%. The contaminated site with an area of 80 by 60 meters has been polluted by DNAPL. The objective of this PhD work within the FAMOUS project was to study foam flow for diverting the flow of groundwater from contaminated soil areas without coming into contact with contaminants. The conceptual illustration of the foam injection process in the contaminated site is presented in Fig. 1.2.

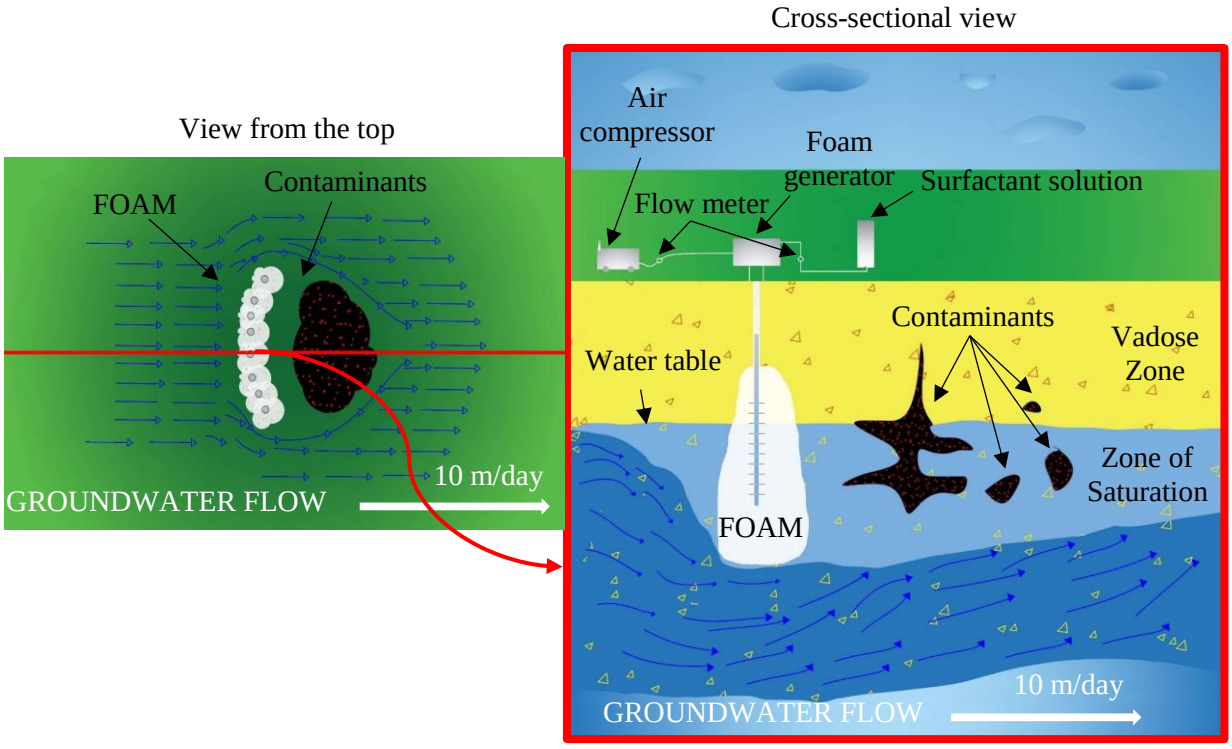

Fig. 1.2 Schematic illustration of the foam injection process in FAMOUS project

1.2. Bulk foam

Foams are close to concentrated emulsions, and the disperse phase in foams is gas. The bulk foam structure is presented in Fig. 1.3, where the presence of gas and liquid phases are shown. The liquid phase of foam consists of surfactants, in which high-molecular-weight substances can be added to increase the stability of the surfactant solutions (Perepelkin & Matveev, 1979). Foam, also called the gas-emulsion, is considered as one of the numerous classes of colloidal systems in the classification of Bikerman (Bikerman, 1973).

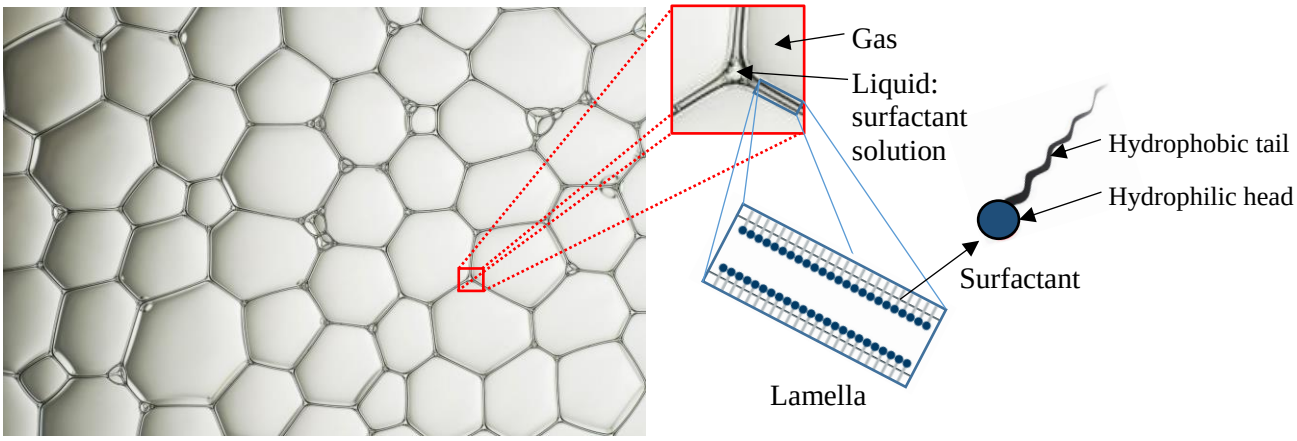

Fig. 1.3 Structure of foam

1.2.1. Surfactant

Surfactant is the essential component of the foam and plays a crucial role in foaming. Surfactants are organic molecules with different polarity parts that lower the interfacial (or surface) tension between two fluids, or between a liquid and a solid (Guozhong, 2004). One aspect of the surfactant is hydrophilic (often called the hydrophilic head) and polar. The other part is a hydrocarbon chain, which is hydrophobic (often called the hydrophobic tail) and lipophilic, hence non-polar (see Fig. 1.3). Thus in foams, the hydrophilic part is directed towards the surfactant solution and the lipophilic part towards the gas phase.

According to Gibbs' law (Gibbs, 1879), the interfacial tension decreases sharply with an increase in the surfactant concentration, thus saturating the interface between two phases with surfactants. When the surfactant concentration reaches a particular concentration called critical micelle concentration (CMC), the surface tension remains relatively constant or changes with a lower slope (see Fig. 1.4).

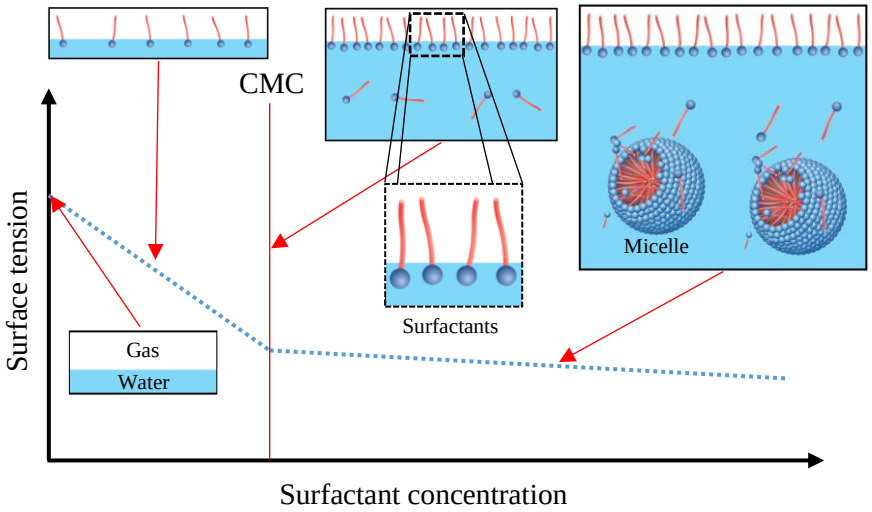

Fig. 1.4 Schematic illustration of surface tension variation as a function of surfactant concentration

1.2.2. Foam formation

Foams can be generated by two methods: dispersion and nucleation (Bikerman, 1973). In the dispersion process, the initial dispersion medium is liquid (the continuous phase). The gas is the dispersed phase introduced in this medium. Thus, foam is the opposite of fog or aerosol, in which a liquid phase in dispersed in a continuous gas phase. Dispersion foams can be made by injection of gas into a surfactant solute, or also by shaking of the surfactant solution by, for example, agitating a can containing solution and air. This foam generation method is mechanical, and there is no chemical modification of the substances present (see Fig. 1.5a). There are numerous foam generation experiments by dispersion method, for instance, air injection into a rotary cylinder, gas injection through a soap or surfactant solution, simultaneous injection of gas and surfactant solution (Bragg & Nye, 1947; Smith, 1949; Neppiras, 1969).

The second type of foaming method is the nucleation method, where the gas molecules are initially present in the liquid phase as a dissolved phase. When the pressure or temperature changes to a specific value, the dissolved gas molecules are transformed into bubbles, thus generating foam. For example, beer and soft drinks (see Fig. 1.5b). Nucleation methods involve more chemical effects than dispersion. The nucleation of gas from a liquid solution requires particular thermodynamic conditions in terms of pressure or temperature.

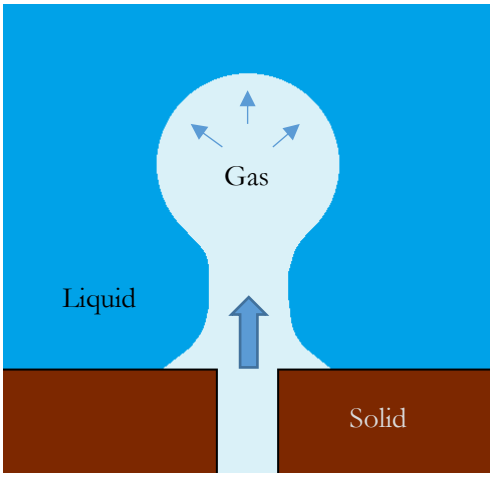

a) Dispersion method

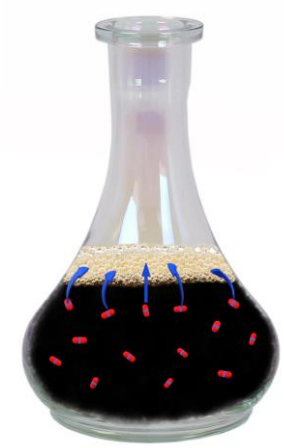

b) Nucleation method

Fig. 1.5 Foam generation methods

Regarding the dispersion method by injection of gas, Bikerman (1973) emphasized the importance of gas injection speed and, therefore, the Reynolds number on the properties of the foams generated. Moreover, the foam generation techniques must be adequately described, since foam quality (the gas fraction) and texture of foam (bubble density) can vary depending on the type of method used. Typically, foam texture is defined as a number of lamellae per unit volume of the gas phase, which is also inversely proportional to the bubble size. In addition, depending on the field of application, it is crucial to choose the best foam formation techniques to have a well-characterized stable foam. The most well-known foam formation

method is the simultaneous injection of gas and surfactant solution through a porous medium, where the porous medium can be stacked glass beads (glass frits) or sand-pack (Burley & Shakarin, 1992; Enzendorfer, et al., 1995; Raza & Marsden, 1967; Patton, et al., 1983).

1.2.3. Foam quality and structure

As mentioned above, in foams, gas bubbles are separated by liquid films called lamellae. The main concept of these lamella or foam films is a sandwich-like structure with three layers in which the inner layer has the same viscosity as a liquid in the system. The two exterior layers, which are in contact with the gas phase, are more viscous and have a non-Newtonian behavior. These outer layers' structures are more like a solid material; they do not flow under minimal stress. For example, consider foam based on soap or high molecular weight surfactant solution and allow it to dry for sufficient time. After a while, we can observe that the liquid between two outer layers of lamella evaporates. A double sheet of solid soap or solid plastic may exist for an uncertain period. It was concluded that there is no hydrostatic equilibrium in the foam films since the pressure varied at each point of a lamella (Bikerman, 1973).

Foams are classified as wet or dry, depending on the gas and liquid fractions (see Fig. 1.6a), which is also called the foam quality. Hence, in a static state, the foam quality can be expressed as,

$$f_g = \frac{V_g}{V_l + V_g} \tag{1.1}$$

where, V_l and V_g are the volumetric contents of liquid and gas in foams, respectively.

The gas fraction of wet foams vary from 64% to 95%, and when the foam quality f_g>95% foams become dry. Foams transform into a more bubbly liquid if f_g<64% (see Fig. 1.6a). The transition from wet foam to bubbly liquid is called the jamming transition.

The shape of bubbles changes from spherical to polyhedral depending on the type of foams. Wet foams produce spherical shape bubbles, while dry foams favored generating polyhedral form. For the polyhedral foams, if three bubbles meet symmetrically, the connection between lamellae called the Plateaus border (Plateau, 1873) creates a three-fold border with a 120° angle (Fig. 1.6b). If four Plateaus borders symmetrically intersect in the space, it forms tetrahedral angles with almost 109° (see Fig. 1.6b).

The change of foam structure also depends on the arrangement of foam bubbles and the size differences between them. Fig. 1.6a shows the most common types of foam structure, depending on the gas fraction. For example, the difference in the structure of dry foams can be polydisperse-disordered (a), monodisperse-disordered (b), and monodisperse-ordered (c). Thus, wet foams (d-f), wet foams at jamming transition (g-i), and bubbly liquid (j-l) can be classified according to the bubble size distribution and the arrangement of foam bubbles (Drenckhan & Hutzler, 2015).

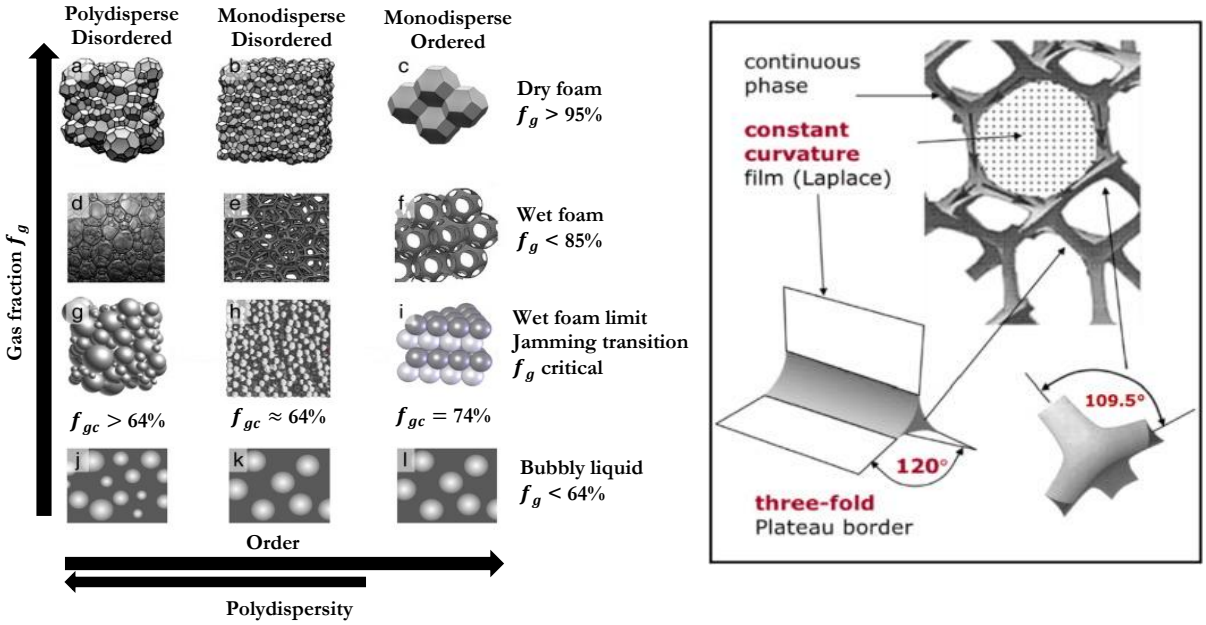

a) b)

Fig. 1.6 Foam property: a) Classification of foams by quality; b) Plateau's border (Drenckhan & Hutzler, 2015)

1.2.4. Foam density

Essentially, foam is a two-phase system, and to calculate the foam density, one must consider the densities of gas and liquid. Therefore it can be expressed as follows:

$$\rho_f = \frac{m_l + m_g}{V_f} \tag{1.2}$$

In which V_f is the volume of foam, m_l and m_g are the mass of liquid and gas, respectively. The mass of foam is usually negligible in very high-quality foams (Zhang, et al., 2009).

1.2.5. Foam stability

Foam stability is a state of being stable of foam texture under static or dynamic conditions. Commonly, foam stability in a static state is estimated by measuring the time necessary for the foam to collapse down to half of the volume initially generated (half-life time). In addition, two other methods can also be used to examine the foam stability: 1) the lifetime of a single bubble; 2) the change of foam volume under dynamic conditions, such as gas flow, shaking or shearing (dynamic) (Schramm, 2006). It is essential to consider both static and dynamic stability aspects to understand the properties of foam better.

The value of the surfactant concentration is also significant for the behavior of foam since the behavior of foam at a high concentration is very different compared to that at a low concentration (Schramm, 2006). For instance, Mulligan and Eftekhari (2003) investigated the foam stability and performed quality tests

for foams made with ten different commercial surfactants. They found a better ability to foam Triton X-100 and JBR425 surfactants when compared to other surfactants. Rothmel et al. (1998) assumed that foam stability is independent of essential properties like hydrophile-lipophile balance and critical micelle concentration. However, some studies showed a significant dependence on foam stability on surfactant concentration and foam quality (Zhang, et al., 2009). Moreover, the highest foam stability was obtained between 90% and 99% of foam qualities.

Since the foam is an unstable disperse system, one of the most common causes of foam instability is the effect of gravity drainage. The drainage of continuous liquid phase through lamellae that leads to the close coming of the bubble surfaces, thus causing coalescence and collapse of the foam. Moreover, foam cannot be considered as a homogeneous system when liquid accumulates at the bottom of the sample (Princen, 1990), which mostly occurs for wet foams. Another reason for foam instability can be caused by the coalescence effect and Ostwald ripening (Voorhees, 1985), where a gas diffuses from small bubbles to large bubbles. The leading root of this effect is the presence of high pressure in small bubbles rather than large ones. Capillary pressure plays an essential role in the coalescence of bubbles, that is to say, that two or more bubbles merge during contact to form a single bubble. As illustrated in Fig. 1.7, the liquid surface between two bubbles is concave to the gas phase, as the pressure at points ***b*** is higher than at point ***a***, the higher pressure from two sides pushes the floating bubbles to each other (Bikerman, 1970; Bikerman, 1973).

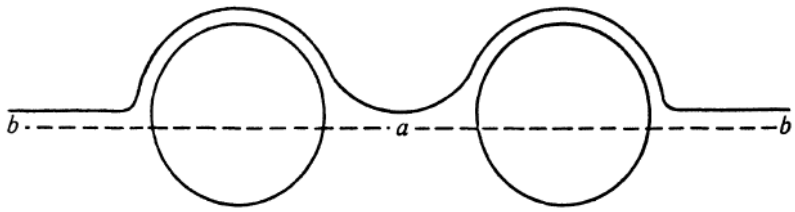

Fig. 1.7 Capillary attraction of two bubbles (Bikerman, 1973)

1.2.6. Bubble size and shape

Foam is a complex fluid, and one of the essential foam parameters is the bubble size that has substantial interconnections with bubble shape. The bubble size can vary according to the gas diffusion (Ostwald ripening) and bubble coalescence effects, which also depend on the foam stability; therefore, the type of surfactant and gas. Moreover, the gas injection rate, the interfacial tension, and the gas quality influence foam bubble size and shape. As already mentioned above, wet foams produce spherical shape bubbles, while dry foams generate polyhedral forms. The bubble shape can also be deformed due to gravitational forces, which change the ideal form of the stationary bubble. Moreover, the resistance of the liquid distorts this shape. For modeling purposes, if the bubble size is relatively small compared to the sample volume, foam can be considered as a continuous phase (Herzhaft, 1999). However, bubble size was ignored as a parameter during some experimental studies (Bikerman, 1968; Achorn Jr. & Schwab, 1948).

1.2.7. Foam rheology and yield stress

Rheology of the foam is also very intricate and requires extensive study to characterize. Moreover, to understand foams thoroughly and, in particular, their flow near a solid surface or in a confined domain, one needs to consider numerous parameters, for instance, foam quality, wall slip velocity, bubble size, viscosity variation, and gas compressibility.

In most of the studies reported in the literature, the bulk foam was highlighted as a yield-stress fluid, and the majority of the results are commonly well fitted by the Herschel-Bulkley law (Cohen-Addad, et al., 2013; Denkov, et al., 2009; Hohler & Cohen-Addad, 2005; Katgert, et al., 2013; Kraynik, 1988; Dollet & Raufaste, 2014; Khan, et al., 1988; Herzhaft, 1999; Denkov, et al., 2005). Mainly, measuring yield stress is not an easy task, especially in capillary geometry. For instance, Khan et al. (1988) measured foam rheology through a rheometer with parallel-plate geometry. They covered the solid plates with sandpaper to avoid wall slip velocity. Elsewhere, the yield stress was measured with the "stress relaxation" method in coaxial geometry (Khan, et al., 1988). They found increasing in yield stress with the foam quality. Some authors experimentally showed the presence of a yield stress in foam by observing behaviors of foam bubbles near the walls of a transparent pipe (Kraynik, 1988). Moreover, when the shear stress is smaller than yield stress and if wall slip velocity exists, the foam flows entirely by 'plug flow,' and many authors experimentally confirmed this behavior (Kraynik, 1988; Beyer, et al., 1972; Thondavadi & Lemlich, 1985).

Denkov et al. (2005) studied foam rheology and wall slip velocity for a foam with 90% gas fraction using a rheometer. The foam used was generated using a syringe with a needle with id (inner diameter) of 2.5 mm. They found a shear-thinning behavior where the shear stress was determined to be a power-law function with the power-law index n equal to 0.25 and 0.42 for tangentially mobile and immobile bubble surfaces, respectively. Denkov et al. (2009) studied the effects of surfactant type and bubble surfaces on bulk foam rheology with $f_g \geqslant 80\%$. They classified the rheological behavior of foam into two different classes depending on the values of the power-law index n, by taking into account the viscous friction between bubbles and also between bubbles and solid walls, qualitatively. Their results with $n \approx 0.5$ referred to a system of the first type corresponding to friction dominance in foam films. The second type $n<0.5$ (mostly between 0.2 and 0.25) was defined as systems with essential energy dissipation on the bubble surfaces. These studies show solid, plastic, or viscoelastic behavior of foam below a yield stress and non-Newtonian liquid regime above the yield stress. The transition from solid-like to liquid-like mechanical behavior is called yielding.

The apparent viscosity of foam is several times larger than the viscosity of the continuous phase, i.e. surfactant solution, even at low shear rates. This can be explained from a description of foam at the molecular and bubble scale (Hohler & Cohen-Addad, 2005).

1.3. Porous media

Porous media are generally a solid material that contains pores (i.e., voids) in which ordinarily the solid matrix and the pore spaces are continuous. However, there are also certain concepts of porous media where naturally closed pores exist. Hence, in a subsurface environment, porous media commonly can be occupied by fluids such as water, oil, and gases. A solid matrix in this medium can be classified as follows:

- Consolidated porous media, where the solid matrix is composed of cemented grains (e.g., sandstones), and the pores in such a media may be connected (permeable) or unconnected (impermeable);
- Unconsolidated porous media, in which solid particles are not bound to each other, therefore the fluid can pass through the pores between the particles (e.g., sand).

1.3.1. Fluid flow in porous media

The study of fluid behavior in porous media is a subject of interest for many industries. For example, filtration technologies commonly used to purify water; reactors filled with porous catalyst support used for chemical reactions; membranes for gas separation; in the oil and gas industry, and soil remediation processes. The main governing law of fluid flow in porous media is Darcy's law, which was formulated by French civil engineer Henry Darcy in 1856 (Darcy, 1856). Hence, Darcy velocity u (m/s) for single-phase fluid flow through a porous medium is presented as follows:

$$\boldsymbol{u} = \frac{\boldsymbol{Q}}{S} = -\frac{\boldsymbol{K}}{\mu} \cdot \nabla(P + \rho g \boldsymbol{z}) \tag{1.3}$$

where $\boldsymbol{K}$ (m^2) is the absolute permeability as a 3×3 tensor, S (m^2) is the cross-sectional area of the porous sample, μ (Pa.s) is the fluid viscosity, ρ (kg/m^3) is the fluid mass density, g (m/s^2) is the gravitational constant, $\boldsymbol{z}$ is the vertical axis oriented up, and ∇P (Pa/m) is pressure gradient linearly dependent on volumetric flow flux $\boldsymbol{Q}$ (m^3/s).

In the case of multiphase flow, the porous medium is saturated (occupied) with several immiscible fluids. The volume fraction of each phase is expressed by a term called saturation, which is defined as follows:

$$S_i = \frac{V_i}{V_p} \tag{1.4}$$

in which V_i is the volume of a fluid i within the porous medium, and V_p (or pore volume, PV) is the fixed volume of the porous space.

Consequently, the flow model of multiphase transport in porous media consists of mass and momentum balance Eqs. (1.5) and (1.6):

$$\frac{\partial(\rho \emptyset S_i)}{\partial t} + \nabla \cdot (\rho \boldsymbol{u}_i) = 0 \tag{1.5}$$

where Ø (-) is the porosity of porous media. Depending on the number of phases i occupied the porous medium, the general form of Darcy's law (Muskat & Meres, 1936; Muskat, et al., 1937) is:

$$\boldsymbol{u}_i = -\frac{\boldsymbol{K} k_i(S)}{\mu_i} \cdot \nabla(P_i + \rho_i g \boldsymbol{z}) \tag{1.6}$$

where, $k_i(S)$ are the relative permeabilities (dimensionless).

In the two-phase theory (i=1, 2), the relative permeabilities are the unique functions of saturation that have a non-linear form (see Fig. 1.8). In order to have a closure relationship of 4 equations (1.5) and (1.6) for two-phase flow system, we need to define equations of state of each phase:

$$\rho_i = \rho_i(P_i) \tag{1.7}$$

$$\mu_i = \mu_i(P_i) \tag{1.8}$$

and capillary law, which is:

$$P_c = P_2 - P_1 \tag{1.9}$$

Capillary pressure is the pressure between two immiscible fluids where the pressure is proportional to the curvature of the interface between two fluids, and when the interface is a plate, P_c=0.

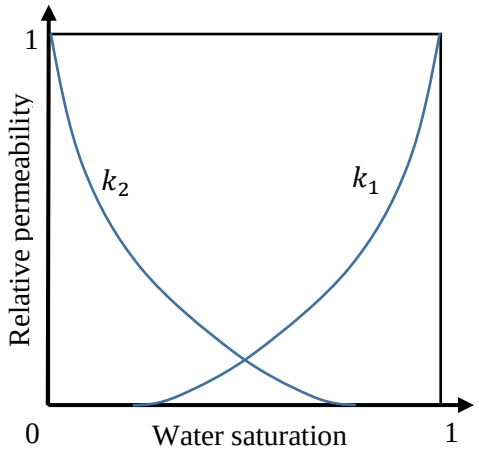

Fig. 1.8 Relative permeability (schematic)

1.4. Foam in porous media

As it was discussed in the previous sections, foam is a complex two-phase fluid. However, it should be noted that the presence of foam in porous media differs from bulk foam because it does not exist as a continuous liquid/film structure that includes gas bubbles (Hirasaki, 1989). Classically, foam flow through porous media is considered as a bubble train, and the bubbles are considered either of the same sizes as the pores or exceeding one pore size. Therefore, it is essential to study the characteristics of foam and porous media, and also the interaction between them. Foam behavior in porous media depends on several factors such as pore structure (shape, pore body-to-throat ratio, pore size distribution) and wettability of porous media, which is mostly (naturally) hydrophilic in aquifers, and that is the case

studied here. As shown in Fig. 1.9, the structure of foam in porous media has been considered either as a continuous-gas or as a discontinuous-gas foam. In continuous-gas foams, lamellae block certain gas flow paths by reducing gas mobility, but some gases can still circulate freely. In discontinuous-gas foams, lamellae block all ways of gas flow. These foams can flow as a train of bubbles or can be trapped, as shown in Fig. 1.9.

.

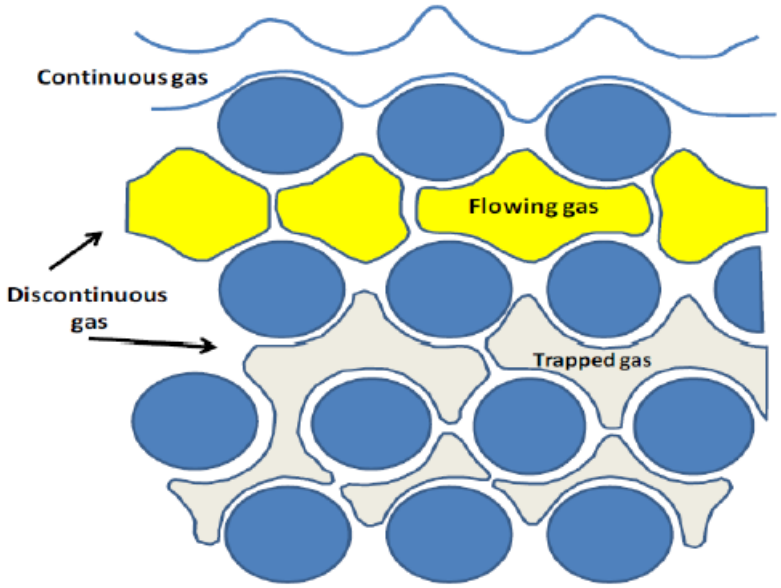

Fig. 1.9 Schematic of foam structures in porous media (Adebanjo & Udofia, 2015)

1.4.1. Mechanisms of foam generation in porous media

Besides the methods mentioned in section 1.2.2, foam can also be generated in porous media, owing to the creation and destruction processes of the lamellae at the pore-scale level. Foam formation in porous media can involve mainly three mechanisms, such as snap-off, lamella division, and leave-behind (Rossen, 1999) (see Fig. 1.10).

a) The snap-off mechanism occurs when the gas enters into a pore while liquid begins to gather in a throat, thereby blocking the throat. This can also be explained by the capillary pressure that increases during gas injection and falls by creating lamellae in pore throats. This mechanism usually generates bubbles of the same size as the pores of the porous medium, and it reduces gas mobility by a factor of one hundred through creating discontinuous-gas foam. Moreover, the snap-off process dominates foam blockage ability in porous media (Rossen, 2003; Kovscek, et al., 2007).
b) The division of lamella (bubble) mostly occurs when bubbles are larger than penetrating pores. Consequently, lamellae form by subdividing the existing foam bubbles.

c) The leave-behind mechanism takes place when gas approaches pore throats from both facing pore bodies. Lamellae created by this process makes the gas phase continues, and an enormous number of lamellae can be created in this way.

Rossen (1999) assumed the existence of the fourth mechanism of lamella creation that can be the production of gas in the middle of the liquid by chemical reaction (changing of temperature and pressure).

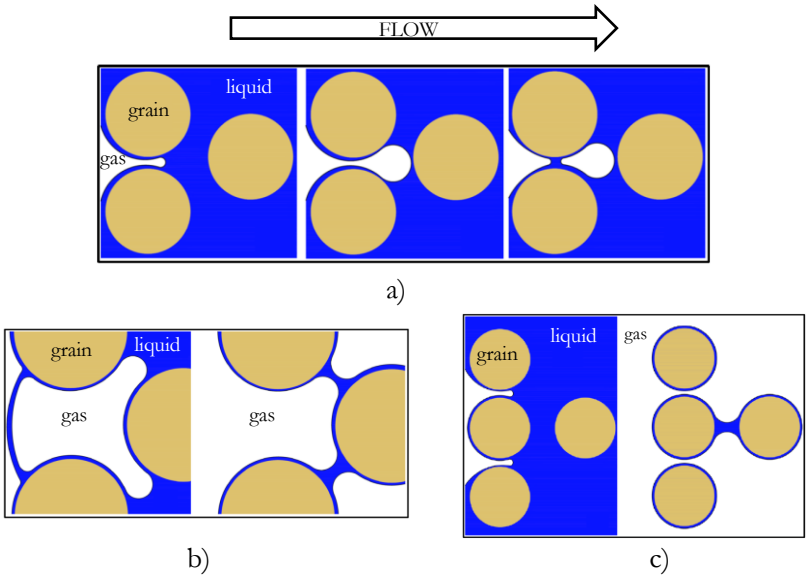

Fig. 1.10 Schematic view of foam generation in porous media: a) Snap-off b) lamella deviation and c) leave behind, adapted from (Almajid & Kovscek, 2020)

In practice, foam can be generated in situ by co-injection of surfactant solution and gas. However, when porous media are very highly permeable (K>1000 darcy), as is the case in soil remediation, foam cannot be generated in situ due to the low capillary pressure. Therefore, in this case, ex-situ generation (i.e. pre-generation) of foam applied in order to make a strong foam.

1.4.2. Foam flow in porous media

Foam flow through porous media is inevitably accompanied by foam formation and destruction, and the foam texture (i.e., bubble density) is a consequence of these two processes. Thus, relying on aqueous and gas flow rates, foam flow in porous media has two regimes: weak (coarse) and strong (fine) foams (see Fig. 1.11) (Gauglitz, et al., 2002). Weak foam is a coarsely textured foam with large bubbles, and the reduction of gas mobility is low or moderate, ranging from 10 to 100 times. Strong foam is a fine-textured foam with small bubbles that has a significant gas mobility reduction, which can range up to 10,000 times. Gauglitz et al. (2002) also pointed out on an unstable intermediate regime between strong and weak foam regimes.

The real application of this foam is doubtful due to its instability. In order to generate a stable foam at a low-pressure gradient, one must look for a surfactant that gives stable lamellae, which is very crucial for soil remediation applications.

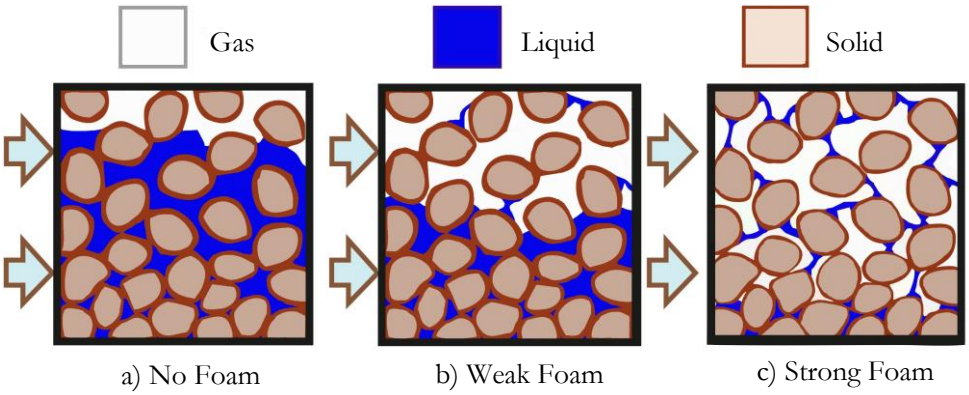

Fig. 1.11 Schematic of foam flow in porous media: a) conventional gas/liquid two-phase flow (no foam) b) weak foam c) strong foam (Lee & Kam, 2013)

As mentioned above, foam is considered as a yield stress fluid in some studies in the literature (Herzhaft, 1999; Denkov, et al., 2009; Hohler & Cohen-Addad, 2005). The yield stress that is related to the bubble size plays a significant role in the mobility of foam through porous media (Falls, et al., 1989). The main issue to keep in mind is a notable effect of the yield stress on foam flow, where sufficiently large pressure gradients are needed before the flow can take place (Friedmann, et al., 1994). This issue has subsequently been controverted by other researchers (Patzek, 1996).

In order to study the foam in porous media, different simplifications can be applied depending on the conditions of foam flow (e.g., dry or wet). Commonly, in a two-phase flow system, the capillary pressure (P_c) goes to infinity when water saturation is near zero. However, in the case of foam flow in porous media, the system always has a nearly zero liquid saturation at high gas fractional flow (i.e., dry foam). According to Khatib et al. (1988), the capillary pressure at first increases and then approaches a specific value at a relatively high fractional gas flow which called "limiting capillary pressure (P_c^*)" (see Fig. 1.12). When the fractional flow of gas increases further, the capillary pressure was found to remain at the limiting value. Nevertheless, they observed the process of coalescence and displacement of the coarse-textured foam near the limiting value. It means that collapsing of foam is not gradual as the P_c rises, but happens abruptly at a single P_c^*. If this hypothesis justifies, many simplifications are possible for strong foams flowing under dry conditions (Rossen, 1999).

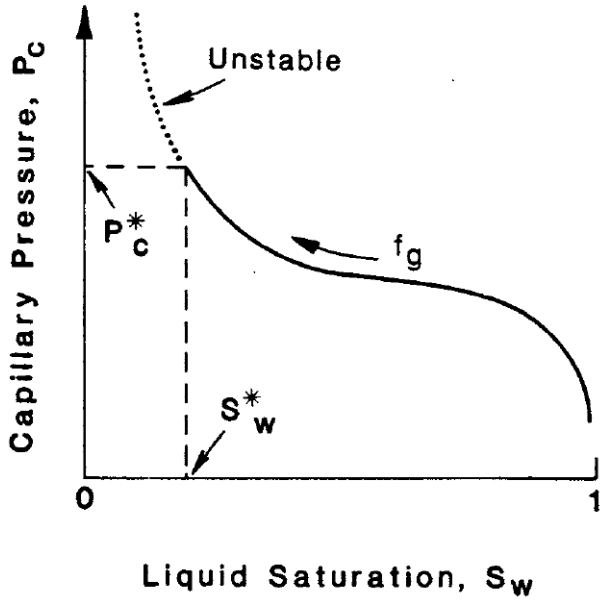

Fig. 1.12 Schematic of capillary pressure curve (Khatib, et al., 1988)

For wet foams, Rossen and Wang (1997) proposed a model in which the foam bubbles were considered to be of fixed size regardless of liquid and gas flow rates. This assumption is based on the idea that bubbles smaller than the pore size disappear due to the diffusion process between the bubbles. Eventually, it must be noted that most of the simplifications are reasonable if assumptions are justified (Rossen, 1999).

1.5. Soil contamination and remediation

Environmental pollution, particularly soil contamination, is a burning problem nowadays. Since the soil is an essential part of the entire ecosystem, it bears the greatest burden of environmental pollution. The presence of contaminants in soils at high concentrations show high potential health and ecological risk. There are many ways of soil pollution, which are directly linked to human activities in the past. In order to eliminate the failures and errors of the past, significant research and technological advances have been performed in the area of soil and groundwater remediation over the past three decades. Nevertheless, the characterization of subsurface contamination is very complex, and this also makes soil remediation very challenging (Fig. 1.13).

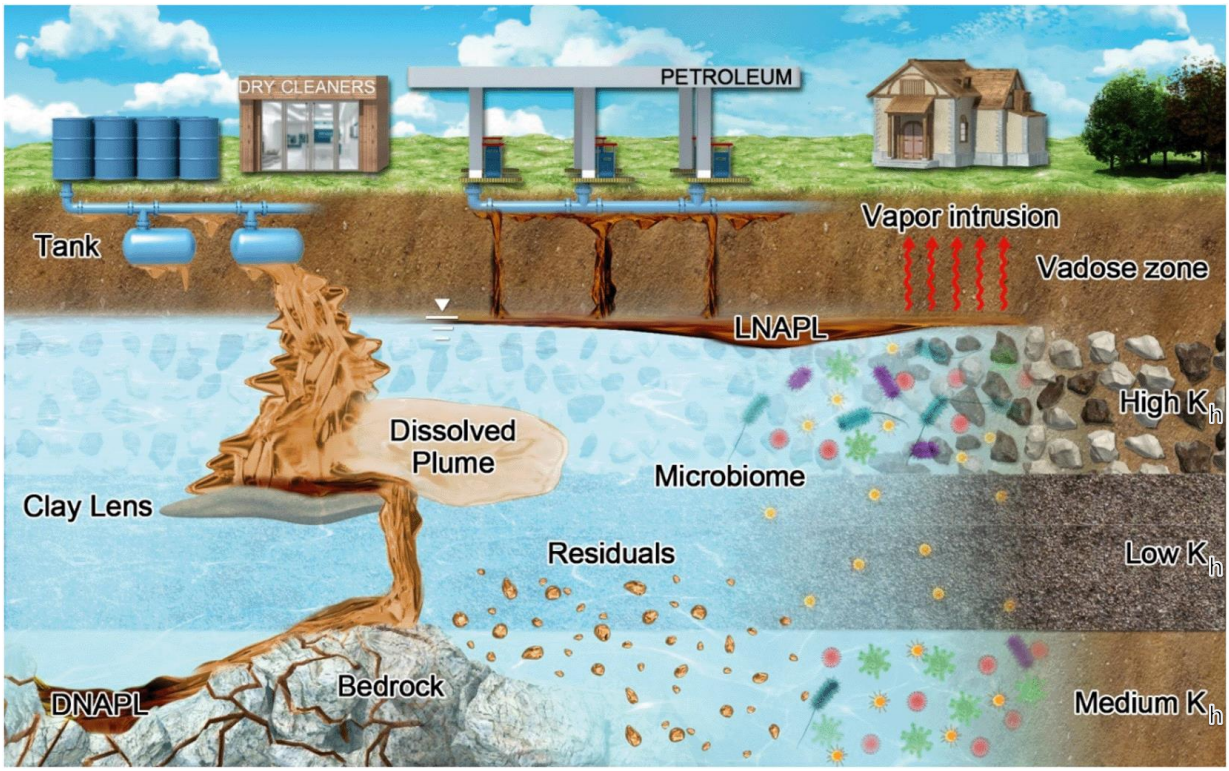

Fig. 1.13 Possible ways of soil contamination, adapted from (Zhang, et al., 2019)

Soil can be contaminated in many different ways, such as:

- discharge of industrial waste, seepage from a landfill;
- rapture of underground storage tanks;
- solid waste seepage;
- excess application of pesticides, fertilizer or herbicides;
- percolation of contaminated water into the soil.

In addition, most common chemicals that cause soil contamination are petroleum hydrocarbons, heavy metals, solvents, and pesticides.

As many organic contaminants are soluble in water, therefore water can be used as the primary control mechanism for soil remediation. In certain cases, some additives can also be used to improve water solubility, thereby cleaning efficiency. Moreover, cleaning efficiency depends on the hydraulic conductivity ($K_h = \frac{K\rho g}{\mu}$) of soil as cleaning in high permeability, i.e. greater than 10^{-5} m/s, gives better results (Mulligan & Eftekhari, 2003). However, non-aqueous phase liquids (NAPL), i.e. immiscible contaminants, remain as a separate phase. Those lighter-than-water NAPLs such as benzene, ethylbenzene, toluene, xylene, and other hydrocarbons are called LNAPLs. The liquid contaminants that sink below the water table, such as chlorinated solvents, coal tar, creosote, and contaminants mixed with metals, are

called dense non-aqueous phase liquids (DNAPLs). Specifically, the remediation of DNAPL is complicated, particularly for complex and heterogeneous subsurface environments (Pankow & Cherry, 1996).

Commonly, treatment technologies for the remediation of contaminated soils and aquifers are based on the following three principles, which are either performed in situ or ex-situ (Zhang, et al., 2019).

1) Extraction (e.g., pump and treat, surfactant flushing, air sparging, thermal methods, foam injection);
2) Degradation/transformation (e.g., biodegradation, chemical oxidation/reduction);
3) Sequestration and immobilization (e.g. encapsulation, sorption).

Currently, the extraction methods mainly related to physicochemical processes can quickly and efficiently remove contaminants but require considerably high energy consumption. Degradation processes, i.e. biological, take a longer time than extraction methods but can save energy. Sequestration and immobilization techniques can be used in places that are difficult to access or to stop and avoid the spreading of contaminants temporarily.

The use of foam for soil remediation purposes is very diverse. For instance, in the scope of our project (FAMOUS project), we use foam as a blocking agent for high-speed groundwater flow to temporarily confine the contaminated area and avoid spreading of contaminants and the chemical treatment agents in aquifers. Besides, foam can also be used as a pollutant sweeping fluid (Hirasaki, et al., 1997), as a vectorization fluid to transport soil cleaning additives or gases (Maire, et al., 2019; Choi, et al., 2009).

1.6. Foam for soil remediation

Foam has been applied for several targets in contaminated-soil remediation. More specifically, it has been used to improve the efficiency of the surfactant flooding and mainly to remove NAPL. In this section, we briefly review the advantages of and the background knowledge on the use of foam, specifically for DNAPL contaminated-aquifer remediation, which is the main focus of our global project.

1.6.1. Benefits of foam application for contaminated-soil remediation

Using foam for soil remediation purposes has the following several advantages:

- It reduces the amount of surfactant required because the surfactant fraction used in foam injection is much lower compared to the surfactant flushing technology (Mulligan & Eftekhari, 2003) from economic and environmental aspects (Roy, et al., 1995).
- It is favorable for mobility control, thereby improves sweeping efficiency as the injection fluid is less mobile than the resident fluids (Hirasaki, et al., 1997). Therefore, it allows the flow to be diverted from high-permeability to low-permeability zones.

- It increases the partition coefficient value that shows the level of absorption/desorption processes and the solubilization of contaminants (Wang & Chen, 2012).

1.6.2. Review of foam applications on contaminated-soil remediation

1.6.2.1 Remediation of soils polluted by DNAPL

The first field demonstration of the soil remediation process using surfactant-based foam was conducted at Hill Air Force Base, UT in USA (Hirasaki, et al., 1997). The DNAPL present consisted of 70% trichloroethylene (TCE), with a smaller amount of other solvents, which was removed from a heterogeneous alluvial aquifer. 3.2 pore volumes of aquifer surfactant solution with a concentration of 3.5% (by weight) of the surfactant sodium dihexyl sulfosuccinate was injected for 3.2 days. In order to generate foam, the air was injected into the aquifer with two-hour interval cycles at the three injection wells on a rotating basis. The remaining amount of contaminants were meager at the end of the test by that showing the efficiency of foam for remediating contaminated soils. Moreover, they observed the dependence of foam strength on the gas injection rate. At low flow rates, foam behaved weakly, and it was too strong at high gas flow rates that could damage the aquifer. They also indicated that the optimal flow rate for a laboratory-scale experiment was inappropriate to scale up for field operations since the characteristics of field differ from a laboratory column due to the three-dimensional geometry of a field site.

Kilbane et al. (1997) pointed out the problem of remediation technology with foam related to the necessity of a high-pressure gradient to move foam through the soil. However, the presence of a high-pressure gradient could lift the soil. The value of the pressure gradient used is usually 1-2 psi/ft (0.2-0.5 bar/m) depending on the injection depth. From an experimental study using a sand-pack with 70 mesh (210 μm) sand, they observed decreasing of pressure gradient with increasing of foam quality. Still, even at the highest foam quality, the pressure gradient was about 12 psi/ft (2.71 bar/m), which exceeded the critical pressure gradient up to 6 times. This means that the adequately stable foam cannot flow through soils at the inquired low pressures. They managed to form ethanol-based foams which propagated well through the soil at the pressure gradient of 1.5 psi/ft (0.34 bar/m) and less. Moreover, these foams efficiently desorbed the contaminated sites with polyaromatic hydrocarbons (PAHs).

Jeong et al. (2000) investigated the removal of residual TCE in homogenous and heterogeneous micromodels using foam. The foam was generated using air and an anionic surfactant, sodium $C_{14\text{-}16}$ olefin sulfonate. They examined the recovery rate of TCE depending on the capillary number values and also showed that the efficiency of foam is higher than surfactant flooding. Further, Jeong and Corapcioglu (2003) studied the effect of surfactant concentration, foam quality (the gas fraction), pore structure, and types of NAPL as contaminants. They found increasing in TCE removal with surfactant concentration at a fixed foam quality. Also, using low-quality foams (50% and 66%) was more efficient in removing TCE

than a higher quality foam (85%). It was concluded that the removal of TCE was mainly dependent on the capillary number rather than surfactant concentration and foam quality since TCE extraction increased notably when the capillary number increased. They indicated that the capillary number is a crucial parameter in defining sweep efficiency in heterogeneous media. They also noted that the instability of foam relies on the type of NAPL, where the foam was more stable with TCE than dodecane (LNAPL).

Mulligan and Eftekhari (2003) studied several surfactants for their capability to generate foam. Based on foam generation characteristics at the high quality and stability tests, they selected Triton X-100 and rhamnolipid (JBR425) surfactants. The foam made through these surfactants were used to volatilize and mobilize pentachlorophenol (PCP) contaminated soil. They considered fine sand and silty-sandy, which were used to pack the test columns. As a result, foam made of Triton X-100 surfactant showed two times higher cleaning efficiency for PCP compared to other liquid surfactant solutions. They also showed the ability of soil remediation by using foam under low pressures.

Wang and Mulligan (2004) assessed contaminated-soil remediation technology using surfactant foam and concluded that a proper selection of a surfactant and its concentration is essential to the success of the remediation. The summary of their work with a review of other studies is reproduced in Table 1.1.

Table 1.1 Summary of contaminated-soil remediation studies using foam (Wang & Mulligan, 2004)

Description	Surfactants	Main Results
Field demonstration of surfactant/foam process for aquifer NAPL (mixture of TCE*, TCA* and PCE*) remediation at Hill Air Force Base in Utah (Hirasaki, et al., 1997)	Sodium dihexyl sulfosuccinate	The average DNAPL saturation of the swept volume was reduced to 0.03%
A laboratory study on foam-enhanced surfactant solution flooding in removing n-pentadecane from contaminated columns (Huang & Chang, 2000)	Triton SP-series	Slightly over 74% of the n-pentadecane was removed at a gas–liquid ratio of 10/1
Micromodel study of surfactant foam remediation of residual TCE* (Jeong, et al., 2000)	Bioterge As-40	99% of the residual TCE was removed
Remediation of PAH*-contaminated soils using foams (Kilbane, et al., 1997)	Biosurfactants +50% ethanol	Foams readily desorbed PAHs from contaminated soils and moved well at pressure of 33.9kPa/m (1.5 psi/ft) or less
A laboratory study on soil flushing using CGA* suspensions generated from a plant-based surfactant to remove HCB* from soil (Kommalapati, et al., 1998)	Natural surfactant from Sapindus mukorossi (Soapnut)	CGA suspension recovered 670l g in 12 pore volumes compared to 8l g by waterflood

Remediation with surfactant foam of PCP*-contaminated soil on laboratory scale (Mulligan & Eftekhari, 2003)	Triton X-100, JBR 425	Triton X-100 (1%) foam removed 85% and 84% of PCP from fine sand and sandy-silt, respectively
Bench-scale study of surfactant foam/ bioaugmentation technology for in situ treatment of TCE*-DNAPLs (Rothmel, et al., 1998)	Steol CS-330	Injecting the foam in a pulsed operation removed 75% of the contaminant, and adding the microbes resulted in 95–99% degradation of the residual
Column tests to evaluate rhamnolipid foam-enhanced remediation of Cd and Ni contaminated soil (Wang & Mulligan, 2004)	JBR 425, Triton X-100	Foam removed 73% of the Cd and 68% of the Ni from the contaminated soil
* TCE – trichloroethylene; TCA – trichloroethane; PCE – tetrachloroethene; PAH – polycyclic aromatic hydrocarbons; HCB – hexachlorobenzene; PCP – pentachlorophenol; CGA – colloidal gas aphrons.		

Maire et al. (2015) studied the use of foam for the remediation of contaminated soil with DNAPL at the bench-scale. They showed the independence of DNAPL recovery on the type of gas in the foam by comparing the N_2 and CO_2 gases. Several authors also demonstrated the ability of DNAPL removal using surfactant foam, some of them examined foam with a solubilizing agent in shallow soils (Maire & Fatin-Rouge, 2017), others used foam as a blocking agent for confining contaminant source zone and refrain from spreading in aquifers (Portois, et al., 2018). Besides, the use of foam with polymers to enhance foam stability also attracts attention (Forey, et al., 2020). Above we mainly considered the remediation of contaminated-soil with DNAPL, and many researchers have also investigated the removal of LNAPL from aquifers (Ossai, et al., 2019).

1.6.2.2 Micro-foams for soil remediation

Micro-foams, i.e. colloidal gas aphrons (CGA), are tightly packed microbubbles with 10 to 100 μm in diameter, and they were firstly presented by (Sebba, 1971). CGAs can be formed through the mixing of surfactant solutions at a very high speed, and it consists of a gaseous inner core surrounded by a thin surfactant film, as shown in Fig. 1.14.

Mostly, surfactant CGAs were used through the flushing of contaminated soil sites (Roy, et al., 1994; Roy, et al., 1995; Roy, et al., 1995; Tao, et al., 2020). Gas content in CGAs is approximately 65-70%, and it forms a low-density liquid. The functional purpose of CGA is to reduce the interfacial tension between water and oil. At the same time, it increases viscosity forces, which tend to sweep soil contaminants.

Roy et al. (1994) reported comparisons of water flooding, a conventional surfactant solution, and CGA for oil waste cleaning experiments. All experiments were done under different flow regimes, but with the same value of residual saturations. With the results, the CGA mixture extracted 56% of oil materials,

which was higher than conventional surfactant solutions 47%, and water flooding 43%, respectively. Also, in similar experiments, the CGA suspensions were found to be more active on the washing of automatic transmission fluid (ATF oil) from the Superfund site (Baton Rouge, LA, USA) soil (Roy, et al., 1995; Roy, et al., 1994). However, it was observed that increasing surfactant concentration did not lead to an increased removal rate of oil. Moreover, during a laboratory investigation for removing naphthalene from a contaminated sample, it was found that flushing by CGA suspensions may clog up pores of the soil matrix, which may affect the overall processes.

Surfactant CGAs have potential applications on transporting and delivering treatments like microorganisms' solutes and oxygen in removing organic pollutants and heavy metal or for bioremediation of contaminated soil. However, more knowledge on the application of CGAs in soil remediation is still required (Tao, et al., 2020).

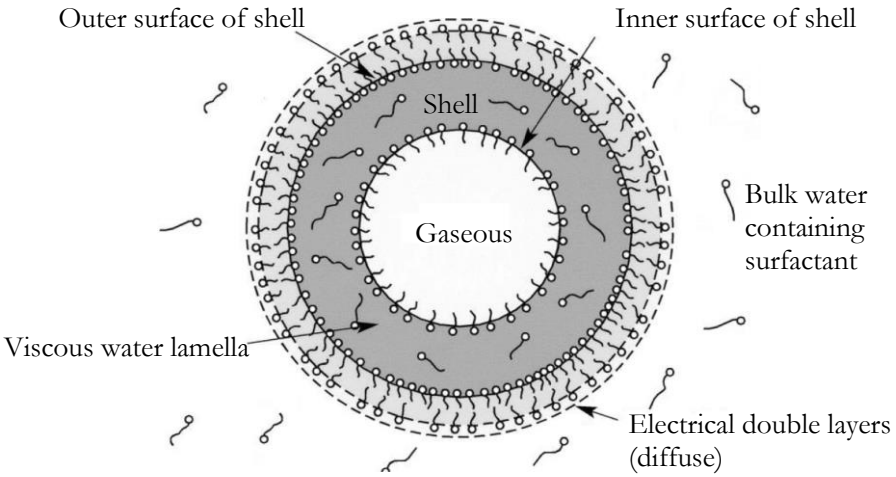

Fig. 1.14 Schematic draw of Colloidal gas aphrons (CGAs) (Pasdar, et al., 2018)

1.6.2.3 Foam as a blocking agent

Foam can also be used as a particular permeability reduction agent (i.e. blocking agent), and several investigations show promising results for this application. The application of foam for this purpose is mainly beneficial for controlling mobility in heterogeneous aquifers, in which the foam can effectively divert the flow from highly permeable areas (Lee & Heller, 1990; Bertin, et al., 1998; Kovscek & Bertin, 2003).

Bertin et al. (2017) conducted 2D laboratory experiments using foam by considering two layers of porous media with different properties. The high-permeability layer was made of sand with a grain size of 450 μm in diameter, and the low-permeability medium was made of calibrated sand with an average diameter of 140 μm. They studied foam behavior by injecting a tracer in the column. A significant reduction in water mobility was observed in the areas where the foam was present. Moreover, it was shown that the foam is more stable in the layer with higher permeability.

Portois et al. (2018 a, 2018 b) demonstrated the use of foam as a blocking agent in a laboratory-scale 1D column, as well as in a field. The investigation aimed to confine the contaminant source area using foam injection and avoid contaminant spreading in an aquifer. In laboratory experiments, they observed that the relative permeability (k_{rw}) of water was reduced by a factor of 100-1000, which was measured by injecting only water in the presence of foam. In the field, they found a reduction of k_{rw} by a factor of 1000 near the well, and it was around 100 at a distance of 1 m from the well. However, the injected foam was much weaker than those tested in the laboratory to respect the compatibility of pressure limit at shallow depth ($\leqslant$ 4 bar). They found that the foam quality increases over the distance, and also noted that the foam could expand at least 2 meters from the injection well.

Some researches were also conducted to study the impact of foam and porous media properties on the blocking ability of foams. For instance, some authors found increasing foam blocking capability with surfactant concentration above the CMC (Lee, et al., 1991; Mannhardt, et al., 2000), others reported sufficient gas mobility reduction at low surfactant concentrations (Mannhardt & Svorstøl, 2001). Pang (2010) tested the blocking ability of foam in a U-shaped sand-pack column where the foams were pre-generated using nitrogen and surfactants. Three types of surfactants, Alpha olefin sulfonate (AOS), Dodecyl dimethyl betaine (BS-12), and Sodium dodecyl sulfate (SDS), were used to generate different foams. As a result, they found an increase in foam resistance with surfactant concentration and permeability. Moreover, the maximum resistance factor ($RF = \frac{\Delta P_{foam}}{\Delta P_{water}}$, at constant flow rate) was observed at the foam quality of 85%.

Based on all these researches and the experimental studies done on foams in porous media, the blocking ability of foam and its behavior depends on surfactant type, surfactant concentration, foam quality, flow rate, and characteristics of porous media. Therefore, each site must be considered independently, depending on the field features and the purpose of using foam.

1.7. Modeling foam flow in porous media

Foam flow in porous media has been modeled mainly by two approaches, which are Local-equilibrium (empirical, semi-empirical) and Bubble population-balance models (mechanistic) (Zhang, et al., 2009; Ma, et al., 2015).

Both models were designed by modifying the parameters of Darcy's law, such as gas relative permeability (k_{rg}) and gas viscosity (μ_g); therefore, these modifications control the foam mobility in porous media. Application of these methods requires certain general agreements and assumptions, for example,

- The presence of foam does not directly modify water relative permeability and viscosity;
- The mobility of water is always controlled by water saturation, without depending on foam (Khatib, et al., 1988);

- The presence of foam reduces gas relative permeability and increases the effective gas viscosity;
- Gas mobility is the function of foam texture (Falls, et al., 1989).

Mathematically, the relative permeability and viscosity of the foam were related to each other and introduced as a mobility term of the gas-phase in Darcy's law, but physically they are divisible.

In Fig. 1.15, all known approaches for modeling foam in porous media are briefly presented.

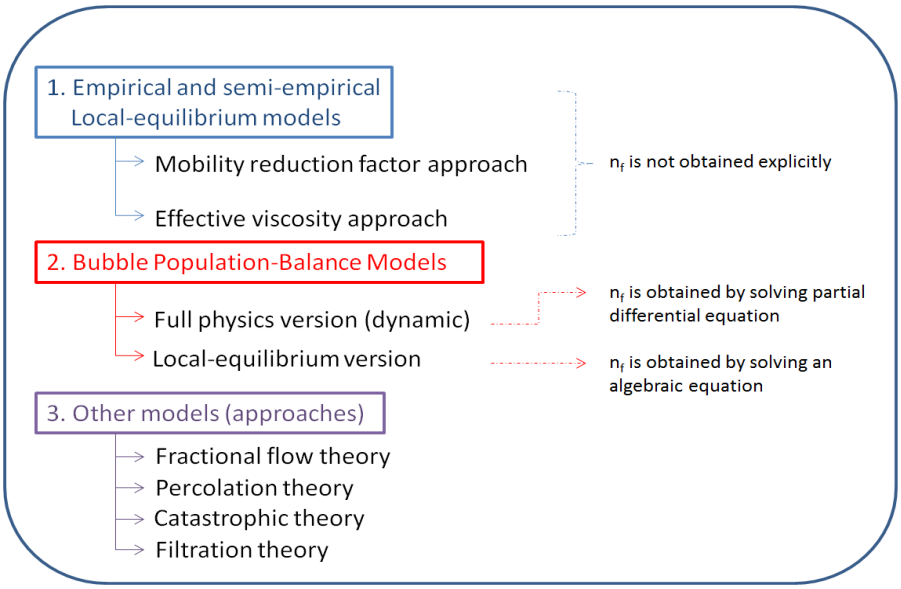

Fig. 1.15 Classification of foam flow models in porous media; n_f, foam texture (modified from (Ma, et al., 2015))

Empirical and semi-empirical, local-equilibrium foam transport models

Local-equilibrium models do not characterize the direct relationship between foam texture and gas mobility, and they are based on the adjustment of relative gas permeability or gas viscosity based on experimental laboratory results, field observations, or hypotheses. In these models, foam texture is implicit, since gas mobility is expressed as a function of flow rates and surfactant concentration. Consequently, the foam texture cannot be obtained through numerical schemes. The advantage of this model is that it requires fewer parameters and less computational time compare to the full-physics version of the bubble population model. Hence, Ma et al. (2015) tabulated the list of these empirical and semi-empirical models chronologically (see Table 1 in (Ma, et al., 2015)).

Bubble population balance models

The primary interest in developing the bubble population approach was the capability to follow the foam texture. Initially, the bubble population balance method was proposed by the analogy of mass balance equations for solutes in subsurface flow. According to the foam texture (n_f), these models evaluate or establish a ratio between the foam texture and foam mobility. Also, foam mobility is combined with other

factors, such as gas velocity, water saturation, and formation permeability. The primary works about the bubble population-balance model in porous media have started since the 1980s (Falls, et al., 1988; Patzek, 1988). The general form of bubble population-balance equation is presented as (Kovscek & Radke, 1994; Kovscek, et al., 1997):

$$\frac{\partial}{\partial t}\left[\emptyset\left(S_{gf}n_f + S_{gt}n_t\right)\right] + \nabla\cdot\left(u_g n_f\right) = \emptyset S_g\left(R_{gr} - R_c\right) + Q_b \tag{1.10}$$

$$S_g = S_{gt} + S_{gf} = X_t S_g + X_f S_g \tag{1.11}$$

where S_g is the gas saturation which includes flowing-gas saturation (S_{gf}) and trapped-gas saturation (S_{gt}); n_f and n_t are the foam texture of flowing and trapped gases, respectively; R_{gr} is the foam generation rate, and R_c is the foam coalescence rate; X_f and X_t correspond respectively to the fraction of flowing and trapped gases; and Q_b is the source-sink term for foam bubbles. Moreover, by the characterization, bubble population balance models have two versions:

1) Full-physics version (dynamic);

2) Local-equilibrium version.

The full-physics version solves the differential equation presented in Eq. (1.10) with numerical schemes to get n_f. However, solving this bubble population-balance model is expensive to reservoir simulators and poses additional numerical problems (Rossen, 2013). In addition, difficulties in practical application due to the problems caused by the estimation of certain parameters from experiments and field data. Therefore, some researchers proposed the local-equilibrium version of this model (Kovscek & Bertin, 2003; Bertin, et al., 1998; Roostapour & Kam, 2013; Li, et al., 2006; Kovscek, et al., 2010), in which the foam texture was obtained as a function of variables obtained through Darcy's law and mass-conservation equations. Local-equilibrium models are based on the assumption that the foam generation and coalescence time is relatively faster than the foam flow through porous media, thereby a dynamic equilibrium in the foam texture is achieved by equalizing the rates of local foam generation (R_g) and local foam coalescence (R_c).

Nevertheless, all these methods were developed for the oil and gas industry, in which pores of porous media are much smaller than in aquifers. Therefore, foam generation in large pore aquifers is doubtful, and the application of these models is questionable.

1.8. Upscaling techniques and upscaling of foam flow in porous media

As we have noticed from the previous sections, like different processes in porous media, foam flow in porous media can be investigated at different scales of observation (see Fig. 1.16), namely:

- Pore-scale (µm), in which the different phases fluid and solid can be distinguished;
- Local-scale (cm) or laboratory scale, in which the local average of the field scale can be studied;

- Field-scale (m) or aquifer scale, in which field-scale can be investigated taking into account heterogeneity.

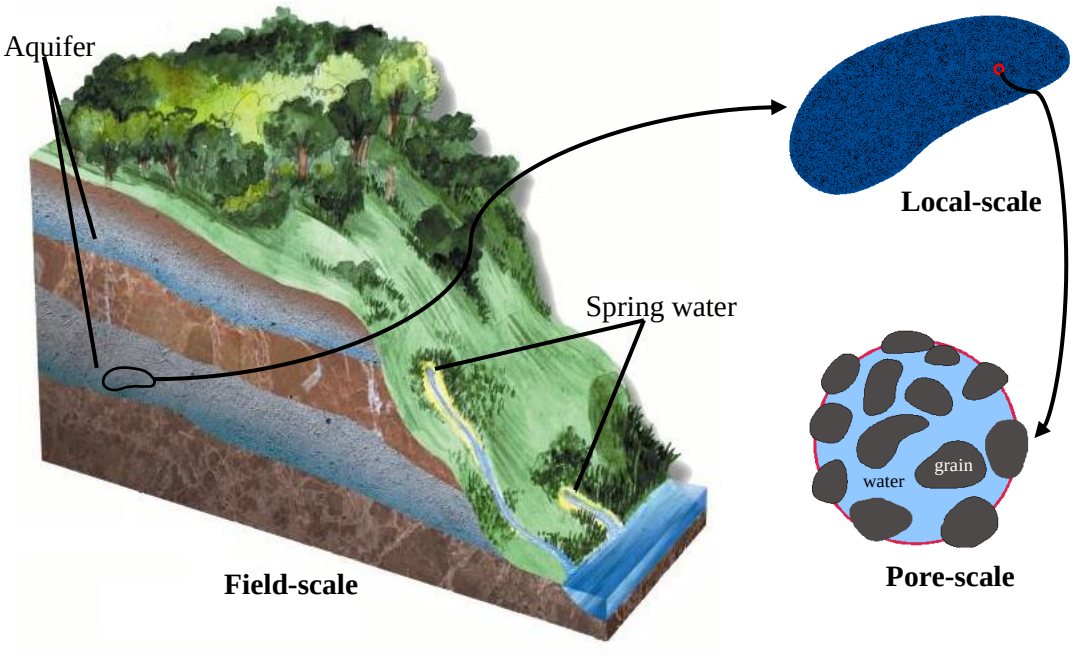

Fig. 1.16 Change of scale

The upscaling process is a fundamental procedure in which the static and dynamic characteristics of a pore-scale model should be taken into account in the local-scale model. Indeed, the direct modeling of fluid flow at the pore-scale of a porous medium sample is practically impossible due to the complexity of the pore structure and the massive demand for computing resources. Therefore, it is necessary to derive a local scale model. Moreover, the upscaling of foam behavior from the bulk-form to the laboratory-scale and the field-scale still needs to be investigated. Since the foam is an unstable system and behaves as a complex, non-Newtonian fluid, it should be carefully studied.

Upscaling and modeling the flow of non-Newtonian fluids through porous media are involved in many problems substantial to science and industry. Appreciable examples are in biological systems, oil recovery operations, food processing, cosmetics, textile, paper industries, and also in soil remediation technologies. For Newtonian fluids, the flow through porous media is modeled by Darcy's law, which has been theoretically derived from the Stokes equation via homogenization (Auriault, 1991) and the volume averaging methods (Whitaker, 1985; Whitaker, 2013). However, the filtration laws for non-Newtonian fluids are more complicated due to their complex rheology and the complex microstructure of porous media. The details on the upscaling of non-Newtonian fluids will be presented in Chapter 3.

1.9. Scope of the thesis and organization

In preceding sections, we acquired a general knowledge of bulk foam, foam flow in porous media, and its application for soil remediation purposes. We found that the selection of a foaming surfactant and its

concentration is crucial to the success of the remediation. Moreover, the selected surfactant must satisfy the biodegradability requirement and be verified for soil remediation applicability. The used gas and its fraction also play critical roles in the formation of foam and stability. We also noticed the non-Newtonian behavior of bulk foam that obeys yield stress models.

Foam can be generated in porous media, but foam generation in highly-permeable aquifers is questionable due to large pores and high permeability. Pre-generated foams can be a solution in these cases that allow foam propagation in a porous medium whose permeability is too high to allow in-situ foam generation. Therefore, we assume that foam in high permeability porous media behaves as a bulk foam when foam bubbles are much smaller than the dimensions of pores, and this assumption will be further investigated in the framework of this thesis program.

The application of surfactant foam for contaminated-soil remediation is widespread, and the properties of the foam in the field are challenging to predict due to the unknown capillary properties of the porous medium. The remediation process also relies on contamination types and other properties of the field, and the choice of the appropriate surfactant type is crucial. Moreover, the foam used must be very stable since it will be used for diverting the high-speed groundwater flow. Consequently, each contaminated site requires an individual approach to achieve significant results.

The final objective of this thesis is to improve our knowledge of the foam application capacity in highly permeable porous media for the remediation of contaminated soil. Mainly, the rheology of pre-generated foam and the behavior of foam in high permeability porous media and different capillary tubes were studied. Moreover, the upscaling of foam flow from the pore-scale to the local-scale was investigated using experimental measurements of bulk foam rheology as input parameters.

In chapter 2, the behavior of pre-generated foam in highly permeable porous media is studied with a special focus on the impact of the foam bubble size, which is related to the choice of the foam generator and the porous medium's permeability. The used surfactant solution and the gas were also examined for further experiments. The experimental results were discussed, and foam behavior in high permeability porous media was characterized.

Chapter 3 focuses on the upscaling of foam flow in porous media using the results of bulk foam rheology as input parameters. The rheology of bulk foam and foam flow through glass beads packings were analyzed for several foam qualities. Upscaling was accomplished by solving a pore-scale problem on different periodic unit cells. The outcomes were compared with the experimental study of foam in 1 mm glass beads packing.

Chapter 4 considers the rheology of pre-generated foam at high shear rates using capillary tubes of different diameters and made of three different materials. The results of foam rheology were analyzed and compared with the outcomes of foam flow in porous media, as well as those obtained through the rheometer.

Chapter 5 provides general conclusions and perspectives from these studies.
Chapters 2, 3, and 4 were written in the form of scientific papers and provide a supplementary literature survey with details.

Chapter 2

Experimental study of non-Newtonian behavior of foam flow in highly permeable porous media

2.1. Introduction

In the following, the paper that has been published in the journal Industrial & Engineering Chemistry Research will be presented. In this work, we studied the behavior of pre-generated foam in highly permeable porous media. The foam characterization depending on the surfactant concentration and the gas type was carried out.

Foam is a two-phase system where gas bubbles are dispersed in a continuous liquid phase. The liquid phase in the foam is generally an aqueous solution containing a surfactant, which plays a crucial role in stabilizing the liquid films between bubbles.

Foam flow in porous media was firstly studied for a variety of applications in the production of petroleum and natural gas, especially in enhanced oil recovery (EOR). At the end of the last century, foam injection also started to be used as a soil remediation technique to remove non-aqueous phase liquids (NAPL) from aquifers (Hirasaki, et al., 1997). The primary use of foam in soil remediation operations is to control the permeability of porous media. By blocking highly permeable zones, foam injection allows remediation agents to be transported from high to low permeable zones in aquifers. Since the fraction of the surfactant used in foam injection is low, this is a better solution than surfactant flushing technology (Mulligan & Eftekhari, 2003) from economic and environmental points of view. However, the differences in context between oil reservoirs and aquifers are significant. For instance, porous media in oil reservoirs are mainly low permeable and consolidated, while polluted aquifers are mostly unconsolidated and highly permeable. Oil reservoirs are subject to much higher pressure and temperature conditions than aquifers. Because of these differences, in situ foam generation in aquifers is questionable, and successfully applying EOR models to highly permeable porous media is doubtful. Additionally, most studies presented in the literature concern low permeability media for EOR applications.

Our understanding of foam flow behavior in porous media is involved, due to the complex behavior of foam and apparent discrepancy in foam studies. For instance, Raza and Marsden (1967) explored pre-generated fine-textured foam flow in four different Pyrex tubes, with radiuses varying from 0.25 to 1.50 mm. They noticed the non-Newtonian shear-thinning behavior of foam with foam quality from 70% to 96%. Moreover, foam at low flow rates exhibited a linear behavior while at high flow rates, a non-linear behavior was obtained. They pointed out an increase in the apparent foam viscosity with both tube radius and foam quality. Hirasaki and Lawson (1985) experimentally measured the apparent viscosity of pre-generated foam in smooth capillaries and developed a mathematical model. They showed shear-thinning behavior in which the dependence of the apparent foam viscosity was proportional to -1/3 power of velocity. Falls et al. (1989) extended these results by examining the apparent foam viscosity in homogenous bead packs, where they demonstrated the shear-thinning behavior of foam flow in porous media. They indicated that the apparent gas viscosity depends on foam bubble size in porous media. Several other authors have considered the existence of yield stress based on a threshold pressure gradient,

which depends on the types of gas and surfactant, surfactant concentration, and petrophysical properties of porous media (Ransohoff & Radke, 1988; Dicksen, et al., 2002). Persoff et al. (1989) studied foam flow through sandstone by co-injecting gas and surfactant solution at elevated pressure. They summarized foam flow in porous media as rheopectic, with Newtonian behavior for the liquid phase and pseudoplastic behavior for the gas flow, at steady-state. Rossen (1991) investigated the rheology of strong foam at steady state by limiting-capillary-pressure concept based on the working hypothesis of Persoff et al. (1989) and Ettinger and Radke (1989). He found that foam behaves as a Newtonian fluid in steady 1D radial flow in which capillary pressure is nearly constant at the value of "limiting capillary pressure," despite that foam with uniform texture behaves as a non-Newtonian fluid. He pointed out the necessity of a quantitative understanding of the mechanisms that control bubbles and rheology for designing foam processes. Moreover, he concluded that the study of the relative permeability and yield stress fluid viscosity individually is debatable, since assumptions on relative permeability strongly affect the foam viscosity. Patzek and Koinis (1990) showed foam's shear-thickening behavior in field cases where the apparent viscosity of steam foam was decayed as much as the foam flowed far from the injector wells. Based on the experimental results of Alvarez (1998), Rossen and Wang (1999) considered bubbles roughly the same size as pores in low-quality regimes, where bubbles smaller than the pore size were expected to grow rapidly to pore size due to gas diffusion between bubbles. As a result, they modeled foam with a fixed bubble size as a Bingham plastic. Vassenden and Holt (2000) presented a model based on the relative permeability concept and validated it by experimental data. They demonstrated a transition of foam flow behavior from Newtonian to shear-thinning, according to increases in the gas flow rate. Alvarez et al. (2001) conducted experimental studies in several types of sandstones and sands for which the permeability ranged from 0.3 to 3 Darcy. They pointed out the dependence of apparent foam rheology on foam quality (foam gas volume fraction, f_g) where foam flowed as a shear-thinning fluid in the low-quality regime and as a shear-thickening fluid in high-quality regimes. Furthermore, in previous studies, the yield stress behavior of stationary lamellae was studied on the pore-scale level (Falls, et al., 1989; Rossen, 1990; Cohen, et al., 1997; Nguyen, et al., 2004). Some authors also considered yield stress as a fixed parameter depending on the ratio of surface tension to pore throat, considering the porous media as a bundle of capillary tubes (Rossen & Wang, 1999; Balan, et al., 2011). Others (Zitha & Du, 2010; Simjoo, et al., 2012; Simjoo & Zitha, 2020) presented foam in low permeability consolidated porous media as a yield stress fluid, which was also described by a threshold pressure (Chen, et al., 2005). For example, Simjoo and Zitha (2020) studied N_2 foam flow in a Bentheimer core in which foam was generated in situ using alpha-olefin sulfonate ($C_{14\text{-}16}$, AOS) surfactant in 0.5 M NaCl brine. The foam behavior with a quality of 91% was analyzed through X-ray Computed Tomography and the results of 6 pressure transducers along the 38.4 cm long core. They observed two foam displacement fronts: 1) the forward primary foam front which was characterized by a low mobility reduction factor (MRF, a ratio of measured pressure drop of foam flow to the corresponding pressure drop for water flow) and high overall liquid

saturation (S_w); 2) the backward secondary front with high MRF and more moderate S_w. This phenomenon explained by the transition of foam from weak to strong state at a liquid saturation of S_w=0.25. They found that yield stress was nearly equal to zero for weak foam, and when S_w is lower than 0.25 (i.e., strong foam), yield stress increased significantly. Nevertheless, in most foam-modeling studies in porous media, foam was described as a pure power-law fluid without considering yield stress (Friedmann, et al., 1991; Kovscek, et al., 1997; Bertin, et al., 1998; Myers & Radke, 2000; Kam, 2008; Kovscek, et al., 2010; Ashoori, et al., 2012).

Recently, Osei-Bonsu et al. (2016) studied pre-generated foams via two sintered glass discs (with the pores size distribution of 16-40 μm and 40-100 μm) to investigate the link among foam quality, apparent viscosity, bubble size and cell permeability in a 2D Hele-Shaw cell with dimensions of 31 × 20 × 0.6 cm. They showed increasing of foam viscosity with foam quality (between 81% and 99%), which was obtained with the fixed gas rate at 10 mL/min and varying the liquid flow rates. The independence of pressure drop from the gas flow rate was assumed based on the outcomes of Osterloh and Jante (1992), which commonly occurs in high-quality regimes. Moreover, they pointed out a decrease of apparent foam viscosity with increasing flow rate for qualities of 93% and 98%. Shojaei et al. (2019) studied pre-generated foam using sintered glass discs (with the pores size distribution of 16-40 μm) like Osei-Bonsu et al. (2016) injected in a Vosges sandstone fracture replica with a length of 26 cm and a width of 14.8 cm. The mechanical and hydraulic apertures were 0.86 mm and 0.5 mm, respectively. They examined the apparent viscosity as a function of foam quality with the same technique as (Osei-Bonsu, et al., 2016). Moreover, the foam with a foam quality of 85% was examined at different flow rates, and all results were compared with the findings of Osei-Bonsu et al. (2016). They observed the shear-thinning behavior of foam with yield stress in which the power-law index was -0.41 compared to the index value of -0.27, found by Osei-Bonsu et al. (2016) for the Hele-Shaw cell. They also observed a decrease of apparent foam viscosity with increasing foam quality that was contrary to the findings of (Osei-Bonsu, et al., 2016). Nevertheless, they admitted that the rheology of bulk foam is not identical to the one observed in porous media.

Most of the studies we reviewed were performed on consolidated media with permeable porosity lower than soil remediation cases, either in capillary tubes or in Hele-Shaw cell at the pore-scale. To the best of our knowledge, the study of foam behavior in highly permeable aquifers is still lacking, mainly when pore size greatly exceeds the bubble size. So for this paper, we studied foam behavior in high permeability porous media with a special focus on the impact of the foam bubble size and quality and the porous medium's permeability. Our goals were two-fold: to characterize the surfactant solution and the gas and to investigate the pre-generated foam flow's experimental behavior. We achieved this by investigating the rheology of foam flow depending on bubble and grain sizes (permeability) in a highly permeable unconsolidated porous medium, performing laboratory experiments in 1D columns.

2.2. Theoretical considerations

Three major foam generation mechanisms are identified at the pore-scale in porous media: snap-off, leave-behind, and lamella division (Kovscek & Radke, 1994). Depending on the generation processes, flow rate, permeability, compressibility, and the length of the system, foam may be classified as "weak" or "strong" (Ransohoff & Radke, 1988; Rossen, 1990), which can be described by a transition from weak continuous gas foam to strong discontinuous gas foam with a particular transition zone (see Fig. 2.1). Weak foam usually occurs through leave-behind processes, while strong foams are generated by all three mechanisms. As previous studies have stated (Rossen & Gauglitz, 1990; Dicksen, et al., 2002; Ransohoff & Radke, 1988; Gauglitz, et al., 2002; Rossen, 1990), foam is generated when the pressure gradient exceeds a critical pressure gradient denoted ∇P^* (Fig. 2.1). This pressure gradient depends on a minimum capillary number for entry into pores by the snap-off mechanism.

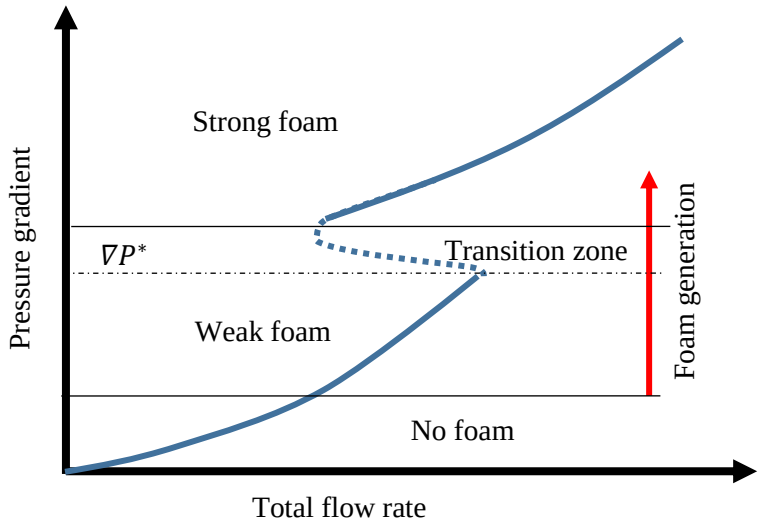

Fig. 2.1 Sketch of foam formation in porous media, inspired by (Gauglitz, et al., 2002)

Several authors (Rossen & Gauglitz, 1990; Dicksen, et al., 2002; Ransohoff & Radke, 1988; Tanzil, et al., 2000) calculated the minimum capillary number to generate foam in porous media. By examining a variety of porous media, Tanzil et al. (2000; 2002) calculated the minimum capillary number N_{cL}=2, with the capillary number N_{cL} defined as

$$N_{cL} = \frac{\Delta P}{\gamma}\sqrt{\frac{K}{\emptyset}} \tag{2.1}$$

where γ (N/m) is gas-liquid interfacial tension, K (m^2) is the permeability of the porous column, $\emptyset$ (-) is porosity, and ΔP (Pa) is the measured pressure drop along the column. ΔP depends on the foam quality, which is the ratio of the gas volume on the total volume and can be written as

$$f_g = \frac{Q_G}{Q_G + Q_L} \tag{2.2}$$

where Q_G (mL/min) and Q_L (mL/min) are the volumetric gas and liquid flow rates, respectively. According to foam quality values, bulk foam can be dry (f_g>99%), wet (64%<f_g<99%), or considered as a bubbly liquid (f_g<64%) (Langevin, 2017).

In porous media, Osterloh and Jante (1992) identified two specific foam-flow regimes in steady-state flow in sand-pack experiments, depending on foam quality. The permeability of the sand-pack was 6.2 Darcy in which nitrogen and surfactant solutions were simultaneously injected, in order to study the behavior of the foam generated in situ. They observed a low-quality regime (wet), in which the pressure gradient was constant regardless of the liquid flow rate, and a high-quality regime (dry), in which the pressure gradient was independent of the gas flow rate. These two regimes were separated by a transition foam quality f_g^*, which depended on the porous media's characteristics, types of surfactants, and gas (Alvarez, et al., 2001). When f_g was lower than f_g^*, foam flowed at the low-quality regime. If foam quality was higher than f_g^*, foam flowed at the high-quality regime. The existence of the transition foam quality became evident when the limiting capillary pressure was reached, as that depends on foam stability in porous media.

Foam flow in porous media is also affected by gravity. The competition between gravity and capillary forces may lead to different flow configurations. This competition is quantified by the Bond number, which is calculated using the following equation (Ransohoff & Radke, 1988):

$$N_{Bo} = \frac{\Delta\rho g R_g D}{\gamma} \tag{2.3}$$

where $\Delta\rho$ (kg/m^3) is the gas-liquid density difference, g (m/s^2) is the gravitational acceleration, R_g (m) is the grain radius, D (m) is the porous column diameter.

The model used in this work to fit the rheological behavior of foam is the Herschel-Bulkley (H-B) model (Herschel & Bulkley, 1926) presented as follows:

$$\mu_{app}(\dot{\gamma}) = a\left|\dot{\gamma}_{eq}\right|^{n-1} + \frac{\tau_0}{\left|\dot{\gamma}_{eq}\right|} \tag{2.4}$$

where τ_0 (Pa) is the yield stress, a (Pa.s^n) is the consistency index, n is the flow index. The Herschel-Bulkley flow index n controls the overall behavior of flow, where 0< n<1 for a shear-thinning fluid, n=1 corresponds to the Bingham fluid model (Bingham, 1916), and n>1 gives a shear-thickening fluid.

2.3. Foam characterization

Since foam is a two-phase system affected by the fractions of gas and surfactant solution, the first step of the investigation was to choose the surfactant and the gas for foam-generation purposes. Careful selection of chemical surfactants was necessary, keeping in mind potential environmental effects since some synthetic surfactants are toxic and poorly biodegradable.

2.3.1. Selection of a surfactant and the surfactant concentration

After considering several studies on chemical surfactants (Mao, et al., 2015), taking account of biodegradability in soils (Tuvell, et al., 1978; Talmage, 1994; Arndt, 2007), market accessibility (Cserháti, et al., 2002), and field tests for soil remediation purposes (Svab, et al., 2009), $C_{14\text{-}16}$ alpha-olefin sulfonate (AOS, Solvay Novecare) was chosen as the most suitable surfactant to generate foam. AOS is an anionic surfactant that is historically the oldest and most commonly used surfactant. It is gentle on the skin and is used in detergents, shampoos, and ordinary bath soaps. The surfactant used contained 40 wt% of active materials in an aqueous solution. To find its critical micelle concentration (CMC), surfactant solutions with different concentrations were examined through a drop-shape analyzer (DSA-100S, KRUSS). The surfactant solution was prepared by using demineralized/degassed water. The measurements were conducted by the pendant drop method (Stauffer, 1965). The results are presented in Fig. 2.2. We found that the CMC and the corresponding surface tension were 1.8±0.1 g/L and 36±1 mN/m, respectively.

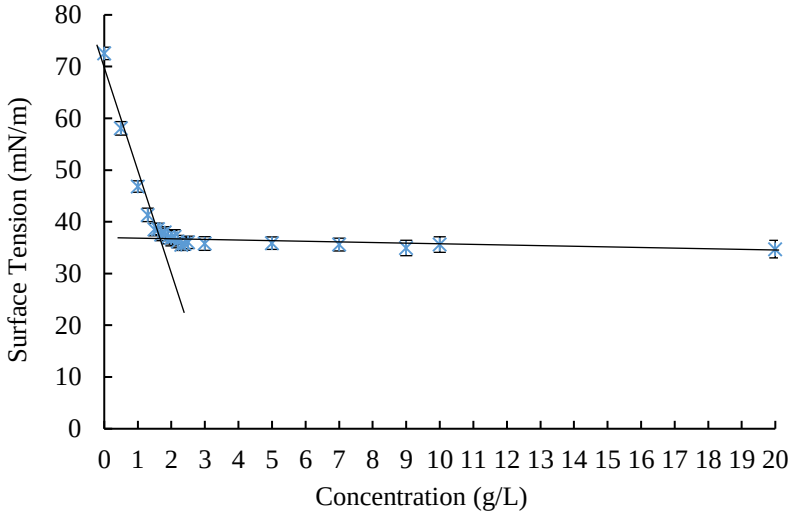

Fig. 2.2 Surface tension as a function of surfactant concentration

We also carried out foam stability experiments using a dynamic foam analyzer (DFA-100, KRUSS) to find the best surfactant concentration for foam formation in terms of stability and foamability. We analyzed the stability of bulk foams generated with different surfactant concentrations (multiples of CMC) by measuring the half-life time and also the foamability. Gaseous nitrogen with 99.98% purity (Air Liquide) was used to generate bulk foam. The investigation methodology we adopted followed Yoon et al. (2019). The results of the test presented in Fig. 2.3 show an increase in foam stability (half-life time) until the concentration of two times CMC that corresponds to the maximum value of half-life time. This phenomenon, i.e. the increasing of foam stability with surfactant concentration, was also observed in previous studies (Simjoo, et al., 2013; Belhaij, et al., 2014; Verma, et al., 2018). However, the values of half-life time dropped after 2 × CMC and were almost constant when surfactant concentration increased further. This means that an optimum concentration exists, which corresponds to the maximum foam

stability. Our conclusion can also be confirmed by the results of Farzaneh and Sohrabi (2015), in which they pointed out the presence of the optimum surfactant concentration for some surfactants in terms of stability. The foamability results also demonstrated increasing behavior with concentration up to the highest value of foamability, which was obtained at three times CMC. Nevertheless, it decreased sharply and followed the trend of half-life time results for higher values of concentration. Consequently, we observed that the dependence of foam stability and foamability on CMC is rather similar. The decrease in foamability at high concentrations can be explained by the achievement of surfactant solubility (Tan, et al., 2005).

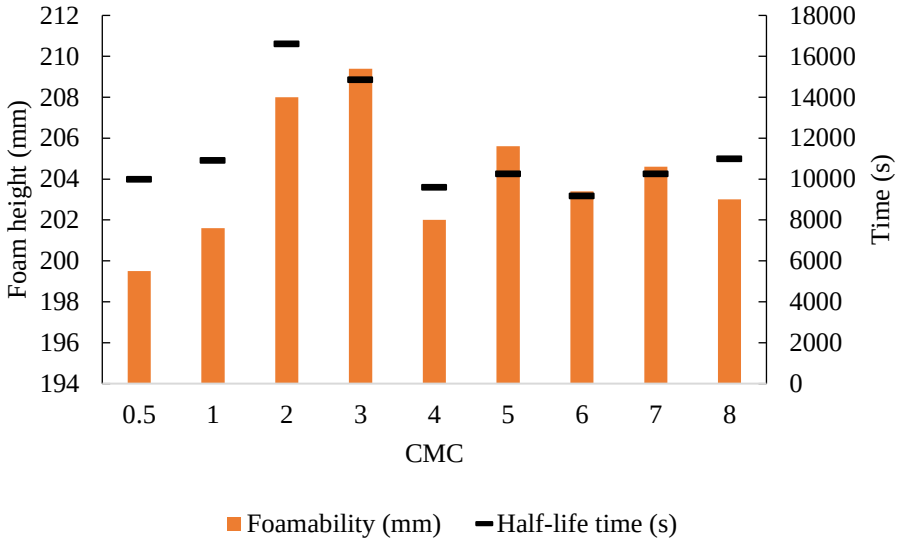

Fig. 2.3 Foam stability and foamability measurements as a function of concentration as multiples of CMC

Foamability, stability, and adsorption issues in the presence of oil have been studied in the literature (Dong, et al., 2010). However, a thorough review of these studies is beyond the scope of this paper, where foam is never in contact with oil. Indeed, the surfactant concentration was chosen to be four times CMC with a margin to ensure not only stability and foamability but also high surfactant concentration in case of adsorption (Wang, et al., 2012) processes in soil (Paria, 2008), although high surfactant concentration may tend to delay the biodegradability process, which is important from the point of view of environmental use.

2.3.2. Gas selection

Gas is the second principal component of foam. We investigated 99.98% pure N_2 and CO_2 gases (Air Liquide) to select the gas for further experiments. We examined stability and foamability using the DFA-100 foam analyzer, where the concentration of the surfactant solution was taken equal to 4 × CMC. The methodology was the same as previous experiments (Yoon, et al., 2019). Fig. 2.4 shows the results of

bulk foam experiments in terms of half-life time and foamability for CO_2 and N_2 gases. Foam generated using N_2 is more stable and has higher foamability than CO_2 foam.

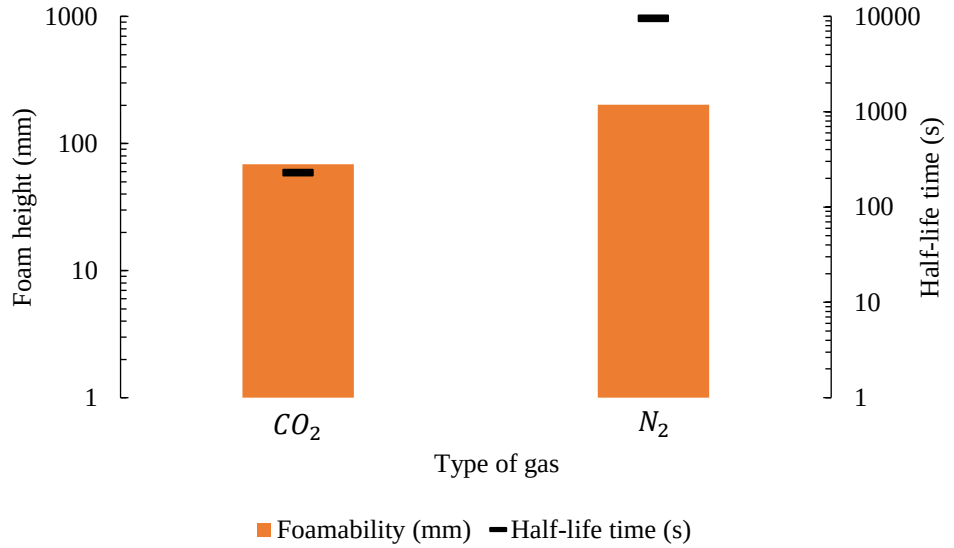

Fig. 2.4 Foam stability and foamability of CO_2 and N_2 gases

Since CO_2 is about 55 times more soluble in water than N_2 gas (Sander, 1999), the foam generated using N_2 is much more stable, as confirmed by the work of Farajzadeh et al. (2009). As a result, we chose N_2 gas for the next experiments.

2.4. Experimental details

2.4.1. Materials

The characterization presented in the previous section demonstrated the consequences of the choices of surfactant and gas used for foam generation. AOS with a concentration of 4 × CMC and N_2 gas were selected for the next experiments. The porous media considered here were unconsolidated, homogenous packings of calibrated glass beads (GB), and quasi-homogeneous silica sand (BR37), provided by Sigma-Aldric and Sibelco, respectively. The grading characteristics of the sand were as follows: the uniformity coefficient (Cu) is 0.72, the curvature coefficient (Cc) is 0.98, the effective size (d_{10}) and the mean grain size (d_{50}) are 0.180 mm and 0.135 mm respectively. The measured properties of all porous media are presented in Table 2.1. Unlike natural soil, porous media made by packing of glass beads prevent adsorption and ensure homogeneous pore distributions. By testing various sizes of calibrated GB, we analyzed the effect of porous media grain size and consequently, pore size, bubble size, or permeability on the foam's rheological behavior.

Table 2.1 Properties of porous columns (Porous Media)

Porous media	Mean grain size diameter, d (mm)	Porosity, $\emptyset$ (%)	Permeability, K (D)	Pore Volume, PV (mL)	Mean pore radius, R_{eq} (µm)
Sand BR37	0.135	38±1	7±1	51±2	11.5
GB 1	1	36±1	830±10	181±2	133.5
GB 2	2	35±1	3017±10	181±2	257.9
GB 4	4	40±1	11032±10	185±2	467.2
GB 8	8	41±1	41125±10	191±2	886.4

The porosity of the medium was determined by measuring the mass of the main column before and after the water saturation processes. The permeability was calculated by relating measured values of the pressure difference for different water flow rates to the corresponding imposed flow rates through Darcy's law given by (Darcy, 1856):

$$u = \frac{Q}{S} = -\frac{\boldsymbol{K}}{\mu}.\nabla P \tag{2.5}$$

where $\boldsymbol{K}$ (m^2) is the intrinsic permeability tensor ($\boldsymbol{K} = K\boldsymbol{I}$ for an isotropic porous medium), μ (Pa.s) is the dynamic viscosity of the fluid, ∇P (Pa/m) is the pressure gradient linearly dependent on Darcy velocity u (m/s). Q and S correspond respectively to the flow rate and the cross-section surface of the sample. The mean pore radiuses were calculated using the following equation proposed by Kozeny (1927), which was derived from Darcy's equation (Eq. (2.5)) and Poiseulle's law (Sutera & Skalak, 1993) using a model porous medium composed of a bundle of parallel capillaries of the identical radius.

$$R_{eq} = \sqrt{\frac{8K}{\emptyset}} \tag{2.6}$$

In the preceding equation, R_{eq} (m) is considered as the mean pore radius.

2.4.2. Experimental setup

The setup used to conduct the foam flow experiments is shown in Fig. 2.5. In this setup, N_2 and AOS-based surfactant solutions were co-injected into the foam-generator column to generate foam. Then the foam was injected into the main column packed with glass beads of the different sizes (Table 2.1).

An El-Flow Select F-201CV mass flow controller (Bronkhorst) 0.16-10 mL_n/min (±0.5 % reading plus ±0.1 % full scale) was used to ensure stability in the gas flow and control the flow rate from the gas bottle. A DCP50 dual cylinder positive displacement pump (Strata) with ±1.5 % setting accuracy was used to inject the surfactant solution at a constant flow rate. The setup consisted of two porous columns, the first "foam generator" (FG) and the second "main" (M) made of transparent PVC (polyvinyl chloride) tubes 10 cm and 40 cm long, respectively. The inner diameter of the columns was 4 cm. A Rosemount 2051 differential pressure transmitter (Emerson), with a range 0-623 mbar (±0.666 mbar at the maximum value)

or 0-2500 mbar (±7 mbar at the maximum value), was used to measure the pressure drop along the main column. The mass of the effluent was measured by a STX 6201 electronic balance model (OHAUS) with

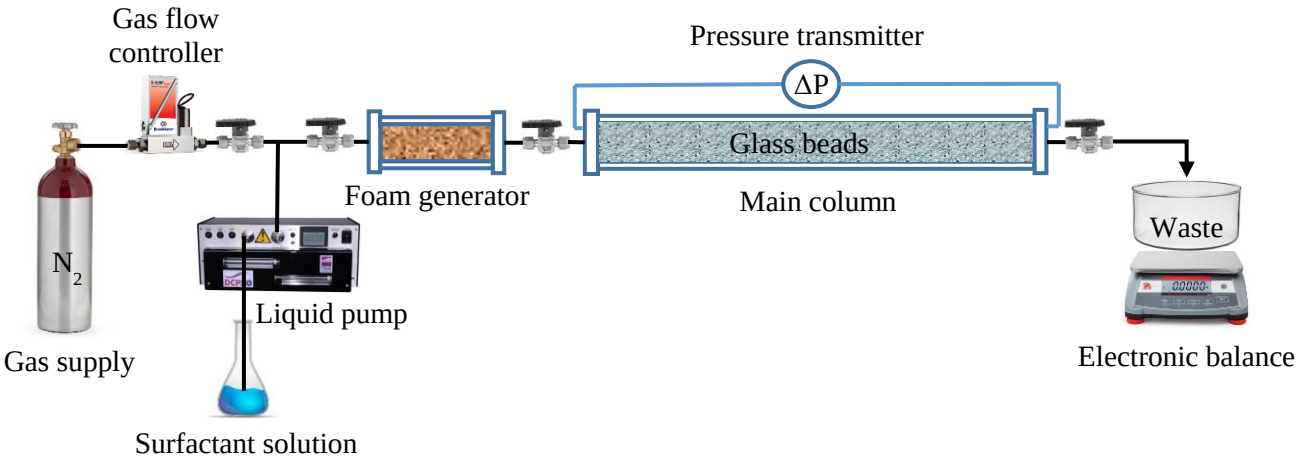

a minimum of 0.1 g readability. The maximum pressure limit of the experimental setup was six bars, which was controlled by the pump's pressure sensor.

Fig. 2.5 Schematic of the experimental setup used to conduct foam flow experiments

Two different foam generators were used. The first pre-generator column was packed with BR37 fine sand, and metallic grids with 42 µm cell size were used to curb the porous media. The second generator column was prepared using 1 mm glass beads. Glass beads with the diameters being tested (d=1, 2, 4, and 8 mm) were used to pack the main column, and metallic grids with 150 µm cell size were used to hold all the glass bead packings. The same foam generator column was used during all the experimental procedures. However, a new main column was prepared for each experimental cycle corresponding to different bead sizes.

2.4.3. Experimental procedure

After packing both columns and checking for leakage, the columns were flushed with CO_2 gas to remove air from the porous samples. Then the columns were saturated with degassed, demineralized water in a vertical position with a 5 mL/min flow rate to dissolve any CO_2 and saturate the columns thoroughly without trapping the gas. In total, around three pore volumes (PV) of demineralized/degassed water were injected. Columns were weighed before and after the water saturation step to measure the pore volume and porosity. The permeability measurements were carried out by injecting demineralized, degassed water with different flow rates, and measuring the pressure differences. Permeability was calculated using Darcy's law (Eq. (2.5)). To satisfy the porous medium's surfactant adsorption capacity (Simjoo & Zitha, 2020), the columns were flushed with 3 PV of surfactant solution. The permeability and porosity of the generator column (fine sand) were rechecked. After checking the porous media parameters, the surfactant solution and the nitrogen gas were co-injected into the generator column to produce foam. 5 PV of fluids

were co-injected to obtain a stable foam from the pre-generator, which was chosen considering the work of (Simjoo & Zitha, 2020). The total flow rate (Q_t=$Q_G + Q_L$) was increased step by step from the minimum (0.2 mL/min) to the maximum (3 mL/min) technically possible values. The proportion of liquid/gas was adjusted simultaneously for each value of the total flow rate (Q_t) in order to keep the foam quality constant. The stabilization time for each experimental cycle was 7 PV. Each experiment was duplicated by at least one descending flow rate experiment. The foam flow experiments were analyzed using the flow rate and pressure drop measurements along the column. The liquid effluent mass was measured using an electronic balance to determine the change of surfactant solution saturation inside the main column (S_w). In addition, each porous column was weighed after the first drainage to establish the initial surfactant solution saturation (S_{wi}). All experiments are carried out at 20°C and atmospheric pressure.

2.4.4. Strategy

First, all the porous media were studied to find the transition (f_g^*) between the two foam flow regimes (low and high-quality regimes) where foam flow behavior was examined at a fixed total flow rate (2 mL/min) by varying the foam quality. The goal of this experiment was to define the transition zone, which would prevent instability during the rheological studies. After determining f_g^*, the rheology of foam in porous media (confined foam) was studied at a given foam quality. Table 2.2 shows the experimental conditions for all the rheological studies. Next, to see the effect of bubble size on foam viscosity, the rheology of two different foams generated through the packing of fine sand and 1 mm GB generators were studied in the main column filled with 1 mm GB at f_g=85%. Note that the foam bubbles were considered to be the same size as the pores of the generator column, according to the model of (Rossen & Wang, 1999).

Finally, the foam generated using the generator column was investigated in four types of glass bead packings at a fixed f_g=85% by varying the total flow rate (0.2 – 3 mL/min). The main idea was to study how foam rheology depends on grain size, and consequently pore size. We analyzed the apparent foam viscosity μ_{app} given by Eq. (2.7) that was obtained from the main column using Darcy's law (Eq. (2.5)) and fitted it to a rheological model of a yield stress fluid.

$$\mu_{app} = \frac{K\Delta P}{uL} \tag{2.7}$$

Table 2.2 Experimental conditions

Foam generator material	Main column material	Foam quality (f_g)
Sand BR37	GB 1	85%
	GB 2	85%
	GB 4	85%
	GB 8	85%
GB 1	GB 1	85%

2.5. Results and Discussion

2.5.1. Foam generation in highly permeable porous media

In situ foam generations (gas and surfactant co-injection) in the foam generator column after the injection of 0.6 PV are shown in Fig. 2.6, for different soil types and flow rates. Fig. 2.6a shows the process during the first drainage experiment in the foam generator column filled with fine sand, where the total flow rate was equal to 2 mL/min. The piston-like displacement of foam in the porous pre-generator was observed with a vertical transition zone.

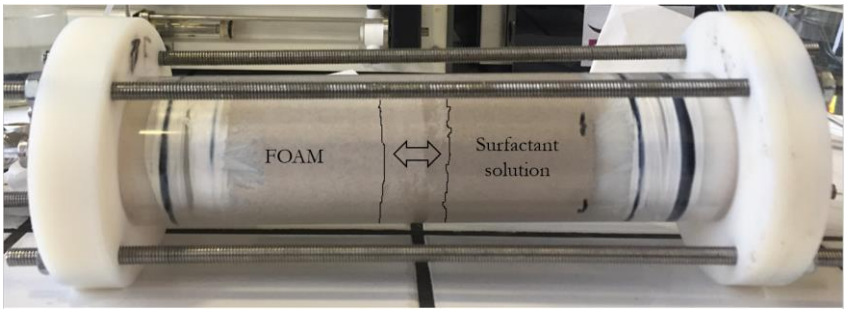

a)

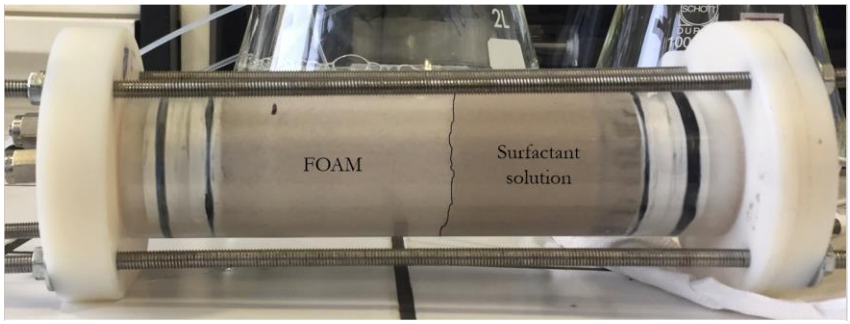

b)

c)

Fig. 2.6 In situ foam generation in foam generator column (after 0.6 PV injection):

a) sand BR37, at Q_t=2 mL/min, b) sand BR37, at Q_t=8 mL/min, and c) 1 mm glass beads, at Q_t = 2 mL/min

This transition zone occurs due to the transition from "weak foam" to "strong foam," which is explained by the foam generation process in porous media (see Fig. 2.1). At this total flow rate, the foam generation mechanism is called "snap-off" and depends on local dynamic capillary pressure. However, when the total flow rate increases further, the pressure drop jumps abruptly to much higher values due to foam generation mechanisms in porous media. Hence, the generation of strong foam requires a high-pressure gradient or depends on injection rates where the "lamella division" mechanism can play a crucial role. The lamella division mechanism concerns foam lamella that already exists and increases the number of bubbles. For this, it is necessary that the static lamellae in the pore throats be displaced by a sufficient pressure gradient. To check this fact, we conducted another drainage experiment by increasing the Q_t. In this experiment (see Fig. 2.6b), the total flow rate was four times higher (8 mL/min) than the previous one, and no transition zone was observed (pure piston-like displacement). Nevertheless, during the experiment, the pressure gradient increased strongly, and we were forced to stop the experiment due to the pressure limitation of the experimental setup. After that, we carried out the co-injection process at Q_t=2 mL/min in the foam generator column packed by 1 mm glass beads. The drainage of the surfactant solution at 0.6 PV is presented in Fig. 2.6c. The border between the foam and the saturated zone is shown clearly to have a given slope due to the weak foam and gravity effects. Indeed, the Bond number (Eq. (2.3)) was nearly ten times larger for the porous pre-generator made by the packing of 1 mm glass beads vs. the one made by sand.

Once the foam generation processes in porous media were analyzed, the pre-generated foam was injected into the main column. Fig. 2.7 shows the front of the foam flow in the main columns packed with 1 mm glass beads, where the foam was pre-generated in the fine sand (a) and in the 1 mm glass beads packing (b), respectively.

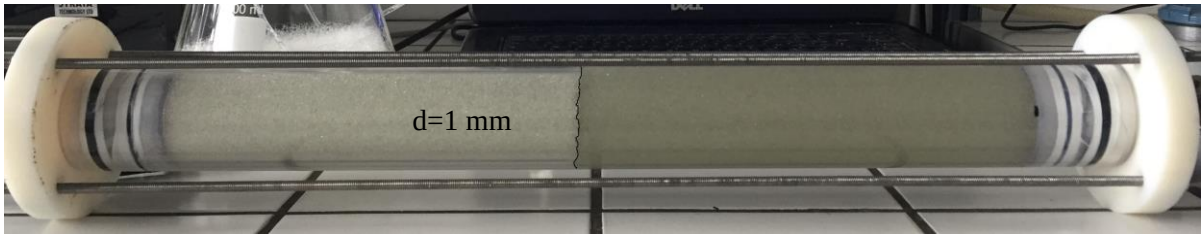

a)

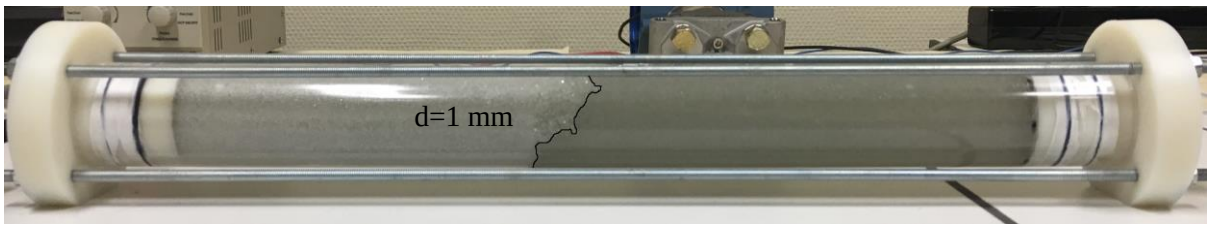

b)

Fig. 2.7 Injection of the pre-generated foam in the main columns at Q_t=2 mL/min: foam generated a) in the fine sand b) in 1 mm glass beads (t=0.5 PV)

If we visually compare the two columns, foam generated in fine sand features strong foam behavior, which has a sharp displacing front. However, the foam produced using a 1 mm glass bead pre-generator has a transition zone with a particular slope, which could be explained by the presence of weak foam at the interface. These circumstances occurred when the pressure drop was lower than ∇P^*in the interface; hence, the weak foam was formed. Since all experimental conditions were identical except for the pre-generator columns, the values of capillary and Bond numbers and the bubble size may explain this phenomenon.

Fig. 2.8 shows the values of capillary and Bond numbers for different foam-generator and main-column systems, which were calculated at the steady-state. Since the value of the Bond number is the same and exceeds one (N_{Bo}=10.9), the capillary forces are small in relation to gravity forces. However, the values of the capillary number in the main column, for Q_t=2 mL/min, were 94 and 79.9 for the foam generated by sand and 1 mm glass beads, respectively. Whereas, the mean size of the bubble in the sand foam generator was 11 times smaller than foam made in 1 mm glass beads if we assume that the bubbles were roughly the same size as the pores (see Table 2.1). Therefore, the foam produced using a sand generator was more viscous, and we can confirm that the variation of foam viscosity depends on the bubble size. In addition, several authors experimentally showed that apparent foam viscosity has a strong dependence on the texture or bubble size at the pore scale (Hirasaki & Lawson, 1985; Falls, et al., 1988; Roof, 1970; Ma, et al., 2012; Ramadan, et al., 2003). Since most of the investigations carried out were for applications in the oil industry, where pore sizes are much smaller than in aquifers, bubble sizes have been considered to be roughly equal to pore size due to the coarsening of small bubbles because of gas diffusion. However, note that coarsening of bubbles in aquifers needs much more time because of large pore sizes.

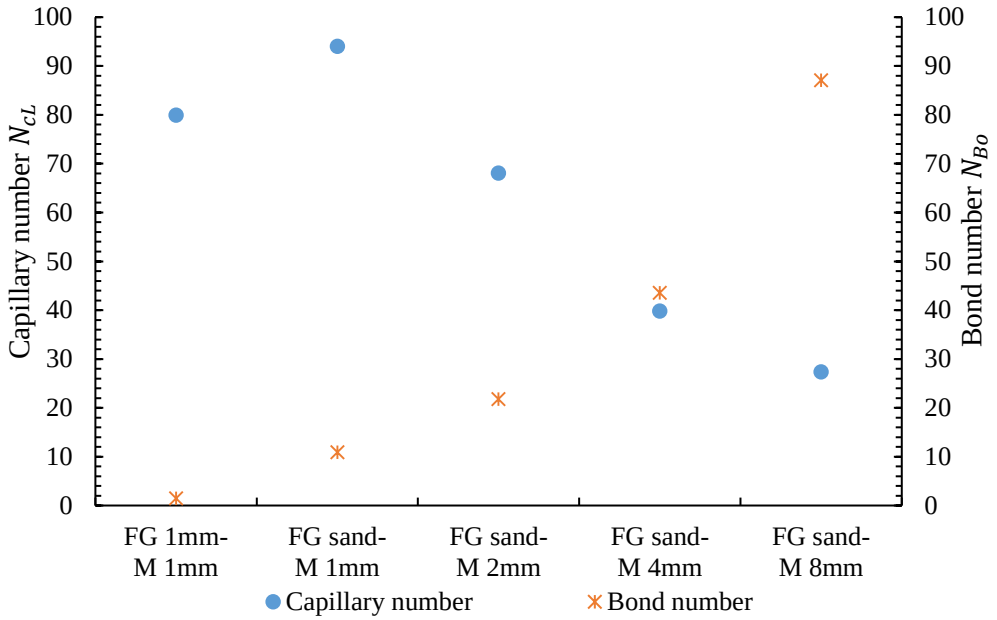

Fig. 2.8 Capillary and Bond numbers for different foam generators and main columns (f_g=85%, Q_t=2 mL/min)

As mentioned above, pre-generated foam in the fine sand was also studied in 2 mm, 4 mm, and 8 mm glass beads packings. The same behavior as in 1 mm glass beads packing was observed in the column packed with 2 mm glass beads. However, with 4 mm glass beads, we observed a foam front with a particular inclination. This slope at the foam front was even more significant in 8 mm glass beads (data not shown). These phenomena can be explained by increasing gravity forces with the grain size. As is shown in Fig. 2.8, values of the Bond number are more critical than capillary numbers for 4 and 8 mm glass beads. We conclude that gravity forces become more dominant than combined viscosity and surface forces.

Additionally, after the first drainage experiment, we determined the initial saturation (S_{wi}) of the surfactant solution for each porous column (Table 2.3). The S_{wi} increased with grain size. Since foam gravity forces were more important with the 4 and 8 mm glass beads (see Fig. 2.8), the effect of gravity-driven drainage increased the liquid saturation of porous media when the pore sizes became larger. We also observed the dependence of S_{wi} on the foam generator (bubble size), which increased with bubble size.

Table 2.3 Initial surfactant solution saturation after the first drainage (f_g=85%, Q_t=2 mL/min)

Foam generator	Main column	S_{wi} (%)
Sand BR37	GB 1	2.82
	GB 2	2.99
	GB 4	4.10
	GB 8	5.58
GB 1	GB 1	4.10

The previous analysis of the mass balance using measurements of the effluent mass as a function of time did not lead to notable differences in production mass for various flow rates. Therefore, we tested an alternative procedure to measure S_w only for the 1 mm GB packed pre-generator and main column. The mass of the main column was measured after each experiment by simultaneously closing the inlet and outlet tubes. Fig. 2.9a shows the saturation of the surfactant solution as a function of the total flow rate. No particular trend on the change of S_w with Q_t was observed, and the average S_w was equal to 4.5%±1.2%. However, a decrease in S_w was observed below 1 mL/min, followed by a slight increase and stabilization above 2 mL/min. Therefore, liquid saturation cannot be considered independent of the flow rate in high permeability porous media, which is contrary to the findings of Ettinger and Radke (1989) and others (Persoff, et al., 1989). Those studies were carried out comparatively in low permeability sandstones, and the saturation was found to be 30-40% regardless of the foam quality. However, Fig. 2.9b shows the linear decrease of S_w with increasing of foam quality that we observed, and that is trivial due to the reduction of the liquid fraction. Hence, in highly permeable porous media, S_w falls with foam quality.

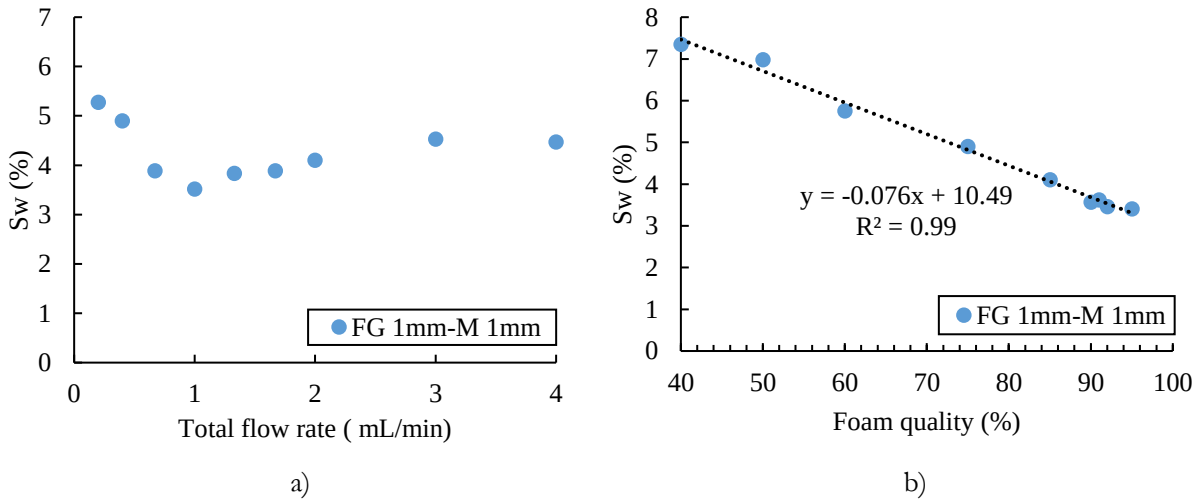

Fig. 2.9 Sw as a function of a) total flow rate at fixed foam quality (f_g=85%), b) foam quality at Q_t=2 mL/min

We also observe that S_w is lower than the fraction of initially injected liquid. This phenomenon can be explained through Fig. 2.10, which plots effluent volume as a function of PV. The gas breakthrough occurred after the injection of 1.44 PV of pre-generated foam, which corresponds to a change of slope in the figure (dashed line). This means that we recover 1.44 times more liquid than the initial volume in the pores of the main column. Since the liquid phase is continuous and S_w in the main column is three times lower than the injected foam quality, we assume that the liquid phase flows faster during the foam formation in porous media, thereby decreasing the liquid saturation in the main column. When the foam was fully formed and stabilized, the change of effluent weight corresponded to the mass of the injected fluid. This phenomenon resembles the drainage effect of foam due to gravity, in which accumulation of liquid can be observed on the bottom.

On the other hand, from the equation of the trend of the first half of the curve, we observed that the effluent flow rate was 12% lower than Q_t, which can also be explained from the compressibility of gas volume. Thus, the compressibility of gas delayed the breakthrough time. However, it should be noted that the cumulated effluent volume was 224.3 mL when the breakthrough occurred, which is greater than the main column PV by 18.5%. Consequently, the liquid saturation in high permeability porous media is much lower and depends on the flow rate, compared with porous media with low permeability.

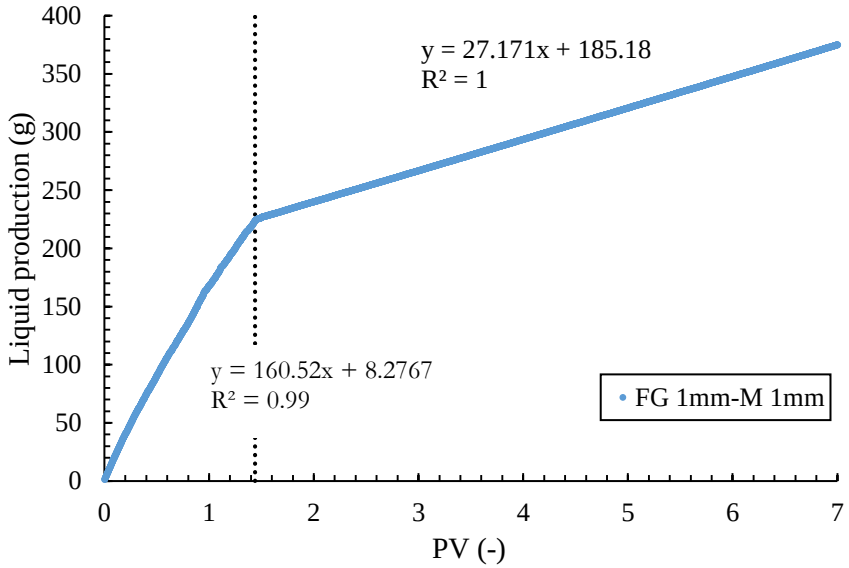

Fig. 2.10 Liquid volume of effluent as a function of PV for the 1 mm GB packed pre-generator and the main column at Q_t=3 mL/min (f_g=85%)

2.5.2. Effect of foam quality on foam flow behavior

We determined the transition foam quality between low-quality and high-quality regimes in order to select the unique foam quality for further investigation of the rheology of foam.

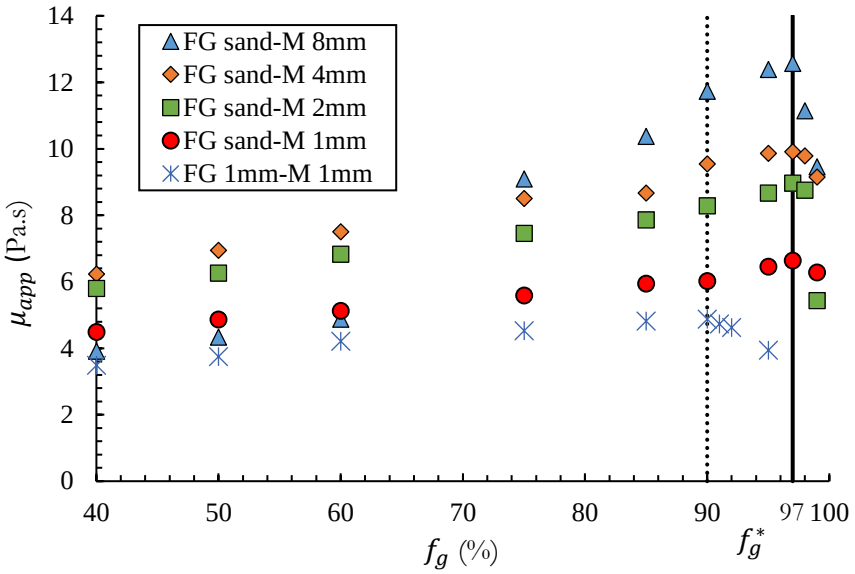

Fig. 2.11 Apparent foam viscosity as a function of foam quality at the fixed total flow rate (Q_t=2 mL/min)

Fig. 2.11 shows the change of the apparent foam viscosity calculated using Darcy's law as a function of foam quality. In this figure, the colored dots represent the results of foam generated by the sand-filled foam generator, and star dots are the result of the foam made through the 1 mm glass beads generator. By comparison of the results for foam generated by the sand column, we see that the apparent viscosity of foam increases with the size of the grain diameter. The vertical lines spot the transition foam quality f_g^*, which is the limit between low-quality and high-quality regimes. The transition foam quality (f_g^*) is 97% for all glass beads and is independent of the grain size (and porous medium permeability). As we observed in the figure, the apparent viscosity of the foams increases with the foam quality up to the f_g^*. Osei-Bonsu et al. (2016) also found an increase in the apparent foam viscosity with the foam quality through the Hele-Shaw cell. However, they did not notice f_g^* even when f_g=99%, which showed the nature of the bulk foam. Alvarez et al. (2001) showed a high f_g^* value (97%) for a foam generated through bronze wool in a high-permeability medium. By highly permeable medium, they insinuated sand-pack with a permeability of 3.1 Darcy. They demonstrated that the f_g^* increases with permeability by taking into account the hypothesis that the bubble size is fixed at the low-quality regime (Rossen & Wang, 1999). Lower capillary pressures in bigger pores accompanied the idea of high values of f_g^*, hence showed a much higher f_g^* in the sandpack.

If we consider that the size of the bubbles can be fixed in a low-quality regime, the results are consistent with the model of Rossen and Wang (1999), where the apparent viscosity only depends on the porous medium's structure and surface tension. However, we admit that the size of the bubbles can be changed due to the diffusion effect at low flow rates. Moreover, the decrease of apparent viscosity for foam quality

lower than 75% for 8 mm GB can be explained by the transition of foam to the state of bubbly liquid (Ramadan, et al., 2003).

On the contrary, foam generated using 1 mm GB and injected into the same porous medium has a lower transition foam quality (90%), which could be explained by the difference in bubble size of pre-generated foams. As previously mentioned, the mean bubble size generated in the sand is smaller than the pore size of the glass beads. Therefore, if the equivalent pore size is larger than the equivalent bubble size, the foam can behave as bulk foam. These circumstances are close to the foam flow in fractures, where the f_g^* for the limiting capillary pressure was predicted to be as high as 99.95% (Pancharoen, et al., 2012). Consequently, we can conclude that f_g^* depends significantly on bubble size (structure of the foam generator).

2.5.3. Effect of foam bubble size on foam rheology

In Fig. 2.12, the results of apparent viscosity as a function of flow rate are compared in 1 mm GB main column, in which foam was pre-generated in the sand (circular points) and 1 mm glass beads (star points). Fig. 2.12 shows non-Newtonian, shear-thinning behavior of foam flow for the foam pre-generated in the sand column. With low flow rates, the apparent viscosity of foam generated by 1 mm glass beads is much smaller than the viscosity for foam made by sand.

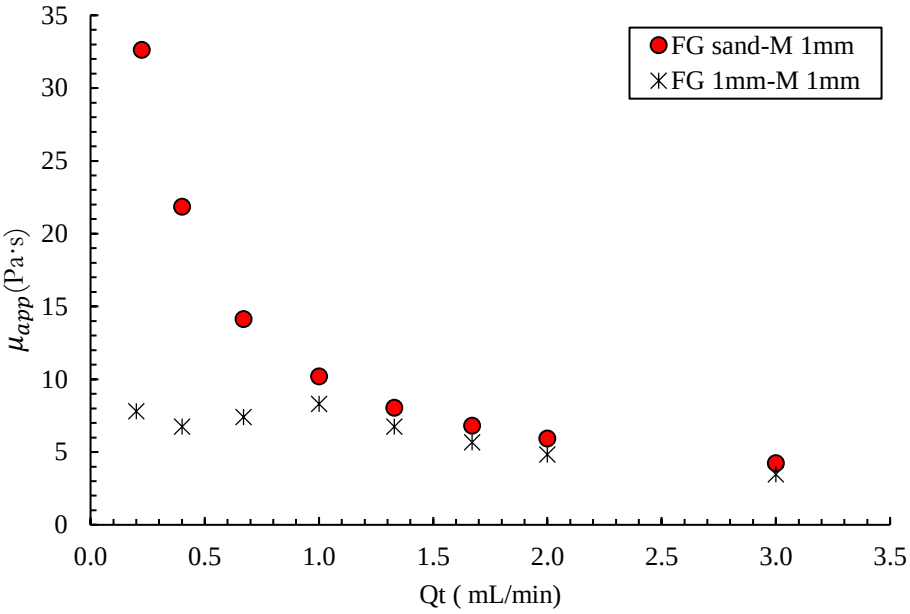

Fig. 2.12 Apparent viscosity of foam versus total flow rate in 1 mm glass bead main column (f_g=85 %)

We observe almost linear variation for apparent viscosity at low flow rates and a gradual transition to shear-thinning behavior when the flow rates are increased (1 mL/min and above) for the foam generated through the FG 1 mm. This behavior is similar to the study of Vassenden and Holt (2000), in which they

demonstrated a model for Newtonian behavior of foam flow at low flow rates and transition to shear-thinning behavior while increasing flow rate. However, their investigation was based on the study of Falls et al. (1989), in which the existence of yield pressure drop stops lamellae flow if the pressure gradient is insufficient to move them, so they demonstrated the transition from Newtonian to shear-thinning behavior by a change from the limiting capillary pressure (Khatib, et al., 1988) to the limiting pressure gradient regime by increasing the rate.

First, for foam formed in the FG 1 mm, we assumed at that this state the foam flow was related to the yield stress: when the flow needs a particular pressure gradient to move out. This phenomenon was also observed during the experiments. At low flow rates, the effluent flow was stopped and resumed with a specific sequence in order to obtain a particular strength to withstand the yield stress. Second, the foam produced through the sand generator had smaller bubbles than pores of a 1 mm GB pack (bulk foam behavior). This means that no foam generation and destruction occur, except coalescence, the coarsening of bubbles due to the gas diffusion from small to big bubbles (Ostwald ripening, (Voorhees, 1985)). However, for foam that is pre-generated and injected in 1 mm GB columns, foam generation, and destruction processes could also take place since the bubble size is assumed to be roughly the same size as the pore.

Fig. 2.13 shows the values of N_{cL} as a function of the flow rate, which is calculated using Eq. (2.1). The capillary number increased with the flow rate and was higher for foam generated in the sand. The changing trend of the foam data produced with 1 mm GB had a particular shift in the region of 1 mL/min. The transition zone between weak and strong foams explains this.

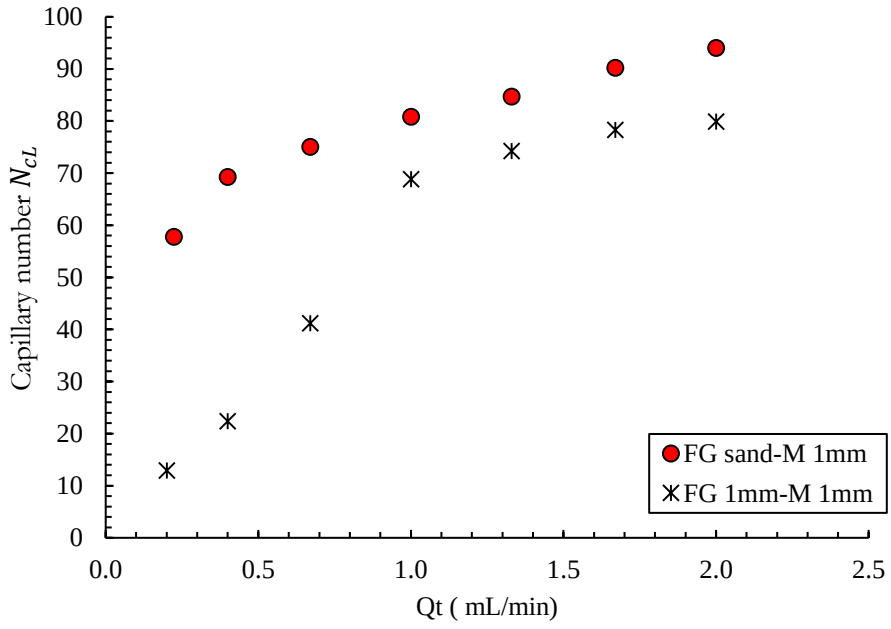

Fig. 2.13 Capillary number as a function of flow rates in 1 mm GB main column

Consequently, these results can also be explained by foam-generation processes, which depend on the flow rate or pressure drop. As shown in Fig. 2.1, strong foam formation occurs at the particular pressure drop, despite the minimum ∇P^*. A specific transition zone exists in terms of ∇P between the generation of weak and strong foams.

2.5.4. Effect of grain size (permeability) on foam rheology

In Fig. 2.14, the apparent viscosity as a function of the total flow rate is plotted for all GB sizes. The apparent foam viscosity in porous media increases with the size of grain diameter and decreases when the flow rate increases. Therefore, shear-thinning foam-flow behavior can be observed. To investigate the foam rheology, the apparent viscosity (μ_{app}) results were considered in terms of the equivalent shear rate ($\dot{\gamma}_{eq}$) using the following equation (Darby, et al., 2001):

$$\dot{\gamma}_{eq} = \frac{4u/\emptyset}{R_{eq}} \tag{2.8}$$

where u (m/s) is the superficial velocity of the fluid (foam) in the porous columns.

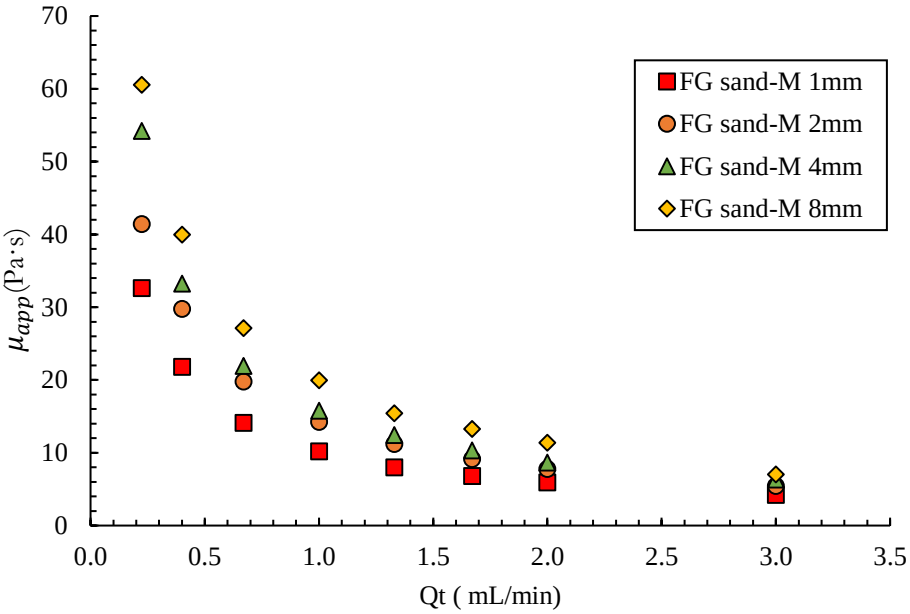

Fig. 2.14 Apparent viscosity versus total flow rate for d=1, 2, 4 and 8 mm glass beads using sand foam generator (f_g=85%)

From Eq. (2.8) and considering the variations of permeability (K) with the pore size (R_{eq}) and porosity ($\emptyset$) given in Table 2.1, it is evident that the shear rate becomes lower when porous media permeability increases for a particular flow rate value.

Fig. 2.15 shows the apparent viscosity results with fitting curves versus the equivalent shear rate. Contrary to Fig. 2.14, for a constant shear rate, the μ_{app} of foam decreases with increasing grain size (permeability). As the same foam was studied with different sizes of glass bead packings made with identical material, the only distinction between the main columns was grain size, consequently, pore size. This phenomenon can be attributed to the ratio of bubble size to pore size. For instance, if we assume that foam bubble size of foam is roughly equal to the pore size of the foam generator and believe that it does not change (hypothetically) during the experiment, the number of bubbles in the pore of 1 mm, 2 mm, 4 mm and 8 mm GB packings will be equal to 11, 22, 40 and 77, respectively. Consequently, friction between bubbles and porous media geometry decreases with increasing bubble numbers per pore.

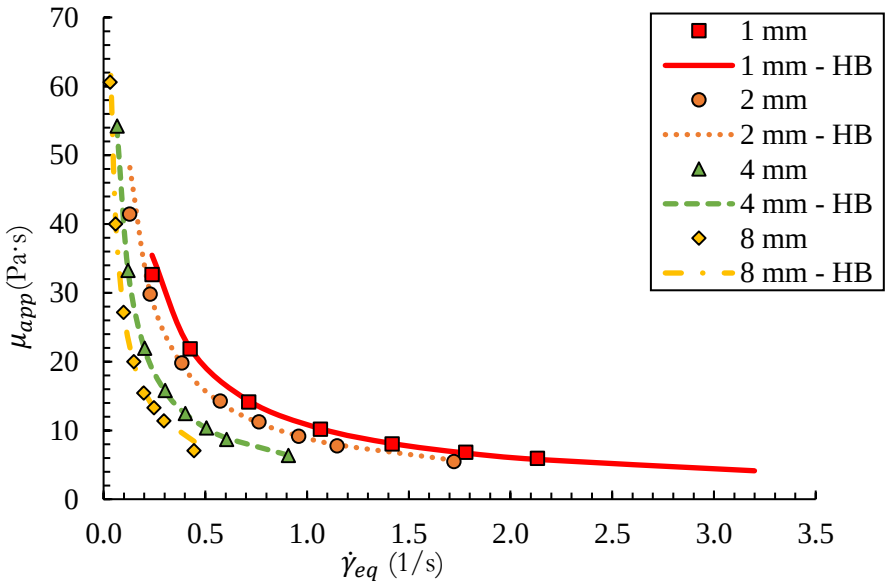

Fig. 2.15 Apparent viscosity as a function of shear rate for d=1, 2, 4 and 8 mm GB and sand foam generator

As can be seen, the experimental results fit the Herschel-Bulkley model very well (Eq. (2.4)). The corresponding fitting values for glass beads are listed in Table 2.4.

Table 2.4 Fitting parameters for H-B model

Grain size diameter (mm)	1 mm	2 mm	4 mm	8 mm
n (-)	0.68	0.66	0.54	0.39
τ_0 (Pa)	7.72	5.83	3.09	1.44
a (Pa.s^n)	2.96	2.97	3.00	3.00
R^2	0.99	0.95	0.99	0.99

The results presented in Table 2.4 show that foam is a yield-stress fluid and that yield stress values, $\tau_{0,}$ decrease with increasing grain size (permeability). The yield stress fluid index n is less than one, which

indicates that in the conditions of our experiments, the foam has a shear-thinning fluid behavior. We also observe that n decreases with increasing glass bead size.

2.6. Conclusions

This work presents a study of foam flow in high permeability porous media. Column experiments were conducted to study the behavior of pre-generated foam in high permeability porous media. Foam generation in packed fine sand and 1 mm glass beads were analyzed to study the effect of bubble size on the apparent foam viscosity. The impact of foam quality on the apparent foam viscosity, with a fixed flow rate, was examined to distinguish low and high-quality regimes. The rheology of foam with 85% foam quality was studied for different glass beads sizes. We drew the following conclusions:

- The foam generator plays a crucial role in foam displacement in porous media. Indeed, the pre-generation of foam in a less permeable column than the main column strengthens the apparent foam viscosity and foam stability. This phenomenon may contribute to the bubble size since the viscosity is higher for a foam containing smaller gas bubbles.
- The liquid saturation in high permeability porous media is much lower and depends on the flow rate compared to porous media with low permeability.
- Foam generated in packed fine sand has a higher foam quality transition value than foam generated in packed glass beads. However, identical foam quality transition values were obtained for all glass bead sizes for foam generated through fine sand packing. Transition foam quality was, therefore, independent of the porous medium's permeability for highly permeable porous media when the bubbles were smaller than the pores. The transition foam quality was lower for foam flow with an equivalent bubble and pore size.
- Foam in high permeability porous media was found to behave as a yield stress shear-thinning fluid regardless of porous medium grain size. The rheological behavior of foam is well fitted with the Herschel-Bulkley model. It was also shown that the apparent foam viscosity in GB packings (main column) increased with the diameter of the glass beads used to pack the main column for a given total flow rate. Hence, we propose considering foam as a yield stress fluid in highly permeable porous media where foam bubbles are much smaller than pores. When the bubbles are the same size as the pores, the foam behaves like a Newtonian fluid at low flow rates and exhibits a shear-thinning fluid behavior by increasing flow rates.

Chapter 3

Experimental and numerical upscaling of foam flow in highly permeable porous media

3.1. Introduction

In the following, the paper that has been recently published in Advances Water Resources journal will be presented. In this work, the upscaling of foam flow from pore to Darcy scale was studied using the results of bulk foam rheology as input parameters. The results were compared with the outcomes of foam flow in porous media that were obtained in Chapter 2.

Foam is a two-phase system where gas bubbles are dispersed in the continuous liquid phase. The liquid phase in foam is generally an aqueous surfactant solution that plays a crucial role in stabilizing the liquid films between bubbles by increasing the surface tension.

Foam is used in a wide variety of industrial applications due to its mechanical behavior combined with its sizeable specific area relative to the density (Prud'homme & Khan, 1996). For instance, foam in the oil industry can be used as a drilling fluid, as a mobility-control agent in enhanced oil recovery processes (Chen, et al., 2014), in matrix-acidization treatments (Rossen & Wang, 1999), and in gas-leakage prevention (Bernard & Holm, 1970). In soil remediation processes, foam can be used as a sweeping pollutant fluid (Hirasaki, et al., 1997), as a fluid that transports soil-cleaning additives or gases (Maire, et al., 2019; Choi, et al., 2009). Moreover, in ordinary life, foam can be found in many food and cosmetic products.

The mechanical behavior of bulk foam is complicated due to elastic, plastic, and viscous properties. Therefore, their complexity is analyzed using rheology (Coussot, 2005; Larson, 1999; Macosko, 1994). Many authors have experimentally studied the rheology of bulk foam in the last sixty years (Cohen-Addad, et al., 2013; Denkov, et al., 2009; Hohler & Cohen-Addad, 2005; Katgert, et al., 2013; Kraynik, 1988; Dollet & Raufaste, 2014; Khan, et al., 1988; Herzhaft, 1999; Denkov, et al., 2005). In most of the studies, the bulk foam was highlighted as a yield-stress fluid, and the majority of the results are commonly well fitted by the Herschel-Bulkley law. For instance, Khan et al. (1988) investigated bulk foam through a rheometer with parallel-plate geometry. The geometry was covered with sandpaper to eliminate the wall slip velocity. The average diameter of foam bubbles was 65 μm, as measured by an optical method. They demonstrated the existence of a yield stress for foams with 92%, 95% and 97% of gas fractions (f_g, foam quality), with increased yield stress with f_g.

A full understanding of foam flow in porous media is hindered due to the complex behavior of foam associated with the complex microstructure of porous media. There are also apparent contradictions in the conclusions of the studies on foam flow presented in the literature. For instance, some authors showed Newtonian (Persoff, et al., 1991) foam flow behavior in porous media, others shear-thinning (Hirasaki & Lawson, 1985; Falls, et al., 1989), a mixture of Newtonian and shear-thinning (Vassenden & Holt, 2000) or related to foam quality (Alvarez, et al., 2001). Hirasaki and Lawson (1985) reported non-linear behavior in foam when flowing through a smooth capillary tube and pointed out the impact of foam

texture (bubble size) on apparent foam viscosity. Shear-thinning behavior of foam flow in homogenous bead packs was shown by Falls et al. (1989). Rossen and Wang (1999) modeled foam as a Bingham plastic flowing in sandstones. They assumed bubble size was fixed and roughly equal to pore size at low-quality regimes. Some authors also considered the presence of yield stress based on a threshold pressure gradient, which was linked with the types of gas and surfactant, surfactant concentration, and petrophysical properties of porous media (Rossen & Gauglitz, 1990; Dicksen, et al., 2002; Ransohoff & Radke, 1988; Gauglitz, et al., 2002; Omirbekov, et al., 2020 a). However, in most of the foam modeling investigations in porous media, foam was characterized as a pure power-law fluid without assuming yield stress (Friedmann, et al., 1991; Kovscek, et al., 1997; Bertin, et al., 1998; Myers & Radke, 2000; Kam, 2008; Kovscek, et al., 2010; Ashoori, et al., 2012). Recently, Aranda et al. (2020) experimentally found the shear-thinning behavior of foam when studying the influence of permeability on the apparent foam viscosity in highly permeable porous media (Aranda, et al., 2020).

Several foam-modeling techniques have been developed since the 1980s, to understand and predict the complex behavior of foam flow in porous media (Ma, et al., 2015). Ma et al. (2015) provided a complete overview of existing methods for modeling foam in porous media. They categorized the modeling techniques into three groups depending on implicit or dynamic foam textures: local-equilibrium models, population-balance models, and others. They also indicated the possibility of using all models for direct incorporation into reservoir simulators based on material balance and Darcy law. They highlighted some studies on the upscaling of foam from laboratory-scale to field-scale in which the upscaling problems were pointed out due to entrance and end effects in laboratory core experiments.

On the other hand, a link between pore or bubble scale (discontinuous) physics and Darcy-scale (continuum) models is missing. This link is often ascertained through a variety of upscaling approaches (Berryman, 2005). For instance, Darcy's law is obtained from the creeping incompressible flow of a Newtonian fluid via the volume-averaging method with a no-slip boundary condition at the liquid-solid interfaces (Quintard & Whitaker, 1993; Quintard & Whitaker, 1994). In this method, intrinsic permeability is calculated as a function of closure variables for a given geometry (porous media) (Whitaker, 1999). However, upscaling is still a challenge for non-Newtonian fluids, which are described by non-linear partial differential equations. There are very few experimental, numerical, or analytical studies on the upscaling of the non-Newtonian fluids flow in porous media. Several authors theoretically/numerically investigated upscaling power-law fluids (Idris, et al., 2004; Wang, et al., 2014; Woods, et al., 2003; Orgéas, et al., 2006), viscoelastic fluids, yield-stress fluids, or considered the case of generalized non-Newtonian fluids (Orgéas, et al., 2007). Therefore, the upscaling of foam flow in porous media is still questionable (Ma, et al., 2015), especially in soil remediation, where the permeability of porous media is considerably high. Some authors also empirically proposed a Darcy-scale equation for non-Newtonian fluids (Larry, et al., 1986; Chauveteau, 1982; Chevalier, et al., 2013; Castro, 2019). Put

simply, the extension of the Darcy scale equation for yield-stress fluid in anisotropic porous media is very complex and still open.

To our knowledge, the modeling of non-Newtonian fluids, especially yield-stress fluid flow in porous media, has received less attention due to strong coupling between the porous medium and the fluid's rheology. Most of the previous studies on foam in porous media were related to the oil industry, where bubble size was considered to be roughly equal to the pore sizes. However, in soil remediation cases, the porous medium is highly permeable and consists of large pores, and there the bubbles can be much smaller than the characteristic length in porous media.

Consequently, the main objective of this study was to show whether foam flow in highly permeable porous media can be deduced from the bulk foam behavior and if we can consider foam as a single-phase yield-stress fluid. We also aimed to characterize the rheological behavior of bulk foam experimentally and to scale-up analytically and numerically the foam flow from pore to laboratory-Darcy scale.

3.2. Theoretical considerations

One of the important characteristics of foam is its foam quality, which is the ratio of the injected gas volume to the total liquid and gas volume, and can be expressed as

$$f_g = \frac{Q_G}{Q_G + Q_L} \tag{3.1}$$

in which Q_G (mL/min) and Q_L (mL/min) are the volumetric gas and liquid flow rates, respectively. The sum of Q_G and Q_L provides the value of total flow rate Q_t. According to the value of the gas fraction, bulk foam can be dry (f_g>99%), wet (64%<f_g<99%), or considered as a bubbly liquid (f_g<64%) (Langevin, 2017). Moreover, foam bubble shape can be transformed from spherical to polyhedral by increasing the gas fraction (Kovscek & Radke, 1994). In porous media, Osterloh and Jante (1992) distinguished two particular foam flow regimes depending on foam quality in sand-pack experiments at steady-state. They found a low-quality regime (wet), in which the pressure gradient was constant regardless of the liquid flow rate, and a high-quality regime (dry), in which the pressure gradient was independent of the gas flow rate. A transition foam quality (f_g^*) divides these two regimes, and depends on porous media characteristics, types of surfactants, and gas (Alvarez, et al., 2001).

Newtonian-fluid flow in porous media can be considered as models of flow through a bundle of tortuous capillary tubes which have uniform radii, R. By the theory of Kozeny-Carman (Kozeny, 1927; Carman, 1997), tortuosity in capillaries is defined as the ratio between the effective length (L_{eff}) i.e. length of the tortuous capillaries and the lengths of equivalent straight capillary tubes (L). Hence, it was assumed that fluid entering into tortuous capillaries flows faster than the fluid flowing through the equivalent straight capillaries in order to reach to the end of the tube at the same time. Using this concept, flow in porous media can be presented as follows:

$$u = \frac{\emptyset R^2 \Delta P}{8\mu L}\left(\frac{L}{L_{eff}}\right)^2 \tag{3.2}$$

u (m/s) and ΔP (Pa) are Darcy velocity and pressure drop in the direction parallel to length L (m), μ (Pa.s) is the fluid dynamic viscosity, $\emptyset$ is the porous media porosity. Eq. (3.2) is then identified with the Darcy velocity for the flow of Newtonian fluids in porous media (Darcy, 1856).

$$u = \frac{Q}{S} = \frac{K\,\Delta P}{\mu\, L} \tag{3.3}$$

where Q (m^3/s) and S (m^2) are the flow rate and cross-section surface area of the porous media. The mean pore radiuses could be calculated as the radius of straight capillaries composing a bundle giving the same flow:

$$R_{eq}^2 = \left(R\frac{L}{L_{eff}}\right)^2 = \frac{8K}{\emptyset} \tag{3.4}$$

In the preceding equation, R_{eq} (m) is the average pore throat radius, K (m^2) is the intrinsic permeability of the porous media. The term $\left(\frac{L}{L_{eff}}\right)^2$ represents the tortuosity in porous media. Hence, an equivalent shear rate ($\dot{\gamma}_{eq}$) for flow in porous media can be expressed as (Darby, et al., 2001),

$$\dot{\gamma}_{eq} = \frac{4\alpha u/\emptyset}{R_{eq}} \tag{3.5}$$

in which α is an empirical shift parameter associated with the bulk rheology of the fluid and the tortuosity of porous media (Chauveteau & Zaitoun, 1981). The tortuosity of packed spheres was assumed to be 25/12 from the derivation of the Blake-Kozeny equation using the capillary model (Christopher & Middleman, 1965; Hirasaki & Pope, 1974). As a consequence, Hirasaki and Pope (1974) proposed to use $\alpha \approx 0.69$ through $\alpha = 1/\sqrt{L/L_{eff}}$ for Newtonian fluids. Recently, Rodriguez de Castro (2019) experimentally found α equal to 0.68 in glass bead packings.

If we consider Darcy's law as applicable for the flow of a non-Newtonian fluid in porous media, the effect of non-linear rheology of the fluid can be incorporated in the definition of an apparent viscosity given by

$$\mu_{app} = \frac{K\,\Delta P}{u\, L} \tag{3.6}$$

This apparent viscosity μ_{app} is not an intrinsic property of fluid and varies with the flow rate. It is a non-linear function of the equivalent shear rate given in Eq. (3.5), which can be varied relying on the flow rate. Moreover, the shear rate varies considerably as a function of the structure and the heterogeneity of porous media that change interstitial velocity.

The rheological behavior of yield-stress fluid for simple shear can be described through the Herschel-Bulkley model (Herschel & Bulkley, 1926):

$$\tau < \tau_0 \Rightarrow \dot{\gamma} = 0 \text{ (solid regime)};\ \tau > \tau_0 \Rightarrow \tau = \tau_0 + a\dot{\gamma}^n \text{ (liquid regime)} \quad (3.7)$$

where τ (Pa) is the shear stress, $\dot{\gamma}$ (1/s) is the shear rate, τ_0 (Pa) is the yield stress, a (Pa.s^n), and n (-) are the consistency and flow indexes, respectively. The continuous, viscous model proposed by Papanastasiou (1987) is used to prevent the main difficulty caused by the Herschel-Bulkley model in numerical studies due to discontinuous behavior at insufficient shear rates that tend the apparent viscosity to infinity. The Herschel-Bulkley-Papanastasiou (H-B-P) model can be written as follows:

$$\mu(\dot{\gamma}) = a|\dot{\gamma}|^{n-1} + \frac{\tau_0}{|\dot{\gamma}|}\left[1 - exp(-m|\dot{\gamma}|)\right] \quad (3.8)$$

in which m (s) is the exponent index.

Based on the models mentioned above, Denkov et al. (2005) studied foam rheology and wall slip velocity with 90% gas fraction using a rheometer. The foam used was generated using a syringe with a needle with id (inner diameter) of 2.5 mm. They found the power-law index equal to 0.25 and 0.42 for tangentially mobile and immobile bubble surfaces, respectively. Denkov et al. (2009) studied the effects of surfactant type and bubble surfaces on bulk foam rheology with $f_g \geq 80\%$. They classified the rheological behavior of foam into two different classes depending on values of power-law index n, by taking into account the viscous friction between bubbles and also between bubbles and solid walls, qualitatively. The results with $n \approx 0.5$ referred to the first system, which was described as the dominant friction in foam films, and the second type $n < 0.5$ (mostly between 0.2 and 0.25) was defined as the essential energy dissipation on the bubble surfaces. These studies show solid, plastic, or viscoelastic behavior of foam below a yield stress and non-Newtonian liquid regime above the yield stress. The transition from solid-like to liquid-like mechanical behavior is called yielding. The yielding can be explained through the complex shear modulus that appears at the transition from a mostly elastic regime where G'(Storage modulus)>G''(Loss modulus) towards predominantly viscous behavior $G' < G''$ (Larson, 1999). The behavior of inverse transition from liquid-like to solid-like is called jamming, which was studied by slightly decreasing the shear rates and measuring the stress (Liu & Nagel, 1998). The apparent viscosity of foam is several times larger than the viscosity of the continuous liquid phase, even at low shear rates. This can be explained from a description of foam at the molecular and bubble scale (Hohler & Cohen-Addad, 2005).

3.3. Experimental approach

Here we present the fluids and materials used. The experimental setups and procedures were provided to characterize the rheology of foam in bulk form and in porous media.

3.3.1. Fluids and materials

Surfactant solution

$C_{14\text{-}16}$ Alpha-olefin sulfonate (AOS) based surfactant Rhodacal® LSS-40/AX (Solvay Novecare) and demineralized/degassed water were used to prepare a surfactant solution. The surfactant contained 40 wt% of active materials in the aqueous solution. The chemical surfactant was chosen based on several factors like soil biodegradability (Tuvell, et al., 1978; Talmage, 1994), market accessibility (Cserháti, et al., 2002), and field tests for soil remediation purposes (Svab, et al., 2009). The critical micelle concentration (CMC) of the surfactant is 1.8±0.1 g/L, which is measured by the pendant-drop method (Stauffer, 1965) using a drop shape analyzer (DSA-100S, KRUSS). The surfactant solution was prepared at a concentration of four times CMC to avoid adsorption (Paria, 2008; Omirbekov, et al., 2020 a; Aranda, et al., 2020) at low concentrations and respect the biodegradability at high concentrations.

Gas

The gas used to generate foam in all experiments was nitrogen, provided by Air Liquide, with a purity of 99.98%. N_2 was selected after considering several studies presented in the literature, including foam stability (Farajzadeh, et al., 2009; Zeng, et al., 2016) and solubility (Sander, 1999) of gases. Also, carbon dioxide (purity > 99.7%), provided by Air Liquide, is used for pre-saturation procedures to avoid trapping of gas bubbles.

Porous media

Unconsolidated porous media made from calibrated silica sand (BR-37) and 1 mm glass beads are used, which are provided by Sibelco™ and Sigma-Aldrich companies, respectively. The sand-grading characteristics were as follows: the uniformity coefficient (C_u) is 0.72, the curvature coefficient (C_c) is 0.98; the effective size (d_{10}) and mean grain size (d_{50}) are 0.180 and 0.135 mm, respectively. Fine-sand packing was used to generate foam, while foam flow was examined in 1 mm glass-bead (GB) packing. The characteristics of the porous media are presented in Table 3.1.

Table 3.1 Properties of porous media

Porous media	**Mean grain size diameter, d (mm)**	**Pore Volume, PV (mL)**	**Porosity, Ø (%)**	**Permeability, K (m^2)**	**Mean pore radius, R_{eq} (µm)**
Sand BR37	0.135	51±2	38±1	7.2 (±1) $\times 10^{-12}$	11.5
GB	1	181±2	36±1	8.30 (±0.1) $\times 10^{-10}$	133.5

3.3.2. Experimental setups

The setups used to conduct the experiments are shown in Fig. 3.1. To generate foam, N_2 and the surfactant solution were co-injected into the foam generator column. Then the rheology of pre-generated foam was studied with different methods: A) in bulk form using a rheometer (bulk); B) in the main porous media column (p.m.).

The mass flow controller El-Flow Select F-201CV (Bronkhorst), providing a range of 0.16-10 mL_n/min (±0.5 % reading, plus ±0.1 % full scale), was used to control the gas flow rate and ensure the flow stability from a gas bottle. A piston pump Model 1HM (Eldex), with a precision of ±0.3 %, was used to inject the surfactant solution at a constant flow rate. The foam generator column was 10 cm long, with 4 cm inside diameter and made of transparent polyvinyl chloride (PVC). The sand-pack was retained using a metallic grid with 42 µm cell size. The following setups were used to investigate the pre-generated foam properties.

D) A rotational rheometer Haake Mars 60, Thermofisher (min. torque rotation 0.02 µNm, torque resolution 0.1 nNm) with serrated parallel plate geometry (P60/Ti/SE and TMP60/SE) was used to examine the rheology of pre-generated foam in bulk form.

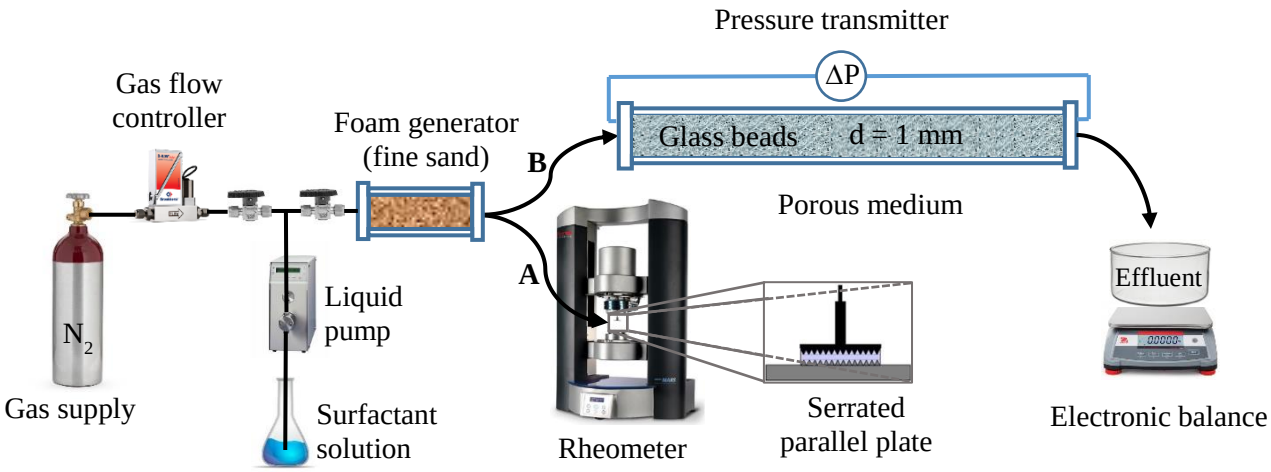

Fig. 3.1 Schematic of the experimental setups used to characterize the rheology of A) bulk foam and B) foam in porous media

E) The main column (made of PVC material) with a length of 40 cm and an inner diameter of 4 cm packed by 1 mm glass beads was used to study foam from the foam generator column. Metallic grids with 150 µm cell size were used on each side of the column to contain the glass bead packing. Pressure drop along the main column was measured through a differential pressure transmitter Rosemount 2051 (Emerson) with a 0-2500 mbar range (±7 mbar at the maximum value). An electronic balance model STX 6201 (OHAUS) with a precision of 0.1 g was used to measure the effluent weight. The maximum pressure limit of the experimental installation was up to 6 bars controlled by the pump pressure sensor.

3.3.3. Experimental procedures

First, the porous columns were carefully packed and checked for leaks. The columns were flushed by CO_2 gas to remove any air. Then, degassed/demineralized water was injected into the columns, in a vertical position, with a 0.5 mL/min for at least five pore volumes (PV) to dissolve any CO_2 and thus to saturate the column thoroughly. As CO_2 is highly soluble in the water, this step was used to provide 100% of porous media saturation. To measure pore volume and porosity, the columns were weighed before and after the water saturation. The subsequent experimental steps were carried out with the column in a

horizontal position. The permeability of the porous media was measured through the injection of degassed water with different flow rates while measuring the pressure difference and calculated via Darcy's law (Eq. (3.3)). The measured properties of porous media were tabulated in Table 3.1. Next, the column was flushed with 3 PV of surfactant solution, to complete adsorption. Finally, to generate foam, the surfactant solution and the nitrogen gas were simultaneously injected into the foam generator. 5 PV of fluids were co-injected to obtain a stable pre-generated foam. The pre-generated foam was further investigated A) using the rheometer and B) in glass bead packing.

A) Pre-generated foams with 60%, 85%, and 95% foam qualities, generated at the same total flow rates (Q =2 mL/min, u =2.65×10^{-05} m/s), were investigated using the rheometer. The mechanical properties of foam were probed through the rheometer, considering previous studies (Larson, 1999; Macosko, 1994). The parallel-plate geometry with serrated surfaces was used to avoid wall-slip velocity (Herzhaft, 1999; Marze, et al., 2008; Princen & Kiss, 1989). The shear gap of the geometry was 1 mm, which was chosen by taking into account previous studies (Herzhaft, 1999). Moreover, before starting the experiments, the dynamic stability of the foam at each quality was verified, based on the study of (Khan, et al., 1988), by examining samples at a constant shear rate. The idea was to observe how long the foam could withstand at constant torque. The decrease in torque values indicates the change in the foam structure. The volume of 3.1 mL of the foam sample was set in the gap, and the experiments were run in triplicate for each foam quality.

B) Firstly, the pre-generated foam was connected to the main column to study the impact of f_g and to determine the transition foam quality (f_g^*). Foam with a fixed total flow rate (2 mL/min) was studied for various foam qualities (40%-99%). The fractions of gas and liquid injected were controlled by the mass flow controller and the pump. The foam flow experiments were examined through the flow rate and pressure drop measurements along the column. Consequently, the apparent foam viscosity was derived from Darcy's law (Eq. (3.3)). After determining f_g^*, foam flow in GB packing was investigated at low-quality regimes. Foam flow with f_g=60%, 85%, and 95% was studied for different total flow rates that were increased step by step from minimum (Q =0.2 mL/min, u =2.65×10^{-06} m/s) to maximum (Q=2.2 mL/min, u=2.92×10^{-05} m/s) technically possible values. Thus, 905 and 82 minutes were required to inject 1 PV of pre-generated foam through the main column at the minimum and maximum flow rates, respectively. Experiments were duplicated by at least a descending flow rate experience. At the same time, the electronic balance measured the liquid effluent to determine the change of surfactant solution saturation (S_w) inside the main column. All experiments were carried out at 20°C, controlled room temperature, and atmospheric pressure.

3.4. Theoretical approach: upscaling technique

Since the direct upscaling of foam flow from pore to laboratory scale is complex, we used upscaling technique to scale up foam flow by using the rheological data of bulk foam as an input. The objective was to examine whether foam-flow behavior in porous media can be predicted from its bulk behavior. For field application in aquifers, a second upscaling from laboratory to aquifer scale should be considered. That was beyond the scope of this study.

In order to numerically study the macroscopic behavior of foam flow, it was first necessary to establish the geometry of representative elementary volume (REV) to correspond to the porous media permeability obtained from the laboratory experiments. To do so, we solved the closure problem for creeping flow of steady-state Newtonian fluids developed through the volume-averaging method (Quintard & Whitaker, 1994; Whitaker, 1999) to define the permeability of the two-dimensional (2D) and three-dimensional (3D) unit cells (see Fig. 3.3). The size of solid inclusion in each kind of unit cell was adjusted to obtain the same permeability as in the 1D column experiment. Then the boundary value problem developed using the homogenization method (Auriault, 1991) was solved to study macroscopic foam flow behavior further. The targets of the upscaling were to study the impact of f_g and the effect of different unit cell geometries on foam flow. Then the outcome of the 1D porous column experiments was used to correlate and validate the findings from upscaling.

3.4.1. Description of foam flow at the pore scale

The concept of porous media is presented in Fig. 3.2, in which we consider the foam flow through a periodic REV with Ωbeing the total volume of REV.

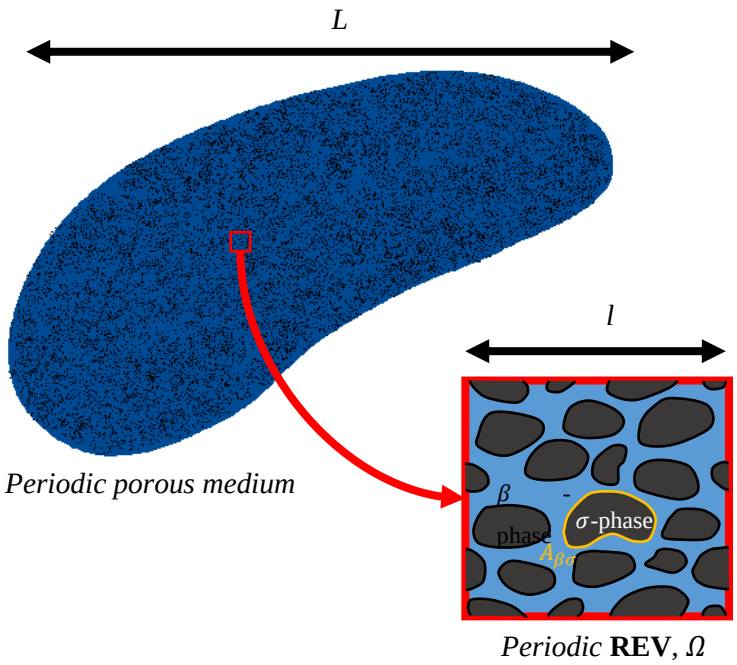

Fig. 3.2 A schematic illustration of a periodic porous medium with the associated REV

The volume considered consists of Ω_σ rigid solid-phase domain and the β yield-stress fluid (foam) of volume Ω_β. The porosity of the porous medium can be defined as $\emptyset = \Omega_\beta/\Omega$. A no-slip boundary condition is considered on the solid-fluid interface denoted $A_{\beta\sigma}$. Also, the fluid is considered as incompressible, purely viscous, and isotropic. Since the flow is in creeping regime (inertial effects are neglected) and steady-state, the mass and momentum balance equations for a yield-stress fluid are written as

$$0 = \nabla \cdot \left(-P\mathbf{I} + \mu(\dot{\gamma})\left(\nabla\mathbf{v} + (\nabla\mathbf{v})^{\mathrm{T}}\right)\right) \qquad \text{in } \Omega_\beta \qquad (3.9)$$

$$\nabla \cdot \mathbf{v} = 0 \qquad \text{in } \Omega_\beta \qquad (3.10)$$

$$\mathbf{v} = 0 \qquad \text{on } A_{\beta\sigma} \qquad (3.11)$$

where $\mathbf{v}$ is the fluid velocity field and P is the pressure. μ is the dynamic fluid viscosity, which can be defined by the H-B-P model (Eq. (3.8)) for our case. Hence, the set of equations is the pore-scale description of the foam flow problem in highly permeable porous media.

3.4.2. Characteristics of the microstructure

Foam flow in model porous media was investigated with fixed permeability. The investigation was carried out in four different periodic 2D and two different 3D unit cells. The pore fraction (porosity) was adjusted to obtain the same permeability as the porous column permeability. The types of unit cells with their porosity values are presented in Fig. 3.3, with a) square-packed cylinders with a circular cross-section (SPC), b) square-packed cylinders with a square cross-section (SPS), c) close-packed cylinders with a circular cross-section (CPC), d) close-packed cylinders with a square cross-section (CPS), e) simple cubic packing of cubes (SCP), f) cubic body-centered packing of spheres (BCP).

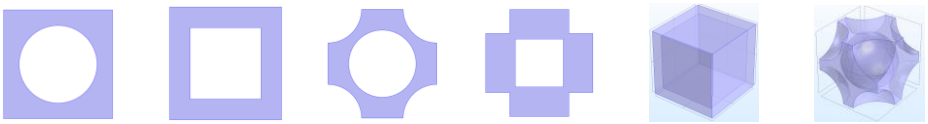

	a) SPC	b) SPS	c) CPC	d) CPS	e) SCP	f) BCP
∅ (-)	0.43	0.37	0.49	0.63	0.41	0.42

Fig. 3.3 2D and 3D periodic unit-cell for an array of parallel cylinders of circular (a, c), square (b, d) cross-sections, (e) simple cubic and (f) cubic body-centered packings

The edge size of the periodic REV was selected to be 1 mm for all cases in order to be close to 1 mm GB size, and the permeability was set equal to 8.3×10^{-10} m^2. The permeability of each porous medium has been calculated by solving the closure problem for a Newtonian fluid flow through the volume-averaging method (Quintard & Whitaker, 1994; Whitaker, 1999). It should be noted that ideally, the unit cells chosen must have the same porosity and permeability as the experimental sample. Moreover, they should feature similar microstructures in terms of the disorder. Although all unit cells considered here are ordered geometries, the porosity values for cells SPC, SPS, SCP, and BCP are relatively close to each other and

also close to the value found for the glass bead packing. The porosity for CPC and CPS are significantly higher for the same value of the permeability.

3.4.3. Upscaling

Separation of scales

In order to meet the requirements of the homogenization method (Idris, et al., 2004; Orgéas, et al., 2007; Auriault, 1991; Papanicolau, et al., 1978; Sanchez-Palencia, 1980), the condition of separation of the scales must be satisfied for the porous media considered. As Fig. 3.2 describes, the characteristic REV length l is supposed to be small compared to the characteristic macroscopic length L, which can be expressed as

$$\zeta = \frac{l}{L} \ll 1 \tag{3.12}$$

where ζ represents the scale-separation parameter.

Boundary value problem

In this work, the homogenization procedure proposed by Orgeas (2007) has been used. Thus, a generalized Newtonian fluid through 2D and 3D elementary unit cells is studied using numerical simulations. To study foam flow in porous media, a boundary value problem concerning the first order velocity $\mathbf{v}^{(0)}$ also, to the second-order pressure $\nabla \mathrm{P}^{(1)}$ is presented in the following way:

$$\boldsymbol{\nabla} \cdot \left(-\zeta P^{(1)} + \left(\frac{\tau_0}{|\dot{\gamma}|} \left[1 - \exp(-m\dot{\gamma}) \right] + a\dot{\gamma}^{n-1} \right) \left(\boldsymbol{\nabla}\mathbf{v}^{(0)} + \left(\boldsymbol{\nabla}\mathbf{v}^{(0)} \right)^{\mathrm{T}} \right) \right) = \boldsymbol{\nabla} P_{\mathrm{x}}^{(0)} \qquad \text{in } \Omega_\beta \tag{3.13}$$

$$\boldsymbol{\nabla} \cdot \mathbf{v}^{(0)} = 0 \qquad \text{in } \Omega_\beta \tag{3.14}$$

$$\mathbf{v}^{(0)} = 0 \qquad \text{on } A_\beta \tag{3.15}$$

Here, the unknowns $\zeta P^{(1)}$ and $\mathbf{v}^{(0)}$ are periodic, and the macroscopic pressure gradient $\boldsymbol{\nabla} P_{\mathrm{x}}^{(0)}$ is given on the whole REV as a source term. Foam was considered as a yield-stress fluid following the rheological model H-B-P (Eq. (3.8)), where the fluid viscosity is supposed to be a function of the magnitude of the shear rate $|\dot{\gamma}|$ given by

$$|\dot{\gamma}| = \sqrt{2\mathbf{S}:\mathbf{S}} \tag{3.16}$$

where the strain rate $\mathbf{S}$ is defined as a function of the velocity field $\mathbf{v}$ at the pore scale,

$$\mathbf{S} = \frac{1}{2}\left(\boldsymbol{\nabla}\mathbf{v}^{(0)} + \left(\boldsymbol{\nabla}\mathbf{v}^{(0)} \right)^{\mathrm{T}} \right) \tag{3.17}$$

The boundary value problem given above was solved in the 2D periodic unit-cell of circular cross-section (Fig. 3.3, a) for f_g=60%, 85% and 95%, where the rheological parameters of the continuous, viscous model were obtained from the experimental study. Foam with f_g=85% was investigated in all geometries

presented in Fig. 3.3. For all simulations in the ordered isotropic porous media, the macroscopic pressure gradient imposed $\nabla P_x^{(0)}$ was in the direction of the x-axis. The non-linear boundary value problem (Eqs. (3.13)-(3.15)) was solved using Comsol Multiphysics Finite Element with a mixed pressure-velocity (P1-P2) formulation. The flow problems were solved through the Creeping flow module, which is designed for solving Stokes flow problems. The dynamic viscosity of the module was user-defined via the Equation View section. Solving this problem was similar to solving the direct flow problem in simple unit cells. The finite-triangular elements were used to mesh the 2D geometries. An example of mesh and boundary conditions used are in Fig. 3.4.

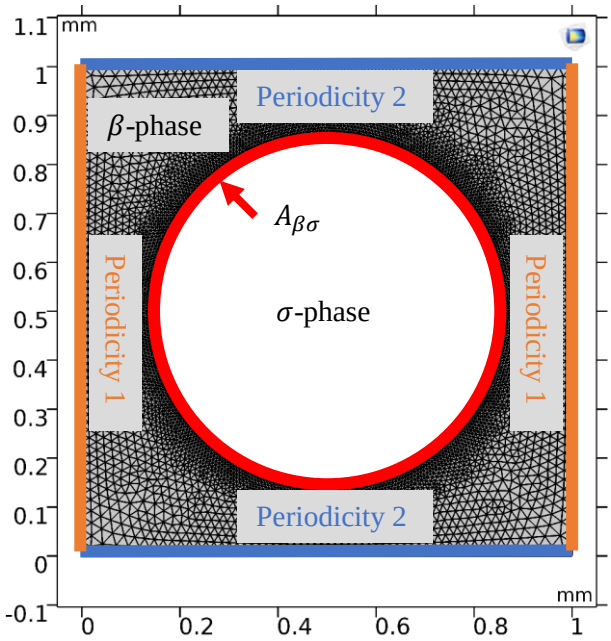

Fig. 3.4 The mesh and boundary conditions used to run the simulations

Results presented in the literature for the same geometries (Idris, et al., 2004; Orgéas, et al., 2007) were used to verify the numerical procedure adopted here in the case of power-law and generalized Newtonian fluids.

3.5. Results and discussion

3.5.1. Rheology of bulk foam

Fig. 3.5 shows the rheology of pre-generated foam for different foam qualities, in which the shear stress τ is displayed as a function of the shear rate $\dot{\gamma}$. The dots represent the average value of experimental results, and the lines describe the results of the H-B-P model. Table 3.2 shows the fitting parameters with coefficients of determination. The exponent index m was chosen to be 10000 in order to better represent the yield stress behavior in numerical studies. From these results, a non-Newtonian fluid behavior with

yield stress is observed that was well fitted by the Herschel-Bulkley-Papanastasiou model. Moreover, we saw that yield stress increases with increasing foam quality thereby raising the bulk foam viscosity and the increasing yield-stress value with the foam quality, which agrees with the literature results (Khan, et al., 1988), where the storage modulus (G') and τ_0 as a function of foam quality (Marze, et al., 2009; Saint-Jalmes & Durian, 1999) were measured. The value of the yield stress increases by a factor 2 from f_g=85% to f_g=95%, which can be explained by the evolution of the bubble shape from spherical to polyhedral-form, thereby increasing the friction between bubbles (Denkov, et al., 2009).

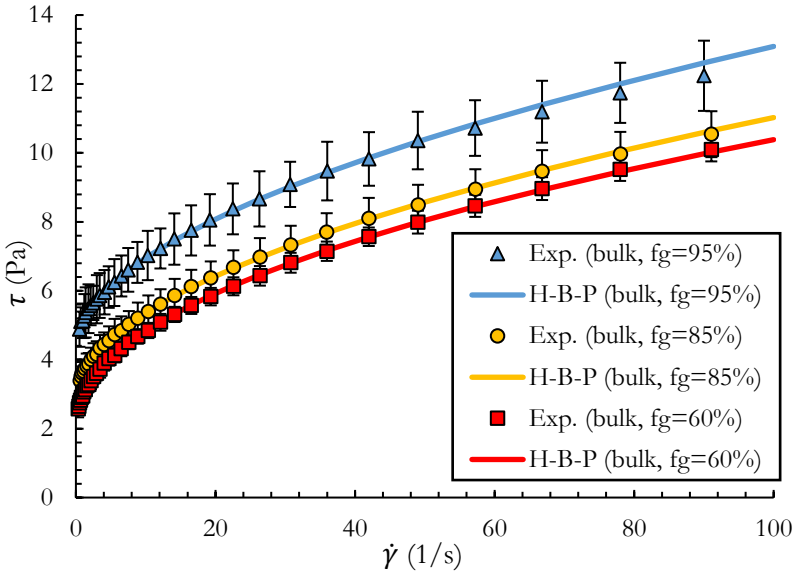

Fig. 3.5 Rheology of bulk foam with different foam quality

Table 3.2 Fitting parameters of H-B-P model

f_g (%)	**60%**	**85%**	**95%**
n (-)	0.48	0.52	0.54
τ_0 (Pa)	2.03	2.87	4.49
a (Pa.s^n)	0.94	0.76	0.7
m (s)	10000	10000	10000
R^2	0.99	0.99	0.99

It can, therefore, be concluded that in our experiments, bulk foam can be clearly considered as a yield-stress fluid. This is in agreement with previous studies in which the value of the flow index, n, obtained experimentally was indicated close to 0.5 (Denkov, et al., 2009; Marze, et al., 2008; Princen & Kiss, 1989; Ovarlez, et al., 2008; Ovarlez, et al., 2010; Tcholakova, et al., 2008).

It should be noted that the measurement of the rheology for the foam with the quality of f_g=60% was found to be complicated due to the drainage of foam liquid-phase from the rheometer geometry. Therefore,

to avoid the liquid draining from the plates, we loaded the exact necessary amount of the foam sample (3.1 mL) by setting the gap to 3 mm, where the foam sample was placed between two plates. Then, the gap was decreased slowly until 1 mm to perform tests at different shear rates. The foam with the quality of f_g=60% was studied with great care at each shear rate by performing additional experiments to ensure accurate results.

These results are analyzed with the outcomes of the experimental study on porous media and further used as inputs for upscaling of foam flow in highly permeable porous media by considering foam as a yield-stress fluid.

3.5.2. Rheology of foam in porous media (Darcy scale)

Since foam was generated in the sand-pack, foam bubble size was expected to be smaller than the pore size of the glass-bead packing. Therefore, the bubble sizes were estimated according to previous studies. For instance, Marsden et al. (1967) noted that some foams generated in porous media could flow with bubbles much smaller than pores, as well as a series of foam films of various sizes, shapes, and configurations depending on the medium. They studied a pre-generated foam through the series of four identical porous media consisting of sand with a porosity of 35% and a permeability of 5.2 d. The foam texture was studied through optical cells and using a microscope. They showed an increase in bubble size with a decrease in foam mobility (the ratio of effective permeability to apparent viscosity). However, in later work, the opposite was revealed (Hirasaki & Lawson, 1985; Falls, et al., 1989). From the results of Marsden et al. (1967), we observed that the bubble size was smaller at high flow rates compared to the pore size, which was estimated to be five times smaller than the grain diameter.

Friedmann and Jensen (1986) found that the size of foam bubbles decreased with increasing velocities at constant foam quality by observing the texture of the foam exiting from several different porous media. Ettinger and Radke (1992) studied the foam texture of pre-generated foam in Berea sandstone. They also observed a decrease in bubble size with an increase in flow rate.

However, according to studies by Falls et al. (1989), the average size of the foam bubbles remained unchanged for the foam, which was pre-generated in 3 mm glass-bead packing and introduced into the second pack with the same grain size. The average size of the bubbles was estimated to be the same as the equivalent capillary radius of the packs. Consequently, in this study, we roughly assumed that the size of foam bubbles is equivalent to the pore size of the sand-pack (see Table 4.1).

The apparent foam viscosity calculated through Darcy's law (Eq. (3.6)) applied to the experimental study of foam flow in the porous sample (1 mm glass bead packing) as a function of foam quality is presented in Fig. 3.6. From these results, the transition foam quality (f_g^*) delimiting low and high-quality regimes is determined.

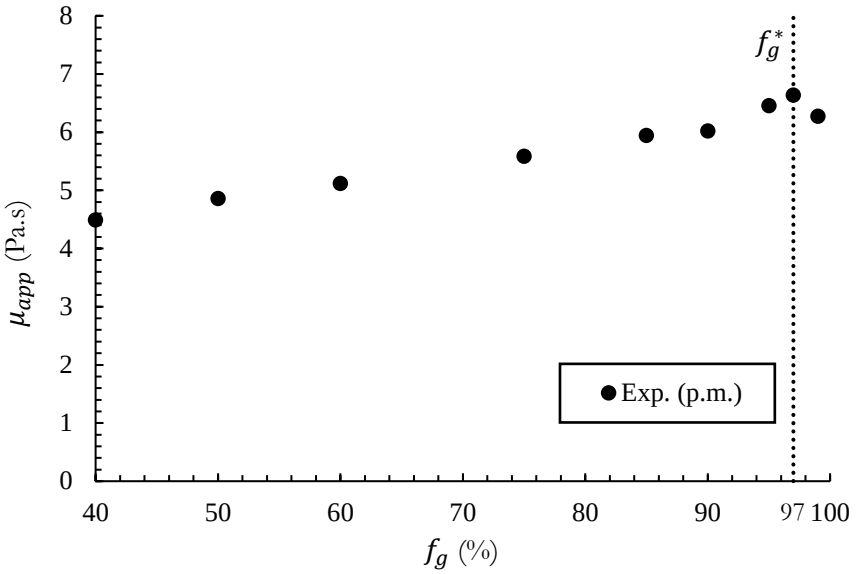

Fig. 3.6 Apparent foam viscosity in porous media (1 mm GB) as a function of foam quality at Q_t=2 mL/min

We observed that the transition foam quality was quite high and equal to 97% (dashed line). Hence, this result is in good agreement with the results of some authors (Alvarez, et al., 2001; Briceno & Joseph, 2003; Omirbekov, et al., 2020 a). For instance, Alvarez et al. (2001) found a value of f_g^*=97% for an experiment study of foam flow in a sand-pack with a permeability of 3.1 Darcy, where the foam was pre-generated through bronze wool (Alvarez, et al., 2001). They used two types of surfactants, an octyl ethoxylated alcohol and AOS, to generate foams. However, the bubble size of the pre-generated foam was not mentioned in their work.

Briceno and Joseph (2003) investigated pre-generated foam flow in a 1.2 m long channel (1 in. tall, 1/4 in. wide) and in a pipe (5/8 in. inner diameter). The foam was formed using an aqueous solution based on a mixture of AOS, polyacrylic acid polymer, cosurfactants (dodecanol), solvent (butanol), and water. They found f_g^*=97% through the pressure gradient vs. foam velocity plot where they discovered a shift in the results at f_g>97%. It was also visually shown that there was a change in the structure of foam at this transition zone, in which foam flow behavior changed from uniform to slug flow.

Recently, Omirbekov et al. (2020 a) also found that transition-foam quality is independent of the porous-media grain size when the average foam-bubble size is smaller than the pore size of the porous medium. The value of transition-foam quality, for the same foam composition and pre-generated foam used in this study, was 97% for 2 mm, 4 mm, and 8 mm glass-bead packing. Nevertheless, the foam's bubble size can be changed depending on time. This is discussed in Appendix A. With these results in mind, all our further studies were chosen to be conducted in low-quality regime (f_g=85%) to avoid the instability around f_g^*.

Fig. 3.7 shows the experimental results in terms of the pressure gradient along the porous column packed by 1 mm GB as a function of the foam flow velocity, for f_g=60%, 85%, and 95%. Non-linear behavior was observed where the pressure gradient of flow increased with foam quality. We were unable to obtain ∇P values above foam injection flowrate of 3-4 mL/min due to the maximum pressure limit of the experimental configuration for f_g=60% and 85% of foams.

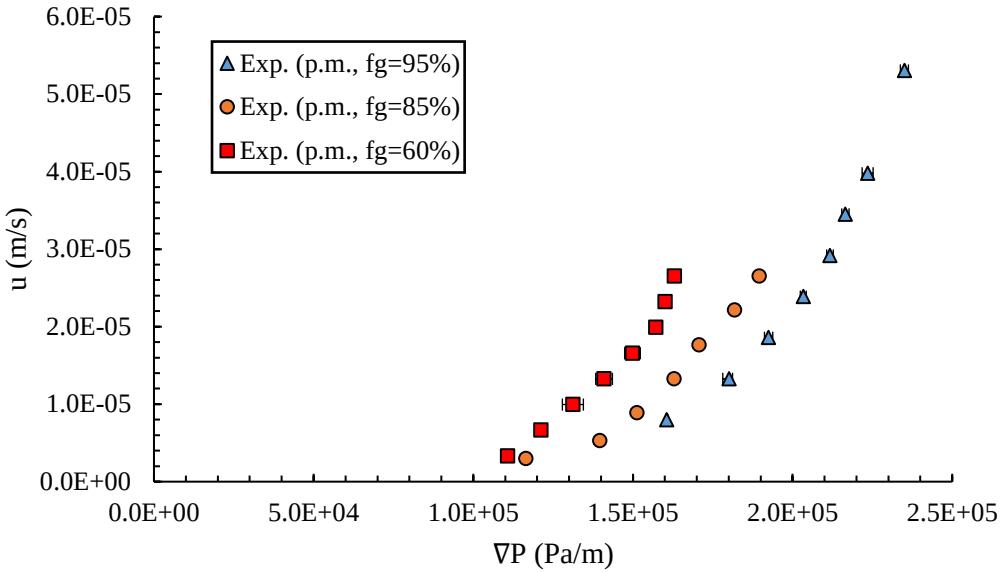

Fig. 3.7 The pressure gradient along the column as a function of the superficial velocity in GB, for f_g=60%, 85%, 95%

To investigate the foam rheology, the apparent viscosity variations versus the equivalent shear rate (Eq. (3.5)) were analyzed. The apparent foam viscosity as a function of the equivalent shear rate (Eq. (3.6)) is plotted in Fig. 3.8, in which points represent experimental data, and the lines correspond to the fitting curves by the H-B-P model (Eq. (3.8)). Results show that foams in porous media behave as non-Newtonian yield-stress fluids and the apparent viscosity of foam increases with foam quality. Therefore, we found that foam flow in porous media behaved as a bulk foam if the bubbles were smaller than the pore size and for a low-quality foam-flow regime. In addition, we observed that the yield-stress values for foams in porous media were about twice as high as those found for bulk foams (see Table 3.3). Moreover, the fluidity index n increased when the gas fractions decreased and had a value of 0.65 for f_g=60%. In the literature, n>0.5 is found for low-quality bulk foams (f_g<75%) (Otsubo & Prud'homme, 1994; Otsubo & Prud'homme, 1994; Larmignat, et al., 2008), so it agrees with our results. However, note that the power-law index n was around 0.5 for all bulk foams. This may be a consequence of the surface roughness, since our porous medium consisted of glass bead packing, and the pore walls are smooth compared to the serrated geometry of the rheometer. Also, it may be a result of the enduring sample preparation time for the foam with the quality of f_g=60% mentioned in section 3.5.1. Consequently, the

foams can be classified into two groups depending on foam quality and values of the power-law index, where we observed n≈0.5 for f_g=85% and 95% and n>0.5 for f_g=60% foams.

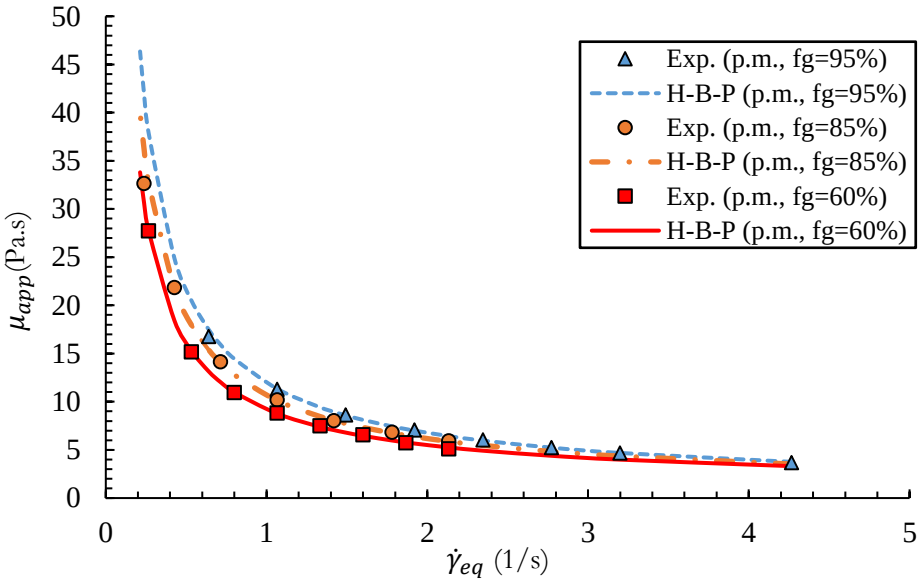

Fig. 3.8 Apparent viscosity as a function of the equivalent shear rate: f_g=60%, 85% and 95%

Table 3.3 Fitting parameters for H-B-P model

f_g (%)	60%	85%	95%
n (-)	0.65	0.53	0.49
τ_0 (Pa)	6.05	6.86	8.06
a (Pa.s^n)	3.15	3.88	3.90
m (s)	10000	10000	10000
R^2	0.99	0.99	0.99

In Fig. 3.9a, the apparent viscosity of the bulk foam defined as $\tau/\dot{\gamma}$ is plotted as a function of shear rate for various foam qualities on a log-log scale. The apparent viscosity obtained from experiments in porous media is also presented in the same figure. The range of the shear rate was restricted in order to facilitate the comparison of the results. Fig. 3.9b shows the fitted results with the shift parameter α for each foam quality (Eq. (3.5)). In this figure, the colored dots represent the outcomes of foam flow in porous media, and star dots are the result of the bulk foam examined through the rheometer. The fitted shift parameters α with the coefficient of determination are tabulated in Table 3.4 for each foam quality. Here, the shift parameter is found to allow a good superposition of the apparent viscosities of bulk and in-situ foam. Moreover, α becomes more significant with increasing foam quality. In previous studies related to yield-stress fluids, it was found that the shift parameter α>1 for sandstones (Fletcher, et al., 1991) and bead packings (Castro, 2019; Zitha, et al., 1995). Also, α was mostly assumed to be constant and independent of the flow rate. Recently, Rodriguez de Castro (2019) showed empirically, in glass beads packings, the

dependence of α on flow rates where α>1 at slow flow rates and α<1 for high flow rates with a constant value at very high velocities. However, note that all these studies were related to the flow of polymer solutions in porous media, and there is a lack of data for foams.

In this study, it was found that the values of α for foams are even smaller than those for Newtonian fluids in glass bead packings (Castro, 2019). Also, we observed that apparent in situ foam viscosity is higher than bulk foam viscosity at the same shear rate. Since bulk foam was examined at ambient conditions, this phenomenon may occur due to the effect of foam compressibility.

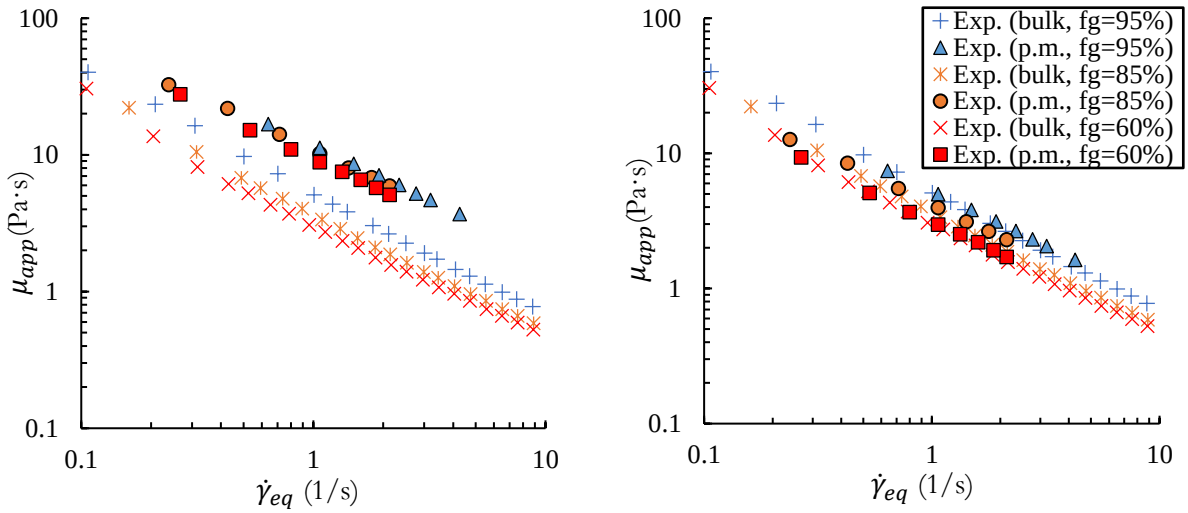

a) b)

Fig. 3.9 Apparent viscosity vs shear rate a) experimental results b) fitted results with α shift parameter

Table 3.4 Shift parameter for various foam qualities obtained from 1 mm GB packing

GB size	**1 mm**		
f_g **(%)**	60%	85%	95%
α **(-)**	0.34	0.39	0.44
$\mathbf{R^2}$	0.99	0.99	0.99

3.5.3. Upscaling of foam flow

3.5.3.1 Influence of foam quality

The outcome of the numerical study on foam flow in the periodic 2D SPC unit cell is compared to the experimental results in terms of the velocity/pressure gradient relationship in Fig. 3.10, for different foam qualities. In order to compare model results and experimental data, Fig. 3.10 was plotted on a semi-logarithmic scale. The dashed lines represent numerical results, in which the size of the solid cylinder was set in order to fit the experimental data in terms of permeability (K=8.3×10^{-10} m^2). The colored dots correspond to experimental results in 1 mm GB packing. Thus, the flow of foam with quality values of 60, 85, and 95% were examined to study the influence of foam quality on foam flow behavior. As

experimental results, it is observed that the foam flow viscosity in porous media increases with f_g. However, results from the numerical study show higher foam mobility even at lower pressure gradients compared to experimental results. The global trend of the curves and the behavior in terms of f_g follow the same tendency as those of the experimental results.

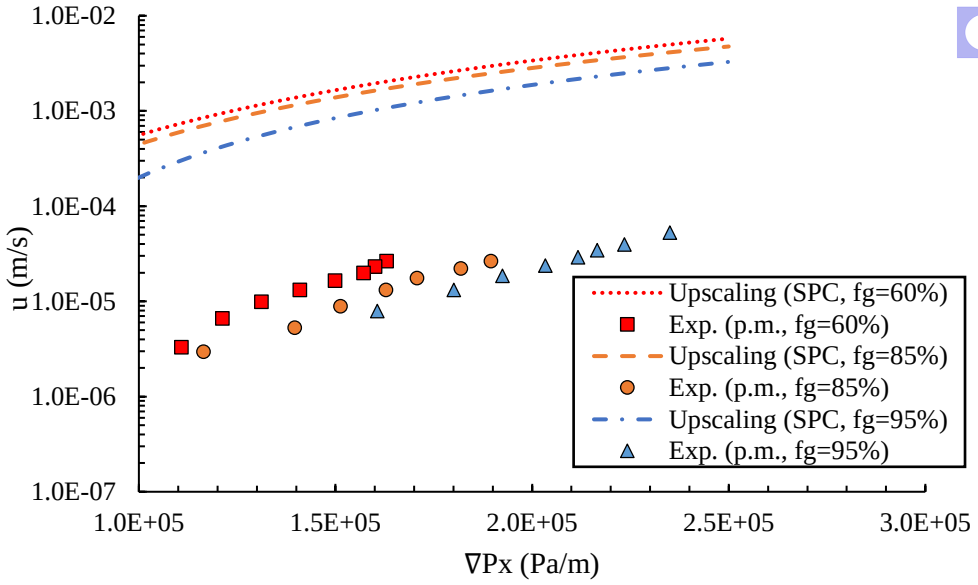

Fig. 3.10 Evaluation of the superficial velocity as a function of the macroscopic pressure gradient in 2D periodic SPC geometry, for different foam qualities (f_g=60, 85 and 95%)

3.5.3.2 Effect of porous media geometry

Fig. 3.11 shows the superficial velocity of foam as a function of the pressure gradient in different 2D and 3D geometries for f_g=85%. The dashed lines correspond to the numerical results where the unit-cell geometry was adjusted to match the K=8.3×10^{-10} m^2 value in Newtonian case, and the colored dots represent the corresponding experimental results of GB packing for f_g=85%.

As Fig. 3.11 shows, the flow is non-linear and depends on the geometry of porous media, which plays a crucial role in the flow of yield stress fluids. Moreover, flow in 2D-SPC and 2D-SPS geometries are close to each other but differ from the outcomes of other unit cells. In addition, the results for 2D unit cells CPC and CPS are very close to those of 3D unit cells SCP and BCP. Since the upscaling results were plotted on the semi-logarithmic scale, the small difference between the results was not explicitly shown. The porosity of 2D-SPC and 2D-CPS cells respectively equal 0.49 and 0.63, which is higher than the porosity of other unit cells where the values are close to 0.4. Therefore, we conclude that although the foam's behavior depends on the porous media structure. The results for the complex 2D and 3D geometries are closer to the experimental data than the simple 2D geometries. The predicted superficial foam velocities are however still a few order of magnitudes higher than the experimental data.

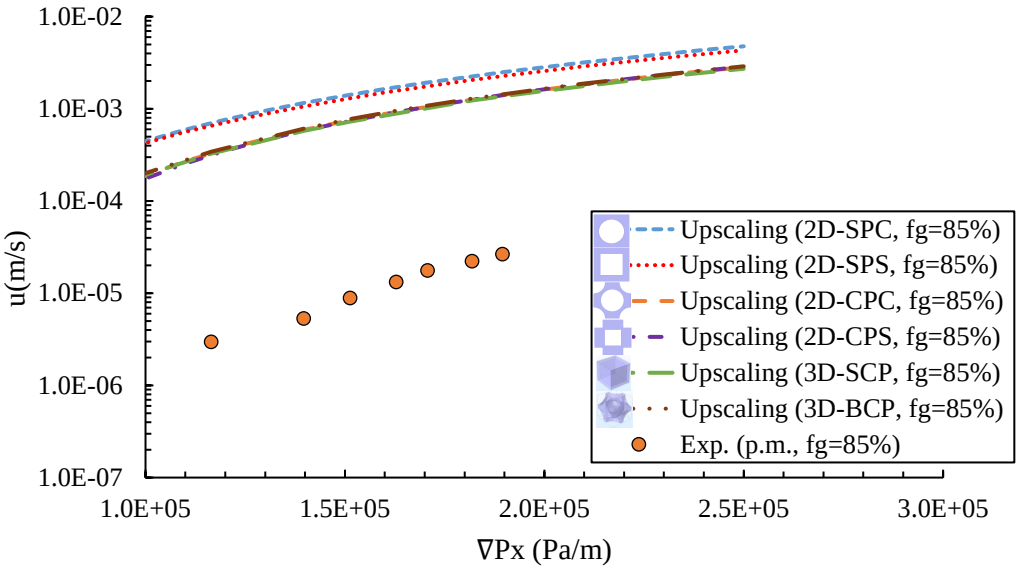

Fig. 3.11 The macroscopic pressure gradient vs. superficial velocity of foam flow in 2D SPC, SPS, CPC, CPS and 3D SCP, BCP unit cells (f_g=85%)

This discrepancy can be attributed to the effects of compressibility and gas trapping, which should be considered during the study of foam flow in porous media. To estimate the trapping effect in foam injection experiments, we calculated the capillary number N_{ca} using the following equation (Satter & Iqbal, 2015),

$$N_{ca} = \frac{K\nabla P}{\gamma} \tag{3.18}$$

where γ=0.036 (N/m) is gas-liquid interfacial tension. Consequently, the capillary numbers as a function of pressure gradient can be written as $N_{ca} = 2.31 \times 10^{-8}\nabla P$. The minimum value of N_{ca} is then 2.55×10^{-3} which corresponds to our minimum measured pressure gradient (110782 Pa/m) where foam quality was 60%. This capillary number is even greater than the critical capillary number of 10^{-5}, above which the capillary forces become negligible according to several studies (Chatzis & Morrow, 1984; Ding & Kantzas, 2007). Therefore, gas trapping can be negligible in our experiments.

To better observe the effects of gas trapping and compressibility of foam with f_g=85% in the porous medium, we closed the outlet of the generator column and measured the pressure drop along the main column at the end of the experiment. From the result presented in Fig. 3.12, it is shown that the pressure in the column reduced gradually even after the foam supply was stopped. During the first two hours, the pressure gradient dropped sharply from 140,000 Pa/m to 37,000 Pa/m, after gradually decreasing, and the experiment lasted four days.

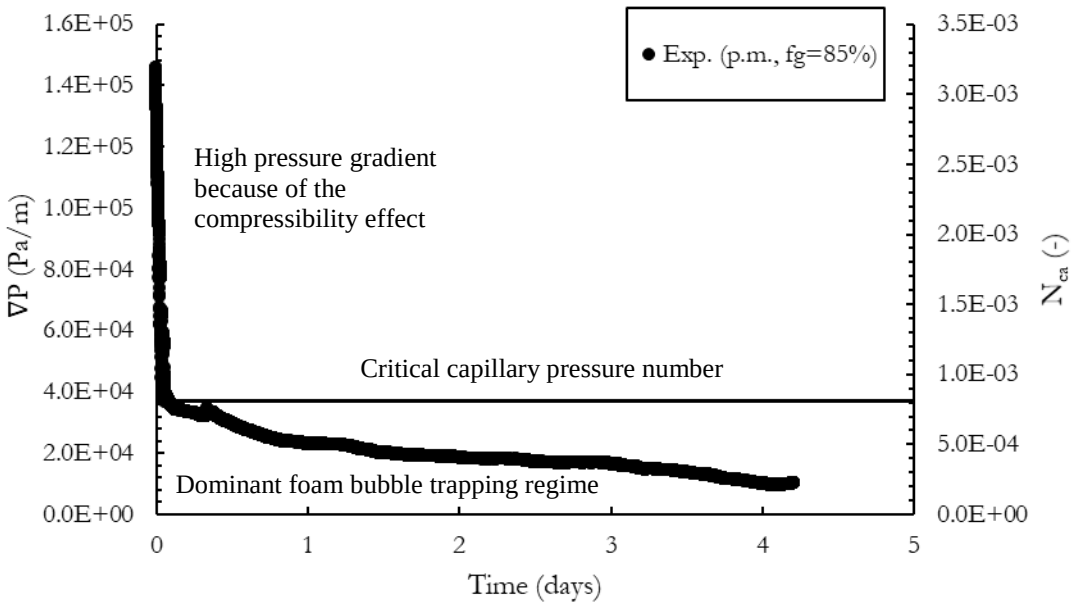

Fig. 3.12 Pressure gradient and capillary number as a function of time after the foam flow has stopped (f_g=85%)

After closing the foam-generator outlet, foam continues flowing through the column. This can be explained by the foam compressibility effect. However, the pressure gradient falls first very fast and then more slowly because of the gas trapping. From the values of the capillary number shown in Fig. 3.12, we can say that the gas trapping occurs below a critical capillary-pressure number, N_{ca}=7×10^{-4}. This shows that our foam flow experiments in 1 mm glass-bead packing (2.55×10^{-3}<N_{ca}<5.42×10^{-3}) are not affected by the gas trapping.

We also observed the foam's compressibility and gas trapping effects by measuring the pressure gradient along the column and weighing the effluent. The pre-generated foam column was first connected to the GB column that was initially saturated by the surfactant solution. Fig. 3.13 shows a plot of the effluent mass and pressure gradient as a function of the main column PV. The PV of the GB packing was 180.9 mL, which is shown in Fig. 3.13 by the continuous black line. The total-injection rate into the foam generator was 2 mL/min, including 1.20 mL/min of N_2 gas and 0.80 mL/min of surfactant solution. However, the gas breakthrough happened after producing of 2.94 PV of liquid, which corresponds to a slope change in the figure (dotted black line). Hence, 2.94 times more liquid was recovered than initially stated in the column.

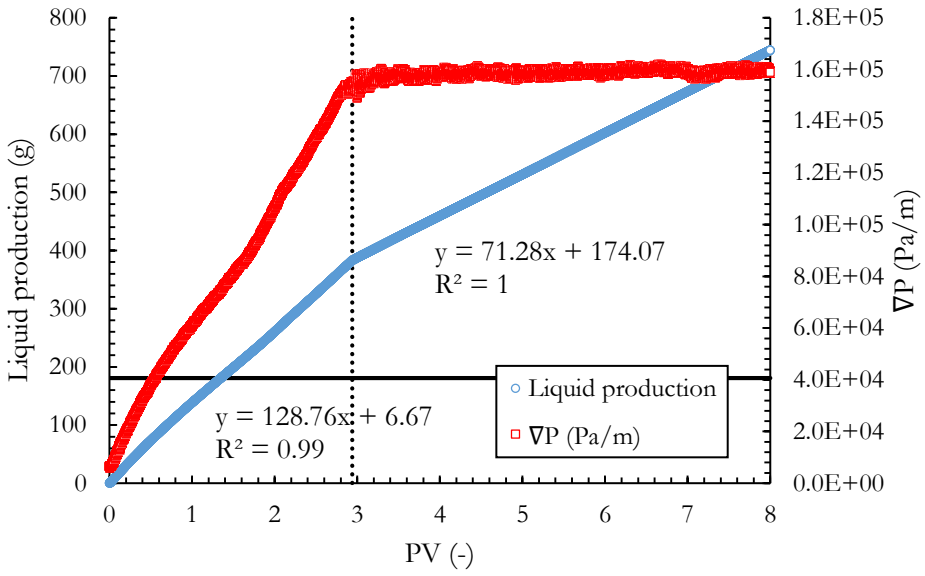

Fig. 3.13 Liquid mass of effluent as a function of PV for GB packing at Q_t=2 mL/min for f_g=60%

This indicates compressibility and trapping of gas in porous media that delayed the gas breakthrough time. From Fig. 3.12, we discovered that the gas was trapped considerably below 37,000 Pa/m. Thus the liquid flowed within foam lamellae at the low pressure gradients. This phenomenon was also observed by Falls et al. (1989). They found the flow of foam lamellae through a single-flow path where stationary lamellae blocked most of the cross-sectional area of the bead-pack at sufficiently low pressure gradients. Since the gas was trapped in the porous medium, all liquids were transported through the lamellae, thus delaying the gas breakthrough. Therefore, we recovered 385 mL of liquid when the gas breakthrough occurred, that is, 2.1 times more than PV. Moreover, based on the trend equation of liquid production for the first half of the curve, the liquid recovery rate was approximately 128.8 mL per injected PV, which is 24% less than the injection volume (180.9 mL). If we consider that the liquid is an incompressible fluid, the volume of gas is reduced to 40%. Therefore, we can conclude that foam flow at low pressure gradients is influenced by the trapping effect and at high pressure gradients by the compressibility, which tends to decrease the foam's gas volume. After the breakthrough, when the foam had reached the column outlet, the change of effluent weight corresponded to the mass of the injected fluid. As a consequence of these results, foam compressibility must be taken into account during the study of foam rheology in confined media.

Since most of the foam volume is gas, compressibility is one of the essential parameters. The compressibility is often described in terms of the expansion ratio ε which is defined as the ratio between the density of liquid phase ρ_l and the foam density ρ_f ($\varepsilon=\rho_l/\rho_f$) (Valko & Economides, 1992). The expansion pressure should be determined for each pressure drop. Using the volume-equalization method proposed by (Valko & Economides, 1992), one should obtain a single master curve by plotting

normalized-shear stress (τ/ε) versus normalized-shear rate ($\dot{\gamma}/\varepsilon$) regardless of the pressure and foam quality. According to Valko and Economides (1992), this method is relevant for low expansion foams (ε<4) with spherical bubbles. Gardiner et al. (1999) highlighted an increase in apparent-foam viscosity with the expansion ratio by analyzing and fitting the foam-viscosity data from previous research. They also found that the volume-equalization method proposed by Valko and Economides (1992) is applicable to polyhedral (ε>5) and bubbly-to-polyhedral (5≥ε≥4) foams (Gardiner, et al., 1998). Most of these studies were done using simple geometries such as pipes. Therefore, the determination of the expansion ratio in a porous medium is more difficult, if only the pressure drop along the column is measured.

To avoid the compressibility effect, we investigated the upscaling of foam flow in a more highly permeable porous medium based on the results of 4 mm glass-bead packing from Omirbekov et al. (2020 a). In this case, foam was pre-generated using the same surfactant solution and sand-pack. The maximum pressure gradient was 23,210 Pa/m at the flow rate of 3 mL/min at f_g=85%. Hence, the permeability of the unit cells was adjusted to the permeability of 4 mm glass-bead packing, K=1.09×10^{-8} m^2. No gas trapping was expected as the capillary numbers were 4.5×10^{-3} and 7×10^{-3} at the flow rates of 0.22 and 3 mL/min, respectively. Fig. 3.14 shows the upscaling results through the different 2D and 3D geometries with the experimental outcomes from Omirbekov et al. (2020 a). In this case, the upscaling results are close to the experimental data. Because the compressibility effect is insignificant in 4 mm glass-bead packing ($\varepsilon \cong 1$), we estimated the expansion ratio for 1 mm glass-bead packing using the volume equalization method of Valko and Economides (1992). In Fig. 3.15, we plotted the shear stress versus the shear rate of f_g= 85% foam in 1 mm glass-bead packings without and with mean-expansion factor, based on the 4 mm GB packing results. We found a mean-expansion factor of $\varepsilon = 2.1$ for 1 mm glass-bead packing. Because the bubble shape of the foam in porous media is more spherical, the method of Valko and Economides (1992) for low expansion foams is applicable.

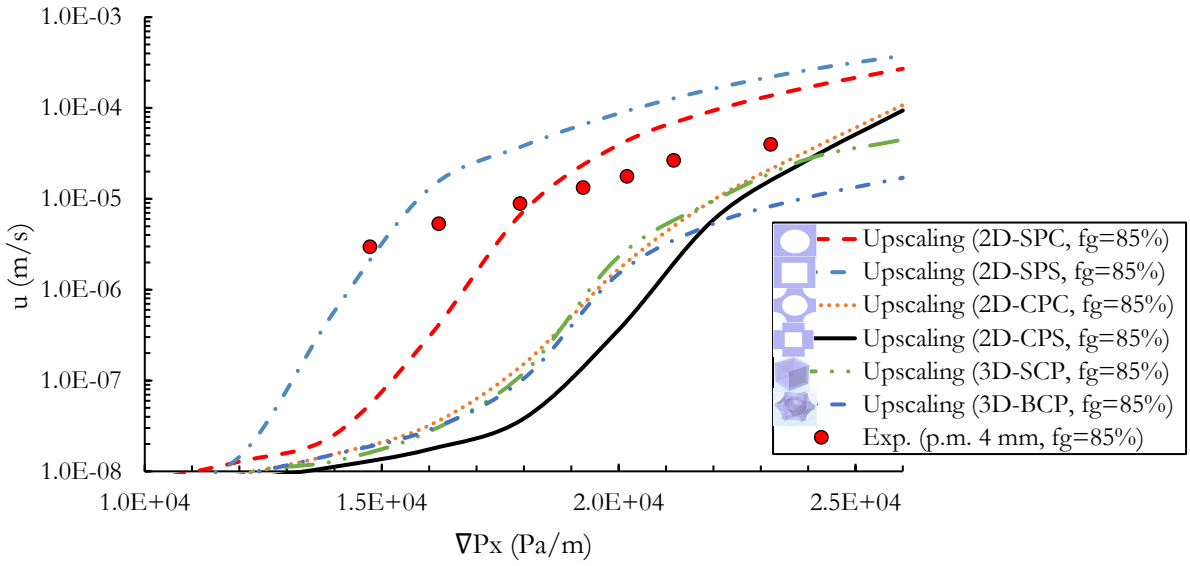

Fig. 3.14 The superficial velocity of foam flow vs. the macroscopic pressure gradient in 2D and 3D unit cells and experimental results in 4 mm GB packing of Omirbekov et al. 2020 a (f_g=85%)

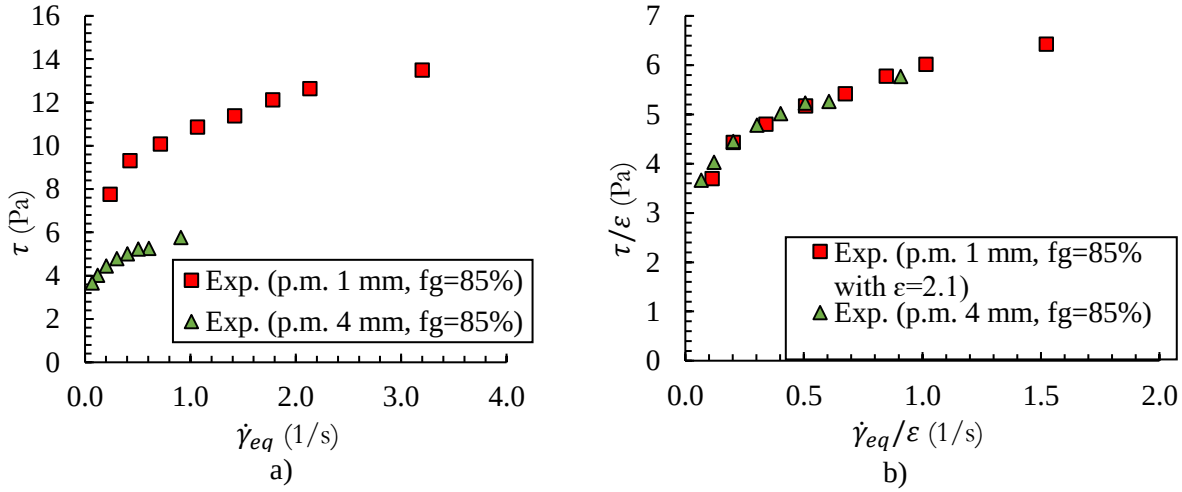

Fig. 3.15 Shear stress as a function of shear rate for foam quality of f_g = 85% in 1 and 4 mm GB packings a) without expansion factor b) with ε=2.1 expansion factor for 1 mm GB packing

We note also the simplicity of the unit cells considered here where the pore-scale structure is highly ordered which may also influence the results and partly explain the discrepancies observed. Consequently, upscaling is an encouraging tool if the input parameters are settled by taking into account not only the real structure of the porous medium but also all phenomena involved for foam flow in confined media. In this chapter, we only investigated the upscaling of foam flow from pore-scale to laboratory-scale. Therefore, the second upscaling from laboratory-scale to field-scale should be explored in the future. Then foam stability, including coalescence and gravity segregation, needs to be investigated. We know that in field applications, foam texture and bubble sizes may be different, as foam-residence time can be much longer.

3.5.3.3 Empirical Darcy-scale law

To further study foam flow in porous media using the bulk foam viscosity as input, we used the purely empirical approach of Chevalier et al. (2013) for the flow of yield-stress fluids (YSF) in glass beads packings with a bead diameter d, which is presented in the following form:

$$\nabla P = \frac{\chi \tau_0}{d} + \frac{\omega a \left(\frac{u}{d}\right)^n}{d} \tag{3.19}$$

They considered a polymer (Carbopol aqueous solution) and an emulsion (water-in-oil emulsion with a surfactant solution) as yield-stress fluids. In their study, the relationship between the pressure gradient (∇P) and the Darcy velocity (u) is of the same form as the constitutive law of the fluid, which contains the yielding term. In the preceding equation, terms χ and ω are dimensionless coefficients that depend on the distribution of shear rate intensity and the power-law index (Chevalier, et al., 2014). To determine the dimensionless coefficients of YSF Darcy's law, we used the H-B-P fitting parameters of bulk foam and deduced χ and ω parameters by adjusting to $u(\nabla P)$ results of foam flow in GB packing. Fig. 3.16 presents the experimental results with the fitted YSF Darcy law, in which the colored dots represent the results of experiments through the GB packing and dotted lines are the results of the extended Darcy's law for yield-stress fluids with fitted parameters. The corresponding dimensionless coefficients and coefficient of determination for each foam quality are presented in Table 3.5.

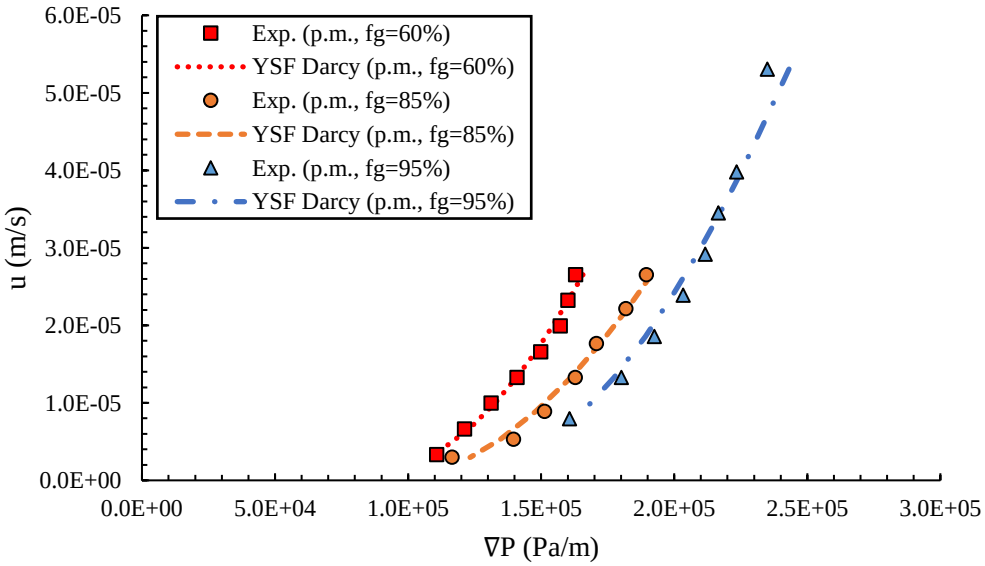

Fig. 3.16 Superficial velocity as a function of the pressure gradient for column experiments and the fitting curve by YSF Darcy's law for different foam qualities (f_g=60%, 85% and 95%)

Table 3.5 The dimensionless coefficients determined for foams (f_g=60%, 85% and 95%)

f_g (%)	60%	85%	95%
χ (-)	38.2	31.8	26.4
ω (-)	535.6	870	870
R^2	0.99	0.98	0.98

The values of the dimensionless coefficients determined are found to be very high in comparison to previous results of Chevalier et al. (2013, 2014), in which they found χ equal to 12 and 5.5 for the polymer solution and the water-in-oil emulsion, respectively. The dimensionless coefficient ω was 85 for both types of fluids.

Our results showed that χ decreases with increasing foam quality and is 2-6 times higher than the values found for the polymer and the emulsion. Therefore, we recommend considering χ as a function depending on foam quality. Moreover, it was observed that the coefficient ω was 870 for foams with 85% and 95% foam qualities, but it was 535.6 for f_g=60%. These results can be an outcome of power-law index values, which was high for f_g=60% foams. Thus in our case, ω should be considered individually for bubbly liquids (f_g<64%), low-quality (64%≤f_g≤97%) and high-quality foams (f_g>97%).

Consequently, we can conclude that the Darcy-scale law depends on foam quality as foam rheology changes with the fraction of gas and liquid.

3.6. Conclusion

This work investigated the upscaling of foam flow for very high permeability porous media. The impact of foam quality on the apparent foam viscosity, with a fixed flow rate, was examined to distinguish the low and high-quality regimes. The rheology of pre-generated foam through the fine sand was studied as a bulk foam in a rheometer. Foams of different qualities were also injected into a porous column filled with 1 mm glass beads, from which the foam rheology was deduced. The results of both methods were fitted by a rheological model (Herschel-Bulkley-Papanastasiou model) and analyzed by comparison with each other. Foam flow's macroscopic behavior was also numerically studied in different periodic 2D and 3D unit cells by using the rheological data of bulk foam as an input. We also used the empirical Darcy scale law proposed by Chevalier et al. (2013) to derive dimensionless coefficients from our experimental results. We draw the following conclusions:

- Bulk-foam was found to behave as a yield stress fluid and the yield-stress values increased with foam quality. The rheological behavior of foam fits well with the Herschel-Bulkley model.
- Foam in highly permeable porous media (K=8.3×10^{-10} m^2) was also found to behave as a yield-stress shear-thinning fluid regardless of the foam quality. It was also shown that the apparent foam viscosity in porous media increases with the foam quality at the same total flow rate.

- Apparent foam viscosity was seen to be 3-4 times higher than bulk foam viscosity at the same shear rate, which may be due to the complexity of the foam flow in porous media. However, this difference was smaller for very highly permeable porous media. Secondly, the values of dimensionless coefficients of empirical extended Darcy's law exhibited high values for foam compared to other yield-stress fluids and varied depending on foam quality.
- Considerable differences were observed in the experimental and numerical results of upscaling. The global trend of the curves and the behavior in terms of f_g followed the same tendency as those of the experimental results. The experimental results for a very highly permeable porous medium, where the compressibility effect is not significant, fitted well to the experimental data. In the absence of the foam trapping (e.g., a high capillary number), the difference between upscaling results and experimental data can be related to the foam compressibility. Therefore, foam rheological behavior in porous media can be easily predicted from the bulk foam in the case where the foam compressibility is negligible. The calculated compressibility coefficients should be increased with increasing pressure gradients.

Upscaling can be an encouraging tool to predict foam-flow behavior from its bulk behavior. However, further investigations are necessary to incorporate the complex nature of the foam flow in porous media into the upscaling model. These insights are a promising point for studying foam flow in highly permeable porous media.

Chapter 4

Experimental study of rheological behavior of foam flow in capillary tubes

4.1. Introduction

The following is the preliminary draft of a paper that is planned to be submitted in the journal of non-Newtonian fluid mechanics. In this work, we studied the foam flow in straight capillary tubes to better understand the behavior of the foam in porous columns that were investigated in preceding chapters.

Aqueous foam is a complex two-phase fluid where a dispersed gas-phase (bubbles) is separated with a continuous liquid-phase forming lamella. The liquid-phase is commonly an aqueous surfactant suspension that plays a significant role in stabilizing the lamellae between the bubbles.

Foams can be used in many industries, for instance, in the cosmetics and pharmaceutical industry, in the production of foods, as isolating material in constructions, as a fire-fighting fluid. It is also widely used in the oil industry as a drilling fluid and especially as a fluid to extract oil through the enhanced oil recovery (EOR) methods (Lake, 1989). Recently, foam has also been used in polluted soil remediation (Hirasaki, et al., 1997). Since the foam has a low density and a considerably sizeable interfacial surface, it can ensure active contact with contaminants and provide a high capacity for removing pollutants (Wang & Mulligan, 2004).

Foam in porous media can be formed by three underlying mechanisms, namely capillary snap-off, lamella division, and leave-behind (Kovscek & Radke, 1994). However, foam could not be generated in situ in very highly permeable porous media due to the big size of the pores, leading to low capillary pressures, which are mainly found in aquifers (Bertin, et al., 2017). Using pre-generated foam to remediate contaminated-aquifers is also not an easy task due to the high groundwater flow rate in some places. Therefore, the pre-generated foam must be very stable in aquifers to avoid foam flushing. The study of foam flow in porous media is a challenging task both due to the complex rheology of foam and the highly complicated microstructure of porous media. The porous media geometry has therefore been greatly simplified in many works where it is considered as a bundle of capillaries (Scheidegger, 1974; Dullien, 1992; Castro, et al., 2016). Capillary tubes are also considered as the basic element used in the more sophisticated pore network modeling approaches (Sochi & Blunt, 2008; Xiong, et al., 2016). Therefore, a thorough study of foam flow in a capillary tube is considered in this work. Indeed, the simplicity of the geometry allows us to address various but inter-related aspects of foam behavior, namely rheology, stability, and bubble size. For instance, foam instability can be caused by bubble coalescence, drainage, and gas diffusion from small to large bubbles (Ostwald ripening) that leads to a change in bubbles size (Voorhees, 1985). Therefore, foam flow behavior must be studied by regarding these aspects with great care.

Rheology of foam in tubes is often described as a shear-thinning with and without yield stress, and several models were used to represent the foam flow like the Bingham model (Khan, et al., 1988), the power-law model (Enzendorfer, et al., 1995; Gardiner, et al., 1999), and the Herschel-Bulkley model (Harris, 1989; Burley & Shakarin, 1992; Herzhaft, et al., 2005). For instance, David and Marsden (1969) studied foam

flow in glass tubes with diameters of 0.4, 0.6, 0.7, and 0.8 mm. They found shear-thinning behavior of foam with a very low yield stress, and also corrected apparent foam viscosity by taking into account wall slip velocity. Hirasaki and Lawson (1987) described the apparent viscosity of foam flow in smooth capillary tubes based on Hagen-Poiseuille law. The generated foams with a gas fraction (f_g, foam quality) of 70% and above were flowing through glass capillaries with radii of 0.1, 0.2, 0.25, 1, and 2.5 mm. The smallest bubble was equivalent to the size of the smallest capillary tube. They observed a shear-thinning behavior for foam flowing in the tubes and described the apparent foam viscosity by three main affecting factors: 1) liquid slugs between gas bubbles; 2) deformation of bubbles shapes due to viscous and capillary forces; 3) the surface tension gradient, which was explained by the accumulation of active surface material at the back of the bubbles. They also noted the dependence of apparent foam viscosity on bubbles size (texture), capillary radius, and on the fraction of gas in foam. However, the change in length of capillary tubes did not affect the foam behavior in capillary tubes. Herzhaft et al. (2005) studied a pre-generated foam in a recirculating pipe rheometer made of two parallel stainless steel pipes with an internal diameter of 7.7 and 10.9 mm. The flow behavior of the foam was examined with respect to the foam quality varying from 20% to 85% for different surfactant concentrations and at various static pressures. They found a Newtonian and yield stress-type behavior for low ($f_g \leq 50\%$) and high quality ($f_g \geq 60\%$) foams, respectively. Bogdanovic et al. (2009) investigated the rheological behavior of foams with foam quality ranging from 86.2% to 99.6% in horizontal stainless steel pipes with a diameter of 0.5 and 1 inch (corresponding to 12.7 and 25.4 mm respectively). The foam was generated by co-injection of nitrogen and a surfactant solution using a filter (50 μm or 90 μm opening size). They examined five different surfactants with three various concentrations. They found an impact of surfactant type on the transition foam quality (f_g^*), where higher values were found for more stable foams. However, the change in pipe diameter did not significantly change the transition foam quality. They also observed a shear-thickening behavior of foam flow in high-quality regimes ($f_g > f_g^*$) in all experiments. In low-quality regimes ($f_g < f_g^*$), foams mostly behaved as a shear-thickening fluid in the 0.5-inch diameter pipe, but in the 1-inch pipe, foams showed nearly Newtonian (slightly shear-thinning) behavior. Gajbhiye and Kam (2011) conducted foam flow experiments in stainless steel and nylon pipes. The foam flow was studied through pressure drop measurement and also visually by filming the foam bubbles since the nylon pipes were transparent. They pointed out the shear-thickening behavior of foam flow in the low-quality regime and indicated the effect of surfactant on the transition foam quality. They showed a schematic of two flow regimes which were observed based on the foam texture during the experiments (Fig. 4.1). The high-quality regime was described by fine-textured foams and showed slug flow. In contrast, foam flow in the low-quality regime was characterized by a stable flow of uniform foam and illustrated by either segregated or plug flow.

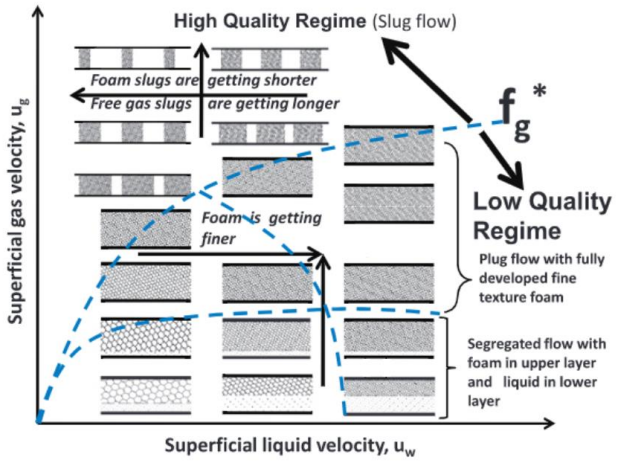

Fig. 4.1 Schematic representation of foam flow in pipes (Gajbhiye & Kam, 2011)

Gumati and Takahshi (2011) studied the flow of foam pre-generated experimentally through glass beads packing in 5 m long acrylic pipe with a diameter of 50 mm. They found a shear-thinning behavior for foams with a quality of 80%, 85%, and 95%, in which shear stress was determined to be a power-law function with the power-law index n respectively equal to 0.44, 0.45 and 0.42. Moreover, Du et al. (2011) admitted the power-law behavior of foam flow in a glass tube with a 5 mm of diameter. As a result, we noticed that foams behave differently in tubes, and these contradictions found among various works may depend on the type of surfactant and gas, as well as on the medium in which foam flows. Another essential feature of foam flow in tubes is a wall slip velocity, which depends on the type of tube material, its surface roughness, and diameter (Stevenson, 2012). This slip velocity is simply useful for a macro-scale description of the boundary condition of the wall. The mechanism of slip at the pore scale depends on the presence of a thin layer of liquid that does not itself slip, but wets the wall and lubricates the foam flow. Hence, when the foam is sheared, a large velocity gradient appears in this liquid layer. Thus, this low viscosity liquid leads to the foam slipping. Indeed, its existence was found in most foam studies through pipes. For example, Jastrzebski (1967) assumed wall slip velocity to be inversely proportional to the pipe diameter. He also, for the first time, proposed to correct the wall slip velocity. Harris and Reidenbach (1987) observed no wall slip velocity in their 3 m long steel pipe with a diameter of 7.75 mm. Thondavadi and Lemlich (1985) found wall slippage for acrylic (Perspex) pipes but did not observe wall slip in galvanized steel pipes (of roughness 100-500 μm). They noted that the acrylic surface is not wetted by foam, but that the galvanized steel is well wetted. However, Denkov et al. (2012) found that a static contact angle of deionized water to be 77.0° and 77.8°, respectively, for Perspex and galvanized steel (Stevenson, 2012). In addition, wall slip velocity was found dependent on the liquid film thickness (Enzendorfer, et al., 1995), which is more significant for low foam qualities (Calvert & Nezhati, 1986).

To our knowledge, the rheology of foam flow in capillary tubes is still under debate. Indeed as mentioned above divers non-Newtonian behaviors are observed for different experimental conditions: Newtonian,

non-Newtonian shear-thinning, shear-thickening, with or without yield stress. Moreover, the impact of the material the tube is made of, which is in relation to the wettability and the wall slip velocity, has not been studied in detail in previous studies. Therefore, the first objective of this study is to investigate foam rheology in capillary tubes in order to understand better foam behavior in porous media and interpret these results both with the rheology of the same pre-generated foams flowing in porous media, and the bulk foam behavior found using a rheometer. Besides, we studied the impact of tube material and the tube diameter on the behavior of the foam in capillary tubes. These goals are achieved by experimentally investigating foam flow in different capillary tubes where foams were pre-generated through a sand-pack.

4.2. Theoretical considerations

The peculiarity of the use of foam in industrial applications is due to a high fraction of gas and a low weight compared to other liquids. The characteristic of foam changes according to the ratio of the gas and liquid phases. It is generally called foam quality, which is expressed as follows.

$$f_g = \frac{Q_G}{Q_G + Q_L} \tag{4.1}$$

where Q_G (mL/min) is the volumetric gas flow rate and Q_L (mL/min) is the volumetric liquid flow rate. The sum of both presents the total flow rate value Q_t. Hence, the shape of the bubbles also changes with the increase in foam quality, from spherical-form (wet foam, 64%<f_g<99%) to polyhedral-form (dry foam, f_g>99%) (Langevin, 2017).

Darcy's law first described the fluid flow through porous media with a linear relationship between the pressure gradient ∇P (Pa/m) and Darcy velocity u (m/s) that can be expressed in the following form when neglecting gravity effects (Darcy, 1856).

$$u = \frac{Q}{S} = -\frac{K}{\mu} \cdot \nabla P \tag{4.2}$$

in which K (m^2) is the intrinsic permeability, μ (Pa.s) is the dynamic fluid viscosity, Q (m^3/s), and S (m^2) the flow rate and the cross-section surface of the porous media sample, respectively. The bundle of capillary tubes model was also one of the first conceptual models for fluid flow in porous media. This concept was also applied for two-phase flow systems where the wetting phase preferably flowed in the smaller capillaries, and the non-wetting phase flowed in the larger capillaries (Lopez & Blunt, 2004). Flow in the capillary tubes was described at first by Hagen-Poiseuille's law (Sutera & Skalak, 1993) through the relationship between the flow rate (Q, in m^3/s) and pressure drop (ΔP, in Pa). It can be presented as follows,

$$Q = \frac{\pi \Delta P R^4}{8 \mu L} \tag{4.3}$$

where R (m) is the tube radius and L (m) is the tube length. In porous media, Kozeny (1927) derived the following equation to calculate a mean pore radius R_{eq} (m) through the laws of Darcy and Poiseuille.

$$R_{eq} = \sqrt{\frac{8K}{\emptyset}} \tag{4.4}$$

in which $\emptyset$ (-) is the porosity of porous media. Hence, wall shear rate $\dot{\gamma}$ (1/s) of a Newtonian fluid in capillary tubes can be calculated using the following equation (Darby, et al., 2001),

$$\dot{\gamma} = \frac{4Q}{\pi R^3} \tag{4.5}$$

and the shear stress at the wall τ_w (Pa) is given by

$$\tau_w = \frac{\Delta P R}{2L} \tag{4.6}$$

It must also be noted that the shear rate is not constant along the diameter and varies with distance from the tube wall. Since the foam flow through the capillary tubes is primarily considered to be a non-Newtonian fluid, the Herschel-Bulkley (H-B) model (Herschel & Bulkley, 1926) may be the best model to represent the foam flow, which is expressed as follows.

$$\mu_{app} = \frac{\tau_0}{|\dot{\gamma}|} + a|\dot{\gamma}|^{n-1} \tag{4.7}$$

with μ_{app} (Pa.s) being the apparent foam viscosity as a function of shear rate $\dot{\gamma}$ (1/s), τ_0 (Pa) the yield stress, a (Pa.s^n) consistency index, and n (-) is the flow index. If the applied stress τ is lower than τ_0, the fluid behaves as a solid, otherwise, it flows as a fluid. In addition, the fluid can be shear-thinning for n<1 or shear-thickening if n>1, and is called a Bingham fluid when n=1. The model reduces to the Newtonian fluid, if τ_0=0 and n=1. Consequently, the volumetric flow rate in a circular tube for Herschel-Bulkley fluids by the following relation (Skelland, 1967):

$$Q = \frac{8\pi}{a^{\frac{1}{n}}}\left(\frac{L}{\Delta P}\right)^3 (\tau_w - \tau_0)^{1+\frac{1}{n}}\left[\frac{(\tau_w - \tau_0)^2}{3 + 1/n} + \frac{2\tau_0(\tau_w - \tau_0)}{2 + 1/n} + \frac{{\tau_0}^2}{1 + 1/n}\right](\tau_w > \tau_0) \tag{4.8}$$

which was derived through the well-known Weissenberg-Rabinowitsch equation (Rabinowitsch, 1929; Mooney, 1931).

4.3. Experimental study

In this section, we present the materials used, the experimental setup, and the procedures for foam flow studies in capillary tubes.

4.3.1. Fluids and materials

Surfactant solution

The surfactant solution was prepared using anionic C_{14-16} alpha-olefin sulfonate (AOS) surfactant Rhodacal® LSS-40/AX (Solvay Novecare) and demineralized water. The surfactant used was chosen based on several essential factors from the point of view of environmental use such as biodegradability in soil (Tuvell, et al., 1978; Talmage, 1994), using field cases (Svab, et al., 2009), and accessibility in the market (Cserháti, et al., 2002). The surfactant critical micelle concentration (CMC) is found to be 1.8±0.1 g/L using a drop shape analyzer (DSA-100S, KRUSS) via the pendant-drop method (Stauffer, 1965). The surfactant solution was prepared with four times CMC, which was chosen after measuring foam stability using a dynamic foam analyzer (DFA-100, KRUSS) by adopting the methodology of Yoon et al. (2009).

Gas

Nitrogen gas with a purity of 99.99% is utilized to generate foam. It was selected after taking into account several studies in the literature on foam stability (Farajzadeh, et al., 2009; Zeng, et al., 2016) and solubility of gases (Sander, 1999). Besides, carbon dioxide with a purity of 99.7% is used for flushing the pre-generation column porous media during the pre-saturation procedures. Air Liquide company supplied both gases.

Porous media

Sand-pack made of calibrated silica sand (BR-37), provided by Sibelco™ company, was used to generate foam, and the grain size distribution of the sand is presented in Fig. 4.2. The measured characteristics of the sand packing are tabulated in Table 4.1.

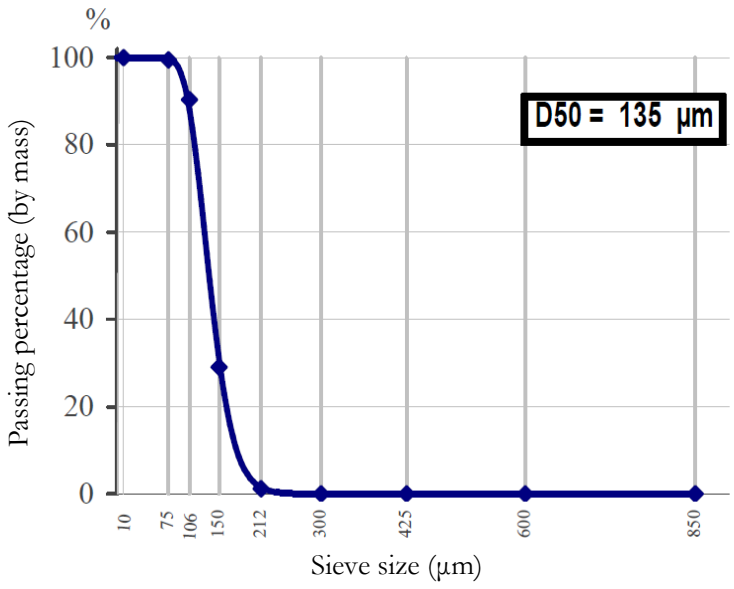

Fig. 4.2 Granulometric distribution of sand BR37 provided by Sibelco company

Table 4.1 Properties of sand-pack

Porous media	**Mean grain size diameter, d_{50} (mm)**	**Pore Volume, PV (mL)**	**Porosity, ∅ (%)**	**Permeability, K (m^2)**	**Mean pore radius, R_{eq} (µm)**
Sand BR37	0.135	51±2	38±1	7.2 (±1) ×10^{-12}	11.5

Capillary tubes

Rheology of pre-generated foam is examined in capillary tubes, the diameters of which were chosen by considering the porous media of our previous experiment (Omirbekov, et al., 2019; Omirbekov, et al., 2020 b) as a bundle of capillary tubes. The diameters of tubes were calculated by Eq. (4.4), which is equal to twice the value of R_{eq}. In addition, according to Prud'homme and Khan (1996), tube diameter must be at least ten times larger than the bubbles to appropriately measure the "bulk" foam rheology as a continuous medium in capillary tubes.

Two types of capillary tube systems are studied to investigate the influence of the tube material on the property of foam: hydrophobic systems (PTFE – polytetrafluoroethylene and FEP – fluorinated ethylene propylene) and hydrophilic (GT – smooth glass tubes). PTFE and FEP tubes were provided by Darwin microfluidics (France) and Adtech (UK) companies, respectively. The glass tubes were obtained from DWK Life Sciences GmbH (Germany). Since the capillary length does not affect the foam flow behavior (Hirasaki & Lawson, 1985), the length of the hydrophobic and the hydrophilic tubes was chosen to be 30 cm and 40 cm, respectively. These lengths were chosen in accordance with the lengths of columns considered in our previous experiments (Omirbekov, et al., 2020 a). The capillary tubes used with their internal diameters (id) are presented in Table 4.2.

Table 4.2 Material type and internal diameters of capillary tubes used in this study

Capillary tube material type		Tube internal diameter (mm)			
Hydrophobic materials	FEP	0.25 (±0.01)	0.3 (±0.01)	0.4 (±0.01)	0.8 (±0.01)
	PTFE	-	0.3 (±0.01)	0.5 (±0.01)	0.8 (±0.01)
Hydrophilic material	Glass tube (GT)	0.2 (±0.01)*	0.4 (±0.01)*	0.5 (±0.01)*	0.8 (±0.01)

*these capillary glass tubes has not been studied due to the delay in delivery

4.3.2. Experimental setup

The experimental setup is presented in Fig. 4.3, where foam was generated by the co-injection of N_2 and the surfactant solution through the foam generator. Next, the flow of pre-generated foam was studied in the capillary tubes.

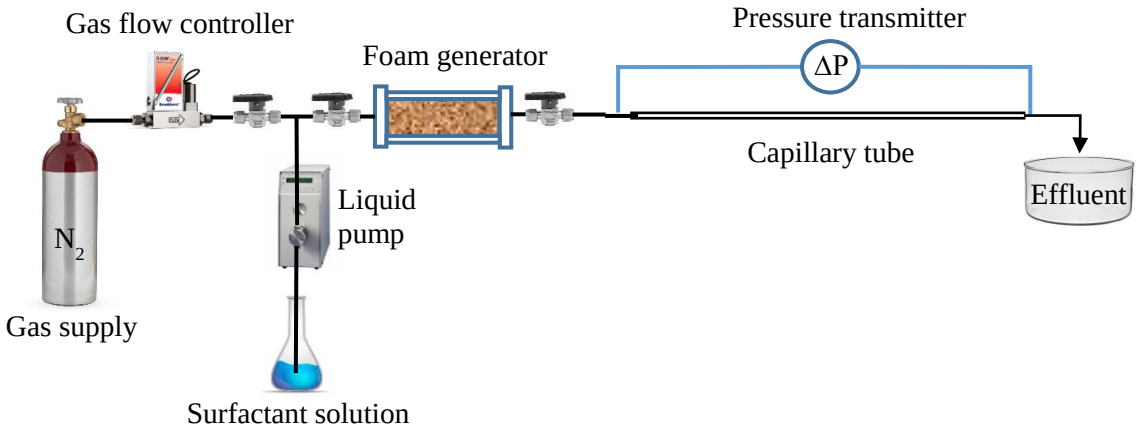

Fig. 4.3 Schematic of the experimental setup used to characterize the rheology of in capillary tubes

The gas was supplied through the mass flow controller El-Flow Select F-201CV (Bronkhorst) with a range of 0.16-10 mL_n/min (±0.5% reading, plus ±0.1% full scale). The surfactant solution was pumped using a piston pump Model 1HM (Eldex) with a precision of ±0.3%. A foam generator column (sand-pack) made of transparent polyvinyl chloride (PVC) with 4 cm internal diameter and 10 cm long was used for foam formation. Two metal grids with a cell size of 42 µm retained the sand in the column on both sides. Rosemount 3051S (Emerson) differential pressure transmitter in the range of 0 to 620 mbar (±0.5 mbar at the maximum value) was used to measure pressure difference along the capillary tubes for a pressure drop less than 620 mbar. When the amplitude of the pressure was more significant than 620 mbar, we used two PR-33X (Keller) pressure transducers to a maximum of 3000 mbar (with an accuracy of 0.01%), installed at both ends of the capillary tubes. In addition, Rosemount 3051S (Emerson) pressure transmitter in the range of 0 to 2500 mbar (±5 mbar at the maximum value) was also used for the tubes with an id of 0.4, 0.5, and 0.8 mm.

4.3.3. Experimental procedure

First, we thoroughly packed the foam generator column with fine sand BR37 and inspected it for leaks. Since CO_2 gas is highly soluble in water, it has been used to rinse the sand-pack, thereby removing air from the porous medium. Demineralized, degassed water was injected vertically into the generator column with 0.5 mL/min to saturate the sand-pack by entirely dissolving CO_2 gas. In order to measure the pore volume (PV), i.e. the porosity, the column was weighed before and after the water saturation step. The sand-pack permeability was obtained by injecting water with different flow rates while measuring the pressure drop along the column. Thereby, the permeability of the sand-pack was calculated through

Darcy's law (Eq. (4.2)). Then, the generator column was flushed by 3 PV of the surfactant solution to complete adsorption. The surfactant solution and N_2 gas were simultaneously injected into the sand-pack to generate foam. 5 PV of foam were co-injected to the sand-pack to obtain a stable foam, which was chosen based on (Simjoo & Zitha, 2020). Then the generated foam was injected horizontally into capillary tubes. The foam flow in each capillary tube was investigated during the injection of a volume equivalent to 1 PV of the foam generator by measuring the pressure drop using the pressure transmitters. In order to examine the impact of foam quality on foam flow behavior in capillary tubes, FEP, PTFE and GT tubes with an id of 0.8 mm and PTFE tube with an id of 0.5 mm were studied at a fixed total flow rate of 1 mL/min while the foam quality was varied from f_g=50% to f_g=99%.

To study the rheology of foam in the capillary tubes with quality of f_g=85%, we measured the pressure drop along the capillary tubes by adjusting the flow rates at each phase. The total flow rate ranged from 0.2 mL/min to 1 mL/min, as it is shown in Table 4.3. In addition, we take pictures of foam bubbles for each flow rate and foam quality, to see the change in the texture of the foam, for the 0.8 mm glass tube. All experiments are conducted at 20°C and atmospheric pressure.

Table 4.3 The values of flow rates used in the experiment for f_g=85%.

Total flow rate, mL/min	Gas flow rate, mL/min	Liquid flow rate, mL/min
1.00	0.85	0.15
0.93	0.79	0.14
0.87	0.74	0.13
0.80	0.68	0.12
0.73	0.62	0.11
0.67	0.57	0.10
0.60	0.51	0.09
0.53	0.45	0.08
0.47	0.40	0.07
0.40	0.34	0.06
0.33	0.28	0.05
0.27	0.23	0.04
0.20	0.17	0.03

4.4. Results and discussion

To verify the experimental configuration, we tested the water flow at different flow rates while measuring the pressure drop along the capillary tubes. The flow through the FEP capillary tube with an id of 0.8 mm was examined by all pressure sensors, and compared to the results calculated using the Poiseuille equation (Eq. (4.3)). Fig. 4.4 shows the set flow rate vs. the measured pressure drop of water flow using the various pressure sensors. Results from the differential pressure transmitter Rosemount 3501S with a range up to 620 mbar was the most reliable one, and the one with a range up to 2500 mbar had an error due to the

calibration range. Still, the results followed the trend of Poiseuille's law results. However, the displayed results from Pressure Transducers PR-33X from Keller were the least secure and gave values with significant discrepancies.

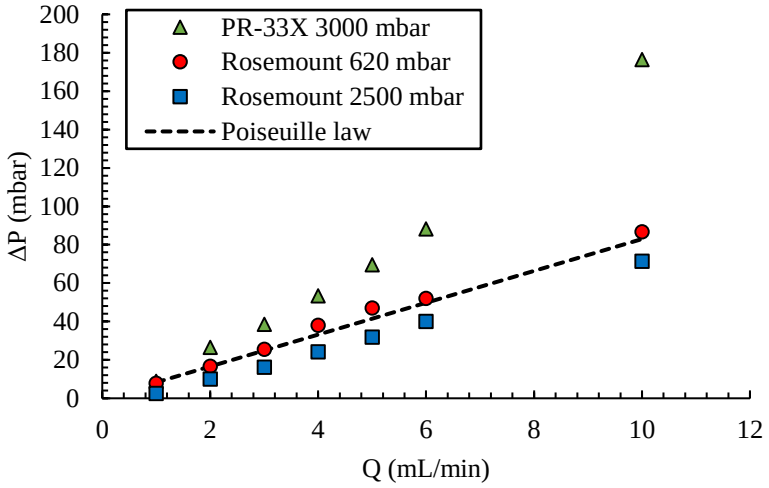

Fig. 4.4 The measured pressure drop for water flow (in id=0.8 mm FEP tube) as a function of the flow rate through PR-33X and Rosemount pressure transducers

Since foam is not a pure single-phase fluid, it requires a particular time to achieve stabilization while measuring the pressure drop along capillary tubes. 5 PV of the N_2 and surfactant solution were co-injected through the foam generator to form a stable foam. Hence, in the capillary tubes, the pre-generated foam has reached stabilization when a foam volume equivalent to 0.5-1 PV of the generator column has flowed through the capillary tubes. For instance,

Fig. 4.5 shows the f_g=85% foam-flow stability test through a 0.8 mm diameter PTFE tube for foam flow with Q=1 mL/min. The stabilization occurred after 0.5 PV (1500 s) of injection, and for lower flow rates, the stabilization time increased up to 1 PV. The average value of the pressure drop obtained was 70.03, with ±8.68 mbar of oscillation that occurs due to the difference between liquid and gas pressures in foams. Consequently, the oscillation bars were presented by the standard deviation for each result.

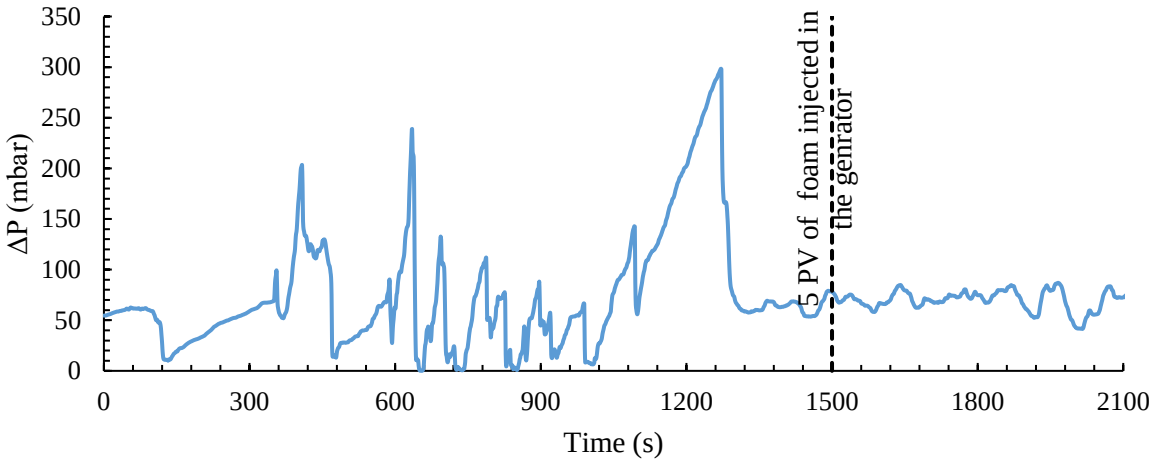

Fig. 4.5 Pressure difference as a function of time for f_g=85% foam in 0.8 mm diameter PTFE tube at Q_t=1 mL/min: the steady state occurs at 5 PV of foam injection in the generator

4.4.1. Foam quality in capillary tubes: effect of tube material and inside diameter on foam flow

Fig. 4.6 shows the apparent foam viscosity as a function of foam quality for FEP, PTFE and GT tubes with id of 0.8 mm, and PTFE tube with id=0.5 mm. The apparent foam viscosity is increased with foam quality up to a transition foam quality value (f_g^*). The domain where $f_g < f_g^*$ corresponds to the low-quality regime. Above the transition foam quality denoted as a high-quality regime, the apparent viscosity of foam decreases with f_g. We noticed that the apparent foam viscosity increased with foam quality until an instability zone that occurred above f_g=90%, for the FEP, PTFE and glass tubes of 0.8 mm id. According to Khatib et al. (1988), this instability caused by capillary pressure, which was found to reach a specific value (the limiting capillary pressure) at a relatively high fractional gas flow. When the fractional flow of gas increases further, the capillary pressure was found to remain at the limiting value. Nevertheless, they observed the process of coalescence and displacement of the coarse-textured foam near the limiting value. Therefore, the instability mentioned above occurred due to the change of foam texture. The maximum μ_{app} of foam for the hydrophobic tubes (i.e., FEP and PTFE) and for the hydrophilic tube (GT) were obtained respectively at f_g=98% (the vertical dotted line) and f_g=97% (the vertical dashed line), which corresponds to the transition foam quality f_g^*. This indicates that the transition foam quality depends on the material type. Moreover, lower values of μ_{app} were noticed for the tube of id of 0.5 mm compared to id of 0.8 mm made with the same material, i.e. PTFE. This means that there is a decrease in the apparent foam viscosity with the tube diameter. This is in agreement with the shear-thinning behavior of the foam. Furthermore, a transition foam quality of f_g^*=96% (the vertical dash-dotted line) was obtained for the PTFE tube with a 0.5 mm diameter against f_g^*=98% for the same tube material but 0.8 mm of diameter. This indicates that the f_g^* depends not only on tube material but also on tube diameter. Decreasing the tube dimeter decreases the transition foam quality.

In low-quality regimes, the bubbles' size of the generated foam was roughly assumed to be the same size as sand-pack pores (Rossen & Wang, 1999), which was determined through Eq. (4.4). However, foam textures were changed above f_g=90%, where we also observed the flow of foam with free gas slugs (see Fig. 4.7) as it was indicated in the literature (Gajbhiye & Kam, 2011). Therefore, bubbles size cannot be considered equal to pores of the foam generator in high-quality regimes.

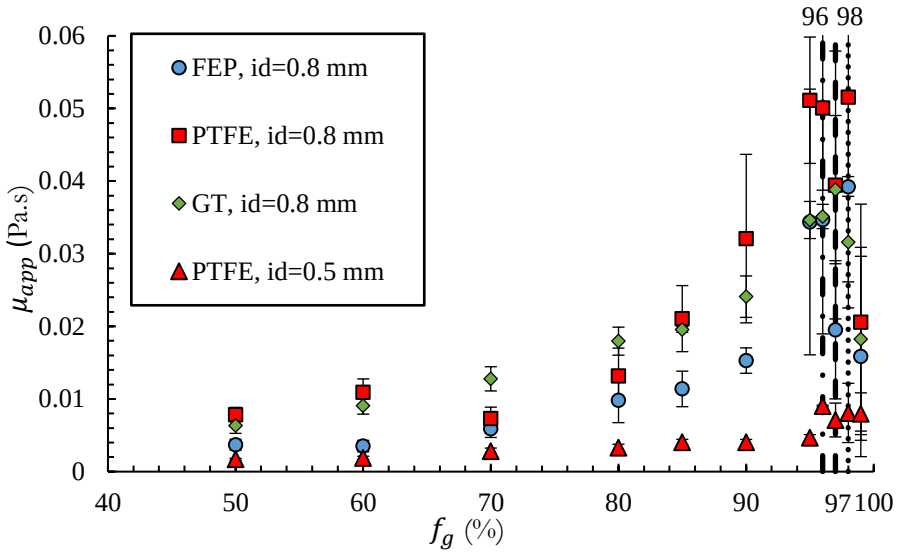

Fig. 4.6 Apparent foam viscosity in capillary tubes (FEP id=0.8 mm; PTFE id=0.5, 0.8 mm; GT id=0.8 mm) as a function of foam quality at Q_t=1 mL/min.f_g^* are shown as dotted (hydrophobic tubes id=0.8 mm) and dashed (hydrophilic material id=0.8 mm), and dash-dotted (PTFE, id=0.5 mm) lines.

For the foam flow in tubes of the same internal diameter (id=0.8 mm), high viscosity values were observed from the experiments in the PTFE tube compared to those performed in the GT and FEP tubes, thus confirming the impact of the tube material. Besides, foam in the glass tube behaved more viscous than in the PTFE tube, although the FEP and PTFE tubes are hydrophobic, the disparities observed could be attributed to the difference in wettability (Qi, et al., 2018) or the effect of wall slip velocity (Herzhaft, et al., 2005), which should be taken into account in future work.

Fig. 4.7 shows the foam texture images for each quality of foam in the glass tube. In the foams below f_g of 70%, we can observe slugs of liquid that refer to the flow of bubbly liquid. The texture of the foams between f_g=70% and f_g=85% is more homogenous, and we can see the appearance of gas slugs in the foams flowing at f_g>90%. Furthermore, these gas slugs become more important with increasing the foam quality.

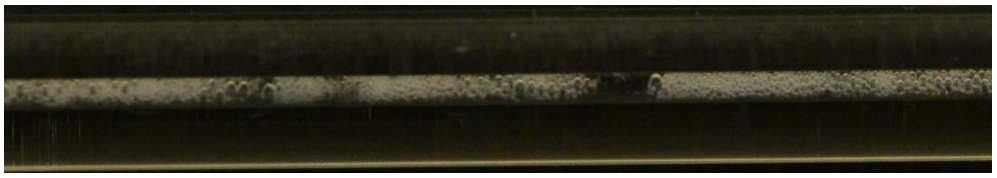

f_g=50%

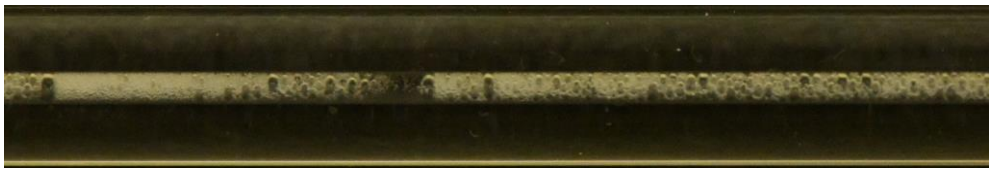

f_g=60%

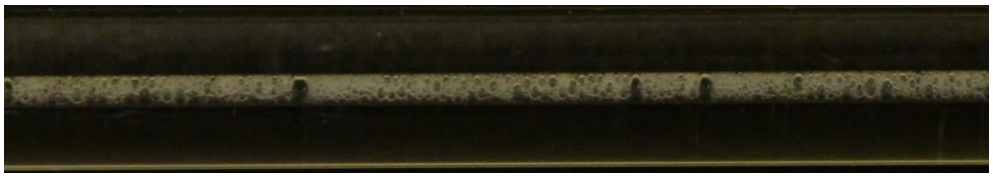

f_g=70%

f_g=80%

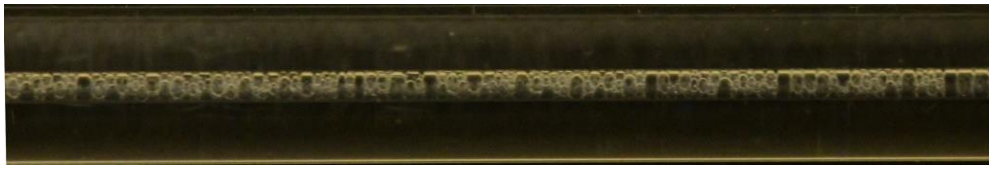

f_g=85%

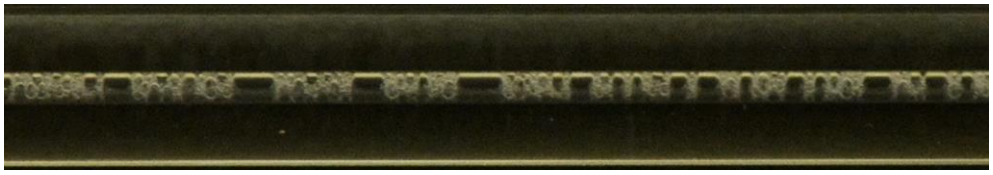

f_g=90%

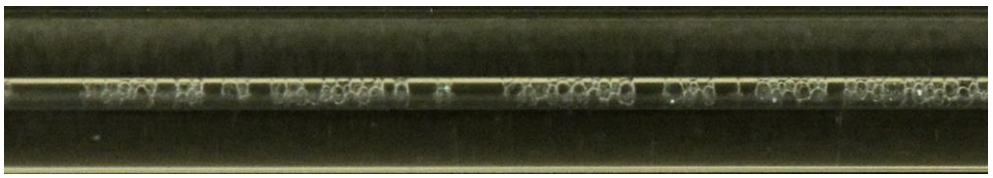

f_g=95%

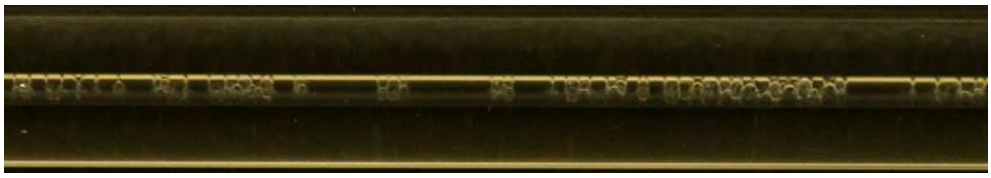

f_g=96%

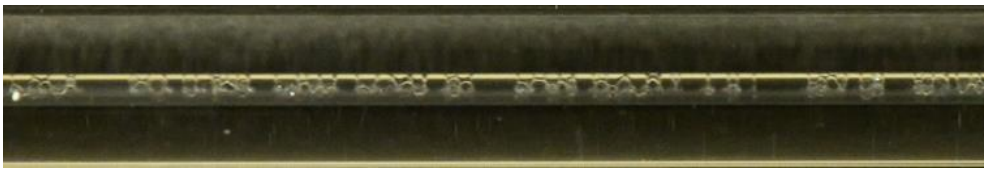

f_g=97%

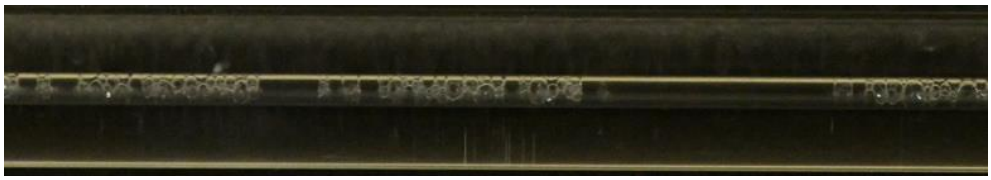

f_g=98%

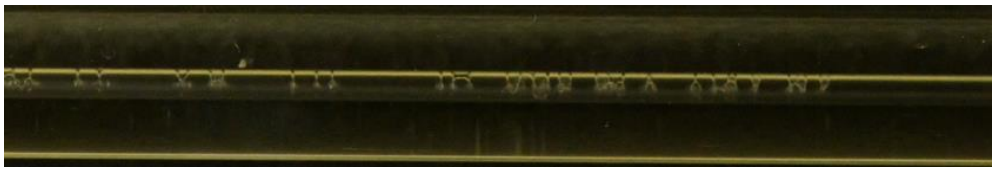

f_g=99%

Fig. 4.7 Foam images in 0.8 mm glass tube for different foam qualities (Q_t=1 mL/min)

4.4.2. Foam rheology in capillary tubes: effect of tube diameter, material and foam texture

In Fig. 4.8 and Fig. 4.9, the apparent viscosity is plotted as a function of the total flow rate respectively for FEP and PTFE tubes, at a fixed f_g=85%. Here, we observed that the apparent foam viscosity in capillary tubes increases with the size of tube diameter at the same total flow rate and decreases when the flow rate increases. Therefore, shear-thinning foam-flow behavior can be noticed. However, an irregularity in the results was observed for smaller tube diameter, where the foam bubbles become larger compare to the tube diameter.

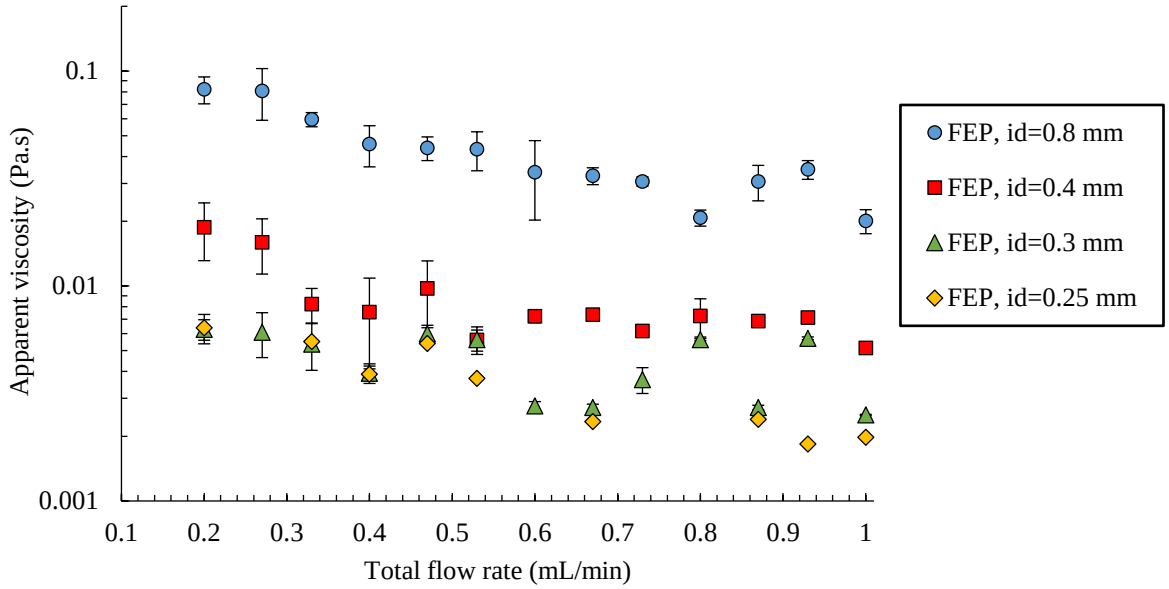

Fig. 4.8 Apparent viscosity as a function of total flow rate for id=0.25, 0.3, 0.4 and 0.8 mm FEP tubes (f_g=85%)

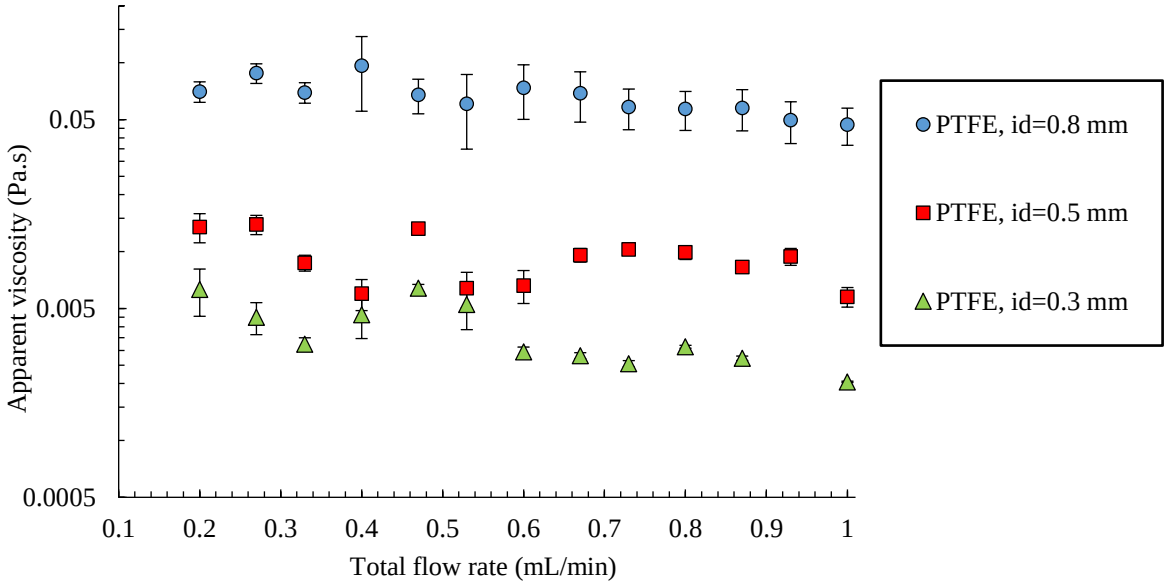

Fig. 4.9 Apparent viscosity versus total flow rate for id=0.3, 0.5 and 0.8 mm PTFE tubes (f_g=85%)

In order to investigate the foam rheology, the apparent viscosity results were considered as a function of the equivalent shear rate. The variation of the apparent foam viscosity in FEP capillary tubes with different inside diameters as a function of shear rate is presented in Fig. 4.10. The equivalent shear rates in capillary tubes were calculated from the flow rates given in Table 4.3 through Eq. (4.5). The experimental results show the non-Newtonian behavior of foam when flowing through a capillary tube, and the results were fitted by the Herschel-Bulkley model (Eq. (4.7)). In Fig. 4.10, Fig. 4.11, Fig. 4.12, and in Fig. 4.14, the

colored dots and the lines correspond respectively to the experimental data and the fitted curves using the Herschel-Bulkley model. The fitting parameters for each tube with the coefficient of determination are tabulated in Table 4.4.

The same experiments under identical conditions were also carried out in all the PTFE capillary tubes. The results with the fit curves are shown in Fig. 4.11, and fitting parameters listed in Table 4.4. Both figures show the scattering of the results with respect to the H-B fitting lines, increases with the reduction of the tube diameter. When we examine the tube with a smaller diameter, the size of the bubbles becomes more significant compare to the tube diameter since the number of bubbles decreases per section of the tubes. As a result, this calls for instability in the pressure drop measurement caused by the pressure differences between gas and liquid phases.

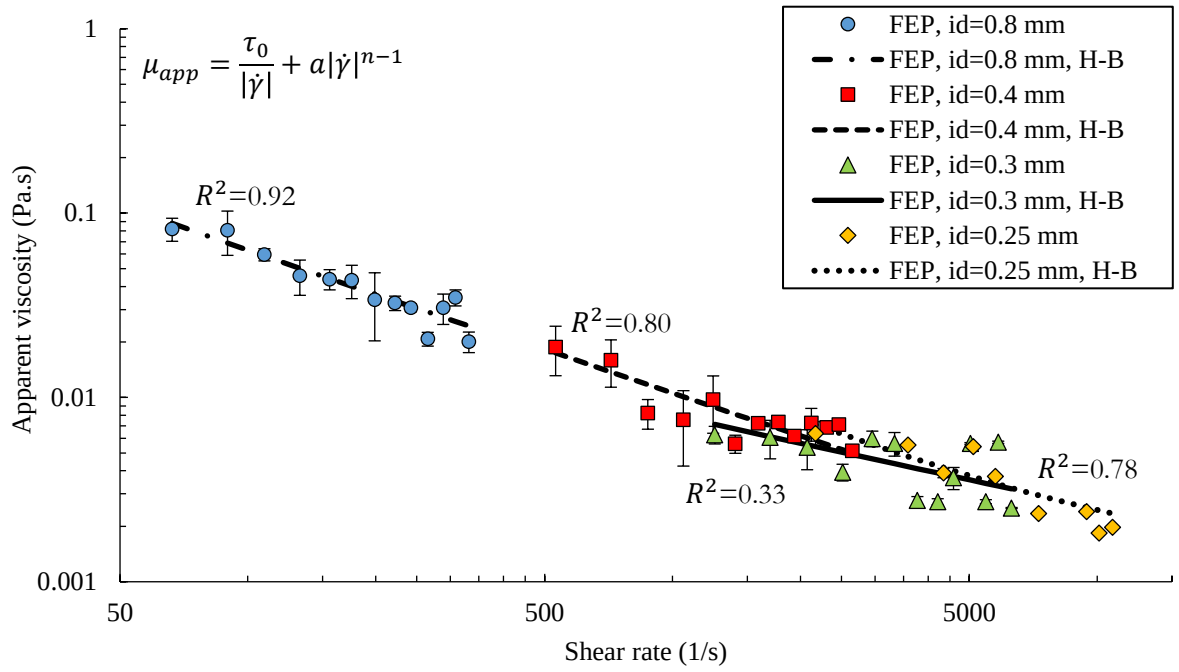

Fig. 4.10 Apparent foam viscosity as a function of shear rate in FEP tubes with an id=0.25, 0.3, 0.4, and 0.8 mm (f_g=85%)

As Table 4.4 shows, we observed the impact of tube diameter on the foam rheology. The shear-thinning behavior of foam was found for all tubes. In PTFE tubes, we noticed an increase in flow indices n with the size of tube diameter. However, for FEP tubes, we found a reverse effect, where the values of n increased with a reduction in tube diameter size. The foam behaved like a Bingham plastic for FEP tubes with id of 0.25 and 0.3 mm, the flow indices of which were 0.95 and 0.99, respectively. Moreover, the values of yield stress increased with the decrease in the diameter of FEP tubes. Nevertheless, the yield stress fitting values were almost zero in all PTFE tubes, thus showing the lack of yield stress in these tubes.

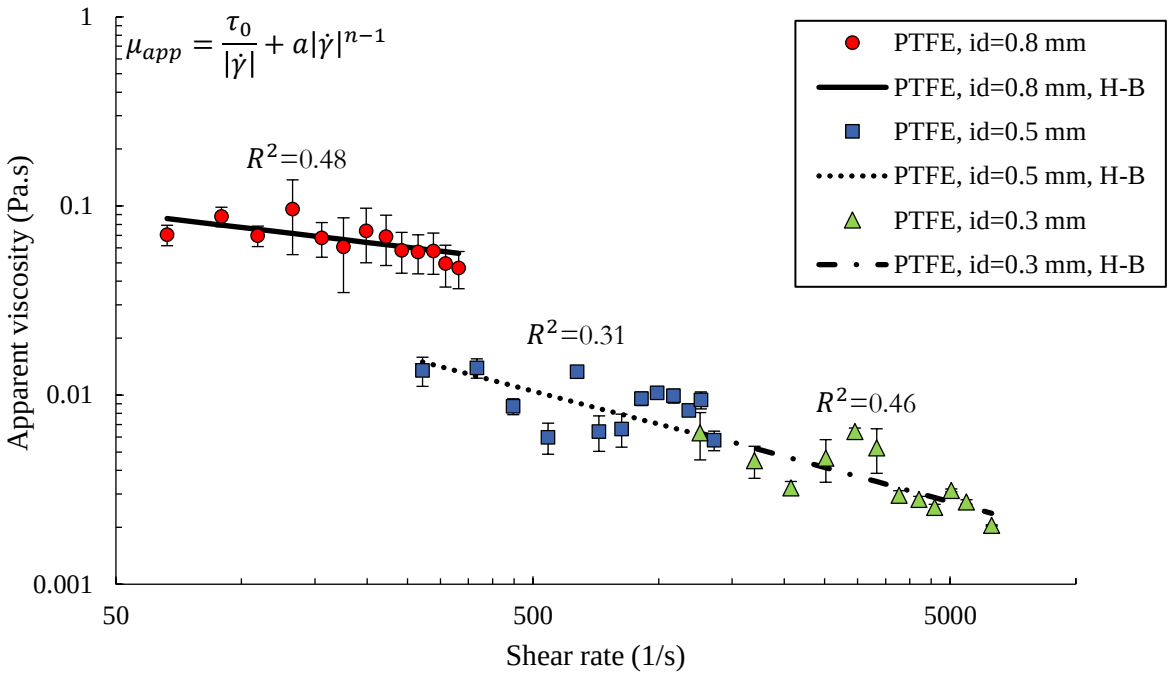

Fig. 4.11 Apparent foam viscosity as a function of shear rate in PTFE tubes with an id=0.3, 0.5, and 0.8 mm (f_g=85%)

In Fig. 4.12, we plotted the apparent foam viscosity as a function of shear rate with an inside diameter of 0.8 mm, and the fitting parameters with a coefficient of determination are tabulated in Table 4.4. We can see that the foam in the glass tube also behaves as a shear-thinning fluid. However, the results do not follow the Herschel-Bulkley model between shear rate values of 66.3 1/s and 155.8 1/s.

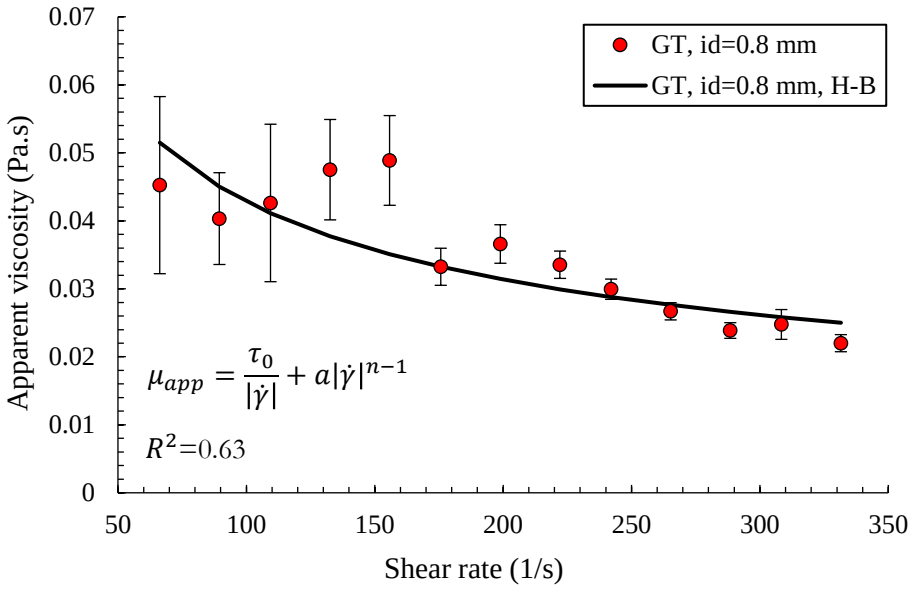

Fig. 4.12 Apparent viscosity of foam vs. shear rate in id=0.8 mm glass tube (f_g=85%)

For low shear rates (i.e. flow rates) up to 155 1/s, the oscillation bars of the apparent viscosity values are relatively high compared to the values at higher shear rates. This phenomenon can be explained by the transition of foam formation from weak to strong state in the generator column, which occurs when the total flow rate increases. During this process, the foam texture changes from coarse to fine, thereby considerably reduce gas mobility. Thus, foam flow at low shear rates has a state of being weak, which tends to the higher oscillations of pressure drop measurements (i.e., apparent foam viscosity).

In order to see this process, we presented in Fig. 4.13 the photographs of steady-state foam flow in a 0.8 mm GT for flow rates in the range of 0.20 to 1 mL/min and foam quality of 85%. According to the images, we see that the high oscillation bars of the apparent viscosity depend on the change of foam texture with flow rates. Notably, at low flow rates from 0.20 mL/min to 0.47 mL/min, we observed slugs of free gas that cause the large fluctuation in pressure drop measurements. As mentioned above, this phenomenon is related to the presence of weak foam, which occurs due to the excess of the bubble coalescence rate compared to the lamellae (i.e., bubble) creation in the foam generator (Sheng, 2013).

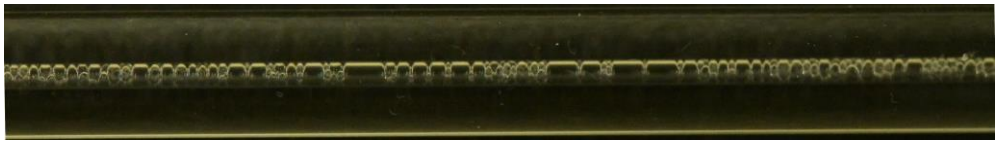

0.20 mL/min (66.3 1/s)

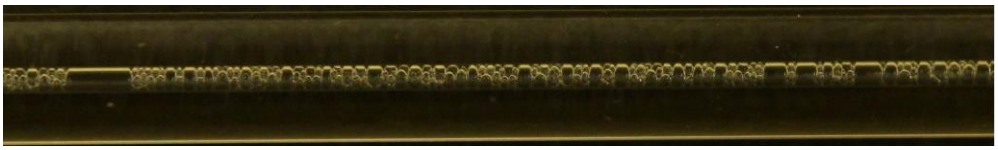

0.27 mL/min (89.5 1/s)

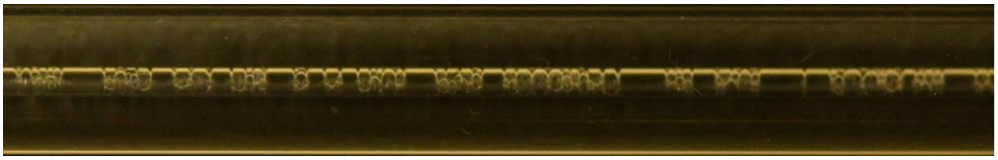

0.33 mL/min (109.4 1/s)

0.40 mL/min (132.6 1/s)

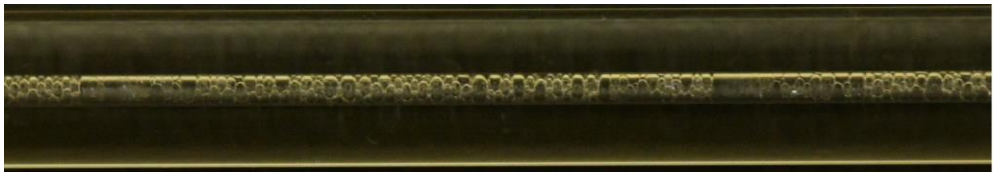

0.47 mL/min (155.8 1/s)

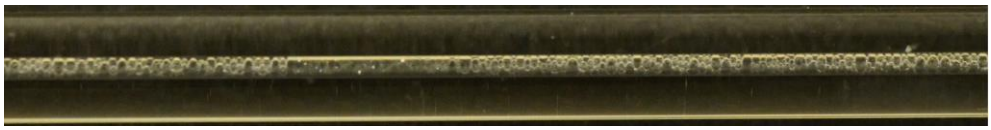

0.53 mL/min (175.7 1/s)

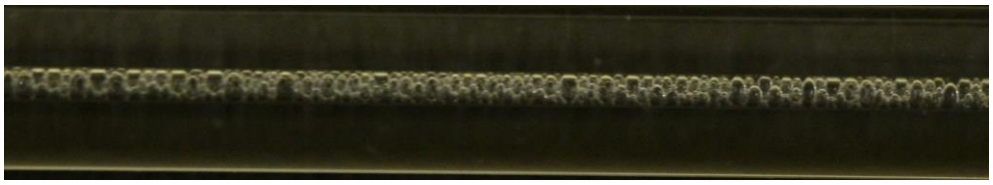

0.60 mL/min (198.9 1/s)

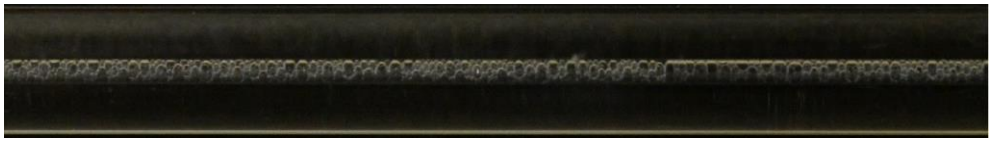

0.67 mL/min (222.1 1/s)

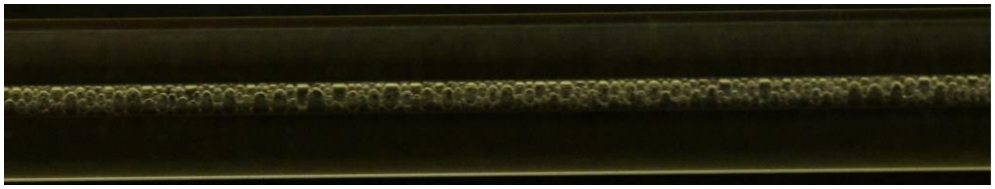

0.73 mL/min (242.1 1/s)

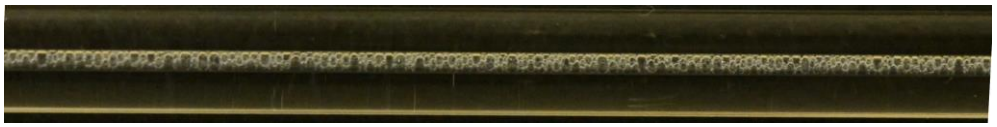

0.80 mL/min (265.2 1/s)

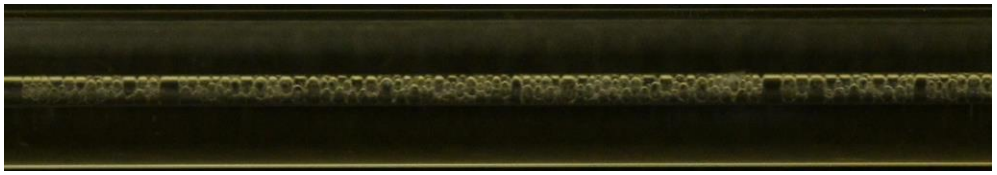

0.87 mL/min (288.5 1/s)

0.93 mL/min (308.4 1/s)

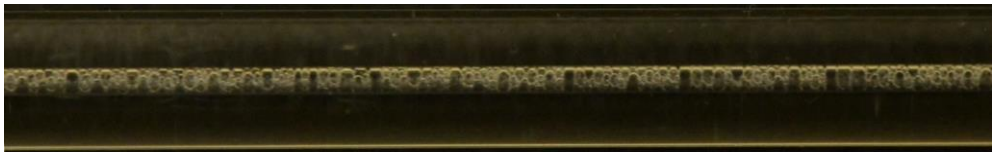

1.00 mL/min (331.6 1/s)

Fig. 4.13 Foam images in 0.8 mm GT for different flow rates (f_g=85%)

In order to compare the apparent foam viscosity results in tubes made of different materials, we plotted the results of the apparent foam viscosity obtained from FEP, PTFE, and GT tubes with the same diameter size in Fig. 4.14. At first sight, we observed that the apparent foam viscosity in hydrophobic systems (i.e. in PTFE and FEP tubes) is higher than in the glass tube, which is a hydrophilic material.

According to fitting parameters presented in Table 4.1, the foam in the PTFE and GT tubes behaved as a power-law fluid while in the FEP tube, the foam flowed as a yield stress fluid. Since the generated foam is identical, the discrepancy can only be attributed to the material used for each tube. However, according to the images presented in Fig. 4.13, we observed that the foam texture is coarse at the low flow rates from 0.20 mL/min (66.3 1/s) to 0.47 mL/min (155.8 1/s). If we do not take into account the data of these flow rates, the results of FEP and glass tubes almost overlap. Nevertheless, even at high shear rates exceeding 155.8 1/s, we observe differences in apparent viscosity of the same foam in the PTFE and FEP tubes, regardless of whether the two tubes are made of hydrophobic materials.

Finally, we found that the behavior of the foam depends on the type of material, which may be a reason for the roughness of the surface.

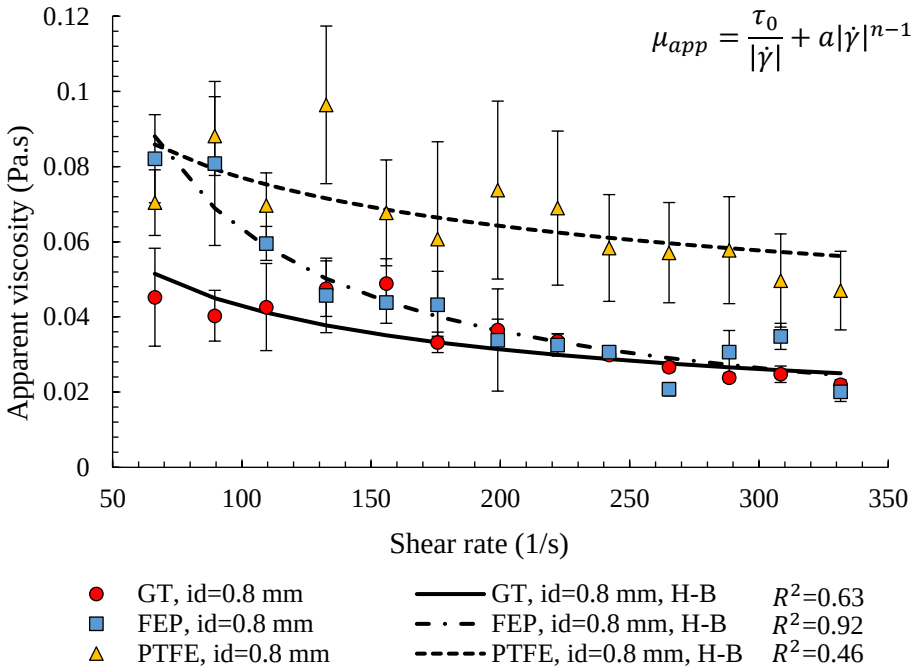

Fig. 4.14 Comparison of apparent foam viscosities for FEP, PTFE and GT tubes with id=0.8 mm at the same range of shear rate (f_g=85%)

Table 4.4 Fitting parameters of H-B model for FEP, PTFE and GT tubes

Tube types	**FEP**				**PTFE**			**GT**
id (mm)	0.25	0.3	0.4	0.8	0.3	0.5	0.8	0.8
$\boldsymbol{n}$ (-)	0.95	0.99	0.36	0.36	0.39	0.42	0.74	0.55
$\boldsymbol{\tau_0}$ (Pa)	12.69	4.49	4.12	2.95	0.01	0	0	0
$\boldsymbol{a}$ (Pa.s^n)	0.01	0.01	0.54	0.64	0.48	0.39	0.26	0.34
R^2	0.78	0.33	0.80	0.92	0.48	0.31	0.46	0.63

4.4.3. Consistency of the foam behavior in capillary tubes with the rheology of bulk foam

In this section, we used the analytical expression of the Herschel-Bulkley model (Eq. (4.8)) for volumetric flow through the circular tubes, in which the measured rheological characteristics of the bulk foam from our previous experiment (Omirbekov, et al., 2020 b) are used as input, to study the consistency with the foam behavior in capillary tubes. The following H-B fitting parameters of bulk foam with a foam quality of f_g=85% is used in the analytical expression: n=0.52, τ_0=2.87 and a=0.76 (see Chapter 3, Table 3.2).

In Fig. 4.15, we plotted the total flow rate versus the pressure loss per unit length of foam flow through the 0.8 mm GT, FEP, PTFE tubes, and the analytical solution of the H-B model using the bulk foam rheology. In the figure, the experimental data and the results of the analytical solution correspond respectively to the colored dots and the dashed line. Here, we observe that the foam mobility in the capillary tubes is greater than that simulated using the bulk foam rheology. This may be a consequence of wall slip velocity in capillary tubes since the rheology of the bulk foam was measured through the serrated parallel-plate geometry to eliminate the wall slip velocity.

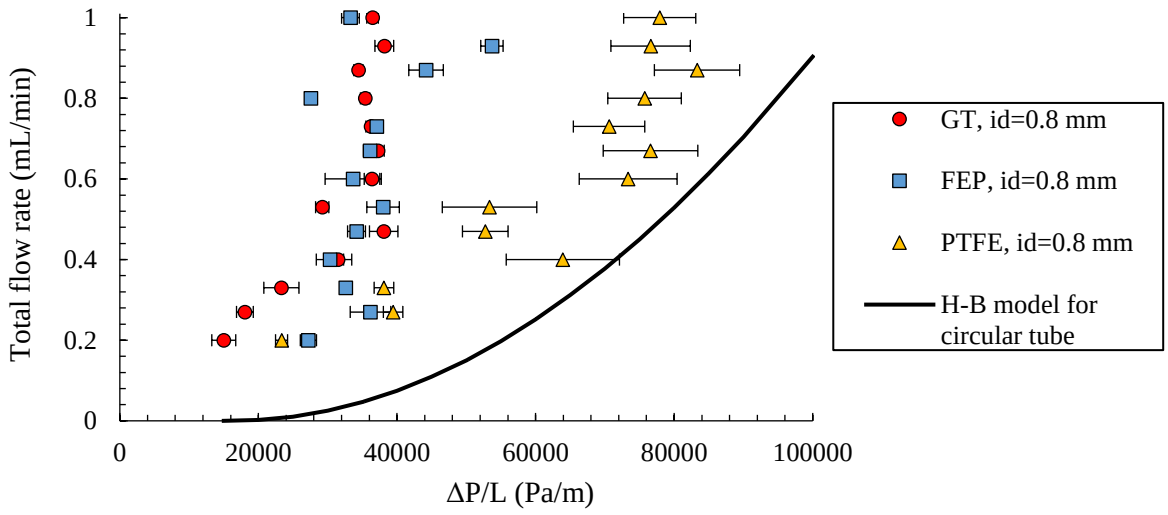

Fig. 4.15 Total flow rate as a function of the pressure loss per unit length for GT, FEP, PTFE tubes with the id of 0.8 mm and the analytical solution for the yield stress fluid (f_g=85%)

Since the tube diameters are the same, only surface roughness and the wettability of foam may affect the surface boundary condition (i.e., wall slip).

As we know, the glass is the hydrophilic material, the static contact angle of which is 47-58° (Mitra, et al., 2016), hence less than 90°. According to Lee et al. (2008), advancing and receding contact angles of water drop on PTFE surfaces are 122° and 94°, respectively. On FEP surfaces, the values of advancing and receding contact angles are almost identical and correspond respectively to 119° and 98°. Since the surfactant solution is able to change the contact angle (Singh & Mohanty, 2016), the contact angle between the surfactant solution and PTFE (or FEP) can be changed (Chaudhuri & Paria, 2009; Henrich, et al., 2016). However, in Fig. 4.15, we can see that the results of FEP and PTFE tubes are dissimilar, and outcomes from the FEP tube are close to the smooth glass tube results. The only reason for this difference can be the effect of surface roughness. According to Lee et al. (2008), the root-mean-square surface roughness (R_{rms}) of the PTFE and FEP materials corresponds respectively to 58.6 and 10.5, where the R_{rms} was measured by an atomic force microscope on scanned areas of 10×10 μm^2. We can see that the roughness of the PTFE surfaces is about 6 times greater than the FEP material. By this, we can assume that the wall roughness of the PTFE tube suppresses the wall slip velocity, but does not completely eliminate it compared to the results of the bulk foam rheology. As a result, the total flow rate should be presented as follows:

$$Q_t = Q_f + Q_s \tag{4.9}$$

in which, Q_f (mL/min) and Q_s (mL/min) are the volumetric flow rate due to the fluidity and slip, respectively. From the preceding equation, Q_s was roughly estimated to be 0.19 mL/min for the 0.8 mm diameter PTFE tube. However, the wall slip velocity should be evaluated with great care, depending on the tube diameter (Jastrzebski, 1967). Therefore, the wall slip velocity will be calculated for all tubes after experiments on glass tubes of smaller diameter are completed.

In order to compare and combine our results, we have gathered the outcomes of bulk foam rheology using a rheometer, as well as with the results of foam flow through high permeable porous media (Omirbekov, et al., 2020 a). Fig. 4.16 shows measured apparent foam viscosity vs. shear rate in GT, FEP and PTFE capillary tubes, in comparison with the results studied in foam flow in the porous column and bulk foam behavior through rheometer. All the foams studied were pre-generated through the same sand-pack and with a foam quality f_g=85%. The experimental results of glass beads column and bulk foam using the rheometer were drawn from (Omirbekov, et al., 2020 b). All results were fitted well using the Herschel-Bulkley model, and the fitting parameters with a coefficient of determination were presented in Fig. 4.16.

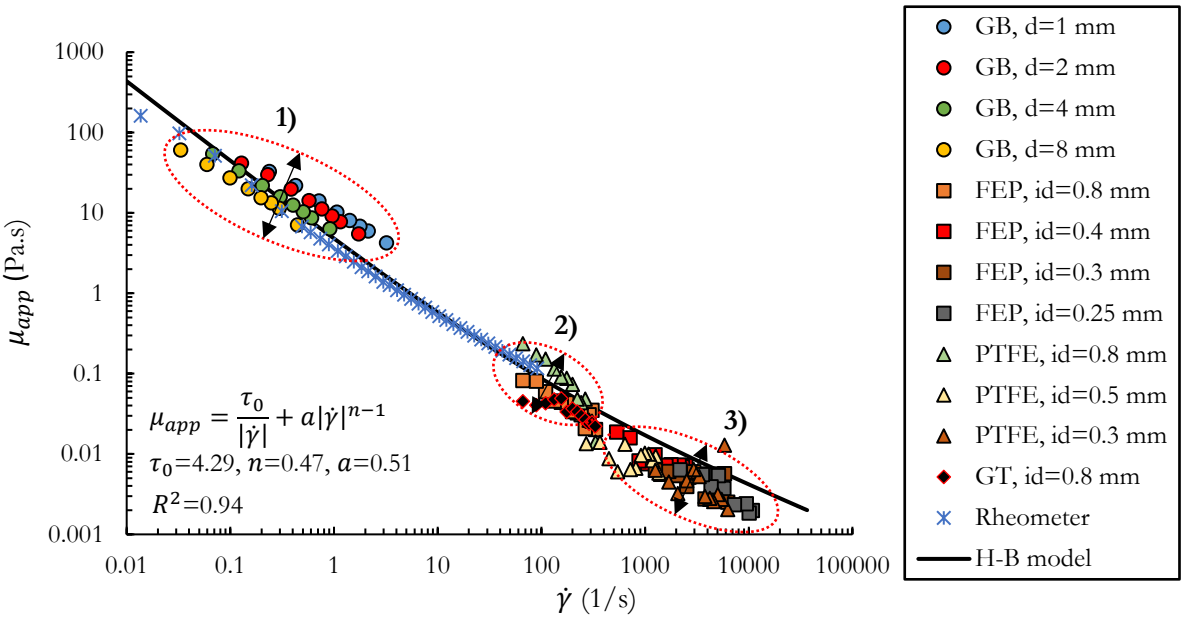

Fig. 4.16 Apparent foam viscosity of f_g=85% as a function of shear rate through different methods: in glass beads packings (GB d=1, 2, 4 and 8 mm), using a rheometer (serrated parallel plate geometry), and in capillary tubes (FEP, id=0.25, 0.3, 0.4 and 0.8 mm; PTFE, id=0.3, 0.5 and 0.8 mm)

These results globally show that the pre-generated foam considered here can be considered as a bulk foam if bubbles are much smaller than pores for the columns or much smaller than tube diameter for the flows in capillary tubes. However, the following inferences can be drawn from each zone in Fig. 4.16 denoted in the figure.

1) Foam flow in porous media, i.e. in confined media, behaves differently from bulk foam under ambient conditions. The apparent foam viscosity increases with the decrease in grain size. These can be an effect of compressibility that is more important in less permeable porous media. Therefore, the results of 4 mm and 8 mm near the fitting curve seem consistent with the results from the rheometer.

2) The effect of tube material on foam viscosity is observed. This can be the impact of inter-related wall slip velocity, which is therefore linked to surface roughness and wettability. Consequently, wall slip velocity can lead to a change in the mobility of foam flow in tubes. However, as it was mentioned in the previous section, it must be studied again with great care.

3) We noticed a dispersion of the results of foam flow in smaller diameter tubes, particularly for very high shear rates. This may also be due to the decrease in the radius of the tube, therefore a decrease in the pore size to bubble size ratio. Foam flow at high flow rates and in smaller diameter tubes must be considered with particular care.

4.5. Conclusion

The following conclusions were drawn from this study:

- From experiments in capillary tubes, the apparent foam viscosity as a function of foam quality follows globally the classical trend with two regimes corresponding to the low-quality and high-quality regimes separated by a transition. However, the apparent foam viscosity increases with foam quality until the occurrence of an instability due to the change of foam textures above f_g=90%.
- For id=0.8 mm tubes, the transition foam quality was found to be f_g^*=98% for the FEP and PTFE tubes, and f_g^*=97% for the glass tube of the same size. Thus, the transition foam quality values depend on material type. However, it was 96% for 0.5 mm FEP tubes that indicates the instability of the foam in smaller diameter tubes.
- The foam flow imaging showed that the foam texture changes from the bubbly liquid at low foam qualities (f_g<70%) to polydisperse homogeneous foam at 70%≤f_g<90% and to foam with gas slugs above f_g≥90%. The texture of the foam also changed depending on the flow rate. At low flow rates, the foam texture is coarse, which is due to the generation of weak foam where the bubble coalescence rate increases compared to the rate of bubble generation. Therefore, the foam rheology is highly dependent on the foam texture and the size of the bubbles.
- Foam viscosity is more significant in the PTFE tube compare to FEP and glass tubes that can be a consequence of surface roughness. However, we were unable to quantify specifically the tube wall slip velocity; therefore further investigations to elucidate this aspect are proposed.
- Foam behaves like a yield stress fluid in the FEP tubes and its behavior can be well fitted by the Herschel-Bulkley model. Nevertheless, yield stress values were found to be zero in GT and PTFE tubes.
- Foam rheology deduced from flow in capillary tubes could be compiled in a master curve along with the rheology obtained through the study of foam flow in glass beads packings and the characterization measured by a rheometer and they could altogether be fitted by a H-B model allowing different comparisons and discussions.
- The scattering of the results found for foam flow in small capillaries, may be the cause of the polydispersed foam generated through the sand-pack.

4.6. Perspectives

The behavior of foam flowing in capillary glass tubes with id=0.2, 0.4, and 0.5 mm has not been studied due to the delay in delivery. Therefore, it will be examined, and the outcomes will be compared to other results. Besides, the wall slip velocity will be calculated using the Jastrzebski method (Jastrzebski, 1967). We propose to thoughtfully study foam texture and wall slip velocity in all tubes to understand the foam behavior in tubes better. Moreover, it will be interesting to consider the foam flow in the tube using the foam of different bubble sizes (e.g., glass bead packings with 0.1 and 1 mm glass beads).

Chapter 5

General conclusions and perspectives

5.1. Conclusions

This thesis aimed to make new contributions to the study of foam behavior in highly permeable porous media that are mainly found in aquifers. More specifically, the behavior of the pre-generated foam in high permeability porous media, where the foam bubbles are much smaller than the pore dimensions, is still lacking. Therefore, we studied the flow of pre-generated foam through highly permeable porous media and capillary tubes, as well as the rheological behavior of the foam in bulk-form using a rheometer. Moreover, the upscaling of foam flow from the pore to the Darcy-scale was conducted using the homogenization technique considering the rheological features of foam as an input. The characterization of bulk foam, including surfactant concentration, gas type, and foam formation depending on an alpha-olefin sulfonate surfactant concentration, were examined. We considered foam formation using a sand-pack (d_{50}=0.135 mm) and bead-pack composing of 1 mm glass beads, in which the foam was pre-generated by co-injection of surfactant solution and nitrogen.

We draw the following conclusions from the characterization of bulk foam.

- The critical micelle concentration (CMC) of the surfactant used was determined experimentally to be 1.8 g/L.
- The maximum stability (i.e., half-life time) of bulk foam was observed with 2 × CMC, and the utmost foamability was obtained with 3 × CMC. The surfactant concentration was chosen to be 4 × CMC with a margin, to ensure not only stability and foamability but also high surfactant concentration in case of adsorption.
- The bulk foam generated via N_2 found to be much more stable and foamable than with CO_2. Specifically, the stability and the foamability were exceeded by 42 and 3 times, respectively.

After selecting the surfactant, surfactant concentration, and gas type, the foam behavior was studied in different packed glass beads with monodispersed size. Foam generation in sand-pack and 1 mm glass beads packing were analyzed to study the effect of bubble size on the apparent foam viscosity. The impact of foam (pre-generated) quality on the apparent foam viscosity at a fixed flow rate was examined to distinguish low and high-quality regimes. The rheology of pre-generated foam with different foam qualities was studied in a porous column filled by 1 mm glass beads. In addition, foam rheology with quality of f_g=85% were examined in the glass beads (GB) packings size of 1 mm, 2 mm, 4 mm, and 8 mm. The following conclusions were extracted from the results.

- Foam generator plays a crucial role in the behavior of foam in porous media. The foam generated in the sand-pack showed a sharp vertical front compared to the 1 mm GB packing (inclined interface) at the same total flow rate, thus demonstrating the strong sweeping behavior of foam generated in finer porous media.

- Pre-generation of foam in less permeable media than the porous media of the main column enhances the apparent foam viscosity and foam stability. This phenomenon may contribute to the bubble size since the viscosity is higher for a foam containing smaller gas bubbles. By this, we confirm the dependence of the apparent foam viscosity on the foam texture and bubbles size.
- We found that the initial liquid saturation (S_{wi}) (i.e., liquid content) in 1 mm glass beads packing is lower than the liquid fraction of injected foam. Moreover, we observed that the initial liquid saturation depends on the flow rate compared to porous media with low permeability. This may be due to the foam compressibility, in which compressed, disconnected gas bubbles displace the continuous liquid phase, thereby reducing the liquid fraction of the foam in a porous medium.
- The pre-generated foam in the sand-pack showed a higher foam quality transition (f_g^*) in 1 mm GB packing than foam generated in the same, i.e. through the 1 mm GB packing. Thus, the foam pre-generated in the less permeable porous media demonstrated better stability. This is related to the higher limiting capillary pressure of the finer foam, which delays the bubble coarsening (foam instability).
- Identical values of transition foam quality were obtained in all glass beads packings for foam generated through the sand-pack. Therefore, the transition foam quality was concluded to be independent of the porous medium's permeability for highly permeable porous media when the bubbles are much smaller than the pores. The transition foam quality, f_g^*, was equal to 97%.
- If the size of the bubble is the same as the pore size, the foam behaves like a Newtonian fluid at low flow rates and exhibits a shear-thinning fluid behavior by increasing flow rates. When foam bubbles are much smaller than pores, foam in porous media was found to behave as a yield stress shear-thinning fluid regardless of porous medium grain size. The rheological behavior of this foam is well fitted with the Herschel-Bulkley model. Hence, we propose considering foam as a yield stress fluid in highly permeable porous media where foam bubbles are much smaller than pores.
- It was also shown that the apparent foam viscosity (μ_{app}) in porous media increased with grain diameter size (i.e., permeability) at the same total flow rate. However, for a constant shear rate, the μ_{app} of foam decreases with increasing grain size, which can be an effect of foam compressibility in less permeable media.

In order to see the difference between the behavior of the foam in porous media and in bulk, the rheology of the foam pre-generated through the fine sand was also studied as bulk foam in a rheometer with serrated parallel-plate geometry. The results were fitted using a rheological model (Herschel-Bulkley-Papanastasiou model) and analyzed according to the results taken from the porous medium. The following conclusions were obtained from the outcomes.

- It was found that the bulk-foam viscosity can be considered as a yield stress fluid, and the rheological behavior of foam fits well with the Herschel-Bulkley-Papanastasiou model (H-B-P). We also observed that yield-stress values, which were determined by the H-B-P model, increased with foam quality.
- We found that the apparent foam viscosity in high permeable porous media is 3-4 times higher than bulk foam viscosity at the same shear rate, which is due to the complexity of the foam flow in porous media.

The rheological data of bulk foam was used as an input for the further upscaling procedures, in which the macroscopic behavior of the foam flow was numerically studied in different periodic 2D and 3D unit cells (e.g., square-packed cylinders with a circular cross-section (SPC), square-packed cylinders with a square cross-section (SPS), close-packed cylinders with a circular cross-section (CPC), close-packed cylinders with a square cross-section (CPS), simple cubic packing of cubes (SCP), cubic body-centered packing of spheres (BCP)). To do that, we solved the non-linear boundary value problem of generalized Newtonian fluid proposed by Orgeas (2007) through 2D and 3D periodic unit-cells and compared the findings with the experimental results obtained from porous media. We also conduct empirical upscaling by using Darcy scale law proposed by Chevalier et al. (2013) to derive dimensionless coefficients from our experimental results. The following conclusions were derived from the results.

- Since the foam is a non-Newtonian fluid, the geometric structure of porous media plays a crucial role in the behavior of foam. However, we did not observe significant variations in results between flows in 2D-CPC and 3D-BCP geometries with the same porosity.
- We found considerable differences between the upscaling and the experimental results. Nevertheless, the global trend of the curve of the superficial velocity as a function of pressure gradient from upscaling and the behavior in terms of f_g followed the same tendency as those of the experimental results.
- The experimental results for a very highly permeable porous medium, where the compressibility effect is not significant, fitted well to the experimental data. In the absence of the foam trapping (e.g., a high capillary number), the difference between upscaling results and experimental data can be related to the foam compressibility. Therefore, foam rheological behavior in porous media can be easily predicted from the bulk foam in the case where the foam compressibility is negligible. The calculated compressibility coefficients should be increased with increasing pressure gradients.
- The fitting values of dimensionless coefficients (χ and ω) from empirical extended Darcy's law exhibited high values for foams compared to other yield-stress fluids and varied depending on foam quality.

Upscaling of foam in high permeability porous media can be an encouraging tool to predict foam-flow behavior from its bulk behavior. However, further investigations are necessary to incorporate the complex nature of the foam flow in porous media into the upscaling model.

In order to avoid the highly complicated microstructure of porous media and to study the foam rheology, we investigated pre-generated foam flow in capillary tubes of different diameters and made of different materials (PTFE – polytetrafluoroethylene, FEP – fluorinated ethylene propylene, and glass). The objectives were to study the effect of foam quality, material type, tube diameter, and bubble size on the foam flow. Furthermore, to compare these results with foam rheology outcomes in porous media and the bulk foam rheology found using the rheometer. The following results were drawn from the results of this study.

- The apparent foam viscosity as a function of foam quality generally follows the classical trend, which occurs in porous media, with two regimes corresponding to the low-quality and high-quality regimes separated by a transition foam quality (f_g^*). However, the apparent foam viscosity increased with foam quality until the instability that occurred above the foam quality of 90% due to the change of foam textures. Consequently, for the tubes with an internal diameter of 0.8 mm, the transition foam quality was found to be f_g^*=98% in the FEP and PTFE tubes, and f_g^*=97% in the glass tube. However, for 0.5 mm FEP tubes, the transition foam quality was observed at f_g^*=96%, that indicates the instability of the limiting capillary pressure is lower in smaller diameter tubes. Thus, we confirm that the transition foam quality depends on material type and tube diameter. Moreover, the values of the transition foam qualities found for the glass tube are compatible with the results found in glass beads packings.
- We observed that the foam texture changes from the bubbly liquid at low foam qualities (f_g<70%) to polydisperse homogeneous foam at 70%≤f_g<90% and to foam with gas slugs above f_g≥90%. The texture of the foam also changed depending on the flow rate. At low flow rates, the foam texture is coarse, which is due to the generation of weak foam where the bubble coalescence rate increases compared to the rate of bubble generation. Thus, the foam rheology should be studied with particular care for the foam texture.
- Foam behaves like a yield stress fluid in the FEP tubes, and its behavior can be well fitted by the Herschel-Bulkley model. However, yield stress values were found to be zero in GT and PTFE tubes. Nevertheless, the apparent viscosity of foam in the glass beads packings and through the rheometer is found to be a pure yield stress fluid. This can be a consequence of the existence of a wall slip velocity in the capillary tubes.

- Foam viscosity is more significant in the PTFE tube compare to the FEP and glass tubes that can be a consequence of surface roughness. However, we were unable to define the tube wall effect; therefore, further investigations to elucidate this aspect are ongoing.
- Foam rheology deduced from flow in capillary tubes could be compiled in a master curve along with the rheology obtained through the study of foam flow in glass beads packings and the characterization measured by a rheometer and they could altogether be fitted by a H-B model allowing different comparisons and discussions.
- The scatter in results found for foam flow in small capillaries may be due to the polydisperse foam formed through the sand-pack, as the number of bubbles decreases per tube section as the tube diameter reduces.

These insights can guide the study of pre-generated foam in highly permeable porous media, particularly for application in soil remediation processes. We expect our study to be an opening point for further investigations on foam flow in high permeability aquifers.

5.2. Perspectives

5.2.1. Surfactant and gas for blocking foam

The selection of surfactant is essential for foam formation, particularly for blocking foam. The formulation of the surfactant was not studied since the project provided it. As the foam is a very encouraging tool to divert high-speed aquifer flow, the bulk foam properties, in particular, the foam stability, should be studied thoroughly. Moreover, biodegradability must be respected with great care.

In our experiments, we examined foam formation using nitrogen and carbon dioxide to be sure of the gas properties. However, the characteristics of foam should also be taken into account, depending on the ultimate purpose of foam application in the field where the air is likely to be used.

5.2.2. Foam generator and main columns

Almost in all experiments, we used the sand-pack to pre-generate foam. As a result, the generated foams were polydispersed, and we also observed high pressure in the generator column. To generate monodispersed foams, we recommend using fine glass beads for further studies. Furthermore, foam quality and initial liquid saturation in foam generator and main columns should be studied very carefully, which can be measured by pressure drop along the column and by weighing the columns during the running experiment. In addition, a back pressure regulator should be used for future experiments to ensure the stability and accuracy of the entire system.

5.2.3. Bubble size

We roughly assumed that the bubbles are equal to the pore size of the foam generator since all experiments were conducted using the same foam generator (sand-pack). Therefore, the bubble size of the foam was not analyzed after the generator column. However, we observed a change in bubble size just after the main column, which was presented in Fig. 5.1. From these results, we found increasing bubbles size with glass beads diameter that is the result of bubble coarsening due to Ostwald ripening (Voorhees, 1985). The quality of images was not good enough to analyze them since the photos were taken using a compact camera. Consequently, changing the size of the bubbles should be studied more precisely through a professional camera. Moreover, bubbles size should also be studied during the foam rheology measurements using a rheometer because we did not know how the bubbles behaved during the experiment.

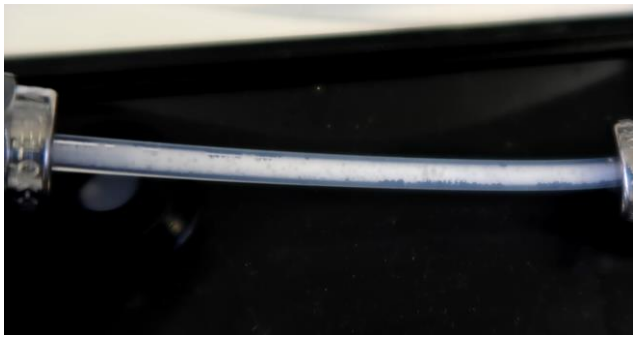

a) Before the main column or after foam generator

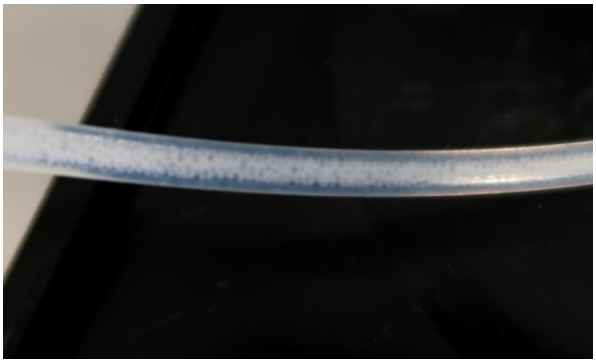

b) After the main column (1 mm GB)

c) After the main column (2 mm GB)

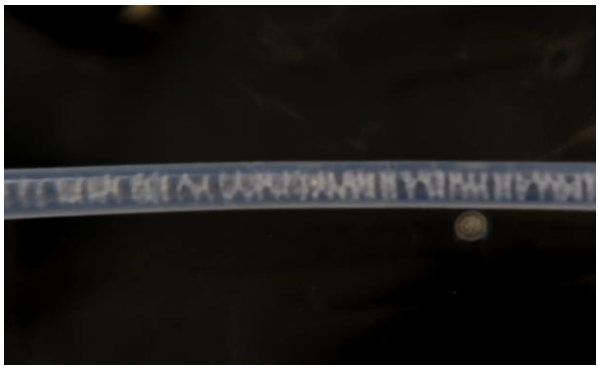

d) After the main column (4 mm GB)

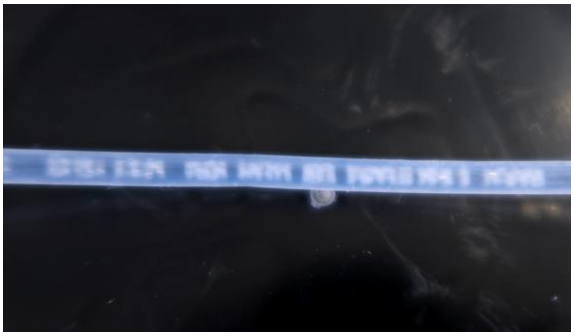

e) After the main column (8 mm GB)

Fig. 5.1 Pre-generated foam bubbles size before and after injection to the main column

5.2.4. Compressibility

From the liquid saturation measurements in 1D porous columns, we observed the lower liquid fraction in porous media than initially injected f_g. This phenomenon can be attributed to the foam compressibility, where the gas-phase of foam squeeze the liquid contained in lamellae, thereby mobilizing the liquid-phase faster before the steady-state flow occurs.

Also, we observed an increase of apparent foam viscosity for less permeable porous media that indicates an increase in the compressibility of the foam with a decrease in porous media permeability. These hypotheses must be investigated in further studies.

5.2.5. Upscaling

Upscaling of foam flow in porous media remains a challenge. More precisely, the resolution of the closure problem via the volume averaging method complicates the integral differential equations contained in the system. Nevertheless, it can also be considered by numerical methods in the outlook.

Scaling up using the rheology of bulk foam as input parameters can be an encouraging tool if bubbles size is much smaller than pores. However, the input parameters must be set with great care. In addition, foam compressibility and coarsening effects should be taken into account in future upscaling studies. Considering geometry should be identical or close to the porous media studied during the experiments.

Moreover, it is essential to note that the upscaling of foam flow from laboratory-scale to field-scale is also necessary for the final application (e.g., considering the heterogeneity effect). In laboratory experiments, we considered columns 40 cm long, which might not be enough to investigate foam behavior over a meter or longer distances. The foam compressibility in columns and fields can also differ since we consider confined media in the laboratory. The heterogeneity of aquifers and the groundwater flow at high speed can also cause a problem, where inertial forces might be dominated.

5.2.6. Wall slip velocity and surface roughness in capillary tubes

In the studies of foam flow through capillary tubes, we observed the impact of material on foam flow behavior despite the fact that PTFE and FEP materials were hydrophobic. However, the foam flow in capillary glass tubes has not been studied, except for the 0.8 mm diameter glass tube, due to the delay in delivery. Foam texture and wall slip velocity will be thoughtfully studied in all tubes to complete the research.

In perspective, wall slip velocity can also be examined as a function of foam quality. Moreover, we recommend studying foam flow at lower shear rates, therefore with different foam generators.

Appendix A

To study the variation of foam bubbles in bulk form (Fig. 1A a) and in 1 mm GB packing (Fig. 1A b), we used a dynamic foam analyzer (DFA-100, KRUSS). The foam analyzer consists of a glass column (250 mm long and 40 mm internal diameter), a camera, and a light source. The experiments were conducted as in studies by Omirbekov et al. (2020 a), where N_2 gas was injected into the surfactant solution (AOS, 4 × CMC) using a porous-glass disc. The porous-glass disc was chosen according to the foam generator, where the pore size varied from 10 to 16 µm. In the porous medium, the used volumetric amount of the surfactant solution and the gas injection time were reduced by 60% since the porosity of the bead-pack was about 40%. In both cases, the camera height was set to 100 mm to record the change in bubble size over time.

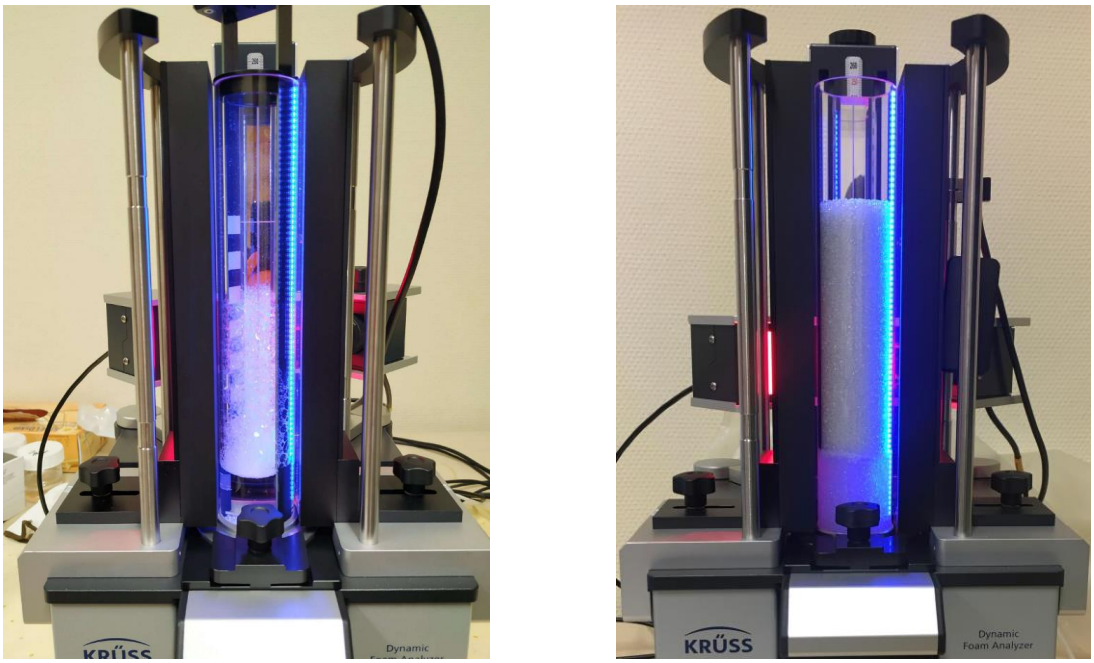

a) b)

Fig. 1A Analysis of foam bubbles using dynamic foam analyzer (DFA-100, KRUSS): a) in bulk form and b) in the porous medium (1 mm GB)

Fig. 2A shows the change of structures in bulk foam and foam in 1 mm GB packing, where the mean bubble area (MBA) was compared after 60, 300, and 900 seconds. We observed that the bulk foam is less stable than foam in porous media. It is the consequence of the drainage process, which is greater for the bulk foam. For instance, the MBA of bulk foam doubled after 300 seconds, while the MBA of foam in 1 mm GB packing increased twice in 900 seconds, which was three times lower than the bulk foam. The bulk foam decays faster than the foam in porous media due to gravity drainage and gas diffusion, which tends to coalescence and coarsen average bubble size. While in porous media, the effect of gravity is small due to the short length scales within the bead-pack; therefore, the hydrostatic pressure differences

are slight (Jones, et al., 2016). Jones et al. (2016) also found a correlation between apparent foam viscosity in porous media and the stability of foam in bulk form.

Moreover, from Fig. 2A, we can see that the shape of the bulk foam bubbles was changed from spherical to polyhedral over time, while the shape of the foam bubbles in porous media did not change, and it took the shape of pores to a greater degree.

Time	60 sec	300 sec	900 sec
Bulk foam	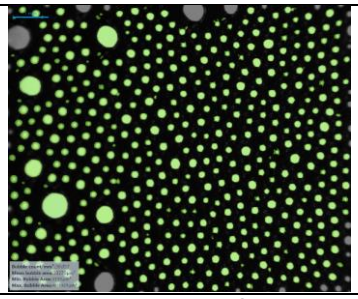	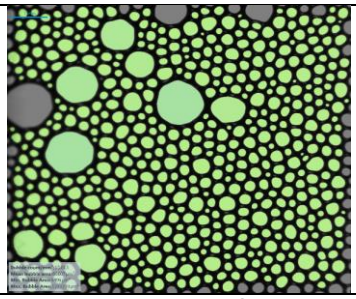	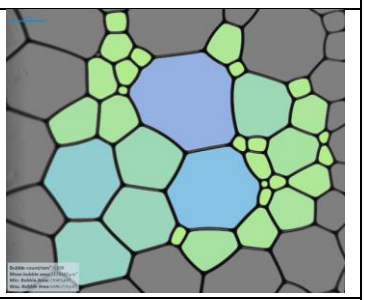
MBA_{bulk}	33,270 µm^2	66,607 µm^2	1,128,160 µm^2
1 mm GB packing	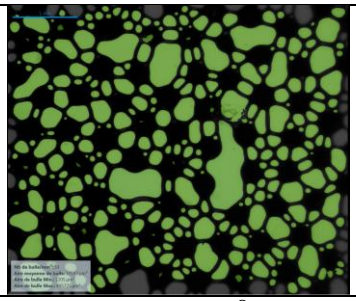	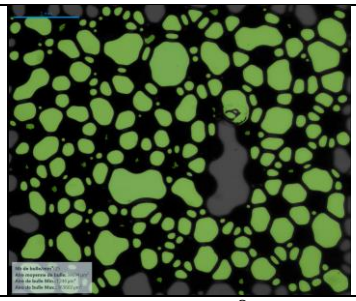	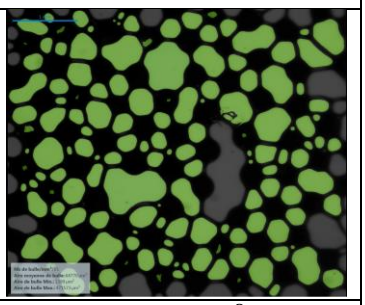
MBA_{pm}	30,543 µm^2	39,694 µm^2	64,770 µm^2

Fig. 2A Change of foam structure as a function of time for bulk foam and foam in porous media (1 mm GB packing): liquid and solid phase in black, gas phase in color

In Fig. 3A, we plot the characteristic ratio of the bubble area (B_c) as a function of time, where B_c is the ratio of MBA_{pm} to MBA_{bulk} at the same time. In the beginning, the ratio is close to one. However, the values of B_c decrease with time showing that the variation of foam bubbles is much higher than for foam in the porous medium. Nevertheless, it must be noted that these experiments were conducted at ambient pressure in the static case. In addition, the height of the system exceeds 200 mm, which tends to increase bubble coalescence due to gravity drainage.

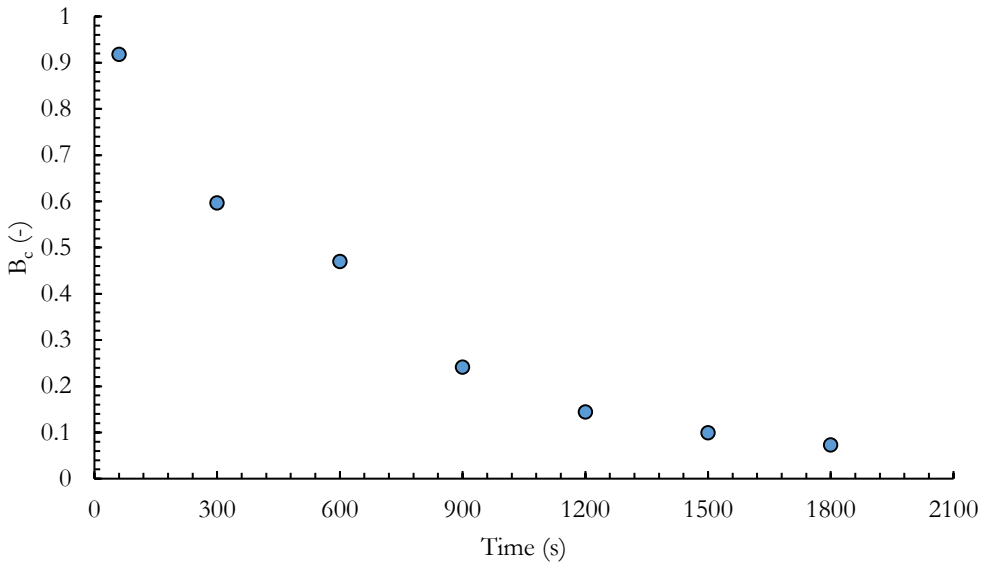

Fig. 3A The characteristic ratio of bubble area versus time ($B_c = MBA_{pm}/MBA_{bulk}$)

In the 1D column experiment, we expected the bubble change to be less than that detected by the foam analyzer. Because the foam was examined horizontally, therefore, the effect of gravity drainage was assumed to be weaker. Moreover, the foam in the 1D column flowed under a certain pressure, and according to the study by Holt et al. (1996), the foam strength (made of AOS surfactant) increases with increasing system pressure.

In our recent study (Omirbekov, et al., 2020 a), we compared the behavior of foams in 1 mm GB packing, where the foams were pre-generated in a 1 mm bead-pack and in a sand-pack used in this study. From the plot of apparent viscosity versus total flow rate, we noticed that the apparent foam viscosities vary greatly even at low flow rates, despite the long residence time of the foam in the column. Thus, it can be concluded that foam stability in confined environments is much longer than in bulk form. Nevertheless, we confirm that there was a small change in the size of the bubbles in the main column outlet. This should be studied with great care in future studies.

References

Achorn Jr., G. D. B. & Schwab, J. L., 1948. A Method for the Aeration of Liquid Cultures of Microorganisms.. *Science (Washington)*, pp. 377-8.

Adebanjo, F. O. & Udofia, J., 2015. Evaluating the application of foam injection as an enhanced oil recovery in unconsolidated sand [J]. *Journal of Petroleum and Gas Engineering*, Volume 6, pp. 22-37.

Almajid, M. M. & Kovscek, A. R., 2020. Pore Network Investigation of Trapped Gas and Foam Generation Mechanisms. *Transport in Porous Media*, Volume 131, pp. 289-313.

Alvarez, J. M., 1998. *Foam-Flow Behavior in Porous Media: Effects of Flow Regime and Porous-Medium Heterogeneity*, s.l.: s.n.

Alvarez, J. M., Rivas, H. J. & Rossen, W. R., 2001. Unified Model for Steady-State Foam Behavior at High and Low Foam Qualities. *Society of Petroleum Engineers.*

Aranda, R. et al., 2020. Experimental Study of Foam Flow in Highly Permeable Porous Media for Soil Remediation. *Transport in Porous Media*, Volume 134, p. 231–247.

Arndt, R., 2007. *Alkyl Sulfonates and Alpha-Olefin Sulfonates: SIDS Initial Assessment Report*, s.l.: s.n.

Ashoori, E., Marchesin, D. & Rossen, W. R., 2012. Multiple Foam States and Long-Distance Foam Propagation in EOR Displacements. *Society of Petroleum Engineers.*

Auriault, J. L., 1991. Heterogeneous medium. Is an equivalent macroscopic description possible?. *International Journal of Engineering Science*, Volume 29, pp. 785-795.

Auriault, J. L., 1991. Heterogeneous medium. Is an equivalent macroscopic description possible?. *International journal of engineering science*, Volume 29, pp. 785-795.

Balan, H. O., Balhoff, M. T. & Nguyen, Q. P., 2011. Modeling of Gas Trapping and Mobility in Foam Enhanced Oil Recovery. *Energy Fuels*, Volume 25 (9), pp. 3974-3987.

Belhaij, A., AlQuraishi, A. & Al-Mahdy, O., 2014. *Foamability and foam stability of several surfactants solutions: the role of screening and flooding.* s.l., s.n.

Bernard, G. G. & Holm, L. W., 1970. Model study of foam as a sealant for leaks in gas storage reservoirs. *Society of Petroleum Engineers Journal*, Volume 10, pp. 9-16.

Berryman, J. G., 2005. Comparison of upscaling methods in poroelasticity and its generalizations. *Journal of Engineering Mechanics*, Volume 131, pp. 928-936.

Bertin, H., Estrada, E. D. C. & Atteia, O., 2017. Foam placement for soil remediation. *Environmental Chemistry*, Volume 14, pp. 338-343.

Bertin, H. J., Apaydin, O. G., Castanier, L. M. & Kovscek, A. R., 1998. *Foam flow in heterogeneous porous media: Effect of crossflow.* s.l., s.n.

Bertin, H. J., Quintard, M. Y. & Castanier, L. M., 1998. Development of a bubble-population correlation for foam-flow modeling in porous media. *SPE Journal,* Volume 3, p. 356–362.

Bertin, H. J., Quintard, M. Y. & Castanier, L. M., 1998. Development of a Bubble-Population Correlation for Foam-Flow Modeling in Porous Media. *Society of Petroleum Engineers.*

Beyer, A. H., Millhone, R. S. & Foote, R. W., 1972. *Flow behavior of foam as a well circulating fluid.* s.l., s.n.

Bikerman, J. J., 1968. *The science of adhesive joints.* s.l.:ACADEMIC PRESS.

Bikerman, J. J., 1970. *Physical surfaces.* s.l.:ACADEMIC PRESS.

Bikerman, J. J., 1973. *Foams.* s.l.:Springer-Verlag Berlin Heidelberg.

Bingham, E. C., 1916. Plastic flow. *Journal of the Franklin Institute,* Volume 181, pp. 845-848.

Bogdanovic, M., Gajbhiye, R. N. & Kam, S. I., 2009. Experimental study of foam flow in horizontal pipes: Two flow regimes and its implications. *Colloids and Surfaces A: Physicochemical and Engineering Aspects,* Volume 344, pp. 56-71.

Bragg, W. L. & Nye, J. F., 1947. A dynamical model of a crystal structure. *Proceedings of the Royal Society of London. Series A. Mathematical and Physical Sciences,* Volume 190, pp. 474-481.

Briceno, M. I. & Joseph, D. D., 2003. Self-lubricated transport of aqueous foams in horizontal conduits. *International journal of multiphase flow,* Volume 29, pp. 1817-1831.

Burley, R. & Shakarin, M., 1992. Experimental study of foam rheology in straight capillary tubes. *International Journal of Engineering Fluid Mechanics,* Volume 5, pp. 115-141.

Calvert, J. R. & Nezhati, K., 1986. A rheological model for a liquid-gas foam. *International journal of heat and fluid flow,* Volume 7, pp. 164-168.

Carman, P. C., 1997. Fluid flow through granular beds. *Chemical Engineering Research and Design,* Volume 75, pp. S32 - S48.

Cassie, A. B. D. & Baxter, S., 1944. Wettability of porous surfaces. *Transactions of the Faraday society,* Volume 40, p. 546–551.

Castro, A. R., 2019. Extending Darcy's law to the flow of yield stress fluids in packed beds: Method and experiments. *Advances in water resources,* Volume 126, pp. 55-64.

Castro, A. R., 2019. Extending Darcy's law to the flow of yield stress fluids in packed beds: Method and experiments. *Advances in water resources,* Volume 126, pp. 55-64.

Castro, A. R., Oostrom, M. & Shokri, N., 2016. Effects of shear-thinning fluids on residual oil formation in microfluidic pore networks. *Journal of colloid and interface science,* Volume 472, pp. 34-43.

Chatzis, I. & Morrow, N. R., 1984. Correlation of capillary number relationships for sandstone. *Society of Petroleum Engineers Journal,* Volume 24, p. 555–562.

Chaudhuri, R. G. & Paria, S., 2009. Dynamic contact angles on PTFE surface by aqueous surfactant solution in the absence and presence of electrolytes. *Journal of colloid and interface science,* Volume 337, p. 555–562.

Chauveteau, G., 1982. Rodlike polymer solution flow through fine pores: influence of pore size on rheological behavior. *Journal of Rheology,* Volume 26, pp. 111-142.

Chauveteau, G. & Zaitoun, A., 1981. *Basic rheological behavior of xanthan polysaccharide solutions in porous media: effects of pore size and polymer concentration.* s.l., s.n., pp. 197-212.

Chen, M., Yortsos, Y. C. & Rossen, W. R., 2005. Insights on foam generation in porous media from pore-network studies. *Colloids and Surfaces A: Physicochemical and Engineering Aspects,* Volume 256, pp. 181-189.

Chen, Y. et al., 2014. Switchable nonionic to cationic ethoxylated amine surfactants for CO2 enhanced oil recovery in high-temperature, high-salinity carbonate reservoirs. *SPE journal,* Volume 19, pp. 249-259.

Chevalier, T. et al., 2013. Darcy's law for yield stress fluid flowing through a porous medium. *Journal of Non-Newtonian Fluid Mechanics,* Volume 195, pp. 57-66.

Chevalier, T. et al., 2014. Breaking of non-Newtonian character in flows through a porous medium. *Physical Review E,* Volume 89, p. 023002.

Choi, Y. J., Kim, Y.-J. & Nam, K., 2009. Enhancement of aerobic biodegradation in an oxygen-limiting environment using a saponin-based microbubble suspension. *Environmental pollution,* Volume 157, pp. 2197-2202.

Christopher, R. H. & Middleman, S., 1965. Power-law flow through a packed tube. *Industrial & Engineering Chemistry Fundamentals,* Volume 4, pp. 422-426.

Cohen-Addad, S., Höhler, R. & Pitois, O., 2013. Flow in Foams and Flowing Foams. *Annual Review of Fluid Mechanics,* Volume 45, pp. 241-267.

Cohen, D., Patzek, T. W. & Radke, C. J., 1997. Onset of Mobilization and the Fraction of Trapped Foam in Porous Media. *Transport in Porous Media,* 01 9, Volume 28, pp. 253-284.

Coussot, P., 2005. *Rheometry of Pastes, Suspensions, and Granular Materials: Applications in Industry and Environment.* s.l.:Wiley.

Cserháti, T., Forgács, E. & Oros, G., 2002. Biological activity and environmental impact of anionic surfactants. *Environment International,* Volume 28, pp. 337-348.

Darby, R., Darby, R. & Chhabra, R. P., 2001. *Chemical engineering fluid mechanics, revised and expanded.* s.l.:CRC Press.

Darcy, H. P. G., 1856. *Les Fontaines publiques de la ville de Dijon. Exposition et application des principes à suivre et des formules à employer dans les questions de distribution d'eau, etc.* s.l.:V. Dalamont.

David, A. & Marsden Jr, S. S., 1969. *The rheology of foam.* s.l., s.n.

Denkov, N. D., Subramanian, V., Gurovich, D. & Lips, A., 2005. Wall slip and viscous dissipation in sheared foams: Effect of surface mobility. *Colloids and Surfaces A: Physicochemical and Engineering Aspects,* Volume 263, pp. 129-145.

Denkov, N. D. et al., 2009. The role of surfactant type and bubble surface mobility in foam rheology. *Soft Matter,* 5(18), pp. 3389-3408.

Dicksen, T., Hirasaki, G. J. & Miller, C. A., 2002. Conditions for Foam Generation in Homogeneous Porous Media. *Society of Petroleum Engineers.*

Ding, M. & Kantzas, A., 2007. Capillary number correlations for gas-liquid systems. *Journal of Canadian Petroleum Technology,* Volume 46.

Dollet, B. & Raufaste, C., 2014. Rheology of aqueous foams. *Comptes Rendus Physique,* Volume 15, pp. 731-747.

Dong, X. et al., 2010. Aqueous foam stabilized by hydrophobically modified silica particles and liquid paraffin droplets. *Colloids and Surfaces A: Physicochemical and Engineering Aspects,* Volume 353, pp. 181-188.

Drenckhan, W. & Hutzler, S., 2015. Structure and energy of liquid foams. *Advances in colloid and interface science,* Volume 224, pp. 1-16.

Drenckhan, W. & Saint-Jalmes, A., 2015. The science of foaming. *Advances in Colloid and Interface Science,* Volume 222, pp. 228-259.

Du, D. X., Li, Y. G. & Sun, S. J., 2011. *Experimental study on pseudo-plastic behavior for film foam flow in a vertical tube.* s.l., s.n., pp. 194-199.

Dullien, F. A. L., 1992. *Porous media: fluid transport and pore structure.* s.l.:Academic press.

Enzendorfer, C. et al., 1995. Pipe viscometry of foams. *Journal of Rheology,* Volume 39, pp. 345-358.

Ettinger, R. A. & Radke, C. J., 1992. The influence of texture on steady foam flow in berea sandstone. *Society of Petroleum Engineers.*

Falls, A. H. et al., 1988. Development of a mechanistic foam simulator: the population balance and generation by snap-off. *SPE reservoir engineering,* Volume 3, pp. 884-892.

Falls, A. H. et al., 1988. Development of a Mechanistic Foam Simulator: The Population Balance and Generation by Snap-Off. *Society of Petroleum Engineers*, 8.

Falls, A. H., Musters, J. J. & Ratulowski, J., 1989. The apparent viscosity of foams in homogeneous bead packs. *SPE (Society of Petroleum Engineers) Reserv. Eng.; (United States),* 5.Volume 4:2.

Falls, A. H., Musters, J. J. & Ratulowski, J., 1989. The apparent viscosity of foams in homogeneous bead packs. *SPE Reservoir Engineering,* Volume 4, pp. 155-164.

Farajzadeh, R., Andrianov, A., Bruining, H. & Zitha, P. L. J., 2009. Comparative Study of CO2 and N2 Foams in Porous Media at Low and High Pressure−Temperatures. *Industrial & Engineering Chemistry Research,* Volume 48, pp. 4542-4552.

Farzaneh, S. A. & Sohrabi, M., 2015. Experimental investigation of CO2-foam stability improvement by alkaline in the presence of crude oil. *Chemical Engineering Research and Design,* Volume 94, pp. 375-389.

Fletcher, A. J. P. et al., 1991. *Measurements of polysaccharide polymer properties in porous media.* s.l., s.n.

Forey, N., Atteia, O., Omari, A. & Bertin, H., 2020. Saponin foam for soil remediation: On the use of polymer or solid particles to enhance foam resistance against oil. *Journal of contaminant hydrology,* Volume 228, p. 103560.

Friedmann, F., Chen, W. H. & Gauglitz, P. A., 1991. Experimental and simulation study of high-temperature foam displacement in porous media. *SPE (Society of Petroleum Engineers) Reservoir Engineering; (United States),* 2.Volume 6:1.

Friedmann, F. et al., 1994. Steam-foam mechanistic field trial in the midway-sunset field. *SPE Reservoir Engineering,* Volume 9, pp. 297-304.

Gajbhiye, R. N. & Kam, S. I., 2011. Characterization of foam flow in horizontal pipes by using two-flow-regime concept. *Chemical engineering science,* Volume 66, pp. 1536-1549.

Gardiner, B. S., Dlugogorski, B. Z. & Jameson, G. J., 1998. Rheology of fire-fighting foams. *Fire Safety Journal,* Volume 31, p. 61–75.

Gardiner, B. S., Dlugogorski, B. Z. & Jameson, G. J., 1999. Prediction of pressure losses in pipe flow of aqueous foams. *Industrial & engineering chemistry research,* Volume 38, pp. 1099-1106.

Gauglitz, P. A., Friedmann, F., Kam, S. I. & Rossen, W. R., 2002. Foam generation in homogeneous porous media. *Chemical Engineering Science,* Volume 57, pp. 4037-4052.

Gibbs, J. W., 1879. On the equilibrium of heterogeneous substances.

Gumati, A. & Takahshi, H., 2011. Experimental study and modeling of pressure loss for foam-cuttings mixture flow in horizontal pipe. *Journal of Hydrodynamics,* Volume 23, pp. 431-438.

Guozhong, C., 2004. *Nanostructures and nanomaterials: synthesis, properties and applications.* s.l.:World scientific.

Harris, P. C., 1989. Effects of texture on rheology of foam fracturing fluids. *SPE production engineering,* Volume 4, pp. 249-257.

Harris, P. C. & Reidenbach, V. G., 1987. High-temperature rheological study of foam fracturing fluids. *Journal of Petroleum Technology,* Volume 39, pp. 613-619.

Henrich, F. et al., 2016. Influence of surfactants in forced dynamic dewetting. *Soft Matter,* Volume 12, p. 7782–7791.

Herschel, W. H. & Bulkley, R., 1926. Konsistenzmessungen von gummi-benzollösungen. *Kolloid-Zeitschrift,* Volume 39, pp. 291-300.

Herzhaft, B., 1999. Rheology of Aqueous Foams: a Literature Review of some Experimental Works. *Oil & Gas Science and Technology,* 7, Volume Vol. 54 (1999), pp. 587-596.

Herzhaft, B., Kakadjian, S. & Moan, M., 2005. Measurement and modeling of the flow behavior of aqueous foams using a recirculating pipe rheometer. *Colloids and Surfaces A: Physicochemical and Engineering Aspects,* Volume 263, pp. 153-164.

Hirasaki, G. J., 1989. Supplement to SPE 19505, The Steam-Foam Process--Review of Steam-Foam Process Mechanisms. *SPE.*

Hirasaki, G. J. & Lawson, J. B., 1985. Mechanisms of Foam Flow in Porous Media: Apparent Viscosity in Smooth Capillaries. *Society of Petroleum Engineers.*

Hirasaki, G. J. et al., 1997. Surfactant/Foam Process for Aquifer Remediation. *Society of Petroleum Engineers,* 1.

Hirasaki, G. J. et al., 1997. *Field demonstration of the surfactant/foam process for aquifer remediation.* s.l., s.n.

Hirasaki, G. J. & Pope, G. A., 1974. Analysis of factors influencing mobility and adsorption in the flow of polymer solution through porous media. *Society of Petroleum Engineers Journal,* Volume 14, pp. 337-346.

Hohler, R. & Cohen-Addad, S., 2005. Rheology of liquid foam. *Journal of Physics: Condensed Matter*, Volume 17.

Huang, C.-W. & Chang, C.-H., 2000. A laboratory study on foam-enhanced surfactant solution flooding in removing n-pentadecane from contaminated columns. *Colloids and Surfaces A: Physicochemical and Engineering Aspects*, Volume 173, pp. 171-179.

Idris, Z. et al., 2004. Microstructural effects on the flow law of power-law fluids through fibrous media. *Modelling and Simulation in Materials Science and Engineering*, Volume 12, p. 995.

Jastrzebski, Z. D., 1967. Entrance effects and wall effects in an extrusion rheometer during flow of concentrated suspensions. *Industrial & Engineering Chemistry Fundamentals*, Volume 6, pp. 445-454.

Jeong, S.-W. & Corapcioglu, M. Y., 2003. A micromodel analysis of factors influencing NAPL removal by surfactant foam flooding. *Journal of contaminant hydrology*, Volume 60, pp. 77-96.

Jeong, S.-W., Corapcioglu, M. Y. & Roosevelt, S. E., 2000. Micromodel study of surfactant foam remediation of residual trichloroethylene. *Environmental science & technology*, Volume 34, pp. 3456-3461.

Jones, S. A. et al., 2016. Surfactant screening for foam EOR: Correlation between bulk and core-flood experiments. *Colloids and Surfaces A: Physicochemical and Engineering Aspects*, Volume 500, p. 166–176.

Kam, S. I., 2008. Improved mechanistic foam simulation with foam catastrophe theory. *Colloids and Surfaces A: Physicochemical and Engineering Aspects*, Volume 318, pp. 62-77.

Katgert, G., Tighe, B. P. & Hecke, M., 2013. The jamming perspective on wet foams. *Soft Matter*, 9(41), pp. 9739-9746.

Khan, S. A., Schnepper, C. A. & Armstrong, R. C., 1988. Foam Rheology: III. Measurement of Shear Flow Properties. *Journal of Rheology*, Volume 32, pp. 69-92.

Khatib, Z. I., Hirasaki, G. J. & Falls, A. H., 1988. Effects of capillary pressure on coalescence and phase mobilities in foams flowing through porous media. *SPE reservoir engineering*, Volume 3, pp. 919-926.

Kilbane, J. J. et al., 1997. Remediation of contaminated soils using foams. *Land Contamination and Reclamation*, Volume 5, pp. 41-54.

Kommalapati, R. R., Valsaraj, K. T., Constant, W. D. & Roy, D., 1998. Soil flushing using colloidal gas aphron suspensions generated from a plant-based surfactant. *Journal of Hazardous Materials*, Volume 60, pp. 73-87.

Kovscek, A. R. & Bertin, H. J., 2003. Foam mobility in heterogeneous porous media. *Transport in porous media*, Volume 52, pp. 17-35.

Kovscek, A. R., Chen, Q. & Gerritsen, M., 2010. Modeling foam displacement with the local-equilibrium approximation: theory and experimental verification. *SPE Journal,* Volume 15, p. 171–183.

Kovscek, A. R., Chen, Q. & Gerritsen, M., 2010. Modeling Foam Displacement With the Local-Equilibrium Approximation: Theory and Experimental Verification. *Society of Petroleum Engineers.*

Kovscek, A. R. & Radke, C. J., 1994. Fundamentals of foam transport in porous media. *ACS Advances in Chemistry Series,* Volume 242, pp. 115-164.

Kovscek, A. R., Tadeusz, W. P. & Radke, C. J., 1997. Mechanistic foam flow simulation in heterogeneous and multidimensional porous media. *SPE Journal,* Volume 2, pp. 511-526.

Kovscek, A. R., Tadeusz, W. P. & Radke, C. J., 1997. Mechanistic foam flow simulation in heterogeneous and multidimensional porous media. *SPE Journal,* Volume 2, p. 511–526.

Kovscek, A. R., Tang, G. Q. & Radke, C. J., 2007. Verification of Roof snap off as a foam-generation mechanism in porous media at steady state. *Colloids and Surfaces A: Physicochemical and Engineering Aspects,* Volume 302, pp. 251-260.

Kozeny, J., 1927. Uber kapillare leitung der wasser in boden. *Royal Academy of Science, Vienna, Proc. Class I,* Volume 136, pp. 271-306.

Kraynik, A. M., 1988. Foam Flows. *Annual Review of Fluid Mechanics,* Volume 20, pp. 325-357.

Lake, L. W., 1989. *Enhanced oil recovery.* s.l.:Prentice Hall.

Langevin, D., 2017. Aqueous foams and foam films stabilised by surfactants. Gravity-free studies. *Comptes Rendus Mécanique,* Volume 345, pp. 47-55.

Larmignat, S., Vanderpool, D., Lai, H. K. & Pilon, L., 2008. Rheology of colloidal gas aphrons (microfoams). *Colloids and Surfaces A: Physicochemical and Engineering Aspects,* Volume 322, pp. 199-210.

Larry, W. L., Russell, J., Bill, R. & Gary, P., 1986. *Fundamentals of Enhanced Oil Recovery.* s.l.:Society of Petroleum Engineers.

Larson, R. G., 1999. *The Structure and Rheology of Complex Fluids.* s.l.:New York: Oxford University Press.

Lee, H. O. & Heller, J. P., 1990. Laboratory measurements of CO2-foam mobility. *SPE Reservoir Engineering,* Volume 5, pp. 193-197.

Lee, H. O., Heller, J. P. & Hoefer, A. M. W., 1991. Change in apparent viscosity of CO2 foam with rock permeability. *SPE reservoir engineering,* Volume 6, pp. 421-428.

Lee, S. & Kam, S. I., 2013. Enhanced oil recovery by using CO2 foams: fundamentals and field applications. In: *Enhanced Oil Recovery Field Case Studies.* s.l.:Elsevier, pp. 23-61.

Lee, S., Park, J.-S. & Lee, T. R., 2008. The wettability of fluoropolymer surfaces: influence of surface dipoles. *Langmuir,* Volume 24, p. 4817–4826.

Li, B., Hirasaki, G. J. & Miller, C. A., 2006. *Upscaling of foam mobility control to three dimensions.* s.l., s.n.

Liu, A. J. & Nagel, S. R., 1998. Jamming is not just cool any more. *Nature,* Volume 396, pp. 21-22.

Lopez, X. & Blunt, M. J., 2004. *Predicting the impact of non-Newtonian rheology on relative permeability using pore-scale modeling.* s.l., s.n.

Macosko, C. W., 1994. *Rheology: Principles, Measurements, and Applications.* s.l.:Wiley-VCH.

Maire, J., Coyer, A. & Fatin-Rouge, N., 2015. Surfactant foam technology for in situ removal of heavy chlorinated compounds-DNAPLs. *Journal of hazardous materials,* Volume 299, pp. 630-638.

Maire, J., Davarzani, H., Colombano, S. & Fatin-Rouge, N., 2019. Targeted delivery of hydrogen for the bioremediation of aquifers contaminated by dissolved chlorinated compounds. *Environmental Pollution,* Volume 249, pp. 443-452.

Maire, J. & Fatin-Rouge, N., 2017. Surfactant foam flushing for in situ removal of DNAPLs in shallow soils. *Journal of hazardous materials,* Volume 321, pp. 247-255.

Ma, K. et al., 2012. Visualization of improved sweep with foam in heterogeneous porous media using microfluidics. *Soft Matter,* Volume 8, pp. 10669-10675.

Ma, K. et al., 2015. Modeling techniques for foam flow in porous media. *SPE Journal,* Volume 20, pp. 453-470.

Ma, K. et al., 2015. Modeling Techniques for Foam Flow in Porous Media. *Society of Petroleum Engineers,* 6.Volume 20.

Mannhardt, K., Novosad, J. J. & Schramm, L. L., 2000. Comparative evaluation of foam stability to oil. *SPE Reservoir Evaluation & Engineering,* Volume 3, pp. 23-34.

Mannhardt, K. & Svorstøl, I., 2001. Surfactant concentration for foam formation and propagation in Snorre reservoir core. *Journal of Petroleum Science and Engineering,* Volume 30, pp. 105-119.

Mao, X., Jiang, R., Xiao, W. & Yu, J., 2015. Use of surfactants for the remediation of contaminated soils: A review. *Journal of Hazardous Materials,* Volume 285, pp. 419-435.

Marze, S., Guillermic, R. M. & Saint-Jalmes, A., 2009. Oscillatory rheology of aqueous foams: surfactant, liquid fraction, experimental protocol and aging effects. *Soft Matter,* 5(9), pp. 1937-1946.

Marze, S., Saint-Jalmes, A. & Langevin, D., 2008. Aqueous foam slip and shear regimes determined by rheometry and multiple light scattering. *Journal of rheology*, Volume 52, p. 1091.

Mitra, S. et al., 2016. Interaction dynamics of a spherical particle with a suspended liquid film. *AIChE Journal*, Volume 62, p. 295–314.

Mooney, M., 1931. Explicit formulas for slip and fluidity. *Journal of Rheology (1929-1932)*, Volume 2, pp. 210-222.

Mulligan, C. N. & Eftekhari, F., 2003. Remediation with surfactant foam of PCP-contaminated soil. *Engineering Geology*, Volume 70, pp. 269-279.

Mulligan, C. N. & Eftekhari, F., 2003. Remediation with surfactant foam of PCP-contaminated soil. *Engineering geology*, Volume 70, pp. 269-279.

Muskat, M. & Meres, M. W., 1936. The flow of heterogeneous fluids through porous media. *Physics*, Volume 7, p. 346–363.

Muskat, M., Wyckoff, R. D., Botset, H. G. & Meres, M. W., 1937. Flow of gas-liquid mixtures through sands. *Transactions of the AIME*, Volume 123, p. 69–96.

Myers, T. J. & Radke, C. J., 2000. Transient Foam Displacement in the Presence of Residual Oil: Experiment and Simulation Using a Population-Balance Model. *Industrial & Engineering Chemistry Research.*

Neppiras, E. A., 1969. Subharmonic and other low-frequency emission from bubbles in sound-irradiated liquids. *The Journal of the Acoustical Society of America*, Volume 46, pp. 587-601.

Nguyen, Q. P., Currie, P. K. & Zitha, P. L. J., 2004. Motion of foam films in diverging–converging channels. *Journal of Colloid and Interface Science*, Volume 271, pp. 473-484.

Olsson, E. & Kreiss, G., 2005. A conservative level set method for two phase flow. *Journal of computational physics*, Volume 210, pp. 225-246.

Omirbekov, S., Davarzani, H. & Ahmadi-Senichault, A., 2020 a. Experimental Study of Non-Newtonian Behavior of Foam Flow in Highly Permeable Porous Media. *Industrial & Engineering Chemistry Research*, Volume 59, p. 12568–12579.

Omirbekov, S., Davarzani, H. & Ahmadi-Senichault, A., 2020. Experimental Study of Non-Newtonian Behavior of Foam Flow in Highly Permeable Porous Media. *Industrial & Engineering Chemistry Research.*

Omirbekov, S., Davarzani, H. & Ahmadi-Senichault, A., 2020. Experimental Study of Non-Newtonian Behavior of Foam Flow in Highly Permeable Porous Media. *Industrial & Engineering Chemistry Research.*

Omirbekov, S., Davarzani, H. & Ahmadi-Senichault, A., 2020. Experimental Study of Non-Newtonian Behavior of Foam Flow in Highly Permeable Porous Media. *Industrial & Engineering Chemistry Research.*

Omirbekov, S., Davarzani, H., Colombano, S. & Ahmadi-Senichault, A., 2019. *Non-Newtonian behaviour of foam flow in porous media: experiments and upscaling.* s.l., s.n.

Omirbekov, S., Davarzani, H., Colombano, S. & Ahmadi-Senichault, A., 2020 b. Experimental and numerical upscaling of foam flow in highly permeable porous media. *Advances in Water Resources,* p. 103761.

Orgéas, L., Geindreau, C., Auriault, J.-L. & Bloch, J.-F., 2007. Upscaling the flow of generalised Newtonian fluids through anisotropic porous media. *Journal of Non-Newtonian Fluid Mechanics,* Volume 145, pp. 15-29.

Orgéas, L. et al., 2006. Modelling the flow of power-law fluids through anisotropic porous media at low-pore Reynolds number. *Chemical engineering science,* Volume 61, pp. 4490-4502.

Osei-Bonsu, K., Shokri, N. & Grassia, P., 2016. Fundamental investigation of foam flow in a liquid-filled Hele-Shaw cell. *Journal of colloid and interface science,* Volume 462, pp. 288-296.

Ossai, I. C., Ahmed, A., Hassan, A. & Hamid, F. S., 2019. Remediation of soil and water contaminated with petroleum hydrocarbon: A review. *Environmental Technology & Innovation.*

Osterloh, W. T. & Jante Jr, M. J., 1992. *Effects of gas and liquid velocity on steady-state foam flow at high temperature.* s.l., s.n.

Otsubo, Y. & Prud'homme, R. K., 1994. Effect of drop size distribution on the flow behavior of oil-in-water emulsions. *Rheologica Acta,* Volume 33, pp. 303-306.

Otsubo, Y. & Prud'homme, R. K., 1994. Rheology of oil-in-water emulsions. *Rheologica acta,* Volume 33, pp. 29-37.

Ovarlez, G., Krishan, K. & Cohen-Addad, S., 2010. Investigation of shear banding in three-dimensional foams. *EPL - Europhysics Letters,* Volume 91, p. 68005.

Ovarlez, G. et al., 2008. Wide-gap Couette flows of dense emulsions: Local concentration measurements, and comparison between macroscopic and local constitutive law measurements through magnetic resonance imaging. *Physical Review E : Statistical, Nonlinear, and Soft Matter Physics,* 9, Volume 78, p. 036307.

Pancharoen, M., Fernø, M. A. & Kovscek, A. R., 2012. Modeling foam displacement in fractures. *Journal of Petroleum Science and Engineering,* Volume 100, pp. 50-58.

Pang, Z.-X., 2010. The blocking ability and flowing characteristics of steady foams in porous media. *Transport in porous media,* Volume 85, pp. 299-316.

Pankow, J. F. & Cherry, J. A., 1996. Dense chlorinated solvents and other DNAPLs in groundwater: History, behavior, and remediation. *Waterloo Press.*

Papanastasiou, T. C., 1987. Flows of Materials with Yield. *Journal of Rheology,* Volume 31, pp. 385-404.

Papanicolau, G., Bensoussan, A. & Lions, J.-L., 1978. *Asymptotic Analysis for Periodic Structures.* s.l.:North Holland.

Paria, S., 2008. Surfactant-enhanced remediation of organic contaminated soil and water. *Advances in Colloid and Interface Science,* Volume 138, pp. 24-58.

Pasdar, M. et al., 2018. Insight into the behavior of colloidal gas aphron (CGA) fluids at elevated pressures: An experimental study. *Colloids and Surfaces A: Physicochemical and Engineering Aspects,* Volume 537, pp. 250-258.

Patton, J. T., Holbrook, S. T. & Hsu, W., 1983. Rheology of mobility-control foams. *Society of Petroleum Engineers Journal,* Volume 23, pp. 456-460.

Patzek, T. W., 1988. Description of foam flow in porous media by the population balance method. In: s.l.:ACS Publications.

Patzek, T. W., 1996. Field applications of steam foam for mobility improvement and profile control. *SPE Reservoir Engineering,* Volume 11, pp. 79-86.

Patzek, T. W. & Koinis, M. T., 1990. Kern River Steam-Foam Pilots. *Society of Petroleum Engineers.*

Perepelkin, K. E. & Matveev, V. S., 1979. *Gas emulsions (Газовые эмульсии).* s.l.:Chemistry. Leningrad division.

Persoff, P. et al., 1989. *A laboratory investigation of foam flow in sandstone at elevated pressure.* s.l., s.n.

Persoff, P. et al., 1991. A Laboratory Investigation of Foam Flow in Sandstone at Elevated Pressure.. *Society of Petroleum Engineers.*, 8.

Plateau, J., 1873. *Statique expérimentale et théorique des liquides soumis aux seules forces moléculaires.* s.l.:Gauthier-Villars.

Portois, C., Boeije, C. S., Bertin, H. J. & Atteia, O., 2018. Foam for environmental remediation: generation and blocking effect. *Transport in Porous Media,* Volume 124, pp. 787-801.

Portois, C. et al., 2018. Field demonstration of foam injection to confine a chlorinated solvent source zone. *Journal of contaminant hydrology,* Volume 214, pp. 16-23.

Princen, H. M., 1990. Gravitational syneresis in foams and concentrated emulsions. *Journal of colloid and interface science,* Volume 134, pp. 188-197.

Princen, H. M. & Kiss, A. D., 1989. Rheology of foams and highly concentrated emulsions: IV. An experimental study of the shear viscosity and yield stress of concentrated emulsions. *Journal of Colloid and Interface Science,* Volume 128, pp. 176-187.

Prud'homme, R. K. & Khan, S. A., 1996. *FOAMS. Theory, Measurements, and Applications.* s.l.:Routledge.

Qi, H. et al., 2018. Effect of pipe surface wettability on flow slip property. *Industrial & Engineering Chemistry Research,* Volume 57, pp. 12543-12550.

Quintard, M. & Whitaker, S., 1993. Transport in ordered and disordered porous media: volume-averaged equations, closure problems, and comparison with experiment. *Chemical Engineering Science,* Volume 48, pp. 2537-2564.

Quintard, M. & Whitaker, S., 1994. Transport in ordered and disordered porous media III: Closure and comparison between theory and experiment. *Transport in Porous Media,* Volume 15, pp. 31-49.

Rabinowitsch, B., 1929. Über die viskosität und elastizität von solen. *Zeitschrift für physikalische Chemie,* Volume 145, pp. 1-26.

Ramadan, A., Kuru, E. & Saasen, A., 2003. Critcal Review of Drilling Foam Rheology. *ANNUAL TRANSACTIONS-NORDIC RHEOLOGY SOCIETY,* Volume 11, pp. 63-72.

Ransohoff, T. C. & Radke, C. J., 1988. Mechanisms of Foam Generation in Glass-Bead Packs. *Society of Petroleum Engineers.*

Raza, S. H. & Marsden, S. S., 1967. The streaming potential and the rheology of foam. *Society of Petroleum Engineers Journal,* Volume 7, pp. 359-368.

Roof, J. G., 1970. Snap-off of oil droplets in water-wet pores. *Society of Petroleum Engineers Journal,* Volume 10, pp. 85-90.

Roostapour, A. & Kam, S. I., 2013. Anomalous foam-fractional-flow solutions at high-injection foam quality. *SPE Reservoir Evaluation & Engineering,* Volume 16, p. 40–50.

Rossen, W. R., 1990. Minimum pressure gradient for foam flow in porous media: Effect of interactions with stationary lamellae. *Journal of Colloid and Interface Science,* Volume 139, pp. 457-468.

Rossen, W. R., 1990. Theory of mobilization pressure gradient of flowing foams in porous media: I. Incompressible foam. *Journal of Colloid and Interface Science,* Volume 136, pp. 1-16.

Rossen, W. R., 1991. *Rheology of foam in porous media at the" limiting capillary pressure.* s.l., s.n., pp. cp--44.

Rossen, W. R., 1999. Foam in porous media. In: *Foams and Emulsions.* s.l.:Springer, pp. 335-348.

Rossen, W. R., 2003. A critical review of Roof snap-off as a mechanism of steady-state foam generation in homogeneous porous media. *Colloids and Surfaces A: Physicochemical and Engineering Aspects,* Volume 225, pp. 1-24.

Rossen, W. R., 2013. *Numerical challenges in foam simulation: a review.* s.l., s.n.

Rossen, W. R. & Gauglitz, P. A., 1990. Percolation theory of creation and mobilization of foams in porous media. *AIChE Journal,* Volume 36, pp. 1176-1188.

Rossen, W. R. & Wang, M. W., 1999. Modeling foams for acid diversion. *SPE journal,* Volume 4, pp. 92-100.

Rossen, W. R. & Wang, M. W., 1999. Modeling Foams for Acid Diversion. *Society of Petroleum Engineers.*

Rossen, W. R., Zeilinger, S. C., Shi, J. & Lim, M. T., 1994. *Mechanistic simulation of foam processes in porous media.* s.l., s.n.

Rothmel, R. K., Peters, R. W., St. Martin, E. & DeFlaun, M. F., 1998. Surfactant foam/bioaugmentation technology for in situ treatment of TCE-DNAPLs. *Environmental science & technology,* Volume 32, pp. 1667-1675.

Roy, D., Kommalapati, R. R., Valsaraj, K. T. & Constant, W. D., 1995. Soil flushing of residual transmission fluid: application of colloidal gas aphron suspensions and conventional surfactant solutions. *Water Research,* Volume 29, pp. 589-595.

Roy, D., Kongara, S. & Valsaraj, K. T., 1995. Application of surfactant solutions and colloidal gas aphron suspensions in flushing naphthalene from a contaminated soil matrix. *Journal of hazardous materials,* Volume 42, pp. 247-263.

Roy, D., Valsaraj, K. T., Constant, W. D. & Darji, M., 1994. Removal of hazardous oily waste from a soil matrix using surfactants and colloidal gas aphron suspensions under different flow conditions. *Journal of Hazardous Materials,* Volume 38, pp. 127-144.

Saint-Jalmes, A. & Durian, D. J., 1999. Vanishing elasticity for wet foams: Equivalence with emulsions and role of polydispersity. *Journal of Rheology,* Volume 43, pp. 1411-1422.

Sanchez-Palencia, E., 1980. *Non-Homogeneous Media and Vibration Theory Lecture Notes in Physics.* s.l.:Springer-Verlag Berlin Heidelberg.

Sander, R., 1999. *Compilation of Henry's law constants for inorganic and organic species of potential importance in environmental chemistry.* s.l.:Max-Planck Institute of Chemistry, Air Chemistry Department Mainz, Germany.

Sander, R., 1999. *Compilation of Henry's law constants for inorganic and organic species of potential importance in environmental chemistry,* s.l.: Max-Planck Institute of Chemistry, Air Chemistry Department Mainz, Germany.

Satter, A. & Iqbal, G. M., 2015. *Reservoir engineering: the fundamentals, simulation, and management of conventional and unconventional recoveries.* s.l.:Gulf Professional Publishing.

Scheidegger, A. E., 1974. The physics of flow through porous media. *University of Toronto, Toronto.*

Schramm, L. L., 2006. *Emulsions, foams, and suspensions: fundamentals and applications.* s.l.:John Wiley & Sons.

Sebba, F., 1971. Microfoams—an unexploited colloid system. *Journal of Colloid and Interface Science,* Volume 35, pp. 643-646.

Sheng, J. J., 2013. *Enhanced oil recovery field case studies.* s.l.:Gulf Professional Publishing.

Shi, J. X. & Rossen, W. R., 1996. *Simulation and dimensional analysis of foam processes in porous media.* s.l., s.n.

Shojaei, M. J., Castro, A. R., Méheust, Y. & Shokri, N., 2019. Dynamics of foam flow in a rock fracture: Effects of aperture variation on apparent shear viscosity and bubble morphology. *Journal of colloid and interface science,* Volume 552, pp. 464-475.

Simjoo, M., Nguyen, Q. P. & Zitha, P. L. J., 2012. Rheological Transition during Foam Flow in Porous Media. *Industrial & Engineering Chemistry Research.*

Simjoo, M., Rezaei, T., Andrianov, A. & Zitha, P. L. J., 2013. Foam stability in the presence of oil: effect of surfactant concentration and oil type. *Colloids and Surfaces A: Physicochemical and Engineering Aspects,* Volume 438, pp. 148-158.

Simjoo, M. & Zitha, P. L. J., 2020. Modeling and Experimental Validation of Rheological Transition During Foam Flow in Porous Media. *Transport in Porous Media,* Volume 131, pp. 315-332.

Singh, R. & Mohanty, K. K., 2016. Foams with wettability-altering capabilities for oil-wet carbonates: a synergistic approach. *SPE Journal,* Volume 21, p. 1–126.

Skelland, A. H. P., 1967. Non-Newtonian flow and heat transfer(Book on quantitative relationships for non- Newtonian systems, considering classification and fluid behavior of materials with anomalous flow properties). *NEW YORK, JOHN WILEY AND SONS, INC., 1967. 469 P.*

Smith, C. S., 1949. On blowing bubbles for Bragg's dynamic crystal model. *Journal of Applied Physics,* Volume 20, pp. 631-631.

Sochi, T. & Blunt, M. J., 2008. Pore-scale network modeling of Ellis and Herschel--Bulkley fluids. *Journal of Petroleum Science and Engineering,* Volume 60, pp. 105-124.

Stauffer, C. E., 1965. The measurement of surface tension by the pendant drop technique. *The journal of physical chemistry,* Volume 69, pp. 1933-1938.

Stevenson, P., 2012. *Foam engineering: fundamentals and applications.* s.l.:John Wiley & Sons.

Sutera, S. P. & Skalak, R., 1993. The history of Poiseuille's law. *Annual review of fluid mechanics,* Volume 25, pp. 1-20.

Svab, M., Kubal, M., Müllerova, M. & Raschman, R., 2009. Soil flushing by surfactant solution: Pilot-scale demonstration of complete technology. *Journal of Hazardous Materials,* Volume 163, pp. 410-417.

Talmage, S. S., 1994. *Environmental and human safety of major surfactants: alcohol ethoxylates and alkylphenol ethoxylates.* s.l.:CRC Press.

Tan, S. N., Fornasiero, D., Sedev, R. & Ralston, J., 2005. The role of surfactant structure on foam behaviour. *Colloids and Surfaces A: Physicochemical and Engineering Aspects,* Volume 263, pp. 233-238.

Tanzil, D., Hirasaki, G. J. & Miller, C. A., 2000. *Mobility of foam in heterogeneous media: Flow parallel and perpendicular to stratification.* s.l., s.n.

Tao, W., Mei, C. & Hamzah, N., 2020. The application of surfactant colloidal gas aphrons to remediate contaminated soil: A review. *Journal of Contaminant Hydrology,* p. 103620.

Tcholakova, S. et al., 2008. Theoretical model of viscous friction inside steadily sheared foams and concentrated emulsions. *Phys. Rev. E,* 7, 78(1), p. 011405.

Thondavadi, N. N. & Lemlich, R., 1985. Flow properties of foam with and without solid particles. *Industrial & Engineering Chemistry Process Design and Development,* Volume 24, pp. 748-753.

Tuvell, M. E. et al., 1978. AOS --- An anionic surfactant system: Its manufacture, composition, properties, and potential application. *Journal of the American Oil Chemists' Society,* 01 1, Volume 55, pp. 70-80.

Valko, P. & Economides, M. J., 1992. Volume equalized constitutive equations for foamed polymer solutions. *Journal of Rheology,* Volume 36, pp. 1033-1055.

Vassenden, F. & Holt, T., 2000. Experimental Foundation for Relative Permeability Modeling of Foam. *Society of Petroleum Engineers.*

Vassenden, F. & Holt, T., 2000. Experimental Foundation for Relative Permeability Modeling of Foam. *Society of Petroleum Engineers.*

Verma, A., Chauhan, G. & Ojha, K., 2018. Characterization of α-olefin sulfonate foam in presence of cosurfactants: Stability, foamability and drainage kinetic study. *Journal of Molecular Liquids,* Volume 264, pp. 458-469.

Voorhees, P. W., 1985. The theory of Ostwald ripening. *Journal of Statistical Physics,* Volume 38, pp. 231-252.

Wang, H. & Chen, J., 2012. Enhanced flushing of polychlorinated biphenyls contaminated sands using surfactant foam: effect of partition coefficient and sweep efficiency. *Journal of Environmental Sciences,* Volume 24, pp. 1270-1277.

Wang, J., Liu, H., Ning, Z. & Zhang, H., 2012. Experimental research and quantitative characterization of nitrogen foam blocking characteristics. *Energy & Fuels,* Volume 26, pp. 5152-5163.

Wang, S. & Mulligan, C. N., 2004. An evaluation of surfactant foam technology in remediation of contaminated soil. *Chemosphere,* Volume 57, pp. 1079-1089.

Wang, S. & Mulligan, C. N., 2004. Rhamnolipid foam enhanced remediation of cadmium and nickel contaminated soil. *Water, Air, and Soil Pollution,* Volume 157, pp. 315-330.

Wang, X.-H., Jia, J.-T., Liu, Z.-F. & Jin, L.-D., 2014. Derivation of the Darcy-scale filtration equation for power-law fluids with the volume averaging method. *Journal of Porous Media,* Volume 17.

Wenzel, R. N., 1949. Surface roughness and contact angle.. *The Journal of Physical Chemistry,* Volume 53, p. 1466–1467.

Whitaker, S., 1985. A Simple Geometrical Derivation of the Spatial Averaging Theorem.. *Chemical engineering education,* Volume 19.

Whitaker, S., 1999. *The Method of Volume Averaging.* s.l.:Springer Netherlands.

Whitaker, S., 2013. *The method of volume averaging.* s.l.:Springer Science & Business Media.

Woods, J. K. et al., 2003. Creeping flows of power-law fluids through periodic arrays of elliptical cylinders. *Journal of non-newtonian fluid mechanics,* Volume 111, pp. 211-228.

Xiong, Q., Baychev, T. G. & Jivkov, A. P., 2016. Review of pore network modelling of porous media: experimental characterisations, network constructions and applications to reactive transport. *Journal of contaminant hydrology,* Volume 192, pp. 101-117.

Yoon, I.-H.et al., 2019. A highly efficient decontamination foam stabilized by well-dispersed mesoporous silica nanoparticles. *Colloids and Surfaces A: Physicochemical and Engineering Aspects,* Volume 560, pp. 164-170.

Zeng, Y. et al., 2016. Role of gas type on foam transport in porous media. *Langmuir,* Volume 32, pp. 6239-6245.

Zhang, T. et al., 2019. In situ remediation of subsurface contamination: opportunities and challenges for nanotechnology and advanced materials. *Environmental Science: Nano,* Volume 6, p. 1283–1302.

Zhang, Z. F., Freedman, V. L. & Zhong, L., 2009. Foam Transport in Porous Media-A Review. *Report.*

Zitha, P., Chauveteau, G. & Zaitoun, A., 1995. *Permeability˜ Dependent Propagation of Polyacrylamides Under Near-Wellbore Flow Conditions.* s.l., s.n.

Zitha, P. L. J. & Du, D. X., 2010. A new stochastic bubble population model for foam flow in porous media. *Transport in Porous Media,* Volume 83, pp. 603-621.

Remédiation des sols pollués par injection des mousses tensioactifs: expériences et changement d'échelle

Résume: L'injection de mousse dans des milieux poreux a été étudiée pour une variété d'applications dans l'industrie pétrolière et récemment pour des procédés de dépollution des sols afin d'éliminer les contaminants. Cependant, l'injection de mousse pour la remédiation des sols n'est toujours pas répandue en raison de la nature complexe de la mousse et des aquifères.

Afin d'étudier l'application de la mousse pour la remédiation des sols, nous avons étudié expérimentalement le comportement de la mousse à l'échelle du laboratoire. Le but final de la recherche était d'étudier l'écoulement de mousse pour détourner l'écoulement des eaux souterraines des zones de sols contaminés en tenant compte des caractéristiques de l'écoulement de mousse en milieux poreux hautement perméables. Ainsi, la rhéologie de la mousse pré-générée a été étudiée dans des milieux poreux hautement perméables, dans des tubes capillaires, ainsi qu'à l'aide d'un rhéomètre. De plus, une étude numérique a été menée pour examiner l'écoulement de mousse à plus grande échelle sur la base des résultats de la rhéologie de la mousse hors milieu poreux.

En conséquence, il a été démontré que l'écoulement de mousse présente un comportement non newtonien. Nous avons constaté que le comportement d'écoulement de la mousse en milieu poreux très perméables et dans les tubes capillaires est cohérent avec le comportement rhéologique de la mousse hors milieu poreux, si les bulles de mousse sont beaucoup plus petites que la taille des pores des milieux poreux. Ces résultats peuvent guider l'étude de la mousse pré-générée en milieux poreux très perméables.

Mots clés: mousse, rhéologie, milieu poreux, changement d'échelle, décontamination des sols, simulation numérique.

Polluted soil remediation using surfactant foam injection: experiments and upscaling

Abstract: Foam injection in porous media has been investigated for a variety of applications in the oil industry and recently for soil remediation processes to remove contaminants. However, foam injection for soil remediation is still not widespread because of the complex nature of foam and aquifers.

In order to investigate application in soil remediation processes, we experimentally studied the behavior of foam on a laboratory scale. The final goal of the research was to study foam flow for diverting the flow of groundwater from contaminated soil areas considering the features of foam flow in highly permeable porous media. Thus, the rheology of pre-generated foam was studied in highly permeable porous media, in capillary tubes, as well as using a rheometer. Moreover, a numerical study was conducted to examine foam flow in a bigger scale based on bulk foam rheology results.

As a result, foam flow was showed to feature non-Newtonian behavior. We found that the foam flow behavior in high permeable porous media and in capillary tubes are consistent with the rheology behavior of bulk foam if bubbles are much smaller than the pore size of porous media. Hence, these findings can guide the study of pre-generated foam in very highly permeable porous media.

Keywords: foam, rheology, porous media, upscaling, soil remediation, numerical simulation.